Université de Montréal

The Role of CBL Family Proteins in Dendritic Cell Development, Homeostasis, and Functional Quiescence

par
Haijun Tong

Département de Sciences Biomédicales
Faculté de Médecine

Thèse présentée à la faculté des études supérieures
en vue de l'obtention du grade de
Philosophiae Doctor (Ph.D.)
en sciences biomédicales

August. 2016

Résumé

Les cellules dendritiques sont des cellules du système immunitaire inné qui jouent un rôle important dans la reconnaissance immunitaire contre les agents pathogènes étrangers. Elles peuvent également prévenir les maladies auto-immunes à l'état basal. En raison de l'importance des cellules dendritiques dans la régulation immunitaire, il est important de comprendre comment le développement, l'état d'homéostasie et de quiescence des ces cellules sont contrôlées dans des conditions physiologiques et pathologiques. Cette étude permettra non seulement de mieux comprendre le contrôle de la régulation immunitaire, mais aussi de contribuer au développement de nouvelles approches pour traiter les maladies infectieuses et auto-immunes, ainsi que les cancers.

Notre laboratoire a montré que C-CBL et CBL-B, deux membres de la famille CBL des ubiquitine ligases E3, jouent un rôle redondant dans la régulation négative du développement et de l'activation des cellules T et B. En l'absence de CBL dans les cellules T ou B, les souris développent des maladies auto-immunes sévères, indiquant que C-CBL et CBL-B jouent un rôle dans le système auto-immun. Partant de ces observations, nous proposons que CBL-B et C-CBL peuvent également jouer un rôle similaire dans le développement et la fonction des cellules dendritiques. Pour étudier cette possibilité, nous avons généré une souris knockout de *Cbl* spécifiques aux cellules dendritiques (dKO). Nous avons trouvé que cette mutation provoque une modification de l'homéostasie d'un sous-ensemble des cellules dendritiques (DC), y compris une augmentation marquée des $CD8\alpha^+$ cDCs et une réduction des pDC dans la rate. Cette modification est causée par la prolifération accrue des $CD8\alpha^+$ cDCs. Dans les $CD8\alpha^+$ cDCs mutantes, les voies de signalisation PKB et ERK sont constitutivement activées. Blocage de la signalisation de MTOR par la rapamycine atténue de manière significative l'hyperprolifération des $CD8\alpha^+$ cDCs *in vitro* et *in vivo*, indiquant que l'hyperactivation de MTOR est en partie responsable de l'augmentation $CD8\alpha^+$ cDCs. Les protéines CBL contrôlent l'ubiquitination et la dégradation du récepteur FLT3, suggérant que les protéines CBL contrôlent ainsi l'homéostasie de $CD8\alpha^+$ cDCs.

Outre ces effets sur le développement des cellules dendritiques, nous avons trouvé que les souris *Cbl* dKO développent des inflammations sévères du foie et d'autres organes, caractérisées par une infiltration massive de leucocytes et une activation importante des cellules lymphocytes T périphériques. Les souris mutantes produisent des niveaux élevés de cytokines inflammatoires et

de chimiokines, telles que le TNF-α, l'IL-6 et le CCL2. Les souris mutantes développent une maladie inflammatoire du foie. L'ensemble de ces observations montrent que les protéines CBL jouent un rôle essentiel dans le maintien de la quiescence immunitaire chez la souris. Puisque les souris dKO *Cbl* développent principalement une inflammation sévère du foie, il serait intéressant d'étudier si les voies contrôlées par les protéines CBL contribuent également au développement d'une inflammation du foie chez l'homme.

Mots-clés: DC; homéostasie; quiescence; CBL-B; C-CBL; FLT3; ubiquitination; dégradation; une maladie inflammatoire chronique

Abstract

Dendritic cells (DCs) are innate immune cells that play an important role in immune recognition against foreign pathogens. They may also sense self-cues and prevent autoimmune diseases under the steady-state. Given the importance of DCs in immune regulation, it is conceivable that understanding how DCs development, homeostasis and functional quiescence are regulated under physiological and pathological conditions will not only bring insight into our knowledge how immune regulation is controlled but also some new approaches to treat infectious and autoimmune diseases and even cancers.

Dr. Gu's lab previously has shown that C-CBL and CBL-B, two members of the CBL family of E3 ubiquitin ligases, play a redundant negative regulatory role in both T cells and B cells development and activation. In the absence of CBL family of proteins in either T or B cells, mice develop severe autoimmune diseases, indicating that C-CBL and CBL-B restrain immune system against self. Based on these discoveries, we propose that C-CBL and CBL-B may also have a similar regulatory role in DC development and function. To study this possibility, we have generated DC-specific *Cbl* dKO mice. We have found that the *Cbl* dKO mutation results in an altered homeostasis of DC subsets, including a marked increase of $CD8\alpha^+$ cDCs and reduction of pDCs in the spleen (SP). This alteration is due to the enhanced proliferation of $CD8\alpha^+$ cDCs rather than the preferential lineage commitment to $CD8\alpha^+$ cDCs. In the mutant $CD8\alpha^+$ cDCs, both the PKB signaling pathway and ERK signaling pathways are constitutively activated. Blockage of MTOR signaling by Rapamycin significantly attenuates the hyperproliferation of $CD8\alpha^+$ cDCs both *in vitro* and *in vivo*, indicating that hyperactivation of MTOR is at least one of the reasons leading to $CD8\alpha^+$ cDC expansion. CBL proteins regulate ubiquitination and degradation of FLT3. Based on these results, we conclude that CBL proteins control $CD8\alpha^+$ cDC homeostasis through promoting FLT3 ubiquitination and degradation.

In addition to the altered DC development, we have found that *Cbl* dKO mice develop severe liver and other organ inflammation characterized by massive leukocytes infiltration and profound peripheral T cell activation. Mutant mice produce high levels of inflammatory cytokines and chemokines including TNF-α, IL-6, CCL2, etc. Most strikingly, the mutant mice develop a similar liver inflammatory disease even in the absence of T and B cells. These findings together indicate that CBL proteins play an essential role in the maintenance of immune quiescence in mice. Since

Cbl dKO mice mainly develop severe liver inflammation, it will be interesting to study whether the pathways controlled by CBL proteins also contribute to the development of liver inflammation in humans.

Keywords: DCs; homeostasis; quiescence; CBL-B; C-CBL; FLT3; ubiquitination; degradation; chronic inflammatory disease

LIST OF FIGURES AND TABLES

I. INTRODUCTION

III. MATERIALS AND METHODS

IV. RESULTS

V. DISCUSSION

LIST OF ABBREVIATIONS

aCML	atypical chronic myeloid leukemia
ADCC	antibody-dependent cell cytotoxicity
AML	acute myeloid leukemia
AMPs	antimicrobial peptides
ALL	acute lymphoblastic leukemia
APCs	antigen presenting cells
BATF3	basic leucine zipper transcription factor ATF-like 3
BCR	B-cell receptor
BM	bone marrow
CBL	casitas B-lineage lymphoma
CCR	C-C chemokine receptor type 9
CDPs	common DC precursors
CLEC-2	C-type lectin domain family 2
CLRs	C-type lectin receptors
CML	chronic myeloid leukemia
CMML	chronic myelomonocytic leukemia
cMoPs	common monocyte progenitors
CRDs	carbohydrate-recognition domains
CSF-1R	colony stimulating factor-1 receptor
DAMPs	damage-associated molecular patterns
DCIR	DC-inhibitory receptor
DCs	dendritic cells
dDC	dermal DC
DECTIN-1	DC-associated C-type lectin 1
dKO	double knockout
DSS	dextran sulfate sodium
dsDNA	double strand DNA
DTR	diphtheria toxin receptor
EAE	experimental autoimmune encephalomyelitis
EGFR	epidermal growth factor receptor

EPCAM epithelial-cell adhesion molecule

EPOR erythropoietin (Epo) receptor

ERK extracellular signal-regulated kinase

ETS E26 transformation-specific

FANCD2 Fanconi anemia complementation group D2

FcRγ Fc receptor γ

FGFR1 fibroblast growth factor receptor 1

FLT3 Fms-like tyrosine kinase 3

FLT3L FLT3 ligand

GEFs guanine nucleotide exchange factors

GM-CSF granulocyte-macrophage colony stimulating factor

GRB2 growth factor receptor-bound protein

GWAS genome-wide association study

HECT homologous with E6-associated protein C-terminus

HGFR hepatocyte growth factor receptor

HLH helix-loop-helix

HMGB1 high-mobility group box 1

HSCs hematopoietic stem cells

HSPs heat shock proteins

HU hydroxyurea

IBD inflammatory bowel disease

ID2 inhibitor of DNA binding protein 2

iDCs inflammatory DCs

IECs intestinal epithelial cells

IFIH1 interferon induced with helicase C domain 1

IFN interferon

Ig immunoglobulin

IKK IkappaB kinase

IL interleukin

iNOS inducible nitric oxide synthases

IP intraperitoneal

IR ionizing radiation

IRAK IL-1 receptor-associated kinases

IRF interferon regulatory factor

ITAM immunoreceptor tyrosine-based activation motifs

ITD internal tandem duplications

ITIM immunoreceptor tyrosine-based inhibitory motif

JM juxtamembrane domain

JMML juvenile myelomonocytic leukemia

JNK Jun N-terminal kinase

KID kinase insert domain

KIRs killer cell immunoglobulin-like receptors

LCs Langerhans cells

Lin- lineage-negative

LNs lymph nodes

LP lamina propria

LTβR lymphotoxin β receptor

LZ leucine zipper

MAMPs microbe-associated molecular patterns

MAPK mitogen-activated protein (MAP) kinases

MARCH membrane-associated RING-CH

MCP monocyte chemotactic protein

M-CSF macrophage colony stimulating factor

MDA5 melanoma differentiation-associated protein 5

MDPs monocyte-DC precursors

MDS myelodysplastic syndromes

MHC major histocompatibility complex

MINCLE macrophage inducible C-type lectin

MIP macrophage inflammatory protein

MLR mixed leukocytes reaction

MMC mitomycin C

moDCs monocyte-derived DCs

MPN myeloproliferative neoplasms

MS multiple sclerosis

MSU monosodium urate

MTOR mechanistic target of rapamycin

MYD88 myeloid differentiation primary response gene 88

NALP3 pyrin domain-containing protein 3

NEMO NF-kappa-B essential modulator

NF-κB nuclear factor kappa-light-chain-enhancer of activated B cells

NK natural killer

NLRs NOD-like receptors

NOD nucleotide oligomerization domain

non-RTK non-receptor tyrosine kinase

p75NTR neurotrophin receptor p75

PAMPs pathogen-associated molecular patterns

pDC plasmacytoid DCs

PDGFR platelet-derived growth factor receptor

PI3K phosphoinositide 3-kinase

PKB protein kinase B

pre-cDCs precursor classical DCs

PRRs pattern-recognition receptors

PSA polysaccharide A

PTKs phosphotyrosine kinases

RF RING finger

RIG retinoic acid-inducible gene

RIP1 receptor-interacting serine/threonine-protein kinase 1

RLRs RIG-I-like receptors

RTK receptor tyrosine kinase

RUNX2 runt-related transcription factor 2

SCF stem cell factor

SFKs Src family kinases

SH2 Src Homology 2

SLE systemic lupus erythematosus

SNPs single-nucleotide polymorphisms

SOCS-1 suppressor of cytokine signaling-1

SP spleen

STAT signal transducer and activator of transcription

SYK spleen tyrosine kinase

T1 transitional 1

T1D type I diabetes

TAK1 transforming growth factor beta-activated kinase 1

TCR T-cell receptor

TF tissue factor

Tg transgenic

TGFβ1 transforming growth factor β1

Th1 T helper 1

TIR Toll/interleukin-1 (IL-1) receptor

TipDCs TNF-α/iNOS-producing DCs

TKB tyrosine kinase binding

tKO triple knockout

TKRs TAM tyrosine kinase receptors

TLRs Toll-like receptors

TNF tumor necrosis factor

TNFAIP tumor necrosis factor, alpha-induced protein

TOLLIP Toll-interacting protein

TPO thrombopoietin

TRAF6 TNF receptor associated factor 6

UBA ubiquitin-associated

UV ultraviolet light

VEGF vascular endothelial growth factor

WT wild type

ZAP-70 zeta-chain-associated protein kinase-70

Hereby, I would like to express my sincere gratitude to my supervisor Dr. Hua Gu for his instructions on my research and knowledge for the past 5 years. Also I would like to thank to all my committee-meeting members and thesis-meeting members for their great help to my research and thesis. Thanks to Dominique Davidson to help me translate the English abstract of my thesis into French. Moreover, I would like to thank my family for their great understanding and support during my study. I would also thank greatly to all my colleagues in the IRCM and Udem, and the core facility members for their help and support during my PhD study. Last but not least, I would like to thank my country and CIHR for their financial support for my study in Canada for the past 6 years.

02-09-2016

Montréal

Haijun Tong

INDEX

I. INTRODUCTION

Overview of DC, immunity, and immune tolerance

Everyday our body encounters various types of pathogens, such as viruses, bacteria and worms. Nevertheless, our immune system can recognize these invaders and mount effective immune responses against these pathogens, thus protecting us from the development of devastating diseases. During these immune defenses, two types of immune response are involved: the innate immune response and the antigen-specific adaptive immune response. Innate immune response normally does not require T cells and B cells, and innate immune cells themselves can provide the first line of defense against pathogens by producing cytotoxic mediators such as cytokines and free radical oxygens. In the adaptive immune response, the participation of T cells and B cells can help the body with a more efficient, long-lasting and specific way to target pathogens and mount immune responses through immunological memory.

Dendritic cells (DCs) are known to play very important roles in both innate and adaptive immune responses. First, they can sense pathogens using their surface and intracellular receptors, and they can efficiently produce large amounts of cytokines to against pathogen. Secondly, they can present antigens to T cells and B cells through their surface major histocompatibility complex (MHC) molecules and co-stimulatory molecules, and they can dictate the types of adaptive immune responses through cytokine production. In addition to recognizing foreign antigens, our body also needs certain abilities to distinguish self-antigens from non-self-antigens. Otherwise, the misrecognition of self-antigens as non-self-antigens may cause disastrous autoimmune diseases. Given that DCs are so important in both innate and adaptive immune response, the altered development, homeostasis and function of DCs could severely affect our ability to prevent various infections or autoimmune diseases. In this regard, it is pivotally important to understand how the development and homeostasis of DCs are regulated and how their functions are properly controlled to support immune responses against pathogens while preventing the development of autoimmune diseases.

I.1. DC subsets and their function

DCs are a group of hematopoietic cells characterized by their dendritic morphology and specialized antigen-presenting function. Since DCs can efficiently activate T cells, they are considered as professional antigen-presenting cells (APCs). DCs were discovered first by Ralph

Steinman in the mouse spleen in 1973[1-3]. Over the following years, Ralph Steinman and his colleagues further provided compelling evidence showing that DCs with prominent expression of MHC class I and II molecules had strong antigen processing and presenting capacities and were unrivaled stimulators of T cells in primary mixed leukocytes reaction (MLR)[4, 5]. Due to his outstanding work in discovering DCs and establishing their function and biology—as well as their application in vaccines—Ralph Steinman was honored with the Nobel Prize in Physiology or Medicine in 2011.

DCs can be classified into many different subsets. Under steady state, DC development occurs in the bone marrow (BM), starting from common monocyte-DC precursors (MDPs) to common DC precursors (CDPs), which give rise to plasmacytoid DCs (pDCs) and precursor of classical DCs (pre-cDCs) but not monocytes. Pre-cDCs migrate to secondary lymphoid organs through high endothelial venules and continue their differentiation into $CD8\alpha^+$ cDCs and $CD11B^+$ cDCs in a fms like tyrosine kinase 3 (FLT3)-dependent manner[6]. In the peripheral non-lymphoid organs, except lamina propria (LP), there is a DC subset, $CD103^+$ cDCs, that follows a related differentiation program as $CD8\alpha^+$ cDCs[7]. In addition to these cDCs, there are also several non-classical DC subsets such as monocyte-derived DCs (moDCs), pDCs, and epidermal Langerhans cells (LCs) that are developed either during infection or in homeostasis[8] (Fig 1.1).

Despite different origins and phenotypes of individual DC subset, DCs are all equipped with several major features that generally distinguish them from other cell types. Firstly, DCs are professional antigen processing and presenting cells. They can efficiently present endogenous and exogenous antigens in both MHCI and MHCII contexts to prime $CD4^+$ and $CD8^+$ T cells through TCR[9]. In this process, the activation of T cells also requires the assistance of interaction between the co-stimulatory molecules expressed on DCs and the corresponding co-receptors on T cells. In addition to the T cell activation, DCs can also present complete and unprocessed antigens through FcγRIIB to B cells[10]. Secondly, DCs harbor pattern recognition receptors (PRRs) such as TLRs to sense the damage associated molecular patterns (DAMP) signals. When DCs recognize these DAMPs, they become activated and promote their antigen-presentation capacity by enhancing lysosomal acidification and antigen proteolysis, elevating the expression

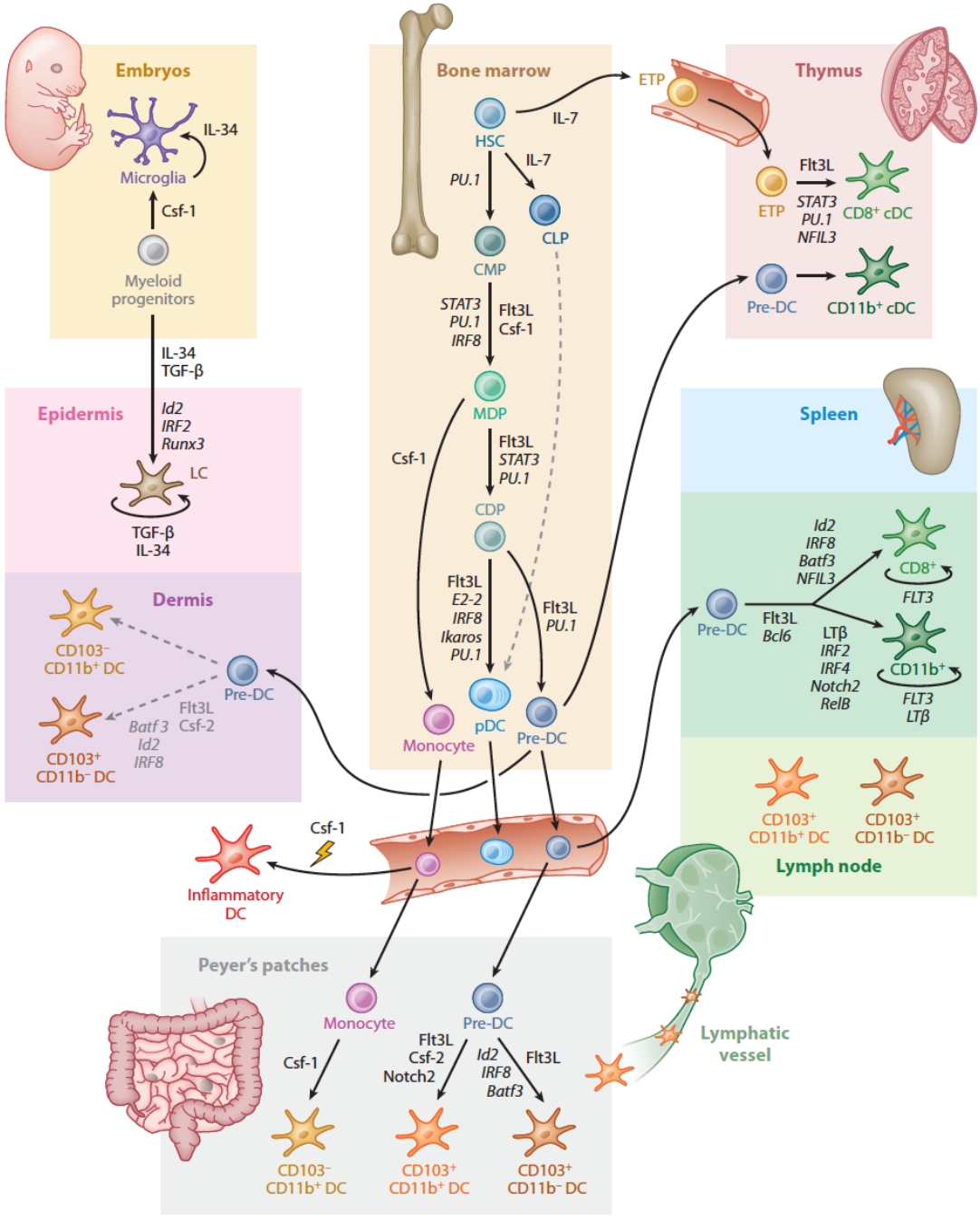

Fig. 1.1. Regulation of DC development and homeostasis in mice. (Cited from Ref.8)
A current model of the developmental pathways of both lymphoid tissue-resident and non-lymphoid tissue-resident murine DCs. Dashed lines indicate pathways that are likely but not yet definitively shown to operate in DC development. Cytokines and transcription factors that are important in each transition are indicated. (HSC, hematopoietic stem cell; CMP, common myeloid progenitor; CLP, common lymphoid progenitor; MDP, macrophage DC progenitor; CDP, common DC progenitor; ETP, early thymic progenitor; mono, monocyte; LC, Langerhans cell)

of their surface co-stimulatory molecules and instructing cytokine production to initiate productive or protective immune responses[11, 12]. Due to these special features, DCs appear to be an important intermediate player between innate immune response and adaptive immune response.

I.1.1. Classical DCs (cDCs)

cDCs can be categorized into at least two main subsets, i.e., the $CD8\alpha^+$ or $CD103^+$ cDCs and $CD11B^+$ cDCs, based on their cell surface markers. Both subsets arise from MDPs in the BM, which later differentiate into common monocyte progenitors (cMoPs) and CDPs. CDPs can further give rise to pDCs and pre-cDCs in BM. Pre-cDCs will migrate to the secondary lymphoid organs or the peripheral non-lymphoid organs to continue their differentiation into $CD8\alpha^+$ or $CD103^+$ cDCs and $CD11B^+$ cDCs, respectively[13].

I.1.1.1. $CD8\alpha^+$ cDC and $CD103^+$ cDC

$CD8\alpha^+$ cDCs and $CD103^+$ cDCs are the best and earliest characterized DC subsets by the efforts from both Shortman and Steinman groups[14, 15]. $CD8\alpha^+$ cDCs are typically located in the lymphoid organs, while $CD103^+$ cDCs are typically located in the non-lymphoid tissues. These $CD103^+$ non-lymphoid tissue cDCs normally do not express $CD8\alpha$[16]. However, they share several functional features with $CD8\alpha^+$ cDCs.

Firstly, both $CD8\alpha^+$ cDCs and $CD103^+$ cDCs require FLT3 signaling to support their development, which is evidenced by the observation that $CD8\alpha^+$ cDCs and $CD103^+$ cDCs are both absent from the lymphoid non-lymphoid organs including dermis, lung, liver, pancreatic islet, kidney, LP and Peyer's patches of mice lacking FLT3 or FLT3 ligand (FLT3L)[7, 17].

Secondly, both $CD8\alpha^+$ cDCs and $CD103^+$ cDCs have a unique, special function to cross-present exogenous extracellular antigens to prime $CD8^+$ T cells, which is necessary for immunity against most tumors and extracellular pathogens that do not readily infect APCs[18]. In general, there are two pathways to process the antigens into peptides. MHCI molecules generally bind peptides generated by proteasomal proteolysis of cell endogenous antigens, while MHCII molecules generally bind peptides generated by lysosomal proteolysis of exogenous antigens[19]. However,

in CD8α$^+$ cDCs and CD103$^+$ cDCs, MHCII can also access peptides from endogenous antigens, and MHCI can also access peptides from exogenous antigens, which enables them to become professional antigen-presenting cells. Although the intracellular mechanism of this MHCI mediated exogenous antigen presentation is so far not very well clarified, this cross-presentation feature is very important because it is the major mechanism to activate cytotoxic CD8$^+$ T cells against extracellular pathogens and tumors[20]. There are accumulating evidences that CD8α$^+$ cDCs and CD103$^+$ cDCs have stronger antigen cross-presentation capacities than CD11B$^+$ cDCs in the steady state[21-23]. However, CD11B$^+$ cDCs and inflammatory moDCs can also exhibit comparable cross-presentation features under inflammatory circumstances[21, 24].

Thirdly, CD8α$^+$ cDCs and CD103$^+$ cDCs share some important master transcription factors to support their differentiation. It is well known that the lineage commitment of different cDC subsets requires a fine transcriptional regulation by certain key transcription factors, and DC-specific knockout of these transcription factors can impair the differentiation of certain cDCs subsets. For example, the zinc finger transcription factor ZBTB46 is the most specific transcription factor for cDCs. Its expression starts at the pre-cDC stage and remains in the CD8α$^+$, CD103$^+$ and CD11B$^+$ cDCs but is absent in pDCs, monocytes, macrophages and other immune cells[25, 26]. This finding makes the *Zbtb46*-specific diphtheria toxin receptor (DTR) mouse a very useful tool to investigate the specific role of cDCs in different types of immune response. Moreover, *Zbtb46* germline deficiency alters the cDC subset composition in the spleen, which favors CD8α$^+$ cDCs development. In addition, ZBTB46 deficiency also changes DC function, which upregulates the MHCII expression and enhances the production of vascular endothelial growth factor (VEGF) in cDCs, leading to the increased vascularization of skin draining lymph nodes (LNs)[27]. In addition, interferon regulatory factor 8 (IRF8) is another transcription factor that plays an important role in the regulation of CD8α$^+$ cDCs and CD103$^+$ cDCs differentiation. *Irf8*$^{-/-}$ mice fail to generate spleen resident CD8α$^+$ cDCs, non-lymphoid tissue resident CD103$^+$ cDCs and pDCs[28,29]. A spontaneous point mutation (R294C) of IRF8 in BHX2 mice also impairs the development of CD8α$^+$ and CD103$^+$ cDCs and also their IL-12 production but without impairing pDCs generation[30]. Inhibitor of DNA binding protein 2 (ID2), which is a member of the helix-loop-helix (HLH) transcription factor family, is required for the development of CD8α$^+$ cDCs and CD103$^+$ cDCs. *Id2*$^{-/-}$ mice have greatly impaired CD8α$^+$ cDCs and CD103$^+$ cDCs development, and enforced *Id2* expression will

inhibit pDCs development without altering the cDCs' development[31-33]. Similarly, the basic leucine zipper transcription factor ATF-like 3 (BATF3) also supports the development of CD8α$^+$ and CD103$^+$ cDCs. Although it is expressed in all cDC subsets, mice lacking *Batf3* have a selective deficiency in CD8α$^+$ cDCs and CD103$^+$ cDCs in the 129S6/SvEv mice strain[34]. For the C57BL/6 mice strain, a lack of *Batf3* causes the loss of CD103$^+$ cDCs and reduction of spleen CD8α$^+$ cDCs but without changing the CD8α$^+$ cDCs' number in the LNs, which suggests that a strain variation may exist in the transcriptional regulation of the development of DCs[35]. In addition to these factors, other transcription factors that have more broad roles in hematopoiesis can also influence DC development. For example, *Ikaros* deficient mice lack thymic and splenic cDCs[36]. PU.1, a member of the E26 transformation-specific (ETS) family of transcription factors, has the important role of controlling cDCs development. Conditional ablation of *Pu.1* in defined precursors including CDPs blocked FLT3L-induced DC generation and also granulocyte-macrophage colony stimulating factor (GM-CSF)-induced DC generation, suggesting that PU.1 is a critical regulator of both cDC and pDC development[37]. The transcriptional regulation and cytokine regulation of the development of different DC subsets are summarized in Table 1.1.

Taken together, it is generally accepted that CD8α$^+$ cDCs and CD103$^+$ cDCs are closely related lineages, based on the evidence that they are conserved through evolution and are also allowed to be aligned based on their transcriptome profiling[38, 39]. They rely on FLT3L/FLT3 signaling to keep their homeostasis. They also express colony-stimulating factor-2 receptor (CSF-2R), receptor of GM-CSF, a cytokine that drives monocytes to give rise to DC-like cells[40]. They share the same transcription factors to control their development, and they have specialized machinery to render them to cross-present exogenous antigens to professionally prime CD8$^+$ cytotoxic T cells. They are also special inducers to promote T helper 1 (Th1) polarization through their professional IL-12 producing function[41].

I.1.1.2. CD11B$^+$ cDC

As a cDC subset, CD11B$^+$ cDCs share some of the same features as CD8α$^+$ cDCs and CD103$^+$ cDCs. For example, FLT3 signaling contributes to the development of CD11B$^+$ cDCs, though to a less extent, since *Flt3l* or *Flt3* knockout mice exert a less severe effect on CD11B$^+$ cDCs than on CD8α$^+$ cDCs. This observation also suggests some other cytokines may also contribute to the

development of CD11B$^+$ cDCs[7]. However, CD11B$^+$ cDCs do have some other unique features that distinguish them from the CD8α$^+$ cDCs and CD103$^+$ cDCs.

Phenotype of mice lacking regulator	pDC	Lymphoid tissue cDC		Nonlymphoid tissue cDC			Langerhans cell
		CD8$^+$ cDC	CD8$^-$ cDC	CD103$^+$ cDC	CD103$^+$ CD11b$^+$ intestinal cDC	CD11b$^+$ cDC	
Batf3	↔	↓↓↓	↔	↓↓↓	↔	↔	↔
Bcl6	↔	↓↓↓	↓↓↓				
Gfi1	↓	↓	↓				↑
ID2	↑	↓↓↓	↔	↓↓↓	↔	↔	↓↓↓
Ikaros C		↓	↓↓↓				
Ikaros DN*		↓↓↓	↓↓↓				
Ikaros L/L**	↓↓↓	↑	↓				
IRF2		↔	↓↓				↓
IRF4	↓	↔	↓↓				
IRF8	↓↓↓	↓↓↓	↔	↓↓↓	↔	↔	↓
Nfil3	↔	↓↓↓	↔				
Notch-RBPJ	↔	↔	↓↓↓				
Notch2	↔	↔	↓↓	↔	↓↓↓	↔	↔
Pten	↔	↑↑	↔	↑↑	↔	↔	
PU.1 (Sfpi)		↓↓↓	↓↓↓				
RelB		↔	↓↓↓				↔
Runx3		↑↑	↓				↓↓↓
SpiB	↓↓↓	↔	↔				
Stat3	↓↓	↓↓↓	↓↓↓				
Stat5	↓↓	↓↓	↓↓				
Tcf4 (E2-2)	↓↓↓	↔	↔				
Xbp1	↓↓	↓	↓				
Zbtb46	↔	↔	↔	↔	↔	↔	
Flt3	↓↓↓	↓↓↓	↓↓↓	↓↓↓	↓↓↓	↓↓	↔
Csf-2R		↔	↔	↓↓↓	↓↓	↓	↔
Csf-1R	↔	↔	↔	↔	↔	↓↓↓	↓↓↓
TGF-β	↔	↔	↔	↔	↔	↔	↓↓↓

Table. 1.1. The transcription factor regulation and cytokine regulation of DC development. (Cited from Ref.8)

The table describes the phenotype of transcription factor knockout mice lacking specific DC subsets. ↓ indicates a reduction in cell numbers; ↑ indicates an increase in cell numbers and ↔ means no change in cell numbers. The number of arrows is representative of the severity of the phenotype, with ↓↓↓ suggesting an almost complete loss of the population.

*Ikaros DN = dominant negative allele.

**Ikaros L/L = low-level expression.

Firstly, CD11B$^+$ cDCs have different surface receptors than CD8α$^+$ cDCs and CD103$^+$ cDCs, which implies that they may rely on different cytokines to support their development. For example,

CD11B$^+$ cDCs have relatively lower surface expression of FLT3 and higher surface expression of CSF-1R compared to CD8α$^+$ cDCs and CD103$^+$ cDCs[7]. Therefore, this may suggest that FLT3 signaling has a greater impact on the development of CD8α$^+$ cDCs and CD103$^+$ cDCs, while macrophage colony stimulating factor (M-CSF), the ligand of CSF-1R, has a more profound impact on the development of CD11B$^+$ cDCs[7]. CSF-2R is expressed on all of these three cDC subsets[40]. *Gm-csf* and *Csf-2r* knockout mice show that there is a clear deficiency of CD103$^+$ cDCs in the lung, lung-draining LNs, LP, dermis and skin-draining LNs, whereas spleen, LN-resident DCs and epidermal LCs developed normally[42-44]. Interestingly, it has been reported that GM-CSF can regulate the expression of CD103 on CD8α$^+$ cDCs, and CD103 upregulation correlates with the maturation process of CD8α$^+$ cDC. In contrast, this positive correlation is not the case in CD11B$^+$ cDCs[45]. In addition, CD11B$^+$ cDCs have more prominent expression of MHCII, which renders them to be more efficient in the induction of CD4$^+$ T cell immunity[46,47]. Mice deficient of the tumor necrosis factor (TNF) receptor family member lymphotoxin β receptor (*Ltβr*) or its membrane-associated ligand *Ltα1β2* have impaired CD11B$^+$ cDC proliferation[48, 49]. Moreover, mice deficient of *Relb*, a downstream molecule of LTβR signaling pathway, have profound reduction of splenic CD11B$^+$ cDCs but not CD8α$^+$ cDCs[50].

Secondly, while CD11B$^+$ cDCs share some transcription factors for their development with CD8α$^+$ cDCs and CD103$^+$ cDCs, they have some unique transcription factors for the regulation of their own development. They include transcription factors such as IRF4 and Notch RBP-J. For example, *Irf4* deficient mice have impaired splenic CD11B$^+$ cDCs development but not CD8α$^+$ cDCs[51]. IRF4 and IRF8 expression are oppositely regulated by GM-CSF through the signal transducer and activator of the transcription 5 (STAT5) signaling pathway[52]. Mice with DC-specific deficiency of *Notch rbp-j* have a selective survival disadvantage in CD11B$^+$ splenic cDCs[53]. In addition to these specific transcription factors, other transcription factors such as ZBTB46 may help to distinguish CD11B$^+$ cDCs from CD11B$^+$ moDCs[25, 26]. By using this marker, it has been proven that LPS-induced DCs originate from cDCs, while *Listeria monocytogenes*-induced TNF-α/iNOS (inducible nitric oxide synthases)-producing DCs (TipDCs) originate from monocytes[26].

Thirdly, $CD11B^+$ cDCs have different functions than $CD8\alpha^+$ cDCs and $CD103^+$ cDCs. In general, $CD11B^+$ cDCs are thought to have a predominant role in priming $CD4^+$ T cells through their relatively higher level of surface MHCII, while $CD8\alpha^+$ and $CD103^+$ cDCs are considered more efficient to prime $CD8^+$ T cells by their specialized cross-presentation machinery in the steady state[46]. However, this notion has been challenged, and further investigation is needed in a more elegant system, because some *ex vivo* assays showed that $CD11B^+$ cDCs can also prime $CD8^+$ T cells[54-56]. One problem is that, in these studies, it remains unclear whether it is due to cross-presentation of infected cell-associated antigens or direct presentation of viral antigens by $CD11B^+$ cDCs. A more recent study clearly showed that lung $CD11B^+$ cDCs were protected from viral infection, and they exclusively stimulated virus-specific $CD4^+$ T cells but were unable to efficiently cross-present virally infected cells[57]. Therefore, further investigations of these controversial results are required, for example, by using a mouse model with specific depletions of $CD11B^+$ cDC. However, such conditional depletion models are still lacking at present.

I.1.2. Non-classical DCs

In steady state, the major non-classical DC subsets in lymphoid organs and non-lymphoid tissues are pDCs and LCs. They have very different features from cDCs in lineage development and functions. Under inflammatory or infectious conditions, lymphoid and non-lymphoid organs can harbor other non-classical DC subsets such as "moDCs" or "inflammatory DCs (iDCs)".

I.1.2.1. PDCs

PDCs were originally identified in human lymph nodes in 1999 and later in mice in 2001[58, 59]. They have plasmacytoid, but not dendritic morphology, as well as a highly developed secretory compartment[60]. PDCs have immunoglobulin heavy chain (*Igh*) rearrangements, which is a very important feature to distinguish them from cDCs[61].

PDCs begin their development in BM from CDPs, which generate both pDCs and cDCs. The CDP is characterized by $Lin^-C\text{-}KIT^{int/lo}FLT3^+M\text{-}CSFR^+$ cells[62, 63]. More recently, a more dedicated pDC progenitor characterized as $Lin^-C\text{-}KIT^{int/lo}FLT3^+M\text{-}CSFR^-$ and a high level of pDC transcription factor E2-2 was identified at CDP downstream development[64]. Fully matured pDCs will then migrate out from BM to peripheral lymphoid organs. During this maturation process, C-

C chemokine receptor type 9 (CCR9), which is a very important surface marker, helps to distinguish mature pDCs from its immature precursors. Upon TLR stimulation, $CCR9^-$ immature pDCs produce greater amounts of type I IFNs and pro-inflammatory cytokines than $CCR9^+$ mature pDCs[65]. Even more interestingly, these $CCR9^-$ precursors show a plasticity to differentiate into cDCs under the induction of intestinal epithelial cells or recombinant GM-CSF[65]. The most commonly used surface markers to distinguish mature pDCs from other DC subsets are $CD11C^{int}B220^+LY6C^+BST2^+SIGLEC\text{-}H^+$[66].

Since CDPs, pDC progenitors and mature pDCs express different levels of cytokine receptors, as discussed above, this suggests that the different cytokines such as FLT3L, M-CSF and GM-CSF may have a great impact on the development and maturation of pDCs. For example, the development of pDCs is strictly dependent on FLT3L. FLT3L can promote pDC development through the activation of STAT3 and phosphoinositide 3-kinase (PI3K)-dependent activation of MTOR[67-69]. The absence of FLT3 signaling in mice can lead to a great reduction of pDC number in the lymphoid organs and BM[17]. However, the role of M-CSF and GM-CSF on pDC development is more complicated. Although both M-CSFR and GM-CSFR are expressed on MDPs and CDPs and cDCs, the expression level of M-CSFR is downregulated on $CD8\alpha^+$ cDC, $CD103^+$ cDCs and pDCs. Therefore, the more general effect of M-CSF on both the development of cDCs and pDCs is probably due to their effects on MDPs and CDPs. In previous experiments, a dramatic reduction of pDC and cDC numbers was discovered in the germline *Csf-1r* knockout mice, which suggests that M-CSF is able to drive pDCs and cDCs development both *in vitro* and *in vivo* in an FLT3-independent manner[70, 71]. By contrast, the GM-CSF inhibits FLT3L-driven pDC development through STAT5-induced ID2 expression but without influencing cDC development[72, 73].

In addition to these regulations by cytokines, some transcription factors have been shown to play very important roles in pDC homeostasis. The best-characterized transcription factor is the HLH family E-protein E2-2, which is required for the development of pDCs[74]. Enforced expression of ID2, an antagonist of E2-2, impairs pDC development, which can be rescued by E2-2 overexpression[75]. SPIB is another transcription factor that is crucial for the development and survival of pDCs. Its deficiency can cause pDC loss in the BM and the dysfunction of type I IFN

production of pDCs upon TLR7 or TLR9 stimulation in a cell-intrinsic manner[76]. A very recent study showed that a transcriptional cofactor of the ETO family, MTG16, could promote pDC development and restrict cDC development through repressing ID2 expression[77]. In addition, runt-related transcription factor 2 (RUNX2), a Runt family transcription factor, can regulate pDC migration, since mature pDCs in *Runx2*$^{-/-}$ mice accumulate in the bone marrow and fail to populate peripheral lymphoid organs due to reduced CCR5 expression[78].

In addition to the aforementioned surface markers and transcription factors, pDCs also have their own unique functions compared to other DC subsets. For example, pDCs have a very high level of TLR7, which is expressed in CD11B^{+} cDCs at an intermediate level and in CD8α^{+} cDCs at a very low level. TLR9 has also a similar expression pattern on these DC subsets. It is known that TLR7 and TLR9 are very important sensors for pathogen-associated molecular patterns (PAMPs) to help pDCs to recognize viruses or self-nucleic acids. PDCs will produce large amounts of type I interferon (IFN) upon TLR7 or TLR9 activation to fight against viruses[79]. Generally, TLR7 senses RNA viruses, endogenous RNA and synthetic oligoribonucleotides, whereas TLR9 detects DNA viruses containing unmethylated CpG-rich DNA sequences, endogenous DNA and synthetic CpG oligodeoxyribonucleotides[66]. The transcription factor IRF7 is essential for the induction of IFN-α/β in pDCs, and *Irf7* deficient mice are more vulnerable than myeloid differentiation primary response gene 88 (*Myd88*)$^{-/-}$ mice to viral infection, which correlates with a marked decrease of serum IFN levels[80]. In addition to initiating innate immunity against virus, pDCs can also initiate adaptive immune response, though they have very limited antigen presentation abilities compared to cDCs in steady state, probably due to their relatively lower surface MHCII expression. However, upon TLR activation, pDCs can also enhance their MHCII expression and other co-stimulatory molecules, leading to more efficient antigen presentation and CD4^{+} T cell activation[81]. Moreover, it has also been shown that activated pDCs are able to cross present antigens, though it is not the case in steady state. However, the mechanism of this cross presentation seems to be controversial. For example, it has been claimed that the endocytosed exogenous antigen would go to the cytosolic proteasome-dependent pathway to be fragmented into peptide, which would later be loaded on MHCI[82]. However, in another study, it was found that the exogenous antigen would be degraded in the endocytic organelles and loaded onto MHCI in the recycling endosomes[83]. Thus, more studies are needed to clarify this issue.

I.1.2.2. Langerhans cells (LCs)

As the largest and most exposed interface with the environment, the skin is a highly sophisticated system with a rich network of DCs to provide immune surveillance—as opposed to an initially perceived passive barrier between the host and the environment[84]. In this network, epidermal DCs are also known as Langerhans cells (LCs), whereas dermal DCs belong to a broader subset of interstitial DCs[85].

LCs are characterized by $CD11B^{+}$ and $CD103^{-}$ as well as lower MHCII levels, intermediate CD11c levels and much higher levels of the C-type lectin LANGERIN (CD207) compared to dermal cDCs[8, 86]. LCs also express E-cadherin, which helps them to anchor to the neighboring keratinocytes, and Epithelial-cell adhesion molecule (EPCAM), another newly discovered adhesion molecule that has a similar function as E-cadherin[87, 88]. LCs also constitutively express DEC205, a lectin that is involved in antigen capture and processing[89]. LCs are radio-resistant and sensitive to ultraviolet exposure, which is an important feature to distinguish them from dermal DCs that are repopulated from BM[90, 91].

LCs have their unique ontogeny and homeostatic properties compared to other DC subsets. In steady state, LCs self-renew locally and independently from BM[92]. Ontogenetically, the precursors of LCs reside in the skin prior to birth and are contributed by yolk sac (less than 10%) and fetal liver-derived monocytes[93-95]. However, in inflammatory conditions, LCs can be repopulated by blood-borne monocytes, and CSF-1R is required in this process[96]. Interestingly, in the *Csf1*$^{op/op}$ mice (*Csf1* loss of function mutation), there is only 40% loss of LCs, which suggests some other ligands can compensate the loss of CSF1[97]. Also, very recently, interleukin-34 (IL-34) was identified as a novel ligand for CSF-1R[98]. In addition to CSF-1, transforming growth factor β1 (TGFβ1) is also crucial for LCs differentiation and survival[99]. However, in contrast to cDCs and moDCs, the development of LCs is not dependent on FLT3L or GM-CSF[84].

In addition to the regulations by cytokines, LC homeostasis can also be regulated by some transcription factors. TGFβ1 induced ID2 expression is required for LC homeostasis in steady state but not in inflammatory conditions, although the exact mechanism is not very clear so far[31, 100]. PU.1 is essential for LC homeostasis in both steady and inflammation states. This regulation

probably operates through its downstream transcription factor RUNX3, because ectopic expression of *Runx3* can rescue LCs differentiation in the absence of PU.1[100]. However, transcription factors IRF8 and IRF4 have no effects on LC homeostasis in both conditions[100].

In addition to these specific cell surface markers and transcription factors, LCs also have their own specialized functions. First, LCs have unique TLR expression profiles. They express high levels of TLR2, intermediate levels of TLR3, TLR4, TLR8 and TLR10 and low to absent levels of TLR1, TLR5, TLR6, TLR7 and TLR9[101]. Second, the LCs have antigen-presenting function to prime $CD4^+$ T cells; however, they have a redundant role to cross-present antigens to prime $CD8^+$ T cell due to the existence of another skin DC subset, the $LANGERIN^+CD103^+$ dermal DC (dDC) subset, which has been proven for their specialized cross presentation ability in skin immune response. For example, it has been proven that the $LANGERIN^+CD103^+$ dDC subset is the only DC subset in the skin that can cross-present the OVA antigen captured from the K5-OVA^+ keratinocytes to prime the OTI^+ T cells *ex vivo*[102, 103]. Further study by using huLangerin-DTR and huLangerin-DTA transgenic mice in which LCs are absent but the $LANGERIN^+CD103^+$ dDCs are kept unaffected has suggested that $LANGERIN^+CD103^+$ dDCs are specialized antigen cross-presenting cells, whereas LCs can somehow suppress antigen-specific immune responses[104].

I.1.2.3. Monocyte-derived DCs (moDCs)

In the inflammatory or infectious conditions, lymphoid and non-lymphoid organs can harbor moDCs or iDCs that originate from monocytes. Monocytes have long been known to give rise to DC-like cells that can efficiently prime T cells under *in vitro* culture by GM-CSF and IL-4[105]. However, its *in vivo* equivalent cell subset had not been identified until 2010[106]. In this study, DC-SIGN (CD209), a type II transmembrane C-type lectin, can be used to distinguish moDCs from other DC subsets in the LNs of mice treated with LPS or *E. coli*. Two years later, these moDCs were further proven to be cDC-like cells, because they express ZBTB46[26]. Interestingly, these moDCs will also lose their monocyte lineage marker LY6C during their differentiation[106]. Based on these features, it is easy to distinguish these $DC\text{-}SIGN^+ZBTB46^+$ moDCs from another *in vivo* moDC subset, the "TipDCs", which was identified much earlier in 2003[107]. In *Listeria monocytogenes*-infected mice, TipDCs ($CD11C^+CD11B^+LY6C^+$ moDCs) produce huge amounts of TNF-α and iNOS to clean up the bacterial infection in a CCR2-dependent manner. Moreover,

these TipDCs are not required for antigen presentation to $CD4^+$ T cells and $CD8^+$ T cells[107]. In later studies, it showed that these TipDCs are M-CSF dependent but not GM-CSF dependent; moreover, they are not $ZBTB46^+$[108, 26]. Taken together, the TipDCs might more represent activated effector monocytes rather than DC-like cells.

I.1.3. The mechanism of DC activation

It is known that DCs can induce both active immune response or suppressive tolerogenic immune response depending on the activation status of DCs. DCs have three major pathways to shape immune responses including antigen presentation, co-stimulatory signals and cytokine or chemokine production. Specifically, through antigen presentation mediated by MHCI and MHCII complexes, DCs are able to prime antigen-specific $CD8^+$ T cells or $CD4^+$ T cells, respectively. By using co-stimulatory signals (e.g., CD40, CD80, CD86, PD-L1), DCs are able to activate or suppress immune response of the cognate T cells or B cells. By producing different cytokines and chemokines, DCs are able to regulate T cell and B cell functions and shape Th1 or Th2 immune responses. However, the regulation of these three pathways is largely correlated with the activation status of DCs. In the steady state, DCs normally keep functional quiescent and only maintain low levels of antigen presentation to prime T cells. In the presence of only self-antigens, DC behavior is complicated, which may dictate the autoimmune status. When DCs are activated by pathogens through their PRRs, they will have enhanced surface levels of co-stimulatory molecules and produce different cytokines to promote the immune responses against these pathogens. This section will summarize what we know about the molecular mechanisms involved in the regulation of DC activation and immune tolerance.

I.1.3.1. TLR

There are mainly four types of PRRs: TLRs, C-type lectin receptors (CLRs), nucleotide oligomerization domain (NOD)-like receptors (NLRs) and retinoic acid-inducible gene (RIG)-I-like receptors (RLRs)[109]. The best-characterized PRR so far is the TLR family, and because of the contribution to the discovery of TLRs in flies and mammals, Jules Hoffman and Bruce Beutler shared the Nobel Prize in physiology or medicine with Ralph Steinman in 2011[110, 111].

As mentioned above, different DC subsets have their own characteristic TLR expression profile to respond differently and specifically to different viruses or bacteria, as has been summarized in Fig 1.2.[112] However, the knowledge about the regulation of TLR on DC functions in steady state remains limited and requires more investigation. One interesting study shows that a 2-fold overexpression of TLR7 alone can develop spontaneous autoimmunity together with a myeloid cell proliferation[113]. However, since this overexpression of TLR7 is germline overexpression instead of DC-specific overexpression, the real effect of TLR7 overexpression on DC still needs further investigation. Furthermore, TLR mis-location could be another mechanism by which autoimmunity arises. For example, wild type TLR9 requires proteolysis by the enzymes in endo-lysosomes prior to their activation by the ligand such as CpG, which provides the protection to sequester these receptors from extracellular self-nucleic acid released from necrotic cells or apoptotic cells. However, a mutation in the TLR9 transmembrane region causes itself to no longer require ectodomain proteolysis for activation, resulting in a lethal auto-inflammatory disease even without the help from lymphocytes[114]. However, since in this study, the mutation is introduced in HSCs, the real effect of such mutation in DC should also be further investigated. Interestingly, there are naturally existing soluble decoy TLRs in the organism to provide a negative regulatory mechanism on DC activation. Iwami et al. found a cDNA encoding a soluble form of TLR4. It contains 122 amino acids, 86 of which are identical to those of the extracellular domain of TLR4. Exogenously expressed soluble TLR4 can significantly inhibit LPS-mediated TNF-α production and nuclear factor kappa-light-chain-enhancer of activated B cells (NF-κB) activation[115]. Later on, such soluble TLRs are also discovered in human plasma and breast milk[116]. Although some of the studies claim that there is a negative effect of these soluble TLRs on cytokine production *in vitro*, its real *in vivo* effect still requires investigation. In addition to these negative regulations, TLRs can also be downregulated

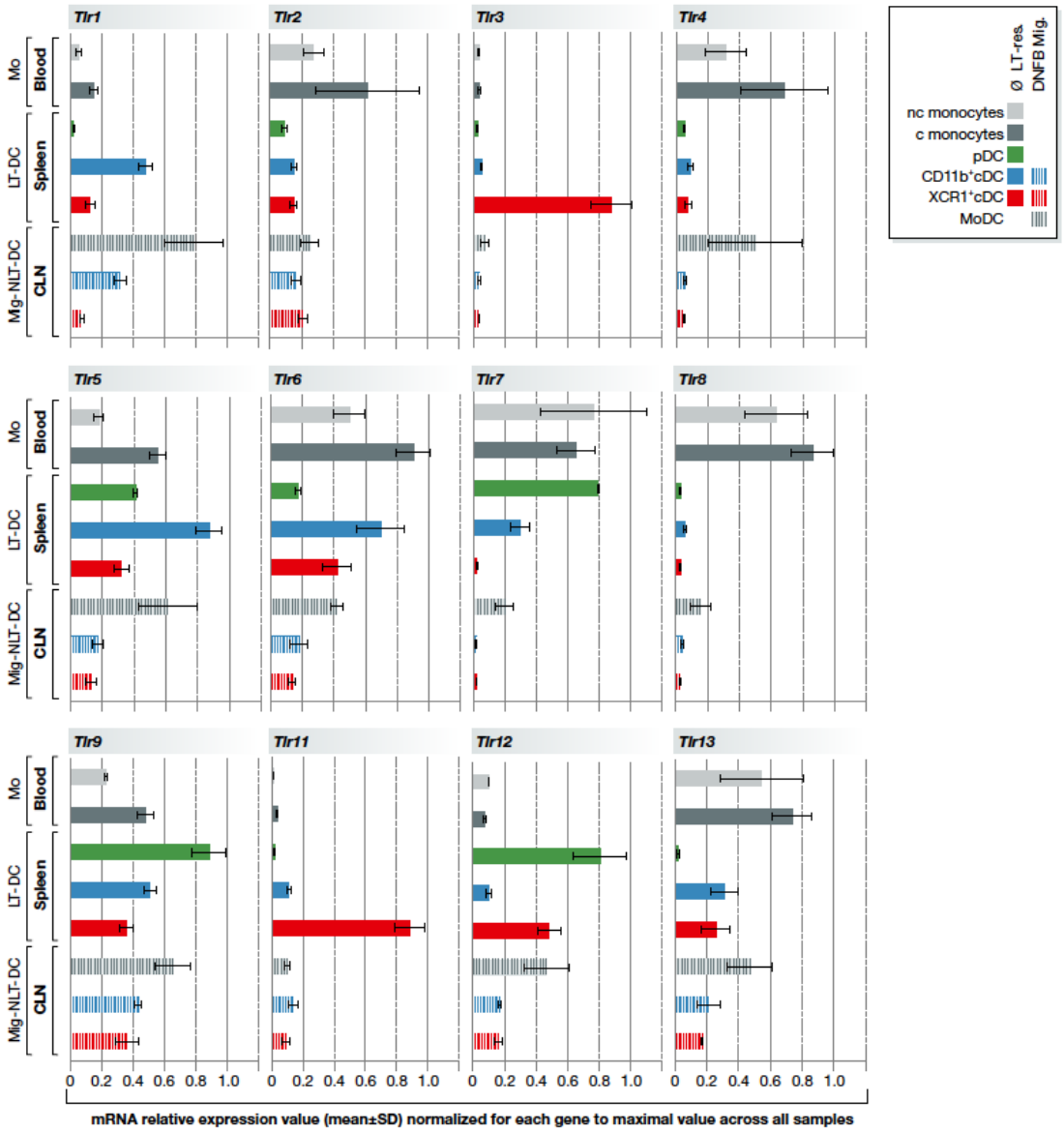

Fig. 1.2. Comparison of the expression patterns of TLRs across DC and monocyte subsets in mice. (Cited from Ref.112)

The bar graphs show relative gene expression (mean± SD) for individual TLRs across blood monocyte subsets (gray bars), spleen LT (lymphoid tissue)-DC subsets from untreated animals (plain color bars) and cutaneous LN (CLN) mig-NLT-DCs from DNFB skin-painted animals (hatched color bars). Key: c monocytes, classical blood monocytes characterized as $CD11B^{+}LY6C^{hi}MHCII^{-}$ cells; nc monocytes, non-classical monocytes characterized as $CD11B^{+}LY6C^{lo}MHCII^{-}$ cells. For each gene, expression values are normalized to maximal expression across all samples and the mean of 2 to 5 replicates for each cell subset is shown.

by either degradation or inhibitory expression. TRIAD3A, the most abundant member of the E3 ubiquitin ligase family proteins TRIAD3, was found to promote the ubiquitination and degradation

of TLR4 and TLR9 but not TLR2 and TLR3[117]. TRIAD3A overexpression or knockdown expression by siRNA can specifically inhibit or enhance TLR4 and TLR9 expression, respectively[117]. Anti-inflammatory cytokine such as TGFβ1 can also inhibit the expression of TLR4. The TGFβ1 null mice show a phenotype of uncontrolled inflammation, cachexia and multi-organ failure as well as more than a 2-fold increase of TLR4 mRNA in multiple organs[118]. However, since TGFβ signaling can promote the generation and function of T regulatory cells (Tregs)[119], the phenotype of TGFβ1 null mice could be contributed from both factors of Tregs expansion and TLR4 upregulation. In some other cases, the co-receptor of TLR can also exhibit negative regulation of TLR function. For example, intestinal epithelial cells (IECs) normally show a very low response to TLR4 activation, since they have low levels of TLR4 and complete lack of its co-receptor MD-2. However, co-transfection of TLR4 and MD-2 in IECs can synergistically restore LPS signaling, whereas individually transfection is not sufficient to restore it[120].

In addition to the regulation of TLRs, DC function can also be regulated by their downstream molecules (e.g., MYD88, an adaptor molecule important for almost all TLRs signaling, except TLR3). Knockout *Myd88* in some mice with disease-prone genetic backgrounds such as MRL.Fas^{lpr} and *Lyn*$^{-/-}$ mice can protect these mice from developing autoimmune diseases, such as systemic lupus erythematosus (SLE)[121, 122]. Furthermore, MYD88 is differentially required for TLR family signaling. *Myd88* deficient DCs are able to enhance their co-stimulatory molecules expression and antigen presentation ability upon TLR4 agonist LPS stimulation, although their cytokine production is severely impaired[123]. However, *Myd88*-deficient DCs cannot enhance their co-stimulatory molecules expression and cytokine production upon TLR9 agonist CpG stimulation, indicating that other signaling pathway may also function downstream of TLRs[123]. Wild type MYD88 is composed of three major domains: the death domain, which mediates downstream interactions with IL-1 receptor-associated kinases (IRAK) family of kinases; the interdomain and the Toll/interleukin-1 (IL-1) receptor (TIR) domain, which mediates the interaction of MYD88 with the TLR[124]. Upon LPS stimulation, MYD88S, an isoform that lacks the interdomain, has enhanced expression and forms heterodimers with MYD88. This heterodimer inhibits the ability of IRAK4 to phosphorylate the downstream molecule IRAK1. The MYD88S may act as a negative regulator and blocks the TLR/MYD88 signaling pathway[125, 126].

There are several other important molecules downstream of MYD88 involved in the regulation of the TLR/MYD88 signaling pathway. For example, MYD88 interacts with the IRAK family, which leads to interaction with the TNF receptor associated factor 6 (TRAF6), and ultimately activates several important signaling pathways, including nuclear factor-κB (NF-κB), mitogen-activated protein (MAP) kinases (MAPK) and Jun N-terminal kinase (JNK). These pathways will initiate the transcription of several pro-inflammatory cytokines, such TNF-α and IL-1β[127, 128]. Therefore, in theory, any negative regulator of these important molecules can also act as the negative regulator of the TLR/MYD88 signaling pathway. The suppressor of cytokine signaling-1 (SOCS-1) was discovered as a negative regulator of LPS-induced macrophage activation, which suppresses NO_2^- synthesis and TNF-α production through inhibiting the phosphorylation of I-κB and p38[129] as well as the phosphorylation of STAT1[130]. PI3K is also a negative regulator of the TLR signaling pathway. It can inhibit IL-12 synthesis and prevent the hyper-activation of a Th1 response[131]. Rapamycin, the inhibitor of MTOR signaling which is the downstream of PI3K signaling pathway, can enhance LPS induced tissue factor (TF) and TNF-α expression in macrophages[132]. However, the detailed mechanism of how the PI3K signaling pathway antagonizes LPS signaling is not very clear. Toll-interacting protein (TOLLIP) can interact with TLR2 and TLR4 through the TIR domain, and its overexpression results in the inhibition of NF-κB activation upon TLR2 or TLR4 stimulation and is related with the decreased level of IRAK1 autophosphorylation[133]. A20, a special protein with both ubiquitylating and deubiquitylating functions, is shown as a negative regulator of the TLR signaling pathway. A20 was initially shown to cleave the ubiquitin chain of TRAF6 to terminate the activation of NF-κB in an earlier study[134]. A more recent study showed that A20 deficiency in DC can drive DC activation through a MYD88-independent pathway, whereas A20-deficient DC-induced T cell expansion was through a MYD88-dependent pathway. These results indicate that DCs need A20 to preserve immune quiescence[135].

I.1.3.2. CLR

CLRs are another important group of PRRs, which can also sense different PAMPs. Distinct pathogens express different PAMPs, and the combination of these PAMP functions act as a fingerprint that triggers a specific set of PRRs, leading to the interaction of signaling pathways to tailor the immune response to that specific pathogen[136]. CLRs consist of a large family of

receptors that bind to carbohydrates in a calcium-dependent manner. The activities of these CLRs are mediated by the conserved carbohydrate-recognition domains (CRDs). Based on their molecular structure, the CLRs can be divided into two groups of membrane-bound CLRs—type I CLRs and type II CLRs—in addition to a group of soluble CLRs. Type I CLRs belong to the mannose receptor family, and type II CLRs belong to the asialoglycoprotein receptor family. These CLRs not only sense the pathogen-derived ligands but also the self-ligands.

One major function of CLRs is to enhance antigen presentation. Because CLR signaling normally does not induce DC activation, this CLR-mediated antigen presentation will lead to immune tolerance. Upon the recognition of ligands, the CLRs will mediate the internalization and transportation of antigens into intracellular compartments for processing and presentation. In the absence of maturation stimuli from TLR signaling, the CLR signaling tends to lead to antigen-specific T cell tolerance rather than to immunity[109]. DEC205, one of the best-studied type I CLRs, has been shown to mediate the induction of antigen-specific immune tolerance by *in vivo* administration of an antigen-conjugated anti-DEC205 antibody[137]. Later on, LANGERIN, a type II CLR, has also been proven to be able to mediate the induction of immune tolerance by using an antigen-conjugated anti-LANGERIN antibody[90]. However, in the presence of other DC maturation signals such as anti-CD40 agonistic antibody co-injection, the outcome of immune response may change from immune tolerance to prolonged T cell activation and enhanced immunity[137].

In addition to the induction of adaptive immune response, a few CLRs can also "self-sufficiently" induce innate immune response to elicit microbicidal effector functions like TLRs[138]. These "self-sufficient" CLRs utilize the spleen tyrosine kinase (SYK) as their proximal adaptor to activate the downstream signaling[139, 140]. SYK normally binds to proteins that contain immunoreceptor tyrosine-based activation motifs (ITAM). There are two tyrosine residues located within ITAM, whose phosphorylation by SRC kinases will create a docking site for the tandem SRC Homology 2 (SH2) domains of SYK, leading to the activation of SYK and its downstream signaling cascade[141]. In addition to the ITAM motif, a small group of CLRs has been shown to have a single tyrosine-based motif in the intracellular tail, which has been termed "hemITAM". The hemITAM group of CLRs includes DC-associated C-type lectin 1 (DECTIN-1), C-type lectin domain family

2 (CLEC-2), CLEC9a and SIGNR3[142-144]. In addition to the hemITAM group, other CLRs such as DECTIN-2 and macrophage inducible C-type lectin (MINCLE) need the help from their associated ITAM-bearing Fc receptor γ (FcRγ) chains to deliver downstream signaling. Ligand binding can cause the phosphorylation of ITAM on the FcRγ chain, which leads to the recruitment of SYK[145, 146]. In contrast to ITAM-associated CLRs, some CLRs possess an inhibitory immunoreceptor tyrosine-based inhibitory motifs (ITIM) that recruit the phosphatases such as SHP-1, SHP-2 and SHIP to initiate their inhibitory signaling. For example, a DC-inhibitory receptor (DCIR) can inhibit TLR8-induced IL-12 and TNF-α production by myeloid DCs and TLR9-induced IFN-α production by pDCs[147, 148]. *Dcir* deficient mice develop sialadenitis and enthesitis characterized by elevated level of serum autoantibodies[149]. How these ITAM and ITIM motif containing receptors coordinate the regulation of DC functions remains to be determined.

In addition to these tyrosine-dependent signaling pathways, CLRs also have a tyrosine-independent signaling pathway, though study in this field is still very limited. For example, SIGNR3 has been shown to activate the serine/threonine kinase RAF1 to induce IL-6 and TNF production together with SYK signaling[144]. However, these two independent pathways of RAF1 and SYK may converge at the level of NF-κB[150].

I.1.3.3. Nod-like and Rig-I-like Receptors (NLRs and RLRs)

NLRs and RLRs are cytoplasmic PRRs that sense the intracellular PAMPs or DAMPs[151]. Based on different N-terminal effector domains, the mammalian NLRs can be divided into four subfamilies: NLRC (also known as NODs), NLRP (also known as NALPs), NLRB (also known as NAIP or BIRC) and NLRA. The best characterized function of these NLRs is the formation of inflammasome, which is important for the generation of mature bioactive pro-inflammatory cytokine IL-1β and IL-18[152]. IL-1β participates in the generation of systemic and local responses to infection, injury and immunological challenge by generating fever, activating lymphocytes and promoting leukocyte infiltration at sites of injury or infection[153]. The major role of IL-18 is similar to IL-12, which is to drive T helper cells to polarize to Th1 cells and induce their IFN-γ production[154].

Since NLRs are so important in pro-inflammatory cytokine production, their mutations have been discovered to be associated with multiple autoimmune and inflammatory diseases. For example, the ligand-binding domain of NOD2, a member of the NLRC subfamily, is frequently mutated in patients with Crohn's disease, a chronic inflammatory bowel disease (IBD) that may be driven by improper immune responses to intestinal commensals[155]. *Nod2* gain-of-function variant knockin mice have enhanced inflammatory cytokine production together with the increased susceptibility to dextran sulfate sodium (DSS)-induced colitis, whereas NOD2-deficient mice are highly susceptible to colitis[156, 157]. Due to these contradictory results, more investigations are necessary to determine the real role of NOD2 in autoimmunity.

RLRs are specialized to recognize cytoplasmic RNA helicases that are critical for host anti-viral response. This function is very similar with TLR3. However, RLRs and TLR3 are differently expressed in different cell types. For example, RIG-I is essential for induction of type I interferon after infection with RNA viruses in fibroblasts and cDCs, whereas in pDCs, they use TLR3 rather than RIG-I for sensing the RNA viruses[158]. RLRs are also involved in autoimmune diseases. Genome-wide association study (GWAS) results revealed that single-nucleotide polymorphisms (SNPs) of interferon induced with the helicase C domain 1 (*IFIH1*) gene, encoding melanoma differentiation-associated protein 5 (MDA5), a member of RLRs family, were associated with autoimmune disease such as type I diabetes (T1D), multiple sclerosis (MS), psoriasis, selective IgA deficiency, dilated cardiomyopathy and SLE[159]. The role of such mutation in *Mda5* has been recently proven in a mice model. The gain-of-function mutation of *Mda5* (G821S) in mice can develop spontaneous lupus-like autoimmune symptoms without viral infection due to the constitutive activation of MDA5[160].

I.1.3.4. The mechanism of self-recognition in DCs

DCs are professional sentinels that sense different PAMPs or DAMPs with their specialized TLRs, CLRs, NLRs and RLRs and respond with their special cytokine production and antigen-presentation capacities to induce innate and adaptive immune responses, respectively. How DCs sense and react to self-ligands is another important issue, because overreaction to self-ligands can cause autoimmune diseases and sterile inflammation, whereas under-reaction to self-ligands can cause cancer. The difference between autoimmune disease and sterile inflammation depends on if

there is an autoantibody involved. In this section, only the mechanism of overreaction to self-ligands will be discussed.

In sterile condition, the most abundant self-ligands come from cell death or injury. PRRs not only recognize the microbes but also recognize the endogenous DAMPs that are released during cellular injury. Under normal physiological conditions, these DAMPs are sequestered intracellularly and are therefore hidden from the PRRs. However, under cellular stress or injury, these DAMPs are released into the extracellular environment to trigger inflammation. Necrosis is one of the most important conditions that is caused by extreme damages such as ischaemia or trauma. In this process, the intracellular DAMPs including chromatin-associated protein high-mobility group box 1 (HMGB1), heat shock proteins (HSPs) and purine metabolites such as ATP and uric acid are released. In addition to these intracellular DAMPs, there are also extracellularly located DAMPs such as hyaluronan, heparin sulphate and biglycan released from the degraded matrix[161].

Determining the PRRs involved in recognizing these self-DAMPs to initiate the sterile inflammation is a very important issue to be addressed here. Firstly, it has been noticed that TLRs not only sense the PAMPs, but they also sense the self-DAMPs. For example, in 2001, a study showed that HSP60s could activate TLR2 and TLR4 and induced pro-inflammatory cytokine production on a macrophage cell line RAW264.7 *in vitro*[162]. However, in 2003, another study showed that a possible contamination of LPS during the preparation of HSP may have caused the activation of TLR2 and TLR4[163]. Furthermore, in 2007, a study showed that mice lacking TLR2 and TLR4 have only a slight reduction in the peritoneal inflammatory response to sterile dead cell *in vivo*, which suggests that some other PRRs may have redundant function of TLR2 and TLR4[164]. More interestingly, in the same study, the authors showed that *Myd88*$^{-/-}$ and *Il-1r*$^{-/-}$ mice have a dramatic reduction of neutrophils recruitment to necrotic EL4 cells and ultraviolet light (UV)-irradiated B16 cells, rather than the TLR null mice, which indicated that the IL-1/IL-1R/MYD88 signaling pathway is more important for the host to respond to sterile inflammation than TLR[164]. This effect is mainly contributed from the non-BM-derived cells rather than the BM-derived cells. Furthermore, in this study, the authors also compared the effects of *Hmgb1*$^{+/+}$ and *Hmgb1*$^{-/-}$ necrotic cells to induce sterile inflammation. Interestingly, they claimed that there were no

differences between these two kinds of cells, which indicated that HMGB1 is not the self-DAMP that triggers the sterile inflammation. The DAMPs that activate the macrophages to release IL-1α have not been identified so far. In another study of the acetaminophen-induced liver sterile inflammation, double strand DNA (dsDNA) released by necrotic hepatocytes can be recognized by TLR9 by some non-myeloid cells to induce IL-1β and IL-18 production through a pyrin domain-containing protein 3 (NALP3) inflammasome-dependent manner[165]. Very little information has been reported about how TLRs act on DCs to sense the self-DAMPs in sterile inflammation, and in most studies, the effects are due to the non-myeloid cells.

In addition to TLRs, CLRs have been reported in several recent studies to sense the self-DAMPs. For example, MINCLE, a type II CLR, has been reported to be able to recognize SAP130, a component of small nuclear ribonucleoprotein released from dead cells, to induce the pro-inflammatory cytokine production of BM derived macrophages[146]. CLEC9A, another type II CLR specially and highly expressed on $CD8\alpha^+$ cDCs, has been reported to be able to sense the exposed actin filaments from the necrotic dead cells to cross-prime the $CD8^+$ T cells[143, 166]. However, the innate immune response of CLEC9A to self-DAMPs is still unknown. Interestingly, CLEC12A has been recently noticed as a function to recognize the self-DAMP uric acid crystals (monosodium urate, MSU) and provide a negative regulation on inflammatory response to this self-DAMP, because *Clec12a* knockout mice show a dramatically enhanced inflammatory response to necrotic cells compared to WT mice[167].

In addition to these self-DAMPs that originate from necrotic dead cells, there is another big group of PAMPs in our body, i.e., the commensal bacteria in the gut: "microbiota". These PAMPs are also sometimes called microbe-associated molecular patterns (MAMPs). These "microbial selves" have evolved to live mutually together with mammals for a long time, and the host will not immunologically reject them during lifelong colonization. Previous opinion thought that these symbiotic bacteria were simply ignored by the host, but more evidences have demonstrated that they can interactively communicate with the host immune system through the PRRs[168]. Firstly, the host can shape the spatial segregation and composition of the microbiota. For example, in *Myd88*-deficient mice, there is a 100-fold increase in bacteria associated with the mucosa compared to wild-type mice, which is probably due to its regulation on the antimicrobial peptides

(AMPs) production in epithelial Paneth cells[169-171]. Similar examples also exist in *Nod2*-deficient and *Rip2*-deficient mice[172]. RIP2 is a downstream molecule of the NOD2 signaling pathway. Second, the microbiota can maintain the intestinal epithelial homeostasis through TLR, because the depletion of microbiota with antibiotics results in increased susceptibility to DSS-induced colitis, whereas LPS and lipoteichoic acid oral administration can correct this predisposition to colitis[173]. In addition to the maintenance of intestinal epithelial homeostasis, the microbiota can even shape the host immune system. For example, the microbiota *B. fragilis* can produce polysaccharide A (PSA) to promote $CD4^+$ T cell differentiation into Tregs rather than Th17 cells in the LP through the TLR2 on $CD4^+$ T cells but not TLR2 on the DCs. By doing so, it can also facilitate *B. fragilis*'s own colonization[174]. Another recent study showed that *Tlr5* deficiency specific in IECs made the mice prone to develop colitis compared to wild-type mice. However, *Tlr5* deficiency specific in DCs did not make the mice prone to develop colitis[175]. To my knowledge, there are very few elegant studies that describe the interactive communication between the PRRs specifically on DCs and the self-MAMPs on microbiota, since it is still a very new field under investigation.

I.2. History, structure and function of the CBL family of proteins

In mammals, there are three members in the CBL family of proteins: CBL-B, C-CBL (also known as CBL) and CBL-C (also known as CBL-3 or CBL-SL)[176]. In mice, CBL-B and C-CBL are ubiquitously expressed in hematopoietic cells; however, CBL-C has a very different expression pattern[177]. CBL-C is specifically expressed in epithelial cells of the gastrointestinal tract and epidermis as well as the respiratory, urinary and reproductive system but is not detected in non-epithelial cells[178]. The discovery of the endogenous CBL family proteins is an interesting story. They were originally identified as a cellular homolog of a murine viral oncogene (*V-cbl*), which is a fibroblast-transforming gene of the CBL tyrosine kinase binding (TKB) domain fused with the viral *gag* sequences[179]. This viral oncogene arises from a recombination event between the ecotropic Cas-Br-M virus and the *C-cbl* oncogene. This recombinant product can induce pre-B cell lymphomas and myeloid leukemia in mice[180]. Therefore, *C-cbl* was originally considered as an oncogene. Later on, further studies showed that C-CBL was associated with some phosphotyrosines and played a negative role in some signaling pathway such as SYK tyrosine kinase and Zeta-chain-associated protein kinase-70 (ZAP-70)[181, 182]. However, the first study

showing that C-CBL can work as an E3 ubiquitin ligase and regulate the ubiquitination and degradation of epidermal growth factor receptor (EGFR) through endocytic sorting to the lysosome did not occur until 1998; this was an important breakthrough in our understanding of the mechanism by which CBL proteins mediate their negative regulatory function[183]. Presently, there are more and more evidences showing that CBL family proteins are in many important pathways (e.g., hematopoietic cell development, immune cell function), which will be introduced in the following sections.

I.2.1. The structure of CBL family proteins

The three members in the CBL family share a highly conserved N-terminal region that encompasses their TKB domain, RING finger (RF) domain and the short linker region between these two domains. However, as a much shorter form in CBL family proteins, CBL-C possesses a much shorter proline-rich domain than CBL-B and C-CBL and lacks their carboxy-terminal leucine zipper (LZ) motif[184, 185] (Fig 1.3). Structural analyses have shown that the TKB domain contains a four-helical bundle, a calcium-binding EF hand and a variant SH2 domain[186]. These structures provide a relatively unique platform to mediate a specific association to the cognate phosphotyrosine-containing motifs of the activated phosphotyrosine kinases (PTKs). The RF domain and the linker region together provide the platform for CBL family proteins to associate with E2 ubiquitin-conjugating enzymes[187]. The C-terminal regions of CBL family proteins have multiple protein-protein interaction domains. The proline-rich domain can bind to the SH3 domain of several important signalling proteins such as SRC family kinases and the Growth factor receptor-bound protein 2 (GRB2) adaptor protein[188, 189]. In addition to the proline-rich domain, there are also three tyrosine residues in the C-terminal of CBL-B and C-CBL. These tyrosine residues will be phosphorylated upon cellular activation and interact with several key signalling mediators including VAV family guanine nucleotide exchange factors (GEFs), P85 regulatory subunit of PI3K and CRK family adaptors, etc[190-192]. The most C-terminal domain is the LZ domain or the ubiquitin-associated (UBA) domain, which is proposed to bind the specific substrate of polyubiquitinated proteins, limit ubiquitin chain elongation and target polyubiquitinated proteins to the 26S proteasome for degradation.

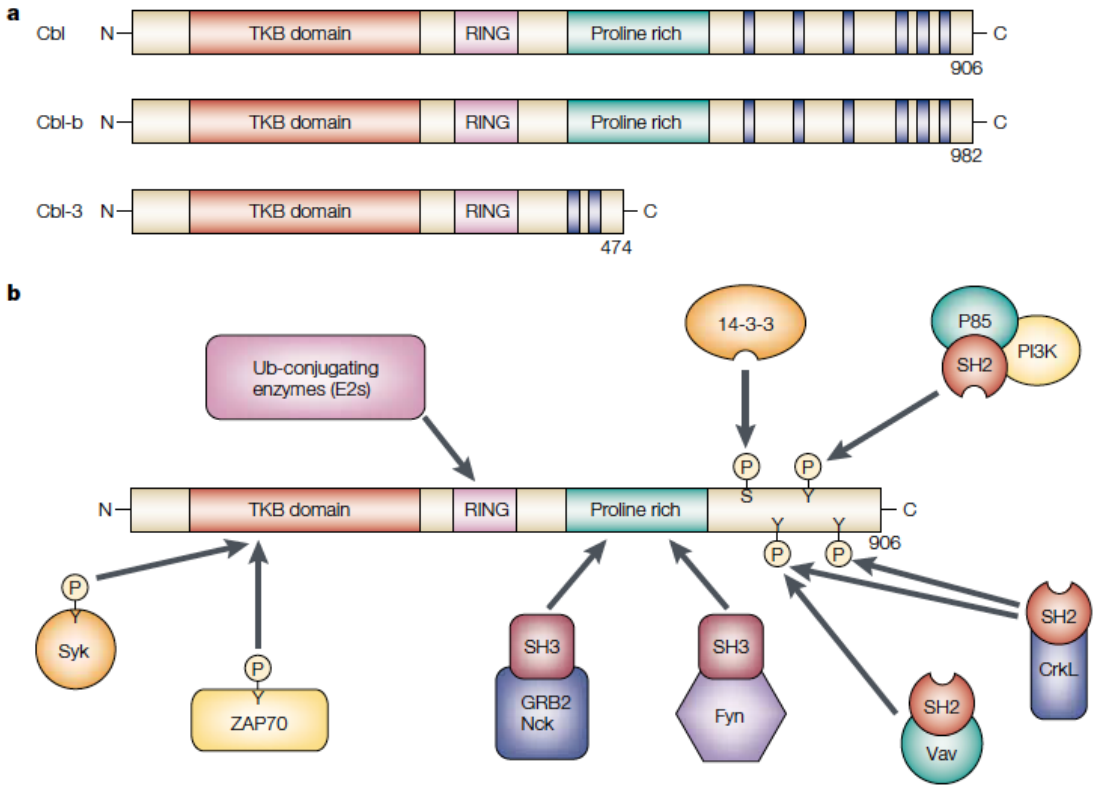

Fig. 1.3. The structure and functional domains of CBL family of proteins. (Cited from Ref.185)

(A) The domain structure of the three members of the mammalian CBL family is outlined. The TKB domain can bind to phosphorylated tyrosines on tyrosine kinases. The RING-finger domain recruits ubiquitin (Ub)-conjugating enzymes. The association between tyrosine kinases and Ub-conjugating enzymes mediated by CBL proteins targets the kinases for proteosomal degradation and hence leads to the decline of regulated responses. The proline-rich regions recruit many proteins containing the SRC-homology 3 (SH3) domain.

(B) The functional domains of CBL family of proteins. CBL proteins can regulate ZAP70 and SYK through their TKB domains. They can interact with GRB2 and FYN through their proline rich domains, and E2 Ub-conjugating enzymes through their RING finger domains. CBL can be phosphorylated on many tyrosine residues, which provide their interaction with other SH domain-containing proteins, such as P85, VAV and CRKL. Phosphorylation on serine residues can also recruit the 14-3-3 family of proteins.

I.2.2. The general principle of ubiquitination pathway

Protein ubiquitination is one of the post-translational modifications in which lysine residues of the proteins are modified with the small molecule ubiquitin, a 76 amino acid polypeptide with a molecular weight around 8500 Da[193]. This modification was originally discovered in the early

1980s by Aaron Ciechanover, Avram Hershko and Irwin Rose, and because of their outstanding contributions to the understanding of energy-dependent protein degradation, they were awarded the Nobel Prize in Chemistry in 2004[194]. In their model, the step-wise ubiquitination modification requires three enzymes. In the ATP-dependent first step, an E1 ubiquitin-activating enzyme transfers the ubiquitin to an E2 ubiquitin-conjugating enzyme by covalently attaching to the cysteine residue via a thioester linkage. In the second step, the E2 ubiquitin-conjugating enzyme further associates with different types of E3 ligase through the RING/U-box or HECT (homologous with E6-associated protein C-terminus) domain. In the third step, because E3 ubiquitin ligase normally has other domains to associate with the substrate, E3 ligases facilitate isopeptide bond formation between ubiquitin on the E2 ubiquitin-conjugating enzyme and the lysine residues on the substrate[195, 196]. After the third step, the ubiquitinated substrate will have various biological functions, depending on its types of ubiquitination. These biological functions will be introduced in more detail later in this section. So far, in the human genome, only 2 E1 enzymes, 37 E2 enzymes and more than 600 E3 ligases have been estimated or discovered[197, 198].

Originally, the major function of ubiquitination is considered responsible for the energy-dependent degradation of proteins after the protein substrates are polyubiquitinated. Later on, more evidences showed that different types of ubiquitination can result in different outcomes. Since ubiquitin itself contains seven lysine residues (K^6, K^{11}, K^{27}, K^{29}, K^{33}, K^{48}, K^{63}) that can serve as receivers of additional ubiquitin molecules to generate ubiquitin polymers, the types of ubiquitin polymers can be categorized into three major types: monoubiquitination, multi-monoubiquitination and polyubiquitination. Monoubiquitination is the modification where protein substrate is ubiquitinated with only a single ubiquitin on a single lysine residue of the substrate. Multi-monoubiquitination is the modification where protein substrate is ubiquitinated with only a single ubiquitin on multiple lysine residues of the substrate. Polyubiquitination is the modification where protein substrate is ubiquitinated with a ubiquitin polymer chain on a single lysine residue of the substrate. Within the polyubiquitination modification, it can be further categorized into two subtypes: homotypic and heterotypic polyubiquitination, which depends on if the ubiquitin is added to the same lysine residue of the previous ubiquitin in the ubiquitin polymer chain[193] (Fig 1.4).

Different types of ubiquitination can lead to different biological functions. For example, multi-monoubiquitination of receptor tyrosine kinase (RTK) EGFR by CBL family proteins is enough to lead EGFR to be sorted to lysosome to be degraded[199]. Monoubiquitination is involved in DNA repair. For example, the protein Fanconi anemia complementation group D2 (FANCD2) is monoubiquitinated specifically at Lys561 in response to different DNA-damaging agents such as mitomycin C (MMC), ionizing radiation (IR), UV and hydroxyurea (HU), which leads to its migration to chromatin-associated nuclear foci to initiate the DNA repair. However, the mutation of Lys561 to Arg561 abrogates the monoubiquitination of FANCD2, thus impairing the DNA repair and leading to disease[200].

There are 7 types of homotypic polyubiquitin chains: K^6, K^{11}, K^{27}, K^{29}, K^{33}, K^{48} and K^{63}. The best characterized homotypic polyubiquitin chains are the K^{48} and K^{63} chains, and they have very different functions. For example, K^{48} polyubiquitination can lead to recognition by the 26S proteasome, and the protein substrate will then be degraded[201]. However, K^{63} polyubiquitination was identified as an important non-degradative modification, which is very different from K^{48} polyubiquitination. K^{63} polyubiquitination has a major function for targeting protein substrate to be sorted to endolysosome to be degraded. Many cell surface receptors are K^{63} polyubiquitinated before their internalization. For example, MHCI internalization and degradation is through K^{63} polyubiquitination, and multi-monoubiquitination is not enough to sort the substrate to lysosome, which is a different mechanism than the degradation of RTK EGFR[202]. Another important function of K^{63} polyubiquitination is involved in the signaling process leading to the activation of NF-κB. In the canonical TLR/MYD88 signaling pathway, the K^{63} polyubiquitination of TRAF6, IRAK1 and the NF-kappa-B essential modulator (NEMO) are important for Transforming growth factor beta-activated kinase 1 (TAK1) activation, which will further lead to the phosphorylation and activation of IKKβ[203].

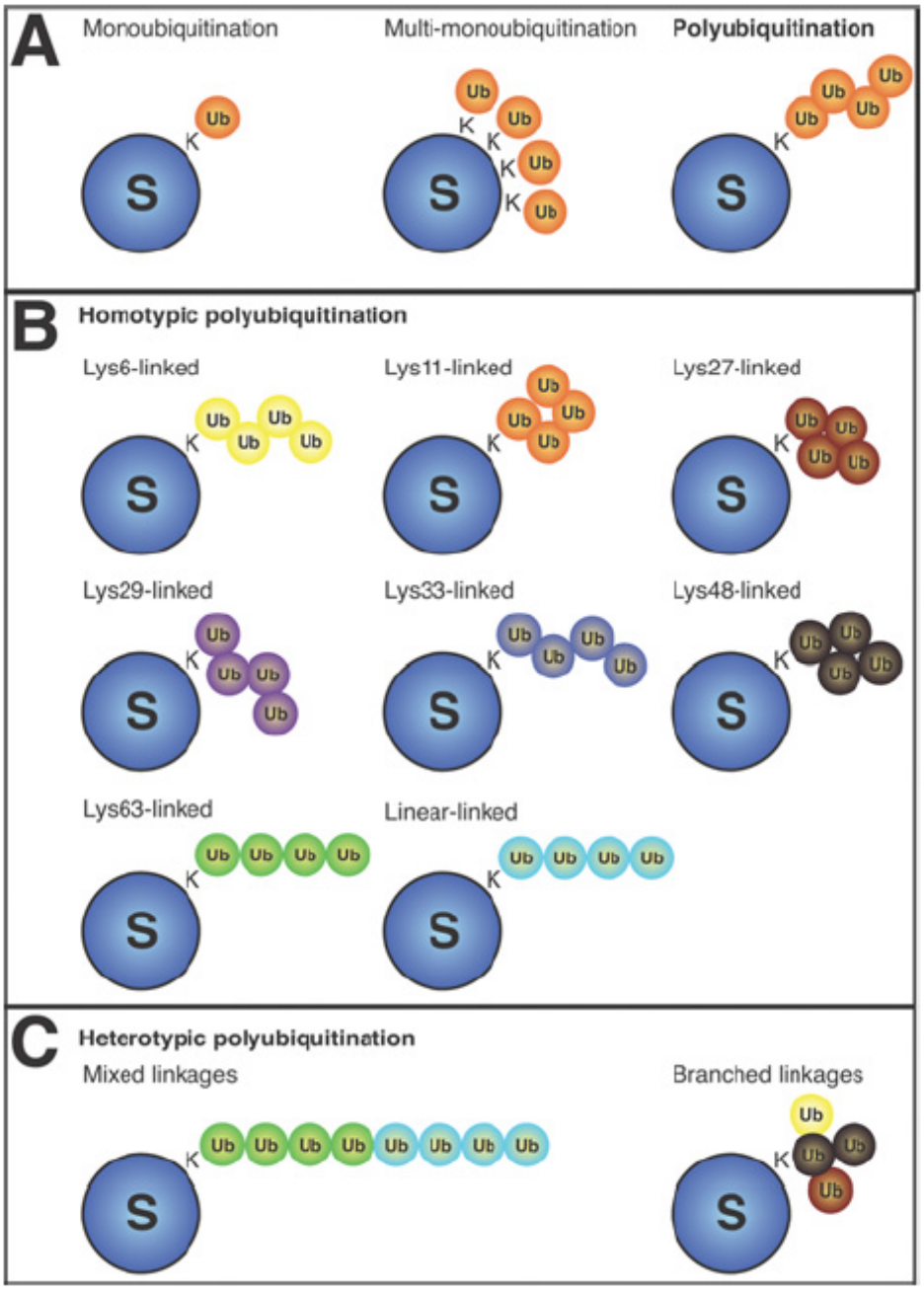

Fig. 1.4. Forms of ubiquitination. (Cited from Ref.193)
(A) The ubiquitin modification has three general layouts: monoubiquitination, multi-monoubiquitination and polyubiquitination.
(B) Forms of homotypic polyubiquitination, where each ubiquitin polymer chain contains a single linkage type. Individual linkages may lead to distinct ubiquitin polymer chain structures, and Lys^{48}- and Lys^{63}-linked/linear chains have different conformations.
(C) Forms of heterotypic polyubiquitination. In mixed linkages, a ubiquitin polymer chain has alternating linkage types; in branched or forked polyubiquitin polymer chains, a single ubiquitin is extended at two or more lysine residues.

I.2.3. CBL related protein ubiquitination and degradation

Since both CBL-B and C-CBL have the RING finger domain, which is the domain that interacts with the E2 enzyme, they function as an E3 ligase and are responsible for the ubiquitination and degradation of multiple target proteins through their TKB domain. The specific E2 enzymes that associate with CBL are UBC4, UBCH7 and UBCH5B/C[204].

The major target substrates of CBL family proteins are RTKs and non-receptor tyrosine kinase (non-RTK). When the RTK or non-RTK received activation signal such as ligand conjugation, their tyrosine residues will be phosphorylated, which leads to the recruitment of CBL family proteins through their TKB domain. Furthermore, the phosphorylation of Tyr371 on C-CBL and Tyr363 on CBL-B make them open their auto-inhibitory conformations and become easier to interact with the E2 enzyme to initiate the ubiquitination of the substrates[205, 206].

Based on different characteristics of these RTKs, they can be divided into several categories. The first major category is the growth factor receptors. The earliest discovery of the target that is ubiquitinated by C-CBL is EGFR, which was discovered in 1998 [183]. Later on, platelet-derived growth factor receptor (PDGFR) was also found as a RTK ubiquitinated by C-CBL[207]. A neuron growth factor receptor neurotrophin receptor p75 (P75NTR) was discovered to be ubiquitinated by C-CBL once P75NTR was phosphorylated[208]. C-CBL has also been proven to mediate the ubiquitination and lysosome sorting of fibroblast growth factor receptor 1 (FGFR1)[209]. The same principle was also applied for the ubiquitination and lysosome sorting of hepatocyte growth factor receptor (HGFR)[210]. In addition to growth factor receptors, another large group of CBL-regulated RTKs are cytokine receptors. For example, C-MPL, the receptor of thrombopoietin (TPO) that is required for hematopoietic stem cell maintenance and megakaryopoiesis, was recently shown to be negatively regulated by C-CBL through both the lysosomal and proteasome-mediated degradation pathways[211]. CSF-1, as we mentioned previously, is a cytokine that is required for macrophage differentiation. Its receptor, CSF-1R, is ubiquitinated and sorted to lysosome to be degraded by C-CBL upon CSF-1 stimulation[212]. KIT, the receptor of stem cell factor (SCF), has also been proven to be regulated by CBL-B and C-CBL mediated ubiquitination and degradation, during which the phosphorylation of Tyr568 and Tyr936 on KIT receptor are required[213, 214]. FLT3, the receptor of cytokine FLT3L, is required for DC development in the steady state. Its

constitutively active mutant FLT3-ITD (internal tandem duplications) is involved in leukemia disease. The regulation of the ubiquitination of wild-type FLT3 by CBL-B or C-CBL has not yet experimentally proven; however, one report has shown that *C-cbl* RING finger mutation can induce leukemia through FLT3 signaling[215].

In addition to the regulation of RTK, CBL family proteins have also been shown to be involved in the regulation of non-RTK. The two earliest examples are the regulation of SYK and TCRζ through C-CBL mediated ubiquitination. SYK, a non-RTK downstream of BCR signaling pathway, will generate phosphotyrosine upon BCR stimulation. Also, C-CBL can promote the ubiquitination of activated SYK, which turns out to be a negative regulator of the BCR signaling pathway[216]. Very recently, two studies have shown that CBL-B can work as a negative regulator of DECTIN-1, DECTIN-2 and DECTIN-3 through the direct regulation of the ubiquitination and lysosome sorting mediated degradation of these CLRs as well as their downstream signaling molecule SYK[217, 218]. This regulation is very important for host immunity against fungi infection such as *Candida albicans*[217, 218]. TCRζ, which can be considered as the intracellular part of TCR, is responsible for the TCR signaling transduction. C-CBL was reported to promote the ubiquitination of TCRζ, which is mediated by the downstream adaptor ZAP-70[219]. P85, a subunit of PI3K, which is the upstream of AKT/MTOR signaling pathway, is also regulated by C-CBL for its ubiquitination upon erythropoietin (EPO) stimulation. This ubiquitination modification is important for EPO receptor (EPOR) endocytosis since it allows P85 to interact with the endocytic protein EPSIN-1 to drive EPOR endocytosis[220].

In addition to the regulation of RTK and non-RTK, C-CBL can also associate with some IRFs such as IRF8 and IRF1 but not IRF4. In 2005, Xiong et al. discovered that C-CBL can regulate IRF8 ubiquitination and degradation through a proteasome-dependent pathway, and because of this negative regulation, C-CBL deficient macrophages produce more IL-12 since IRF8 can regulate the promoter of P40 subunit of IL-12. However, in their study, IRF4 is found not to be regulated by C-CBL[221]. Another study in 2011 showed that C-CBL can associate with IRF1, but in this case, it is not known whether C-CBL regulates the ubiquitination and degradation of IRF1[222]. CBL-B has been shown to regulate the ubiquitination and degradation of MYD88; however, the conclusion is not very convincing[223], because in Han's study, it was claimed that

the TKB domain was required for CBL-B mediated ubiquitination of MYD88; however, the redundant effect by C-CBL was not examined yet. Moreover, the expected enhancement of MYD88 signaling in *Cbl-b*$^{-/-}$ macrophages was also not investigated. Therefore, more evidences need to be collected to fully understand the regulatory role of CBL family proteins on MYD88 signaling. In another study by Kurt et al., CBL-B was shown to regulate the ubiquitination but not the degradation of TLR4[224]. However, the detailed mechanism of this regulation has not been fully investigated yet. For example, which domains of CBL-B and TLR4 are required for this regulation? What type of ubiquitination is involved in this regulation that does not cause the degradation of TLR4?

I.3. Roles of the CBL family of proteins in immune system development and function

Because of the specific structure of CBL family proteins, they can interact with the E2 enzyme to ubiquitinate the target proteins that associate with their TKB domain. Moreover, through the proline-rich domain and the tyrosine residues in the C-terminal, CBL family proteins can also work as adaptors to transduce the signaling to downstream molecules. Since they are ubiquitously expressed in immune cells, this implies that CBL family proteins may have important roles in the development and function of immune cells. Previously, in Dr. Gu's lab, a large amount of work has been focused on their roles in T cells and B cells.

I.3.1. Roles of CBL family proteins on the homeostasis and function of T cells

CBL family proteins have several effects on the homeostasis and function of T cells. First, they affect thymic selection. It is known that $CD4^+CD8^+$ double-positive thymocytes will differentiate into $CD4^+$ and $CD8^+$ single-positive thymocytes in the thymus, which require moderate TCR signal. This process is called thymic positive selection. However, too strong or too weak TCR signals will lead to negative selection or death by neglect[225-227]. C-CBL can selectively inhibit thymic-positive selection of $CD4^+$ but not $CD8^+$ T cells, because the ablation of C-CBL in 5C.C7 TCR transgenic (Tg) mice enhances the $CD4^+$ T cell selection but not the $CD8^+$ T cell selection in the female H-Y TCR Tg mice[228]. However, ablation of CBL-B does not cause any alteration in thymic positive or negative selection in the same model, which is probably due to the fact that the expression level of CBL-B is much lower than C-CBL in the thymocytes. The underlying molecular mechanism is further illustrated in the same study that the TCR downstream signaling such as Zap70 and MAPKs

was significantly enhanced in the C-CBL mutant DP thymocytes[228]. However, the difference between MHCI- and MHCII-mediated positive selections in those two TCR transgenic mice models can also be explained by the different affinity and avidity of these two antigens to the TCR repertoire. Actually, C-CBL-deficient thymocytes do have higher surface expression of CD3 and CD4, which may consequently increase the avidity of TCR/MHCII/co-receptor interaction[228]. In addition to these regulations, it has also been shown that C-CBL can regulate the ubiquitination of CD3ζ[219].

To exclude the possible redundant interference of CBL-B to C-CBL in the thymic development, the next step is to investigate the effects of double knockout *C-cbl* and *Cbl-b* on thymic development. Interestingly, *Cbl* dKO in T cells have enhanced $CD8^+$ T cell selection instead of enhanced $CD4^+$ T cell selection in the *C-cbl* KO mice, which suggests CBL double deficiency leads to MHC-independent $CD4^+$ and $CD8^+$ T cell development[229]. Furthermore, the underlying molecular mechanism points to the fact that CBL family proteins positively regulate surface TCR downmodulation[230].

In addition to the role in thymic selection, CBL family proteins also have an important function in the activation of peripheral T cell, which is regulated by both TCR signaling and the co-stimulatory receptors. Previously, it is shown that different co-stimulatory receptor engagement can lead to different T cell response. For example, CD28 engagement helps to activate T cell function, whereas CTLA4 engagement inhibits T cell function[231-233]. Similarly to a negative regulator in TCR signaling, CBL-B also plays a critical negative regulatory role in CD28 co-stimulatory signaling. In the absence of CBL-B, anti-CD3 stimulation alone can induce the T cells to produce a large amount of IL-2 and proliferate vigorously without the requirement of the help from CD28 co-stimulation[234, 235]. The underlying molecular mechanism that allows T cell activation to bypass CD28 co-stimulation is probably due to the negative effect of CBL-B on VAV and P85[236]. Obviously, this is just a proposed model; more investigations are needed to draw a clearer picture of the underlying molecular mechanisms. Since C-CBL and CBL-B have redundant negative regulatory roles on TCR signaling, the T-cell-specific *C-cbl* and *Cbl-b* double knockout [*Cbl*-dKO(T)] mice exclusively develop lethal systemic vasculitis and also severe autoimmune disease with high concentrations of anti-dsDNA antibodies in the serum[230]. Furthermore, because

Cbl-b KO T cells exhibit a low threshold for activation upon TCR stimulation without the requirement of CD28 co-stimulation, and also these mutant T cells are resistant to TGF-β suppression, these mutant $CD8^+$ T cells have enhanced anti-tumor immunity[237, 238].

Overall, CBL-B and C-CBL have redundant regulatory functions on the TCR signaling pathway, especially through the ubiquitination and lysosome sorting-mediated degradation of CD3ζ. However, the downstream signaling in the *Cbl-b* single knockout T cells may be a little different compared to that in the *Cbl* double knockout T cells, which is probably because as an adaptor, CBL-B and C-CBL could associate with different molecules. This difference needs more investigation to provide further clarification.

I.3.2. Roles of CBL family proteins on the homeostasis and function of B cells

Since CBL family proteins have negative regulatory roles in the homeostasis and function of T cells, it is easy to speculate that they will also have similar roles in the homeostasis and function of B cells, because the BCR signaling pathway is very similar with the TCR signaling pathway. For example, both pathways share the SYK molecule as a downstream signaling molecule. In fact, it has been proven that C-CBL negatively regulates SYK signaling in B cells, and this regulation is correlated with C-CBL-mediated ubiquitination and lysosome sorting[239]. In Dr. Gu's lab, we also generated B-cell-specific *C-cbl* and *Cbl-b* dKO [*Cbl*-dKO(B)] mice to bypass the influence of the functional redundancy between C-CBL and CBL-B. In the spleen of these *Cbl*-dKO(B) mice, B1 cell number and marginal zone B cell number are doubled. There is also an increase of the ratio of transitional 1 (T1) B cells versus T2 B cells. Furthermore, these *Cbl*-dKO(B) mice have a 5-fold increase of serum immunoglobulin (Ig) M but not other Ig isotypes. Also, more than half of the mice develop SLE-like autoimmune disease based on the detection of anti-dsDNA IgG and anti-nuclear antigen IgG antibodies in the serum[240]. These results strongly imply that CBL family proteins play a critical redundant role in B cell tolerance induction.

The underlying mechanism is further proven due to an accelerated maturation of *Cbl* mutant B cells, and this is correlated with the enhanced BCR signaling. The tyrosine phosphorylation of Igα, SYK, PCL-γ2, VAV and ERK1/2 were all enhanced in the mutant cells upon BCR stimulation, which shares a very similar pattern in *Cbl* dKO T cells. Similar to the role on CD3ζ ubiquitination

in T cells, C-CBL and CBL-B also have redundant roles on the ubiquitination of Igα and SYK in B cells[240].

I.3.3. Role of CBL family proteins on the homeostasis and function of other immune cells

Natural killer (NK) cells are a type of cytotoxic lymphocytes that are important in the innate immune system. They express TLRs to sense the PAMPs and professionally produce IFN-γ upon TLR stimulation. NK cells also express the low-affinity Fc receptor CD16 to enable them to detect antibody-coated target cells and to exert antibody-dependent cell cytotoxicity (ADCC). In addition, they are also good sensors to detect the MHCI-deficient non-self tumor cells through their killer cell immunoglobulin-like receptors (KIRs)[241]. Very recently, Penninger's group discovered that *Cbl-b* knockout NK cells have an anti-metastatic effect on mammary cancer and melanoma cells through the ubiquitination regulation on TAM tyrosine kinase receptors (TKRs) TYRO3, AXL and MER[242].

CBL family proteins are also expressed in monocytes, another important type of innate immune cells. On ontogeny, monocytes share the early progenitors MDP with DCs; therefore, there is a close relationship between monocytes and DCs[243]. MDPs are lineage-negative (Lin-) and express CD117 (KIT), CD135 (FLT3) and CD115 (CSF-1R, or M-CSFR)[244, 245]. They give rise to DCs and monocytes depending on FLT3L and M-CSF, respectively. Under inflammatory circumstances, the $LY6C^{hi}$ monocytes will migrate to peripheral tissue to generate monocyte-derived DCs or monocyte-derived macrophages. However, recent discoveries show that in steady state, the tissue resident macrophages have the ability to self-renew, and they originate from the fetal liver[243]. A detailed investigation of the role of CBL family proteins in monocyte has not been done yet. However, it has been proven in macrophages that C-CBL stimulates CSF-1R multi-monoubiquitination and endocytosis, which will attenuate macrophage proliferation[212]. Another more recent study has shown that CBL-B deficient macrophages have enhanced infiltration and activation in adipose tissue, which leads to the peripheral insulin resistance in the mice[246]. Furthermore, CBL family proteins can regulate TLR signalling in monocytes. It is reported that CBL-B has a negative regulatory role of surface TLR4 expression, which leads to an accentuated acute lung inflammation in *Cbl-b*$^{-/-}$ mice upon *in vivo* administration of LPS[224]. It has also been reported in the same study that *Cbl-b* deficiency has no appreciable effect on TLR3-dependent

cytokine and chemokine production[224]. Furthermore, another study showed that CBL-B could regulate the ubiquitination of TLR4 downstream adaptor molecules such as MYD88 and TRIF in the macrophage cell line RAW264.7[223]. In a more recent study, it was shown that CBL-B could regulate the ubiquitination of DECTIN-2 and DECTIN-3 in BM-derived macrophages; therefore, *Cbl-b* deficiency could lead to the hyper-activation of macrophages and more efficient clearance of fungi infection[218].

Since CBL family proteins are highly expressed in DCs, there are also several studies investigated the role of CBL-B and C-CBL in the development and function of DCs. In one study, it was shown that *C-cbl*$^{-/-}$ BMDC could produce more pro-inflammatory cytokines and chemokines upon TLR4 stimulation. These cytokines and chemokines include IL-1α, IL-1β and CXCL1[247]. Interestingly, the *C-cbl*$^{-/-}$ BMDC has a constitutively higher level of IL-6 even without LPS stimulation. Furthermore, the OVA-pulsed *C-cbl*$^{-/-}$ BMDCs have an enhanced ability to induce the proliferation of $CD4^+$ and $CD8^+$ T cells *in vivo* compared to the OVA-pulsed WT BMDCs. These mutant BMDCs are also more potent inducers of Th1 immune response[247]. In another study, *Cbl-b* deficiency was shown to have no effect on BMDC generation and surface receptor expression, except DEC-205. However, the underlying mechanism for this overexpression of DEC-205 in *Cbl-b* mutant cells has not been investigated yet[248]. Furthermore, upon LPS stimulation, the CBL-B deficient BMDCs produce more TNF-α, IL-6 and macrophage inflammatory protein (MIP)-1α, whereas upon CpG stimulation, the CBL-B-deficient BMDCs produce more IL-1α, TNF-α and monocyte chemotactic protein 1 (MCP-1, also known as CCL2). Furthermore, the CBL-B-deficient BMDCs also exhibit increased allogeneic T cell priming potential but not the potential of the induction of antigen-specific T cell responses and cross-presentation[248]. Very recently, two reports claimed that CBL-B can regulate and ubiquitinate DECTIN-1 and DECTIN-2 in BMDCs, and its deficiency leads to the prevention from the infection of fungi *Candida albicans*[217, 249].

For the role of CBL family proteins in the development and function of neutrophils, however, there have been no such reports yet.

I.3.4. Role of CBL family proteins on the homeostasis and function of hematopoietic cells

Since CBL family proteins can regulate the ubiquitination and lysosome sorting of so many important cytokine receptors and growth factor receptors (e.g., EGFR, KIT, CSF-1R), it is easy to speculate that CBL family proteins should have important roles on the homeostasis and function of hematopoietic cells. In fact, a large number of investigations related to CBL family proteins have shown that mutations of CBL family proteins, especially the mutations in the RING finger domain, are highly correlated with leukemia disease such as acute myeloid leukemia (AML) [250, 251] and myelodysplastic syndromes/myeloproliferative neoplasms (MDS/MPN)[252]. In MDS/MPN, there are three subgroups, including the chronic myelomonocytic leukemia (CMML), atypical chronic myeloid leukemia (aCML) and juvenile myelomonocytic leukemia (JMML). In the JMML, *C-cbl* mutations are known to account for 12.5 % of the cases, while mutations of the Ras-MAPK signaling pathway-related molecules account for 75 % of the cases[253]. Interestingly, in these cases, *Cbl-b* mutations are very rare compared to *C-cbl* mutations. Furthermore, in the cases of *C-cbl* mutations, missense mutations or small deletions around the linker region and within the RING finger domain are the majority; complete *C-cbl* gene deletion, truncation or mutations outside of the linker/RING finger domain are rare[253]. Since CBL-B has a function that is redundant with C-CBL, how can *C-cbl* mutations only cause myeloproliferative disorder without *Cbl-b* mutations? It has been proposed and experimentally proven that mutations in the RING-finger or linker region of C-CBL can make them work as a dominant-negative form, which means the mutant C-CBL still can associate with these activated RTKs, but these RTKs will not be sorted to lysosome or proteasomes to be degraded. Due to the high structure similarity between C-CBL and CBL-B, the dominant-negative mutant C-CBL can still compete with CBL-B to associate with these activated RTKs to abolish the normal function of CBL-B[215]. Furthermore, it has also been shown in the same study that the FLT3 signaling pathway is highly involved in *C-cbl*-mutation-mediated leukemia, because crosses between *C-cbl* mutant mice with FLT3L-deficient mice can significantly prevent the development of leukemia[215].

I.4. Role of FLT3 in immune system development and function

The RTK FLT3 is a member of the so-called “split-kinase domain” or type III RTKs, which include PDGFR, KIT, CSF-1R and FMS[254]. It was first discovered by William Matthew et al. in 1991 and was originally isolated from a cell population enriched for stem cells and primitive

uncommitted progenitors but is absent in populations containing more mature cells[255]. Later on, by the same group, FLT3 was shown to be very important for both multipotent stem cell generation and lymphoid progenitor generation[256]. Furthermore, one year later, another group discovered that *in vivo* administration of FLT3L could dramatically expand DC populations[257]. In 2000, it was discovered that in FLT3L-deficient mice, there was a severely impaired homeostasis of DCs and NK cells[258]. Another study in 2015 showed that FLT3 was re-expressed in germinal center B cells and was required for antibody class switch to IgG1[259]. Due to the highly expression of FLT3 in short-term repopulating hematopoietic stem cells, some FLT3 mutations have been discovered to induce about 30 % of AML cases[254]. Since FLT3 signaling is so important in immune cell homeostasis and function, it is necessary to further elaborate.

I.4.1. FLT3 molecular structure and its signaling

As a member of type III RTKs, FLT3 has a very similar structure to the other members in this family. FLT3 is composed of an immunoglobulin (Ig)-like extracellular ligand-binding domain, a single transmembrane domain, a juxtamembrane domain (JM) and a highly conserved intracellular kinase domain interrupted by a kinase insert domain (KID)[260, 261] (Fig 1.5). The JM domain and intracellular kinase domain are the two domains that are important for the activation of FLT3 when it binds to the FLT3L. Without ligand binding, the FLT3 keeps auto-inhibitory conformation of its JM domain[260]. However, upon interaction with FLT3L, FLT3 undergoes a conformational change, allowing a homodimer to form. This receptor dimerization is the prelude to the tyrosine kinase, leading to the phosphorylation of various sites in the intracellular domain[260]. Interestingly, the maturation of FLT3 requires a glycosylation modification on the asparagine residues of the extracellular portion of the receptor. Only fully glycosylated, mature receptors are finally transported to and inserted into the plasma membrane and ready to be exposed to the FLT3L[262, 263]. In addition, the soluble FLT3L itself is a non-covalently linked homodimer and contains six cysteine residues that apparently form intramolecular disulfides[264, 265].

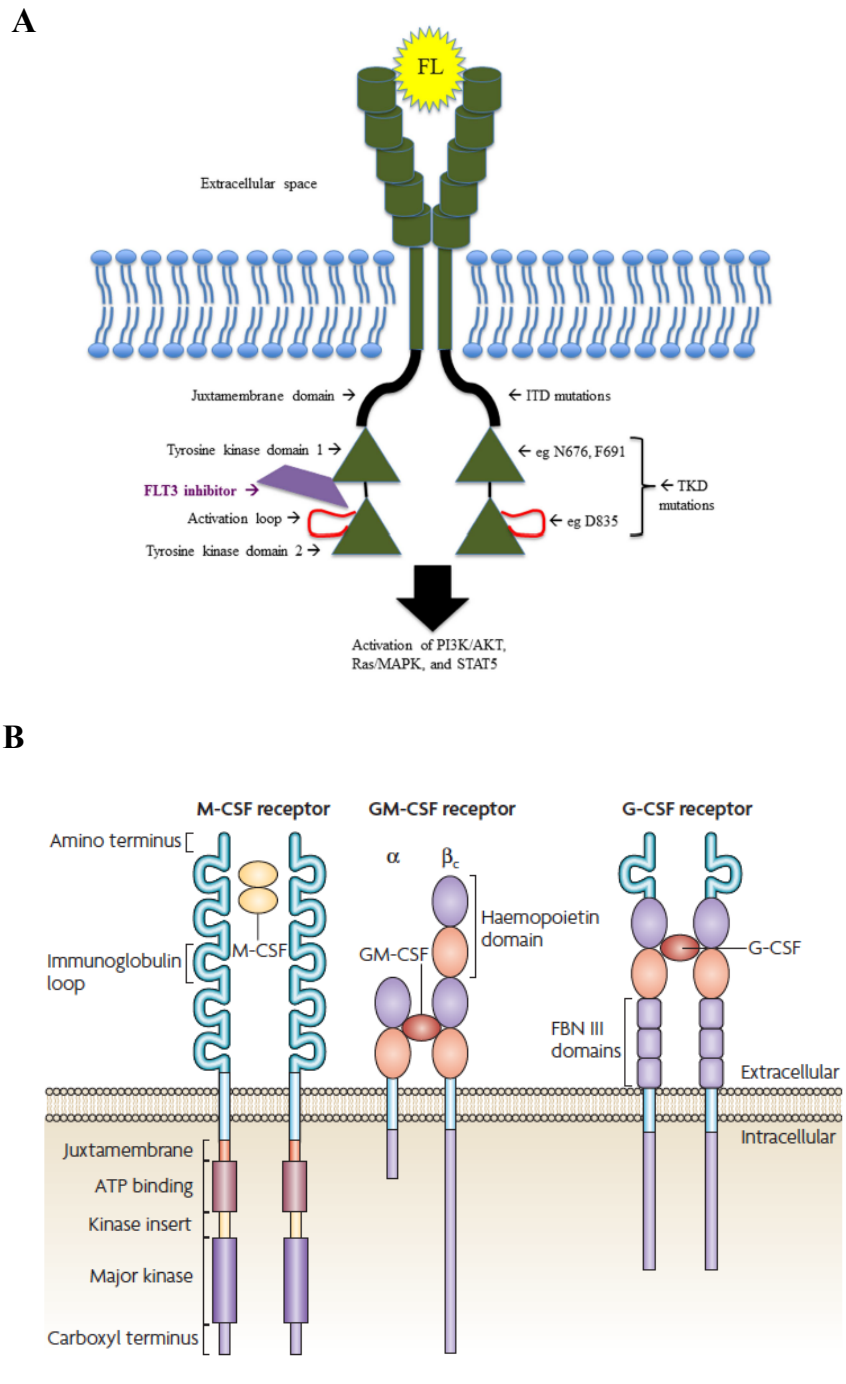

Fig. 1.5. The structure of FLT3 and M-CSFR. (Cited from Ref. 260 and 261)
(A) Schematic illustration of the structure and function of FLT3, including the sites of the most common activating mutations.
(B) The structure of colony-stimulating factors (CSF) receptors. Schematic representation of M-CSFR, GM-CSFR, and G-CSFR. M-CSFR is a homodimeric type III receptor tyrosine kinase, while the G-CSF receptor is a typical member of type I cytokine receptor family. The GM-CSFR consists of a unique α-chain and a common β-chain, through which signaling occurs.

The JM domain and the intracellular kinase domain of FLT3 are also highly involved in the constitutively active form of mutation that leads to multiple leukemia and myeloproliferative disorder. For example, FLT3-ITD mutation was discovered in multiple hematologic malignancies, occurring in chronic myeloid leukemia (CML) (5-10 %), myelodysplasia (MDS) (5-10 %) and AML (15-30 %). FLT3 activation loop mutation, another major type of constitutive active mutation in the intracellular kinase domain, was found in the malignant cells from patients with CML (≈1 %), ALL (acute lymphoblastic leukemia) (1-3 %), MDS (2-5 %) and AML (5-10 %)[260]. One of the highly frequent mutations in this subtype is the aspartate-to-tyrosine substitution at codon 835[266]. Interestingly, individual patient seldom harbours both two types of mutations.

Upon FLT3L stimulation, the FLT3 form homodimer and induce self-phosphorylation to activate downstream signaling pathways such as SRC family kinases (SFKs). Interestingly, this interaction between FLT3 and SFKs is bidirectional instead of being unidirectional, which means SFKs are not just a signal transduction of molecules downstream of FLT3 but also modulate the activity of it. For example, one SFK family member, HCK, is able to phosphorylate FLT3 on tyrosine residues located in the JM region, which is also the region for auto-phosphorylation[267]. Interestingly, this HCK-mediated phosphorylation of FLT3 can induce an accumulation of the immature, intracellular form of FLT3 at the expense of the mature, plasma membrane-inserted form of FLT3[267]. In addition to the association with SFKs (e.g., HCK, LYN, FYN), intracellular C-terminal of FLT3 can also associate with P85 subunit of PI3 kinase, SHP2, GRB2 and SHC upon FLT3L stimulation[268-270]. The major further downstream signaling pathways are the RAS/MAPK and AKT/MTOR signaling pathways, which are important for cell proliferation and anti-apoptosis[271]. Moreover, in leukemia cancer cells, the constitutively activated FLT3 signaling also leads to the constitutively activated RAS/MAPK and AKT/MTOR signaling pathways[272]. STAT5 was also found to be constitutively phosphorylated at tyrosine residues when FLT3 has its constitutive active mutation[273].

I.4.2. Role of FLT3 signaling in DCs

FLT3 is highly expressed mainly in two types of cells: one is short-term repopulating HSCs, and the other one is DCs. Therefore, this implies that FLT3 signaling may have important roles in DCs. Within DCs, although their development requires FLT3 signaling, different DC subsets have

different surface expression levels of FLT3. For example, $CD8\alpha^+$ cDCs have much higher surface FLT3 expression than $CD11B^+$ cDCs, which will also be shown in the results section of my thesis.

Previous studies demonstrated that FLT3L overexpression can directly expand pDCs and cDCs *in vivo* through their surface receptor FLT3 and also indirectly expand NK cells through an expansion of IL-15 expressing DCs[274, 275]. Interestingly, overexpression of FLT3L *in vivo* can also expand Tregs in a DC-dependent manner[276, 277]. Also, FLT3L overexpression-induced DC expansion is probably through the AKT/MTOR signaling pathway, because DC-specific PTEN knockout mice also show a similar dramatic expansion of different DC subsets[278]. However, the impact of the FLT3/MAPK signaling pathway on DCs is still unknown.

The function of FLT3L in tolerance or immunity is not quite clear yet, because controversial results have been reported. For example, FLT3L can be used as an adjuvant to boost antibody response to soluble antigens, which alone can only induce clonal anergy. This boost is probably through the enhanced CD40 expression on DCs by FLT3L stimulation, because blocking the CD40/CD40L interaction can impair adjuvant function of FLT3L[279]. However, in fact, FLT3L can also expand the Treg population via a Treg-DC interaction, which is proposed to be able to promote immune tolerance in a variety of clinical settings[280]. However, more investigations need to be done to prove this hypothesis.

I.5. Role of E3 ubiquitin ligase on the homeostasis and function of DCs

Although it is estimated that there are more than 600 E3 ligases in the human genome, not very many of them have been identified in DCs so far. In addition to CBL family proteins, there are also several other important E3 ubiquitin ligases that have certain effects on the homeostasis and function of DCs.

The well-characterised E3 ubiquitin ligases in DCs are membrane-associated RING-CH (MARCH) family proteins that belong to the RING subgroup of E3 ligases. The most important substrates of the MARCH family proteins are MHCI and MHCII[281, 282]. For example, MARCH1 was first discovered to regulate the MHCII ubiquitination and the subsequent lysosome sorting for degradation. Furthermore, LPS-induced surface MHCII upregulation is dependent on the

downregulation of MARCH1[283]. Later on, it was discovered that the ubiquitination and degradation of CD86 was also regulated by MARCH1[284, 285]. Interestingly, the members in the MARCH family also have redundant functions with what CBL family proteins do. For example, MARCH8 was reported to have the redundant function of regulating the ubiquitination and degradation of MHCII as MARCH1[286]. MARCH4 and MARCH9 can both regulate the ubiquitination and degradation of MHCI[282]. Due to this important feature, MARCH family proteins are considered to have a protective role in autoimmune diseases by impairing $CD4^+$ T cell activation. For example, overexpression of MARCH8 in mice showed resistance to the onset of experimental autoimmune encephalomyelitis (EAE)[286].

Another well-characterised E3 ubiquitin ligase in DCs is the tumor necrosis factor alpha-induced protein 3 (TNFAIP3, also known as A20). However, A20 is more complicated than MARCH family proteins, because it has both ubiquitination and deubiquitination functions[287]. A20 was first identified when its transcription was dramatically induced after TNF-α mediated NF-κB activation[288]. Later on, A20 was discovered as an inhibitor of programmed cell death[289]. Furthermore, A20 was an important player in innate immune response because it was a negative regulator of TNF-α and TLR4-induced NF-κB activation. Due to this negative regulatory function, A20 knockout mice develop severe inflammation and cachexia in a T/B cell-independent manner and die prematurely. In addition, these A20 mutant mice are also hypersensitive to both LPS and TNF[290]. The underlying mechanism of A20 mediated inhibition of TNF and LPS signaling pathways is due to the ubiquitin-editing function of A20. For example, A20 can cleave lysine 63 (K63)-linked polyubiquitin chains on receptor-interacting serine/threonine-protein kinase 1 (RIP1) and then conjugate lysine 48 (K48)-linked polyubiquitin chains that target RIP1 for degradation by the proteasome to inhibit the TNF signaling pathway[291]. In the TLR/MYD88 signaling pathway, two A20-mediated inhibitory mechanisms have been discovered. One is A20, which inhibits the polyubiquitination and activation of TRAF6. The logic behind this is that TRAF6 requires K63-linked polyubiquitination to stabilize its interaction with IκB kinase (IKK) to activate downstream IκBα degradation; therefore, the deubiquitination function of A20 will inhibit TRAF6/IKK interaction, thus leading to the block of IκBα degradation[292]. The other more recently discovered mechanism could be that A20 inhibits the E3 ligase activities of TRAF6, TRAF2 and CIAP1 by antagonizing interactions with the E2 ubiquitin conjugating enzyme UBC13

and UBCH5C with the help of the regulatory molecule TAX1BP1[293]. The role of A20 in DCs was also reported recently in two studies in 2011. In the first study, it was shown that *A20* knockout cDCs and pDCs have enhanced levels of co-stimulatory molecules such as CD40, CD80 and CD86. These mutant DCs also produce more pro-inflammatory cytokines such as IL-6 and TNF-α upon LPS stimulation, which is dependent on the MYD88 signaling pathway. Moreover, these *A20* (DC) mutant mice also develop colitis, IBD and IBD-associated arthritides[135]. In the other study, DC-specific *A20* knockout mice also showed a systemic autoimmune disease phenotype with spontaneously mature DCs that are hyper-responsive to activation stimuli. In the *A20* (DC) mutant mice, the homeostasis of DCs also changed, where there is a significant increase of cDCs and decrease of pDCs ratio in the spleen, which is probably due to the anti-apoptotic effect of A20 deficiency. Furthermore, the *A20*-mutant DCs have enhanced uptake of apoptotic cells and presentation to T cells, which could be one reason that causes the autoimmunity in the *A20* (DC) mutant mice[294].

TRAF6, a member of the RING subgroup of E3 ubiquitin ligase, was also shown as a critical player in the development and maturation of DCs. In DC-specific *Traf6* [*Traf6* (DC)] knockout mice, there is a deficiency of $CD4^+CD8\alpha^-$ cDC subsets. These TRAF6-mutant DCs have impaired responses such as inflammatory cytokines production and surface co-stimulatory molecules upregulation to either microbial components or CD40L stimulation. Moreover, *Traf6*-mutant DCs also have impaired capacity to stimulate naïve T cells after LPS activation[295]. These results suggest that TRAF6 may be required for autoimmunity. However, some controversial results are reported in another study in which the *Traf6* (DC) mutant mice develop eosinophilic enteritis and fibrosis in the small intestine with the characterization of spontaneous development of Th2 cells and decreased Treg cell number in the LP. Further studies showed that this eosinophilic enteritis phenotype is dependent on gut commensal microbiota but independent of MYD88[296]. Due to these controversial results in those two studies, more evidences are needed to fully understand the role of TRAF6 in the regulation of DC activation.

II. QUESTIONS AND HYPOTHESES

In the adaptive immune system, the CBL family proteins play a critical role in both the development and maintenance of immune quiescence. In addition, *C-cbl* and *Cbl-b* are also highly expressed in DCs. Since they are important regulators for various receptors and intracellular signaling molecules, we are interested in understanding whether they also play a similar role in DC development and function.

Our working hypothesis is that CBL-B and C-CBL have redundant and negative regulatory roles to regulate the homeostasis of DCs. They may also play a critical role to maintain DC functional quiescence under the steady-state, thus immune tolerance to self.

III. MATERIALS AND METHODS

III.1. Animals and cell lines

C57BL/6J mice were purchased from the Jackson Laboratory (#000664, USA). Germline *Cbl-b*$^{-/-}$ mice were originally generated in former lab at National Institutes of Health (NIH), USA. In brief, the neomycin resistance gene was inserted into the third exon of *Cbl-b* gene, immediately after the translation-initiation codon ATG, in the antisense orientation. Originally, the *Cbl-b*$^{-/-}$ mice have mixed genetic background of 129 and C57BL/6J mice, but the *Cbl-b*$^{-/-}$ mice in my experiments have already been backcrossed with C57BL/6J mice for many generations, and have been verified to contain 99.9% of C57BL/6J genetic background by Jackson Laboratory. The *C-cbl*$^{f/f}$ mice were also originally generated in the former lab at NIH, USA. In brief, the floxed *C-cbl* allele was generated by introducing two *loxP* sequences into the introns flanking one of the exon of *C-cbl* corresponding to nucleotides 681-837 of the mouse *C-cbl* cDNA by gene targeting. The *C-cbl*$^{f/f}$ mice originally also have mixed genetic background of 129 and C57BL/6J mice, and later backcrossed with C57BL/6J mice for many generations, which have been verified to contain 99.9% of C57BL/6J genetic background by Jackson Laboratory. The *Cd11c* Cre mice are obtained from Boris Reizis lab (Columbia University Medical Center, USA), and they are C57BL/6J background. To generate the *Cd11c* Cre; *C-cbl*$^{f/f}$ (*C-cbl* KO) mice, I crossed the *C-cbl*$^{f/f}$ mice with the *Cd11c* Cre mice. And to generate the *Cd11c* Cre; *C-cbl*$^{f/f}$; *Cbl-b*$^{-/-}$ (*Cbl* dKO) mice, I crossed the *Cbl-b*$^{-/-}$ mice with the *C-cbl* KO mice. The *Rag1*$^{-/-}$ mice are obtained from Woong-Kyung Suh lab at the Institut de Recherches Cliniques de Montréal (IRCM), CA, which also have C57BL/6J background. To generate the *Cd11c* Cre; *C-cbl*$^{f/f}$; *Cbl-b*$^{-/-}$; *Rag1*$^{-/-}$ (*Cbl* tKO) mice, we crossed the *Cbl* dKO mice with *Rag1*$^{-/-}$ mice. The OTI and OTII mice are obtained from André Veillette lab at the Institut de Recherches Cliniques de Montréal (IRCM), CA, which both have C57BL/6J background. The C57BL/6J background *Cbl-b*^{C373A} mice are obtained from Wallace Y. Langdon lab at school of pathology and laboratory medicine, university of Western Australia, AU. To generate the *Cd11c* Cre; *C-cbl*$^{f/f}$; *Cbl-b*$^{C373A/-}$ mice, I crossed the *Cbl* dKO mice with the *Cbl-b*$^{C373A/C373A}$ mice. B6.SJL mice (#002014) were purchased from The Jackson Laboratory.

FLT3L-secreting B16 melanoma cell line was obtained from Boris Reizis (Columbia University Medical Center, USA). Embryonic kidney 293T cell line was originally purchased from ATCC, USA. (#CRL-3216). The J588 GM-CSF-secreting myeloma cell line was obtained from André Veillette lab at the Institut de Recherches Cliniques de Montréal (IRCM).

III.2. Genotyping

The genotype of these transgenic mice in my experiments are verified by genotyping through polymerase chain reaction (PCR), except for OTI mice, which are genotyped through fluorescence-activated cell sorting (FACS). The genotyping primer sequences are listed in Table 3.1.

For PCR genotyping, in brief, the mouse tail was digested in lysis buffer (100mM Tris-HCl, 5mM EDTA, 0.2% SDS, 200mM NaCl, 100μg/ml proteinase K) for overnight at 55˚C. After centrifugation at maximum speed, the supernatant containing the genomic DNA was collected and transferred to a new tube. The genomic DNA was further precipitated by adding equal volume of 100% ethanol. After centrifugation at maximum speed, the genomic DNA pellet was collected and resuspended in 200μl 10mM Tris-HCl buffer. 3μl genomic DNA was used in the PCR for genotyping.

The 3-step PCR program of *Cd11c* Cre genotyping is as follow: 5 mins at 94˚C for initial denaturation (Step 1); 35 cycles of 30 secs at 94˚C, 30 secs at 60˚C, 45 secs at 72˚C for DNA amplification (Step 2); 5 mins at 72˚C for final extension and inactivation (Step 3). The 3-step PCR programs of *Cbl-b and C-cbl* genotyping are as follow: 5 mins at 94˚C for initial denaturation (Step 1); 35 cycles of 30 secs at 94˚C, 30 secs at 58˚C, 45 secs at 72˚C for DNA amplification (Step 2); 5 mins at 72˚C for final extension and inactivation (Step 3). The 3-step PCR program of *Ot2β* genotyping is as follow: 5 mins at 94˚C for initial denaturation (Step 1); 35 cycles of 30 secs at 94˚C, 60 secs at 60˚C, 60 secs at 72˚C for DNA amplification (Step 2); 5 mins at 72˚C for final extension and inactivation (Step 3). The 3-step PCR program of *Rag1* genotyping is as follow: 5 mins at 94˚C for initial denaturation (Step 1); 35 cycles of 30 secs at 94˚C, 30 secs at 58˚C, 60 secs at 72˚C for DNA amplification (Step 2); 5 mins at 72˚C for final extension and inactivation (Step 3). The 3-step PCR program of *Cbl-b*^{C373A} mutation genotyping is as follow: 5 mins at 94˚C for initial denaturation (Step 1); 35 cycles of 30 secs at 94˚C, 45 secs at 55˚C, 60 secs at 72˚C for DNA amplification (Step 2); 5 mins at 72˚C for final extension and inactivation (Step 3).

For FACS genotyping of OTI mice, 2-3 drops of mouse blood were collected by cheek bleeding and collected in the resuspension buffer (20mM EDTA and 0.1% sodium azide in 1×PBS). Cell

pellets were collected by centrifugation at 1500 rpm for 5 mins, and erythrocytes were removed by ACK lysing buffer (#10-548E, LONZA). The rest peripheral blood mononuclear cells (PBMC) were stained with anti-mouse CD3e (145-2C11), anti-mouse CD8α (53-6.7), anti-mouse V alpha 2 TCR (B20.1), and anti-mouse V beta 5.1/5.2 TCR (MR9-4) at a concentration of 2.5ng/μl of each antibody in the FACS buffer (1% BSA and 0.05% sodium azide in 1×PBS) for 30 mins on ice and protected from light. Stained cells were then washed with FACS buffer, and subsequently analyzed by using the CyAn ADP analyzer, or Fortessa analyzer. Acquired flow cytometry data were analyzed further with Flowjo software Version 9.

Gene Name	Primer name	Sequence
Cd11c Cre	Cre1	GGTTTCCCGCAGAACCTGAAG
	Cre4	GCTAAGTGCCTTCTCTACACC
Cbl-b	CBL-B0	CTTGCAAAAAGGACTAAGATTC
	CBL-B8	TTCCTCGTGCTTTACGGTAT
	CBL-B17	CCCAGCAAAAGTAGCCAATG
C-cbl	C-CBL3 Short	TGGCTTGCAATTATAATCCTAC
	C-CBL4 Short	AGATGTCTGGCTGTGTGTAC
Rag1	Rag1-1	GAGGTTCCGCTACGACTCTG
	Rag1-2	CCGGACAAGTTTTTCATCGT
	Rag1-3	TGGATGTGGAATGTGTGCGAG
Ot2β	OT2β_S	GCTGCTGCACAGACCTACT
	OT2β_AS	CAGCTCACCTAACACGAGGA
Cbl-b^{C373A}	CBL-B C373A	GGCTCCACTTTTCAGCTGGCG
	P281_10	ATCTTCCCAGGAGCACGACG

Table. 3.1. The genotyping primer sequences.

III.3. Antibodies

Here is the list of FACS antibodies. Anti-mouse CD3e (145-2C11), anti-mouse TCRβ (H57-597), anti-mouse B220 (RA3-6B2), anti-mouse CD4 (RM4.5), anti-mouse CD8α (53-6.7), anti-mouse CD24 (M1/69), anti-mouse CD135 (A2F10), anti-mouse MHC Class II (I-A/I-E) (M5/114.15.2), anti-mouse MHC Class II I-Ab (AF6-120.1), anti-mouse CD11c (N418), anti-mouse CD11b (M1/70), anti-mouse CD62L (MEL-14), anti-mouse CD44 (IM7), anti-mouse F4/80 (BM8), anti-mouse Ly6G (Gr-1) (RB6-8C5), anti-mouse CD317 (BST2, PDCA-1) (eBio927), anti-mouse NK1.1 (PK136), anti-mouse CD80 (B7-1) (16-10A1), anti-mouse CD86 (B7-2) (GL1), anti-mouse CD274 (PD-L1, B7-H1) (MIH5), anti-mouse CD103 (Integrin alpha E)

(2E7), anti-mouse CD195 (CCR5) (HM-CCR5), anti-mouse TER-119 (TER-119), anti-mouse CD172a (SIRP alpha) (P84), anti-mouse CD45.2 (104), anti-mouse CD45.1 (A20), anti-mouse V alpha 2 TCR (B20.1), anti-mouse V beta 5.1/5.2 TCR (MR9-4), anti-mouse Foxp3 (FJK-16s), anti-mouse IFN gamma (XMG1.2), anti-mouse IL-4 (11B11) were purchased from eBiosciences, US. Anti-mouse Ly6G (1A8), anti-mouse Ly6C (AL-21), anti-mouse CD40 (3/23), anti-mouse IL-2 (JES6-5H4) were purchased from BD Biosciences, CA.

Here is the list of western blot antibodies. Akt (pan) (C67E7) Mouse mAb (#4691), Phospho-Akt (Ser473) (D9E) XP® Rabbit mAb (#4060), Phospho-FLT3 (Tyr589/591) (30D4) Rabbit mAb (#3464), FLT3 (8F2) Rabbit mAb (#3462), Cbl-b (D3C12) Rabbit mAb (#9498), Phospho-p44/42 MAPK (Erk1/2) (Thr202/Tyr204) Rabbit antibody (#9101), p44/42 MAPK (Erk1/2) Rabbit antibody (#9102) were purchased from Cell Signaling Technology, USA. Anti-beta actin antibody [AC-15] (HRP) (#ab49900), and anti-FLT3/CD135 antibody (#ab33092) were purchased from Abcam, CA. Anti-Cbl antibody (C-15) (#sc-170), and Anti-HA-probe antibody (Y-11) (#sc-805) were purchased from Santa Cruz, USA.

III.4. Plasmid and cloning

HA tagged ubiquitin expression plasmid, and pcDNA3.1(+) plasmid are obtained from Tarik Möröy lab at the Institut de Recherches Cliniques de Montréal (IRCM), CA. RNA was isolated and purified from sorted $MHCII^{+}CD11C^{+}$ splenic cDCs of the WT C57BL/6J mice by using the Qiagen RNeasy mini kit (#74104, Qiagen). In brief, the cDCs were first lysed and homogenized in the RLT lysing buffer. Then, 1 volume of 70% ethanol was added to the lysate and the mixture was passed through the RNeasy spin column to isolate the RNA from the mixture. The column was washed by RW1 and RPE buffer, respectively. Finally, the RNA was eluted by RNase-free water and quantified by the Nanodrop 2000 (ThermoFisher Scientific).

The purified RNA was then used as a template to generate the cDNA by reverse transcription PCR (RT-PCR). In brief, the 10µl RNA was first mixed with 1µl $Oligo(dT)_{12-18}$ primer (#18418012, ThermoFisher Scientific) and 1µl 10mM dNTP (#DD0056, BIO BASIC). Then the mixture was heated at 65˚C for 5 mins and quickly chilled on ice for 5 mins to anneal the $Oligo(dT)_{12-18}$ primer with mRNA. The annealed mRNA was then reverse transcribed to cDNA by using the

SuperScript™ II reverse transcriptase kit (#18064014, ThermoFisher Scientific) in a reaction buffer for 50 mins at 42˚C. The reaction was stopped by heating inactivation at 70˚C for 15 mins. Finally, the generated cDNA was used to amplify the mouse *Flt3* CDS (NM_010229.2), mouse *Cbl-b* CDS (NM_001033238.1), and mouse *C-cbl* CDS (NM_007619.2) by classical PCR. The primers for generating these CDSs are in Table 3.2. The PCR was carried out by using the AccuPrime™ Taq DNA Polymerase, High Fidelity kit (#12346-086, ThermoFisher Scientific). In a 50μl reaction system, 5μl 10×AccuPrime PCR buffer I, 2μl 10mM primer (1μl each), 2μl cDNA, 0.2μl DNA polymerase and 40.8μl H_2O were mixed together and put into the PCR machine. The 3-step PCR program of these PCRs are as follow: 5 mins at 94˚C for initial denaturation (Step 1); 35 cycles of 30 secs at 94˚C, 30 secs at 60˚C, 3 mins at 68˚C for DNA amplification (Step 2); 5 mins at 72˚C for final extension and inactivation (Step 3).

These different PCR products were then cloned into the pcDNA3.1(+) vector, respectively. For *Flt3* CDS PCR, there is a HindIII restriction site in the 5'-end overhang of the forward primer, and a XhoI restriction site in the 5'-end overhang of the reverse primer. The PCR product was first isolated and purified by gel electrophoresis and gel extraction by using the QIAquick gel extraction kit (#28704, QIAGEN). In brief, the DNA fragment was excised and dissolved by using buffer containing sodium iodide at 50˚C for 10 mins. Then 1 gel volume isopropanol was added to the dissolved gel to precipitate the DNA. The precipitated DNA was further passed through a column to make the DNA bind to the membrane of the column. The isolated DNA was washed and then eluted from the column by 10mM Tris-HCl buffer. 2μg eluted PCR product was digested by 2 units HindIII (#R0104S, NEB) and 2 units XhoI (#R0146S, NEB) restriction enzymes in NEB buffer 2.1 (#B7202S) at 37˚C for 2 hours. Meanwhile, 2μg pcDNA3.1(+) vector was also digested by 2 units HindIII and 2 units XhoI restriction enzymes in NEB buffer 2.1 at 37˚C for 2 hours. The digested *Flt3* cDNA fragment and the digested pcDNA3.1(+) fragment were then purified by gel electrophoresis and gel extraction as the same procedures as described previously. Finally, the purified *Flt3* cDNA fragment was cloned into the purified pcDNA3.1(+) fragment by using the T4 DNA ligase (#EL0014, ThermoFisher Scientific). In brief, total 100ng *Flt3* cDNA fragment and pcDNA3.1(+) fragment were added together at a 3:1 molar ratio plus 5 units T4 DNA ligase. This mixture was then incubated in the 1×reaction buffer for 15 mins at room temperature.

2μl from the 20μl ligation product was then used to transform to the DH5α competent cells (#18258012, ThermoFisher Scientific). In brief, 2μl ligation product was incubated with 50μl DH5α competent cells for 30 mins on ice. The cells were then heat-shocked for 45 secs in a 42˚C water bath and quickly chilled on ice for 2 mins. 0.9ml S.O.C. medium (#15544-034, ThermoFisher Scientific) was then added to the transformed cells for a 1 hour incubation in a shaker with a speed of 225 rpm and at 37˚C. The cells were then collected, resuspended, and spread on a LB plate with 100μg/ml ampicillin (#400-110-IG, WISENT BIOPRODUCTS) for an overnight incubation at 37˚C.

On the next day, several clones were picked from the LB plate and each clone was grown overnight in 6ml LB medium with 100μg/ml ampicillin in a shaker at 37˚C and with a speed of 225 rpm.

On day 3, the cells were collected and the plasmids were isolated from the cells by using the QIAprep spin miniprep kit (#27106, QIAGEN). In brief, the collected cells were first resuspended in 250μl buffer P1, and then mixed with the same volume of buffer P2 to completely lyse the cells. 350μl buffer N3 was added to the lysed cells to denature and precipitate the proteins in the lysate. The supernatant was collected after a centrifugation at maximum speed for 10 mins, and then passed through a column to make the plasmids bind to the membrane of the column. The plasmids were then washed by buffer PE and eluted from the membrane by using the 10mM Tris-HCl buffer. The concentration of the plasmid was then quantified by Nanodrop 2000. 1μg plasmid was sent to the sequencing department of IRCM to verify the sequence. The sequences of sequencing primers are listed in Table 3.2.

For the cloning of *Cbl-b* and *C-cbl* expression constructs, the basic procedures were the same as the way of making the *Flt3* expression construct. The major differences are the choices of the cloning sites. For *Cbl-b* expression vector, NheI and XhoI were chosen as the 5'-end overhang cloning sites of forward and reverse primers respectively. For *C-cbl* expression vector, the same cloning sites were chosen as *Cbl-b* expression vector. The sequences of sequencing primers are listed in Table 3.2 also.

Gene Name	NM number	Sequence
Flt3	NM_010229.2	Fwd: ATCAAGCTTATGCGGGCGTTGGCGCA
		Rvs: ATCCTCGAGCTAACTTCTTTCTCCGTGAAT
		CMV Fwd: CGCAAATGGGCGGTAGGCGTG
		Seq1: CACCAAGCTGTTCACCATAG
		Seq2: GGTGTCGAGCAGTACTCTAA
		Seq3: GCAGAAGAAGAGGAGGAAGA
Cbl-b	NM_001033238.1	Fwd: ATCGCTAGCATGGCAAATTCTATGAATGGC
		Rvs: ATCCTCGAGCTATAGATTCAGACGTGGGG
		CMV Fwd: CGCAAATGGGCGGTAGGCGTG
		Seq1: GAATTGGAACTTCTTGGCTGT
		Seq2: CCGCCTAGATCTCATTCAGA
		Seq3: TTTGATGCTCTCCCTCCATC
C-cbl	NM_007619.2	Fwd: ATCGCTAGCATGGCCGGCAACGTGAAGAAGA
		Rvs: ATCCTCGAGCTAGGTGGCTACGTGAGCAGGA
		CMV Fwd: CGCAAATGGGCGGTAGGCGTG
		Seq1: CATGGCTCTGAAGTCCACTA
		Seq2: AAAGGCCTTCCTCTCCATTC
		Seq3: GCTGTACCTATGAAGCGATG

Table. 3.2. The sequences of cloning and sequencing primers.

III.5. Flow cytometry

Single cell suspensions were prepared from spleen, lymph nodes, or bone marrow by passing through 70μM nylon cell strainers (#352350, BD Biosciences). Erythrocytes were lysed with ACK lysing buffer (#10-548E, LONZA). Cells were incubated with appropriate antibodies labeled with fluorescence in FACS buffer (1% BSA and 0.05% sodium azide in 1×PBS) with a concentration of 2.5ng/μl for 30 mins at 4°C in the dark. After washes with FACS buffer, the stained cells were subsequently analyzed using the CyAn ADP analyzer (Beckman Coulter), or Fortessa analyzer (BD ebioscience). Acquired flow cytometry data were further analyzed with Flowjo software Version 9 (Tree Star Inc).

Intracellular staining of Foxp3 was performed following the instruction of Foxp3/Transcription Factor Staining Buffer Set (#00-5523-00, ebioscience). In brief, the single cell suspensions were first stained with cell surface markers. After twice washes by FACS buffer, the cells were fixed in the Foxp3 fixation/permeabilization working solution for 30-60 mins at 4°C in the dark. The fixed cells were then washed by using 1×permeabilization buffer twice and incubate with anti-Foxp3

antibody (2.5ng/μl) in the 1×permeabilization buffer for 30 mins at room temperature in the dark. After washes with FACS buffer, the stained cells were subsequently analyzed using the CyAn ADP analyzer, or Fortessa analyzer. Acquired flow cytometry data were further analyzed with Flowjo software Version 9.

Intracellular staining of BrdU was performed following the instruction of BD Pharmingen™ BrdU Flow Kits (#559619, BD Biosciences). In brief, on day 6 of FLT3L culture, the DCs were pulsed by 10μM BrdU for overnight culture at 37˚C and 5% CO_2. The pulsed cells were then stained with cell surface markers following the same procedures as mentioned before. The stained cells were then fixed in 1×BD cytofix/cytoperm buffer for 15-30 mins on ice and washed twice by 1×BD perm/wash buffer. The fixed cells were then further incubated with BD cytoperm permeabilization buffer plus for a second fixation about 10 mins on ice. These cells then had a third fixation step for 5 mins on ice by using the 1×BD cytofix/cytoperm buffer. After three steps of fixation, the fixed cells were then treated with DNase I (300μg/ml) in 1×PBS for 1 hour at 37°C to expose the incorporated BrdU. After wash twice with BD perm/wash buffer, the cells were then resuspended in BD perm/wash buffer with anti-BrdU antibody (2.5ng/μl) for 20 mins at room temperature in the dark. After washes with FACS buffer, the stained cells were subsequently analyzed using the CyAn ADP analyzer, or Fortessa analyzer. Acquired flow cytometry data were analyzed further with Flowjo software Version 9.

III.6. Enrichment of splenic DCs and liver DCs

To purify splenic DCs, single cell suspensions from spleens were washed and lysed with ACK lysing buffer (#10-548E, LONZA) to remove the erythrocytes. Then the splenic DCs were resuspended in PBS supplied with 2% FBS. The resuspended splenic DCs were first enriched by depleting T cells, B cells, NK cells, and macrophages by using EasySep™ Mouse Pan-DC Enrichment Kit (#19763, STEMCELL Technologies). In brief, the single cell suspension was prepared in a concentration of 1×10^8 cells/ml. For every 100 million cells, 50μl enrichment cocktail antibodies were added to the sample and incubated for 15 mins at 4°C. After labeling, the extra antibodies were removed through centrifugation and the cell pellet was resuspended in the same volume of 1×resuspension buffer (1× PBS + 2% FBS) and incubated with 100μl biotin selection cocktail antibodies for 10 mins at 4°C. 75μl well mixed magnetic particles were then

added to the sample and incubated for 10 mins at 4°C. Then 1×resuspension buffer was added to the sample topping up to 2.5ml. The tube was then placed into the magnet and incubated for 5 mins at room temperature. The tube was then removed from the magnet and the enriched unlabeled cell suspension was transferred to a new tube.

The enriched DCs were then stained with anti-mouse MHCII (AF6-120.1 or M5/114.15.2), anti-mouse CD11c (N418), anti-mouse CD317 (eBio927), anti-mouse CD11b (M1/70) and anti-mouse CD8α (53-6.7) for subsequent sorting of pDC subset ($MHCII^{int}CD11c^{int}CD317^{+}$), $CD8\alpha^{+}$ cDC subset ($MHCII^{+}CD11c^{+}CD8\alpha^{+}CD11b^{-}$), and $CD11b^{+}$ cDC subset ($MHCII^{+}CD11c^{+}CD8\alpha^{-}CD11b^{+}$). Finally, these pure DC subsets were sorted by AriaII (BD ebioscience).

To purify liver DCs, the blood of the sacrificed mice was first removed. Then the fresh isolated liver was rinsed with PBS to remove the blood residual. The rinsed liver was further homogenized to make single cell suspension by passing 70μM nylon cell strainers (#352350, BD Biosciences). Then the single cell suspension was incubated with the digestion buffer (RPMI 1640 (#21870-076, ThermoFisher Scientific) supplied with 0.1mg/ml collagenase D (#11088866001, Roche) and 0.01mg/ml DNase I (#10104159001, Roche)) at 37°C for 40mins with rotation. After digestion, the cells were collected by centrifugation and resuspended in 10ml 1×PBS. Then 5ml Percoll (#17-0891-02, GE Healthcare Life Sciences) was mixed with the sample. Mononuclear cells were collected by centrifugation at 2000rpm for 20mins at room temperature. The enriched mononuclear cells were then lysed with ACK lysing buffer to remove the erythrocytes. The rest of the cells were further stained with anti-mouse MHCII (AF6-120.1 or M5/114.15.2), anti-mouse CD11c (N418), anti-mouse CD11b (M1/70), and anti-mouse CD103 (2E7) for subsequent sorting of $CD103^{+}$ cDC subset ($MHCII^{+}CD11c^{+}CD103^{+}CD11b^{-}$), and $CD11b^{+}$ cDC subset ($MHCII^{+}CD11c^{+}CD103^{-}CD11b^{+}$). Finally, pure DC subsets were sorted by AriaII (BD ebioscience).

III.7. *In vitro* generation of FLT3L-derived BMDC and GM-CSF-derived BMDC

For the generation of FLT3L-derived BMDC, the BM single cell suspensions were prepared as follow. In brief, the mice femora and tibiae were cut out and the muscles were removed. The bone marrow cells were flushed out through the end of the bone with RPMI culture medium by using a 1ml syringe with a 26-gauge needle. The cells were then collected by centrifugation and the red

blood cells were removed by ACK lysing buffer. The bone marrow cells were seeded at a concentration of 1×10^6 cells/ml and cultured in 10% FLT3L conditional medium at 37°C and 5% CO_2 for 7-9 days. The mature FLT3L-derived BMDCs were then used for other experiments such as FACS analysis, sorting, and cytokine production, etc. The FLT3L conditional medium stock was obtained from the supernatant of the FLT3L-secreting B16 melanoma cell culture. The FLT3L conditional medium stock was further diluted by RPMI culture medium to 10% when it was used for bone marrow cells culture.

For the generation of GM-CSF-derived BMDC, the BM single cell suspensions were prepared the same way as described before. Then the red blood cells were removed by ACK lysing buffer. The bone marrow cells were seeded at a concentration of 1×10^6 cells/ml and cultured in 10% GM-CSF conditional medium at 37°C and 5% CO_2 for 9 days. The medium was changed to 10% fresh GM-CSF conditional medium every three days. The mature GM-CSF-derived BMDCs were then used for other experiments such as LPS stimulation and FACS analysis. For the LPS stimulation experiment, 1×10^6 mature GM-CSF-derived BMDCs were activated by 100ng/ml LPS for overnight at 37°C and 5% CO_2. On day 2, the cells were collected and analyzed the surface expression of co-stimulatory molecules by FACS. The GM-CSF conditional medium stock was obtained from the supernatant of the culture of J588 GM-CSF-secreting myeloma cell line. The GM-CSF conditional medium stock was further diluted by RPMI culture medium to 10% when it was used for bone marrow cells culture.

III.8. Cytokine ELISA (enzyme-linked immunosorbent assay)

To measure the cytokine concentration in the mice serum, 50μl serum from each mouse was first collected. In brief, 4-5 drops of blood were collected by cheek bleeding, and rested for 15 mins at room temperature. The coagulated blood was centrifuged at 5000 rpm for 10 mins at room temperature. The serum supernatant was transferred to a new tube for further measurement of cytokine concentration by using the ELISA method.

ELISA kits for IL-6 (#88-7064-22), IL-12 p70 (#88-7121-22), and TNF-α (#88-7324-22) were purchased from eBiosciences, USA. The assays were performed as described by the manufacturer. In brief, the Nunc Maxisorp ELISA plate was coated with 100μl/well of capture antibody in

1×coating buffer (1:250 dilution). The plate was sealed and incubated overnight at 4°C. On day 2, the capture antibody was aspirated and the well was washed 3 times with wash buffer (0.05% Tween-20 in 1× PBS). The well was then blocked with 200μl/well of 1×ELISA/ELISPOT diluent for 1 hour at room temperature. The blocking buffer was then aspirated and 100μl diluted serum sample was added to each well. Meanwhile, the 2-fold serial diluted standard cytokines were also added to the well to make a standard curve of total 8 wells. All the dilutions were made by using 1×ELISA/ELISPOT diluent. The plate was sealed and incubated at room temperature for overnight at 4°C. On day 3, the sample was aspirated and the well was washed by wash buffer for 3-5 times. Then 100μl detection antibody diluted in 1×ELISA/ELISPOT diluent (1:250 dilution) was added to each well and incubated for 1 hour at room temperature. The detection antibody was then aspirated and the well was washed by wash buffer for 3-5 times. Then 100μl Avidin-HRP diluted in 1×ELISA/ELISPOT diluent (1:250 dilution) was added to each well and incubated for 30 mins at room temperature. The Avidin-HRP was then aspirated and the well was washed by wash buffer for 5-7 times. Then 100μl 1×TMB substrate solution was added to each well and incubated at room temperature for 15 mins. Then 50μl stop solution was added to each well to terminate the reaction. Finally, the absorbance of plate was read at 450nm and 570nm. The value of 570nm was subtracted from the value of 450nm.

To measure the cytokine production of DCs, 1×10^5 cells or 0.5×10^5 cells (dependent on different experiments) were cultured in flat-bottomed 96-well plate for overnight culture with or without stimulus. For the IL-12 production experiment, 1×10^5 sorted splenic CD8α^+ cDCs were seeded in 96-well plate and stimulated by 5μM CpG (#ODN 1826, InvivoGen) or without stimulation for overnight at 37°C, 5% CO_2. For the TNF-α and IL-6 production experiment, 0.5×10^5 sorted splenic CD8α^+ cDCs were seeded in 96-well plate and stimulated by 5μM CpG or without stimulation. On day 2, the culture supernatants were collected and the concentration of TNF-α and IL-6 were measured by using the same ELISA kits and methods as the serum samples.

III.9. Reverse transcription/quantitative polymerase chain reaction (RT/qPCR)

Total RNA from different types of cells or tissues were extracted by using RNeasy Mini Kit (#74104, Qiagen) and then reverse transcribed with SuperScriptII Reverse Transcriptase (#18064-

014, ThermoFisher Scientific) and together with Oligo(dT)$_{12-18}$ primer (#18418-012, ThermoFisher Scientific). For the RNA purification and cDNA generation procedures, they are the same as described in the plasmid and cloning section. For RNA purification from the liver tissue, it was also followed by the protocol provided by the RNeasy Mini Kit. In brief, 20-30mg liver tissue was excised and homogenized in 600µl lysis buffer RLT. The lysate was then cleared by centrifugation at full speed to remove the tissue pellet. 1 volume of 70% ethanol was then added to the cleared lysate to precipitate the RNA and the mix was transferred to the RNeasy spin column including any precipitation. The mix was passed through the membrane of the column through centrifugation to let the RNA bind to the membrane. The membrane was then washed by buffer RW1 and buffer RPE respectively. Finally, the RNA was eluted from the membrane by using RNase-free water and quantified by Nanodrop 2000 as described previously. The purified RNA was then used as template for further cDNA generation by using the same SuperScript^{TM} II reverse transcriptase kit, Oligo(dT)$_{12-18}$ primer, and method as mentioned before.

For each qPCR reaction, 10-50ng cDNA, 10µl dye SYBR (#4472903, ThermoFisher Scientific), and 400nM primers were mixed together in a total 20µl reaction system. The primer sequences are listed in the following table. (Table 3.3.) The qPCR program was as follows: 2 mins at 50°C (Step 1), 2 mins at 95°C (Step 2), 40 cycles of 15 secs at 95°C and 1 min at 60°C. The reactions were performed by the machine ViiA7-96 (ThermoFisher Scientific). β-actin, and Glyceraldehyde-3-phosphate dehydrogenase (GAPDH) mRNA level was used as internal controls depending on different experiments.

III.10. Immunoblotting and immunoprecipitation

For immunoblotting, each 1×10^6 sorted primary splenic DC subsets, FLT3L-cultred BMDC subsets, or transfected 293T cells were lysed in 30µl RIPA buffer (25mM Tris pH8.0, 150mM NaCl, 1% NP-40, 1% sodium deoxycholate, 0.1% SDS) supplemented with protease and phosphatase inhibitors (#11836153001, Complete^{TM} Protease Inhibitor Cocktail and #04906837001, PhosSTOP Phosphatase Inhibitor Cocktail, Roche) on ice for 20 mins. The lysate supernatant was then collected by full speed centrifugation for 10 mins. For every 30µl lysate, 6µl 6×laemmli sampling buffer (12% SDS, 30% 2-mercaptoethanol, 60% glycerol, 0.012%

bromophenol blue, 0.375M Tris-HCl, pH=6.8) was added to the lysate and the mix was incubated at 100°C for 5 mins to denature the proteins.

Gene Name	NM number	Sequence
Tnf-α	NM_001278601.1	Fwd: AATTCGAGTGACAAGCCTGTAG
		Rvs: TTGAGATCCATGCCGTTGG
Il-6	NM_001314054.1	Fwd: TTCACAAGTCGGAGGCTTAAT
		Rvs: AAGTGCATCATCGTTGTTCATAC
Cxcr4	NM_009911.3	Fwd: CTGTAGAGCGAGTGTTGCC
		Rvs: CAATCCATTGCCGACTATGC
Ccr5	NM_009917.5	Fwd: CCAGCAAGACAATCCTGATC
		Rvs: AACCATTCCTACTCCCAAGC
Ccl2	NM_011333.3	Fwd: GTTGGCTCAGCCAGATGCA
		Rvs: AGCCTACTCATTGGGATCATC
Actb	NM_007393.5	Fwd: CGATGCCCTGAGGCTCTTT
		Rvs: TGGATGCCACAGGATTCCA
Gapdh	NM_001289726.1	Fwd: TCGTCCCGTAGACAAAATGGT
		Rvs: CGCCAAATACGGCCAAA

Table. 3.3. The qPCR primer sequences.

The denatured lysates were resolved on 10% SDS-PAGE gel plus 6% stacking gel. The recipe of 10% SDS-PAGE gel was 3.2ml H_2O, 2.67ml 30% acrylamide (#161-0156, Bio-rad), 2ml 1.5M Tris pH8.8 (#161-0798, Bio-rad), 80µl 10% SDS (#71736-500ML, Sigma), 80µl 10% ammonium persulfate (APS) (#161-0700, Bio-rad), 8µl TEMED (#161-0801, Bio-rad). The recipe of 6% stacking gel was 2.6ml H_2O, 1ml 30% acrylamide, 1.25ml 0.5M Tris pH6.8 (#161-0799, Bio-rad), 50µl 10% SDS, 50µl 10% APS, 5µl TEMED. The lysate from 1×10^6 cells was then loaded on the gel and gel was run in the running buffer (25mM Tris base, 190mM glycine, 0.1% SDS, pH=8.3) at 90V until the sample accumulate at the border between stacking gel and the SDS-PAGE gel, and another 2 hours running at 120V to separate the proteins based on their molecular weight. The Kaleidoscope protein ladder (#1610395, Bio-rad) was used to label the molecular weight.

Proteins on the gels were then transferred to a PVDF membrane (#IPVH00010, EMD Millipore). In brief, the PVDF membrane was first activated by rinsing at 100% methanol for 1 min. The gel/membrane were stacked between filter paper and sponge and run in the transfer buffer (25mM Tris base, 190mM glycine, 20% methanol, pH=8.3) for 2 hours at 30V.

The membrane was then rinsed in Tris-buffered saline with tween-20 (TBST) buffer (20mM Tris, 150mM NaCl, 0.1% tween-20) for 5 mins. After rinsing, the membrane was blocked by blocking buffer (5% milk (#1706404XTU, Bio-rad) in TBST) for 1 hour at room temperature with shaking. After blocking, the membrane was blotted with different primary antibodies (1:1000 dilution) in the blocking buffer for overnight at 4°C. On day 2, the primary antibody was discarded and the membrane was washed by TBST for 3 times, 10 mins each time. The membrane was further blotted with secondary antibodies (1:10000 dilution) in the blocking buffer for 1 hour at room temperature. After incubation with secondary antibodies, the membrane was washed by TBST for 3 times, 10 mins each time. Finally, the membrane was developed by the ECL^{TM} Prime Western Blotting Detection Reagent (#RPN2232, GE Healthcare) at room temperature for 3 mins. The signals on the membrane were exposed to the high performance chemiluminescence films (#28906839, GE healthcare life sciences).

For immunoprecipitation, 1×10^6 CD24$^+$ FLT3L-cultured BMDCs were lysed in 500µl 1× TNE buffer (1% NP40, 50mM Tris pH8.0, 2mM EDTA) supplemented with protease and phosphatase inhibitors, and the lysate was prepared the same way as described before. The lysate was then incubated with 2µg rabbit anti-FLT3/CD135 antibody at 4°C for overnight with rotation. On day 2, 20µl Protein A agarose beads (#9863, Cell Signaling Technology) were added to the lysate and incubated for 2hs at 4°C with rotation. Two hours later, the beads were collected by centrifugation at 10000 rpm for 1 min. The beads were then washed by 1×TNE buffer supplemented with protease and phosphatase inhibitors for 5 times. The beads pellet was then resuspended by 20µl 3×SDS sampling buffer (6% SDS, 15% 2-mercaptoethanol, 30% glycerol, 0.006% bromophenol blue, 0.185M Tris-HCl, pH=6.8) and incubated at 100°C for 5 mins. Finally, the supernatant was collected by centrifugation for 1 min at 14000 rpm.

The supernatant was then loaded and run on a 10% SDS-PAGE gel and 6% stacking gel the same way as mentioned before. The proteins were then transferred to a PVDF membrane and blotted with primary antibody (1:1000 dilution) at 4°C for overnight with shaking also as mentioned before. The membrane was then washed and blotted with HRP-conjugated secondary antibody (1:10000 dilution) following the same procedures. Finally, the membrane was washed and developed by the ECL^{TM} Prime Western Blotting Detection Reagent at room temperature for

3 mins. The signals on the membrane were exposed to the high performance chemiluminescence films.

III.11. Generation of bone marrow chimeras

8 to 10-week-old B6.SJL background ($CD45.1^+$) mice were lethally irradiated at the dose of 9.5Gy. On the next day, these mice will receive a total 2×10^6 bone marrow cells in a 1:1 ratio from B6.SJL ($CD45.1^+$) mice together with WT or *Cbl* dKO C57BL/6J background ($CD45.2^+$) mice. Based on the literature, by day 21 after bone marrow transplantation, a complete reconstitution of peripheral blood has been discovered, although many of these innate cellular effectors are not yet fully functional[297, 298]. Therefore, one month after BM reconstitution, the spleen cells of the recipients were used for analysis by FACS.

III.12. Antigen presentation assay

OVA-specific OTI^+ T cells and $OTII^+$ T cells were purified from the spleens of OTI mice and OTII mice respectively by using the EasySepTM Mouse $CD8^+$ T cell enrichment kit (#19753, STEMCELL Technologies) and Mouse $CD4^+$ T cell enrichment kit (#19752, STEMCELL Technologies) respectively. In brief, for OTI^+ T cell purification, the spleen from the OTI mice was first excised and homogenized into single cell suspension by passing through the 70μm strainer. The cells were collected by centrifugation and resuspended to 1×10^8 cells/ml. For every 1×10^8 cells, 50μl enrichment cocktail was added to the sample and the mix was incubated at 4°C for 15 mins. Then 100μl selection cocktail was added to the sample and the mix was incubated at 4°C for another 15 mins. Then 100μl magnetic particles were added to the sample and the mix was incubated at 4°C for 5 mins. The 1×resuspension buffer was added to the sample to top up to 2.5ml. The tube was then placed into a magnet and incubated at room temperature for 5 mins. The enriched OTI^+ T cells were then poured out into a new tube and then collected by centrifugation. For $OTII^+$ T cells purification, the spleen from the OTII mice was first excised and homogenized into single cell suspension by passing through the 70μm strainer. The rest procedures are the same as OTI^+ T cell purification.

The purified OTI^+ T cells and $OTII^+$ T cells were counted and labeled with cell proliferation dye eFluor 450 (dye e450, #65-0842-85, ebioscience). In brief, for every 1×10^6 cells, the cells were

resuspended in 1ml 1×PBS, and incubated with 5μM dye e450 for 20 mins at 37°C, protected from light. Then 5 volumes of pre-chilled RPMI complete medium were added to stop the labeling reaction for 5 mins on ice. Then the cells were collected by centrifugation and resuspended in RPMI complete culture medium.

For antigen presentation assay, 5×10^4 dye e450 labeled OTI^+ or $OTII^+$ T cells were incubated with 40μg/ml OVA (#9006-59-1, InvivoGen) and together with graded doses of sorted splenic $CD8\alpha^+$ cDC subset in a U-bottom 96-well plate for 3-4 days. For OTI^+ T cells, 3 days after activation, the proliferation of T cells was evaluated by dye e450 dilution and staining with mAb to Vα2 and Vβ5. For $OTII^+$ T cells, 4 days after activation, the proliferation of T cells was evaluated by dye e450 dilution and staining with mAb to Vα2 and Vβ5.

III.13. DAPI staining

1×10^6 FLT3L-cultured BMDCs were first collected between day 7-9 and stained with surface antibodies following the procedures as described in Flow cytometry method section. The cells were then fixed by using the Foxp3/Transcription Factor Staining Buffer Set (#00-5523-00, ebioscience) and following the same procedures as described in Flow cytometry method section. After fixation, the cells were then incubated with 1×PBS to rehydrate for 15 mins at room temperature. The DAPI (4', 6-Diamidino-2-Phenylindole, Dilactate, #422801, Biolegend) was then diluted to 3μM in the 1× Foxp3 permeabilization buffer (#421402, Biolegend) to make a DAPI staining solution. The fixed cells were then resuspended in 1ml DAPI staining solution and incubated for 15 mins at room temperature. The sample was then analyzed by flow cytometry following the same procedures as described in Flow cytometry method section.

III.14. Cellularity analysis

For the cellularity analysis of the SP in WT and *Cbl* dKO mice, the splenocyte single cell suspention was prepared as described in previous sections. The splenocyte cell number was counted and the cells were then stained with different antibodies to distinguish different cell populations: T cells ($TCR\beta^+$), CD4 T cells ($TCR\beta^+CD4^+$), CD4 T effector/memory cells ($TCR\beta^+CD4^+CD44^+$), CD8 T cells ($TCR\beta^+CD8^+$), CD8 T effector/memory cells ($TCR\beta^+CD8^+CD44^+$), B cells ($B220^+$), GC B cells ($B220^+GL7^+FAS^+$), monocytes

($LY6C^{hi}CD11B^{+}$), granulocytes ($LY6C^{+}CD11B^{hi}$), and macrophages ($CD11B^{+}F4/80^{+}$). For the cellularity analysis of the liver in WT and *Cbl* dKO mice, the liver mononuclear cells were purified as described in the previous sections. The liver mononuclear cell number was counted and the cells were then stained and analyzed by the same way as spleen cellularity analysis.

For the cellularity analysis of the SP in *Rag1* KO and *Cbl* tKO mice, the splenocyte single cell suspention was prepared as described in previous sections. The splenocyte cell number was counted and the cells were then stained with different antibodies to distinguish different cell populations: cDCs ($MHCII^{+}CD11C^{+}$), $CD8\alpha^{+}$ cDCs ($MHCII^{+}CD11C^{+}CD8\alpha^{+}$), $CD11B^{+}$ cDCs ($MHCII^{+}CD11C^{+}CD11B^{+}$), pDCs ($Lin^{-}(CD3^{-}CD19^{-}TER119^{-}NK1.1^{-})PDCA\text{-}1^{+}CD11C^{+}$), monocytes ($LY6C^{hi}CD11B^{+}$), granulocytes ($LY6C^{+}CD11B^{hi}$), macrophages ($CD11B^{+}F4/80^{+}$), and NK cells ($NK1.1^{+}CD3e^{-}$). For the cellularity analysis of the liver in *Rag1* KO and *Cbl* tKO mice, the liver mononuclear cells were purified as described in the previous sections. The liver mononuclear cell number was counted and the cells were then stained and analyzed by the same way as spleen cellularity analysis.

III.15. Rapamycin treatment

For the *in vitro* rapamycin (#R-5000, LC Laboratories) treatment, on day 3 of FLT3L BMDC culture, different concentrations of rapamycin (0.5ng/ml to 10ng/ml) was added into the culture medium until day 7 when the cells were collected for flow cytometry analysis.

For the short-term *in vivo* rapamycin treatment, the rapamycin was first dissolved in the injection buffer (5% DMSO, 10% ethanol in 1×PBS). Then 10-week-old mice were injected i.p. (intraperitoneally) with or without 30μg rapamycin per day for 7 consecutive days.

For the long-term *in vivo* rapamycin treatment, 90-day-old *Cbl* tKO mice were injected i.p. with or without rapamycin (300μg/week, 3 times/week) for 45 days to analyze the progression of the disease or until they die to draw the survival curve.

III.16. Degradation and downmodulation assay

2μg pcDNA-*Flt3* plasmid was co-transfected with 2μg pcDNA empty vector, 2μg pcDNA-*Cbl-b* plasmid or 2μg pcDNA-*C-cbl* plasmid to 293T cells by calcium transfection method. In brief, on day 1, 1×10^6 293T cells /well were seeded in the 6-well plate. On day 2, the transfection medium was prepared as follow. For each well, 4μg plasmid DNA (for example, 2μg pcDNA-*Flt3* plasmid plus 2μg pcDNA empty vector) was mixed with 9.4μl 2M $CaCl_2$ and H_2O up to a total volume of 75μl. Then the mixture was added dropwise to 75μl 2×HBS buffer (1% HEPES, 0.07% KCl, 1.6% NaCl, 0.025% Na_2HPO_4, pH=7.05). Total 150μl transfection medium was then added to the culture medium. On day 3, the medium was removed and fresh DMEM culture medium was added to the cells. 48 hours later, the transfected cells are treated with FLT3L (100ng/ml) or without, and blocked with or without either proteasome inhibitor 10μM MG132 (#2194, Cell Signaling Technology) or 50μM lysosome inhibitor chloroquine (#14774, Cell Signaling Technology) for 2 hours at 37°C and 5% CO_2. During this process, the protein synthesis was also blocked by 100μg/ml Cycloheximide (#2112, Cell Signaling Technology).

Two hours later, the cells were collected and 10% of the cells were used for downmodulation assay by examining the surface FLT3 expression level through FACS analysis. The rest 90% of the cells were used for degradation assay by using western blot to test the protein level of FLT3. In brief, the cells were collected and lysed in 100μl RIPA buffer supplemented with protease and phosphatase inhibitors. The lysate preparation and denaturation were followed the same procedures as described in section III.10 “Immunoblotting and immunoprecipitation”. 30μl lysate was then loaded and run on a SDS-gel, and transferred to a PVDF membrane also following the same procedures as described in section III.10 “Immunoblotting and immunoprecipitation”. The membrane was then blocked by blocking buffer and immunoblotted by anti-mouse FLT3/CD135 antibody (1:1000 dilution, #ab33092, abcam) for overnight at 4°C. On the next day, the membrane was washed by TBST and incubated with the Protein A HRP Linked Ab (1:10000 dilution, #GENA9120, GE Healthcare) for 1 hour at room temperature. Then the membrane was washed by TBST and developed by the ECL™ Prime Western Blotting Detection Reagent following the same procedures as described before.

III.17. Ubiquitination detection assay

2μg pcDNA-*Flt*3 plasmid and 2μg pcDNA-HA-Ub plasmid were co-transfected with 2μg pcDNA empty vector, 2μg pcDNA-*Cbl-b* plasmid or 2μg pcDNA-*C-cbl* plasmid to 293T cells by calcium transfection method as mentioned in the previous section. In brief, on day 1, 1×10^6 293T cells were seeded in the 6-well plate. On day 2, the transfection medium was prepared as follow. For each well, 6μg plasmid DNA (for example, 2μg pcDNA-*Flt3* plasmid, 2μg pcDNA empty vector, and plus 2μg pcDNA-HA-Ub plasmid) was mixed with 14.1μl 2M $CaCl_2$ and H_2O up to a total volume of 112.5μl. Then the mixture was added dropwise to 112.5μl 2×HBS buffer. Total 225μl transfection medium was then added to the culture medium. On day 3, the medium was changed to fresh DMEM culture medium. 36 hours later, the transfected cells were collected and incubated with 100μg/ml Cycloheximide, and together with either 10μM MG132 or 50μM lysosome inhibitor chloroquine for 30 mins at 37°C heat block. Then the cells were treated with FLT3L (100ng/ml) or without for additional 15 mins at 37°C heat block.

The cells were then collected, and lysed in 500μl 1×TNE buffer. 10% of the lysate was heated and denatured in 1×laemmli sampling buffer at 100°C for 5 mins to be used as total lysate control. The other 90% of the lysate was immunoprecipitated with 2μg rabbit anti-FLT3/CD135 antibody at 4°C for overnight with rotation. On day 2, 20μl Protein A agarose beads were added to the lysate and incubated for 2 hours at 4°C with rotation. Two hours later, the beads were collected by centrifugation at 10000 rpm for 1 min. The beads were then washed by 1×TNE buffer supplemented with protease and phosphatase inhibitors for 5 times. The beads pellet was then resuspended by 20μl 3×SDS sampling buffer and incubated at 100°C for 5 mins. 20μl lysate was then loaded and run on a SDS-gel, and transferred to a PVDF membrane following the procedures as described in section III.10 “Immunoblotting and immunoprecipitation”. Finally, the supernatant was collected by centrifugation for 1 min at 14000 rpm. The membrane was then blocked by blocking buffer and immunoblotted by anti-HA-probe antibody (1:1000 dilution, #sc-805, Santa Cruz) for overnight at 4°C. On the next day, the membrane was washed by TBST and incubated with the Protein A HRP Linked Ab for 1 hour at room temperature. Then the membrane was washed by TBST and developed by the ECL™ Prime Western Blotting Detection Reagent following the same procedures as described before.

III.18. Anti-nuclear autoantibody detection

Kallestad HEp-2 Kit (#32583, Bio-rad) was used to detect the anti-nuclear antigen autoantibodies in the serum of WT and *Cbl* dKO mice. In brief, the mouse blood was collected by cheek bleeding, and the serum was prepared following the same procedures as mentioned in the section III.8. Then the serum was diluted 1:100 in 1×PBS and 50μl diluted serum was incubated with the slide coupled with HEp-2 substrate for 30 mins at room temperature. The slide was then washed by 1×PBS, and incubated with FITC conjugated anti-mouse IgG (1:500 dilution, #11-4011, eBioscience) at room temperature for 30mins. The slide was then washed by 1×PBS for three times. Finally, the samples were observed by fluorescent microscope (Axiophot, Zeiss). The normal human serum and human serum with a specific autoantibody activity provided in the same kit were used as positive control and negative control. In brief, 50μl the positive control serum and the negative control serum were also incubated with the slide coupled with HEp-2 substrate for 30 mins at room temperature. The slide was then washed by 1×PBS, and incubated with the provided FITC conjugated antiserum to human immunoglobulins at room temperature for 30mins. Finally, the samples were observed by fluorescent microscope.

III.19. Screen of mouse serum cytokines and chemokines

The screen of mouse serum cytokines and chemokines was carried out by using the mouse cytokine array panel A kit (#ARY006, R&D). In brief, the pooled serum from 3 sick *Cbl* tKO mice and other 3 age-matched *Rag1*$^{-/-}$ mice were collected respectively. The way of serum collection was described previously. Following the manual, the membrane provided in the kit was first blocked by array buffer 6 for 1 hour at room temperature on a rocking platform shaker, and then incubated with premixed serum/detection antibody cocktail mix (500μl serum, 500μl array buffer 4, 500μl array buffer 6, and 15μl reconstituted Mouse Cytokine Array Panel A Dection Antibody Cocktail) for overnight at 4°C on a rocking platform shaker. On day 2, the serum/antibody mix was removed and the membrane was washed twice by 1×Wash Buffer for 10 mins at room temperature on a rocking platform shaker. Then the membrane was further incubated with diluted streptavidin-HRP for 30mins at room temperature on a rocking platform shaker. After twice wash by 1×Wash Buffer, the membrane was developed by Chemi Reagent Mix for 1 min, and exposed to X-ray film for 1-10 mins.

III.20. RNA-Seq experiment

The splenic DCs from WT mice and *Cbl* dKO mice were collected and enriched as described before. In brief, the splenic cells from 10 mice of each genotype were made single cell suspension and enriched by the EasySep^{TM} Mouse Pan-DC Enrichment Kit. The CD8α^+ cDCs (MHCII$^+$CD11C$^+$CD8α^+) and CD11B$^+$ cDCs (MHCII$^+$CD11C$^+$CD11B$^+$) were then sorted through FACS. The RNA of these cDC subsets was then purified by using the Qiagen RNeasy mini kit as described previously. After washing the membrane of column by buffer RW1, there was an additional step of DNase digestion to clean up the RNA. In brief, add 80μl DNase I (10μl DNase I stock solution plus 70μl Buffer RDD) to the membrane and incubate at room temperature for 15 mins. Then the membrane was washed by 350μl RW1 and the RNA was eluted by RNase-free water. Finally, the RNA was quantified by Nanodrop 2000 and 1μg RNA was used for RNA-Seq experiment.

For the RNA-Seq data analysis, the quality of the data was assessed with FASTQC Version 0.10.1 (http://hannonlab.cshl.edu/fastx_toolkit/). Sequence data were mapped to GRCm38 mouse reference genome with TopHat Version 2.0.13[299]. The raw alignment counts were calculated with featureCounts Version 1.4.6[300]. Normalization of the raw reads counts relative to sequencing depth and calculations of differential gene expression were performed with both DESeq Version 1.10.6 and Cufflinks v2.2.1[301, 302].

III.21. HE staining and Masson staining

Different tissues (spleen, liver, lung, kidney, et al.) were first excised from the mice, and fixed by 4% formaldehyde solution. The fixed tissues were then rinsed with PBS and dehydrated by using ethanol following the sequence: 10 mins of 50% ethanol, 10 mins of 70% ethanol, 10 mins of 80% ethanol, 10 mins of 95% ethanol, 10 mins of 100% ethanol, 10 mins of 100% ethanol, 10 mins of 100% ethanol. Then the ethanol was exchanged with xylene in the following sequence: 10-15 mins of 2:1 ethanol: Xylene, 10-15 mins of 1:1 ethanol: Xylene, 10-15 mins of 1:2 ethanol: Xylene, 10-15 mins of 100% Xylene, 10-15 mins of 100% Xylene, 10-15 mins of 100% Xylene. Then the xylene was exchanged with paraffin in a vacuum oven set for 54-58°C in the following sequence: 30 mins of 2:1 Xylene: Paraffin, 30 mins of 1:1 Xylene: Paraffin, 30 mins of 1:2 Xylene:

Paraffin, 1-2 hours of 100% Paraffin, 1-2 hours of 100% Paraffin. After paraffin exchange, the tissue was finally embedded in fresh new paraffin.

After embedding, the tissue was cut into 5μm section and placed on the slide for HE staining and Masson staining. For HE staining, the sample was first deparaffinised and rehydrated based on the following sequence: 3×3 mins of Xylene, 3×3 mins of 100% ethanol, 1×3 mins of 95% ethanol, 1×3 mins of 80% ethanol, 1×5 mins of deionized H_2O. Then the slide was stained with hematoxylin in the following sequence: 1×3 mins of hematoxylin (#s212A, Poly Scientific), rinsed with deionized water, 1×5 mins tap water to allow stain to develop, 8-12 times of acid ethanol (1ml concentrated HCl + 400ml 70% ethanol) to destain the hematoxylin, 2×1 min of rinse in tap water, 1×2 mins rinse of deionized water. Then the slide was stained with eosin in the following sequence: 1×30 secs Eosin (#s176, Poly Scientific), 3×5 mins of 95% ethanol, 3×5 mins of 100% ethanol, 3×15 mins of Xylene. The slide was then covered by Permount (#SP15-100, ThermoFisher Scientific).

For masson trichrome staining, the sample on the slide was first deparaffinised and rehydrated as described before. The slide was placed in a preheated (56-64°C) Bouin's Fluid for 60 mins followed by a 10 minutes cooling period. The slide was then rinsed in tap water until the section is completely clear. Then the slide was rinsed once in distilled water. Mix of equal parts of Weigert's (A) and Weigert's (B) was used to stain the slide for 5 mins. The slide was then rinsed in running tap water for 2 mins. The slide was then stained with Biebrich Scarlet/ Acid Fuchsin solution for 15 mins and followed by a rinse of distilled water. Differentiate in Phosphomolybdic/Phosphotungstic Acid solution for 10-15 mins until the collagen is not red. Without rinsing, the slide was stained with Aniline Blue Solution to slide for 5-10 mins. The slide was then rinsed once in distilled water, and followed by 1% Acetic Acid Solution destaining for 3-5 mins. The sample was then dehydrated in 2 changes of 95% Alcohol, followed by 2 changes of absolute alcohol. Finally, the slide was cleared in Xylene and mounted.

III.22. Antigen capture assay

$CD24^+$ cDCs ($MHCII^+CD11c^+B220^-CD24^+CD11b^-$) were sorted by FACS as described in previous sections. 0.5×10^6 cells were incubated with 15 μg/ml $Alexa488^+$ OVA antigen (#O34781,

ThermoFisher Scientific) at 4°C or 37°C for 30 mins in RPMI complete culture medium. After incubation, the cells were washed in FACS buffer for twice, and further analyzed through FACS to detect the antigen capture in $CD24^+$ cDCs.

III.23. PMA/ionomycin stimulation and intracellular cytokine staining

Spleen single cell suspensions from WT mice and *Cbl* dKO mice were prepared as described in the previous sections. 5×10^6 cells were seeded in 12-well plate in 1ml RPMI complete culture medium, and stimulated by PMA (20ng/ml, #524400, Calbiochem) and ionomycin (1μg/ml, #407950, Calbiochem) for 6 hours with the blocker brefeldin A (2.5μg/ml, #423303, Biolegend) at 37°C and 5% CO_2. After stimulation, the cells were collected and stained with anti-mouse CD3e (2.5ng/μl), anti-mouse CD8α (2.5ng/μl), and anti-mouse CD4 (2.5ng/μl) for 30 mins on ice as described before. After surface staining, the cells were washed by FACS buffer and fixed in 200μl 4% formaldehyde solution for 30 mins on ice. After fixation, the cells were washed in 1×permeabilization buffer and stained with anti-mouse IL-2 (2.5ng/μl) or anti-mouse IFN-γ (2.5ng/μl) for 30 mins at room temperature in 1×permeabilization buffer. After intracellular staining, the cells were washed in FACS buffer and analyzed further by using the CyAn ADP analyzer, or Fortessa analyzer.

III.24. Statistical analysis

Statistical significance was determined by unpaired t test using Prism software (GraphPad Software Inc). The default setting of this unpaired t test is using the parameter of "Fewer assumptions. Analyze each row individually. Do not assume consistent SD.", and "Correct for multiple comparisons using the Sidak-Bonferroni method". P value of ≤0.05 was considered as statistically significant and labeled "*".

IV. RESULTS

IV.1. Generation of DC-specific *Cbl* dKO mice

As mentioned previously, to generate DC-specific *Cbl* dKO mice, I crossed germline *Cbl-b*$^{-/-}$ mice to the *Cd11c* Cre; *C-cbl*$^{f/f}$ (*C-cbl* KO) mice. To confirm that *Cbl-b* and *C-cbl* were specifically knocked out in DCs of the *Cbl* dKO mice, I sorted out MHCII^{+}CD11C^{+} cDCs, PDCA-1^{+}MHCII^{int} pDCs, B220^{+} B cells, and CD3^{+} T cells from the spleens of both WT and *Cbl* dKO mice by FACS, and did the Western blot analysis to verify the knockout efficiency of CBL-B and C-CBL proteins in these mutant cells. The sorting strategy was shown in Fig. 4.1A to describe how these four cells subsets were sorted. They were MHCII^{+}CD11C^{+} cDCs, PDCA-1^{+}MHCII^{int}CD11C^{int} pDCs, MHCII^{-}CD11C^{-}CD3^{+} T cells, and MHCII^{-}CD11C^{-}B220^{+} B cells (Fig. 4.1A). In all these 4 cell populations, the CBL-B proteins were completely absent because the mutant mice carried a germline *Cbl-b* knockout. However, the C-CBL proteins were only absent in the cDCs and pDCs, but not in the T cells and B cells of the *Cbl* dKO mice. These results indicate that in our *Cbl* dKO mice, *Cbl-b* and *C-cbl* are specifically double knocked out in cDCs and pDCs (Fig. 4.1B).

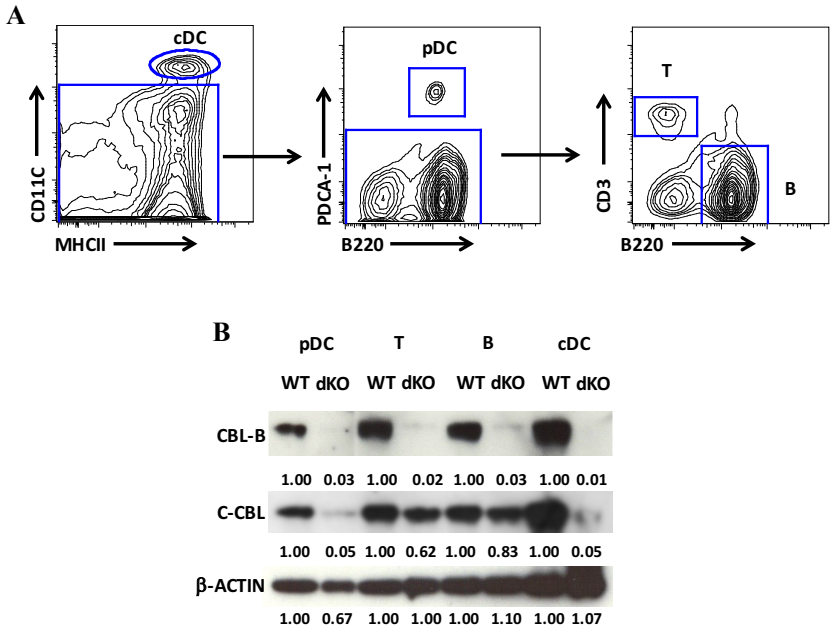

Fig. 4.1. Generation of *Cbl* dKO mice.
(A) FACS sorting strategy to isolate different cell populations from the splenocytes of WT and *Cbl* dKO mice. The 4 cell populations: pDCs (PDCA-1^{+}MHCII^{int}CD11C^{int}), cDCs (MHCII^{+}CD11C^{+}), T cells (MHCII^{-}CD11C^{-}CD3^{+}), B cell (MHCII^{-}CD11C^{-}B220^{+}) are shown in the corresponding gates.
(B) Western blot analysis of *Cbl-b* and *C-cbl* expressions in sorted pDCs (0.2×10^{5} cells), cDCs (0.5×10^{5} cells), T (0.5×10^{5} cells) and B cells (0.5×10^{5} cells). β-ACTIN is used as the loading control. The Western blot results are then quantified by ImageJ software. The values of dKO samples are normalized by WT samples, which are set as 1.00.

IV. 2. Altered homeostasis of cDCs and pDCs in *Cbl* dKO mice

IV. 2.1. The Cbl dKO mutation results in overexpansion of CD8α$^+$ cDCs in the SP and LN

Analysis of the SP cellularity of the *Cbl* dKO mice revealed that the ratio of CD8α$^+$ cDC versus CD11B$^+$ cDC was significantly increased (Fig. 4.2A). In particular, I found that the absolute number of CD8α$^+$ cDC was enhanced 5-fold in the SP of *Cbl* dKO mice compared to that in the WT mice; however, the absolute number of CD11B$^+$ cDC was not significantly changed in WT, *Cbl-b* KO, *C-cbl* KO, and *Cbl* dKO mice, indicating that *Cbl* dKO mutation selectively alters the homeostasis of CD8α$^+$ cDC (Fig. 4.2B).

To further determine whether CBL proteins control DC homeostasis in other tissues, I also examined the DC subsets in the LNs. I found that the ratio of CD8α$^+$ cDC versus CD11B$^+$ cDC in the LN tissue-resident DCs was significantly increased compared to that in the WT mice (Fig. 4.2C). However, the ratio of CD103$^+$ cDC versus CD11B$^+$ cDC in the LN migratory DCs was not significantly changed, which is consistent with the notion that CBL proteins affect only the development of CD8α$^+$ cDCs (Fig. 4.2D).

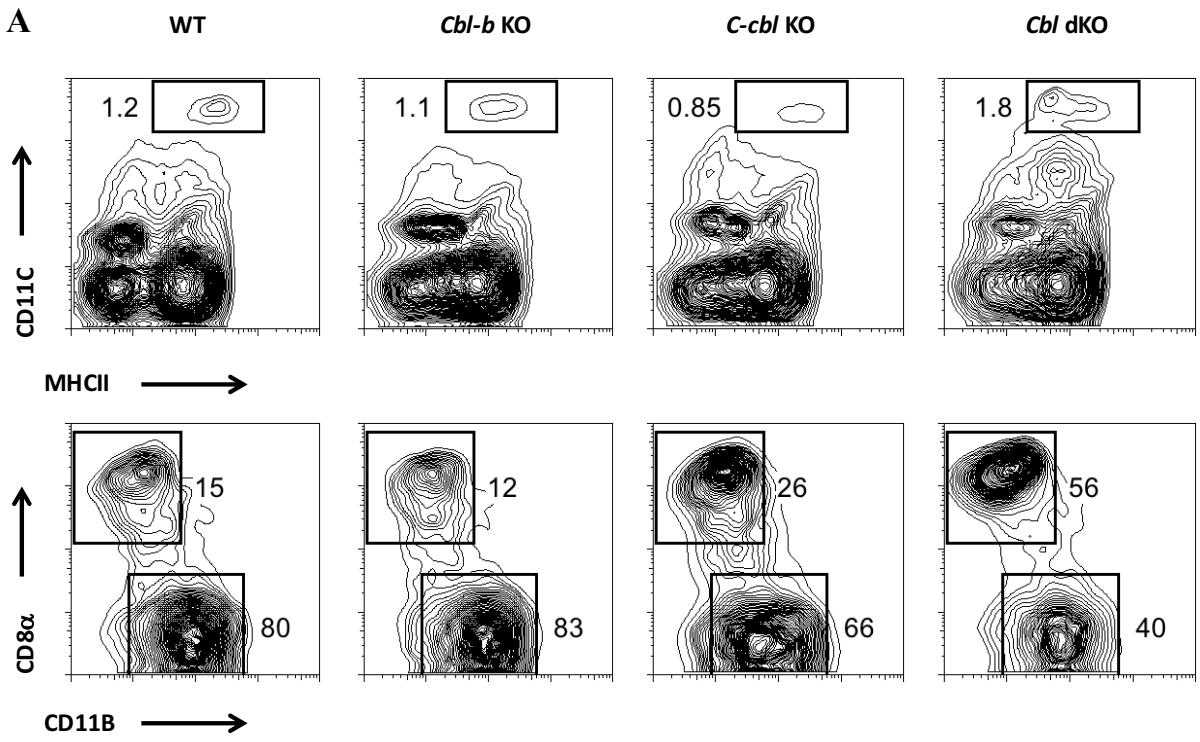

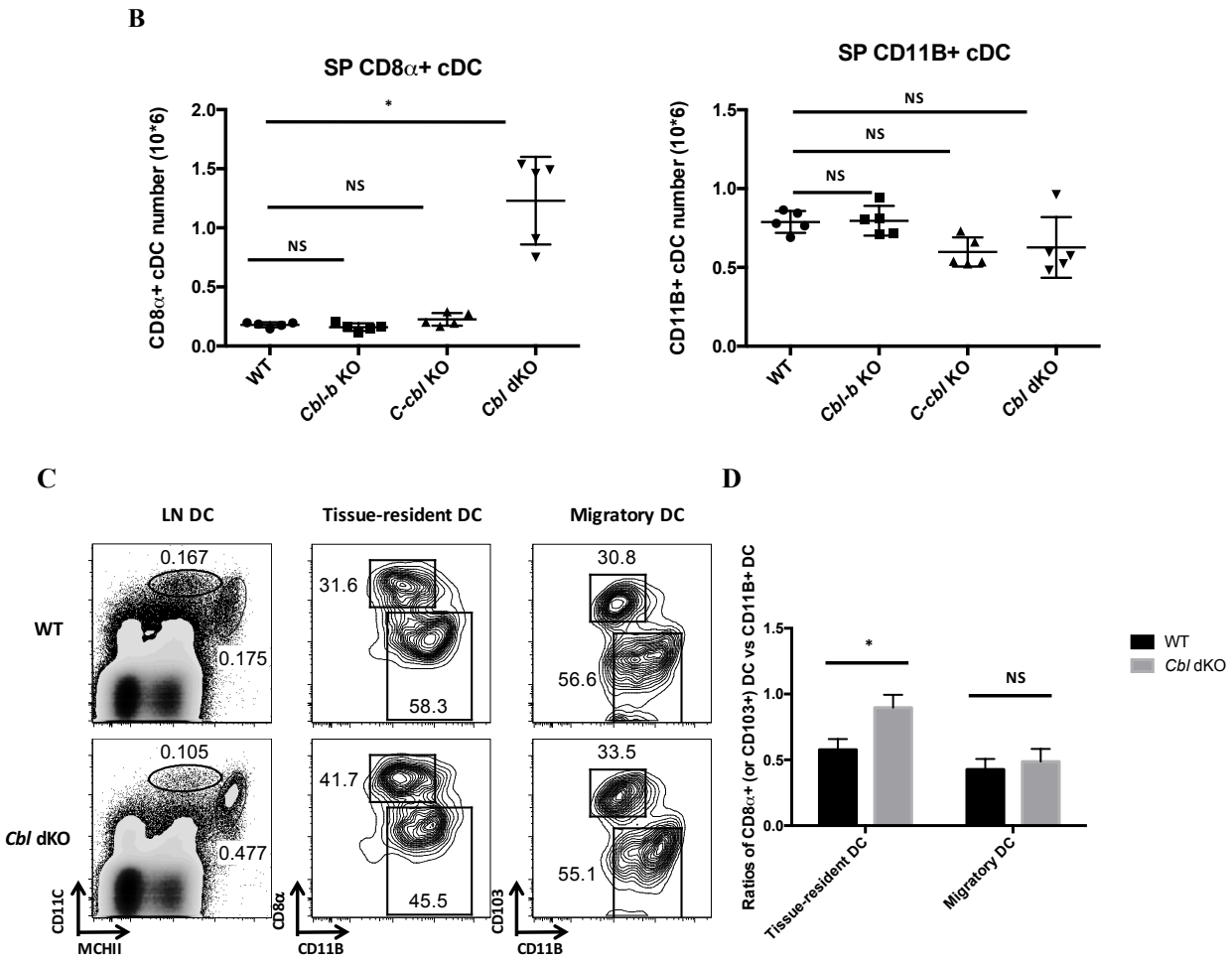

Fig. 4.2. Overexpansion of CD8α$^+$ cDCs in the SP and LN of *Cbl* dKO mice.

(A) Flow cytometry analysis of splenic conventional DC (cDC) subsets. Shown are the contour maps of splenic DC subsets in 10-week-old WT, *Cbl-b* KO, *C-cbl* KO, and *Cbl* dKO mice. The percentages of total MHCII$^+$CD11C$^+$ cDC (top panel), MHCII$^+$CD11C$^+$CD8α$^+$ cDC and MHCII$^+$CD11C$^+$CD11B$^+$ cDC subsets (bottom panel) are indicated in the plots.

(B) The statistics of splenic CD8α$^+$ cDC and CD11B$^+$ cDC numbers in 10-week-old WT, *Cbl-b* KO, *C-cbl* KO, and *Cbl* dKO mice. (n=5) Ordinary one-way ANOVA and Dunnett's multiple comparisons test with a single pooled variance were applied in the statistics. P value <0.05 was considered significant.

(C) FACS analysis of skin-draining LN cDC subsets. Shown are the contour maps of LN tissue resident DCs (MHCII$^+$CD11C$^+$) and migratory DCs (MHCII^{hi}CD11C$^+$) from 10-week-old WT and *Cbl* dKO mice. The percentages of CD8α$^+$ cDCs and CD11B$^+$ cDCs amongst the total LN tissue-resident DCs, and CD103$^+$ cDCs and CD11B$^+$ cDCs amongst the total LN migratory DCs of the WT and *Cbl* dKO mice are indicated in the plots.

(D) The ratios of CD8α$^+$ cDCs versus CD11B$^+$ cDCs in the LN tissue-resident DCs, and CD103$^+$ cDCs versus CD11B$^+$ cDCs in the LN migratory DCs. (n=3) Multiple t tests with fewer assumptions and Holm-Sidak correction method were applied in the statistics. P value <0.05 was considered significant.

IV. 2.2. The Cbl dKO mutation leads to reduced SP pDC number

To examine whether *Cbl* dKO mutation influences pDC development, I analyzed the BM and SP pDCs by flow cytometry. Analysis of BM and SP pDCs revealed that although the percentage and absolute number of BM pDCs did not change in *Cbl* dKO mice compared to WT mice, there was a significant decrease of the percentage and absolute number of SP pDCs in *Cbl* dKO mice compared to WT mice (Fig. 4.3A and Fig. 4.3B). These results could suggest that the pDC migration from BM to secondary lymphoid organ was blocked by *Cbl-b* and *C-cbl* double deletion. Since it was reported recently that chemokine receptors CCR5 and CXCR4 are required respectively for pDC migration from BM to secondary lymphoid organ and retention in the BM[78], I examined the expression of these chemokine receptors in the *Cbl* dKO BM pDCs by qPCR analysis. The results revealed that there was a slight downregulation of CCR5, as well as a moderate upregulation of CXCR4 in the mutant pDCs compared to the WT pDCs (Fig. 4.3C). This result thus suggests that dysregulation of pDC migration from BM to the periphery as guided by CCR5 and CXCR4 signaling could be one of the reasons leading to the impaired SP pDC homeostasis in *Cbl* dKO mice. This finding of course cannot exclude that other mechanisms may also influence pDC homeostasis in the periphery, which will be discussed later.

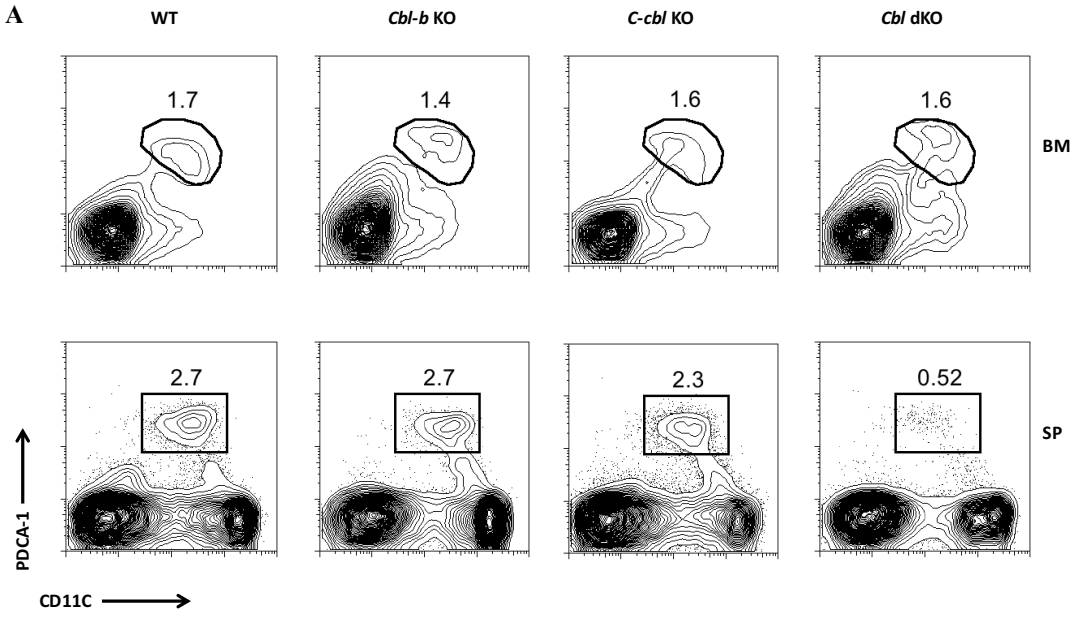

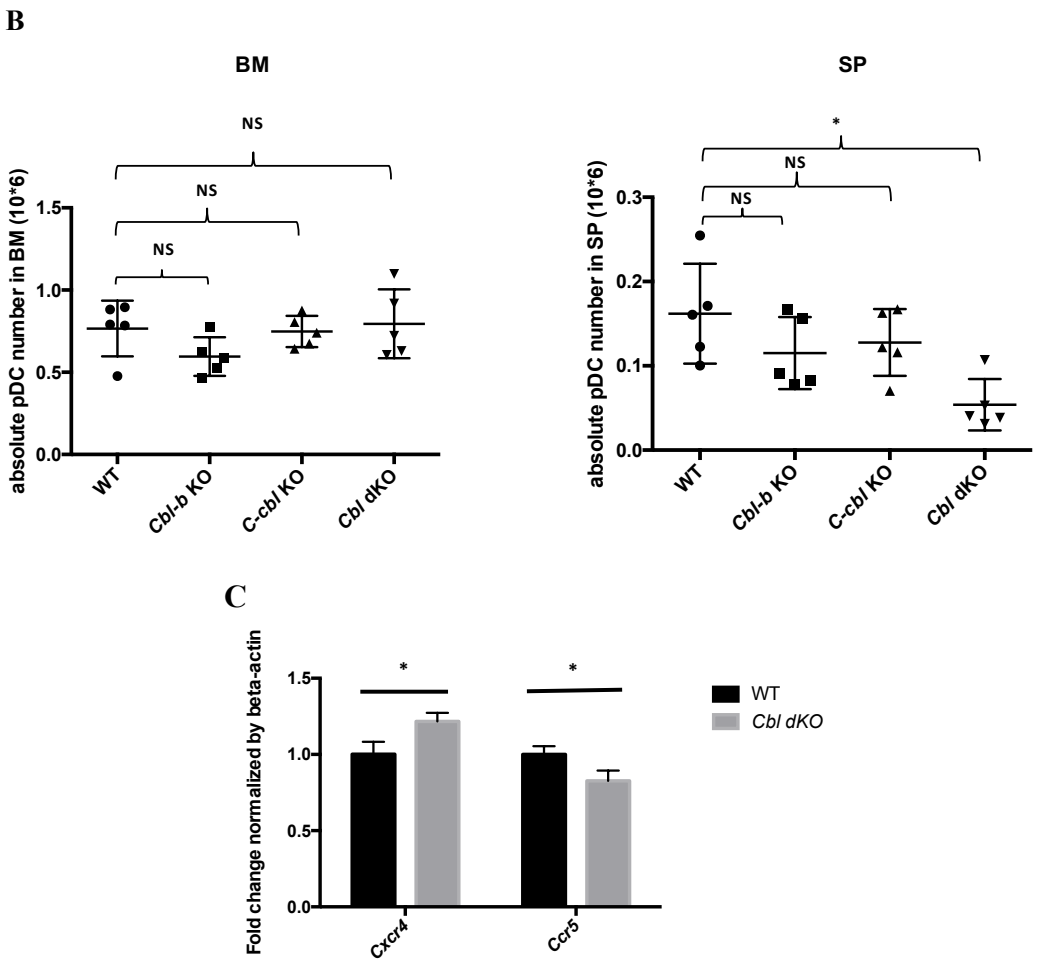

Fig. 4.3. Impaired homeostasis of SP pDCs in *Cbl* dKO mice.

(A) Flow cytometric analysis of pDCs in the BM and SP. Shown are contour maps of PDCA-1 vs CD11C staining of BM and SP pDCs in 10-week-old WT, *Cbl-b* KO, *C-cbl* KO, and *Cbl* dKO mice. The percentages of pDC ($Lin^-(CD3^-CD19^-TER119^-NK1.1^-)CD11C^+PDCA\text{-}1^+$) in the BM (upper panel) and SP (lower panel) of WT, *Cbl-b* KO, *C-cbl* KO, and *Cbl* dKO mice are indicated in the plots.

(B) The statistical analysis of pDC absolute number in the BM (left panel) and SP (right panel) of 10-week-old WT, *Cbl-b* KO, *C-cbl* KO, and *Cbl* dKO mice. (n=5) Ordinary one-way ANOVA and Dunnett's multiple comparisons test with a single pooled variance were applied in the analysis. P value <0.05 was considered significant.

(C) qPCR analysis of CXCR4 and CCR5 expressions in pDCs. BM cells from three WT and *Cbl* dKO mice were pooled together respectively. $CD11C^+PDCA\text{-}1^+$ pDCs were purified through sorting. 0.5×10^6 cells were used for RNA purification and cDNA generation. The CXCR4 and CCR5 expressions were measured by qPCR. Triplicates were done in the experiment. qPCR primer sequences and programs were listed in the Materials and Methods section. Multiple t tests with fewer assumptions and Holm-Sidak correction method were applied in the analysis. (n=3) P value <0.05 was considered significant.

IV. 3. Cellular mechanisms that contribute to the impaired homeostasis of CD8α$^+$ cDCs and pDCs

The previous results in my study demonstrate that there is selective CD8α$^+$ cDC expansion and pDC reduction in the SP of *Cbl* dKO mice compared to WT mice. Since overexpansion of CD8α$^+$ cDCs can be caused by a biased lineage commitment from pre-cDCs to CD8α$^+$ cDCs or preferential proliferation and survival of peripheral committed CD8α$^+$ cDCs, I decided to determine which cellular mechanisms are used by CBL proteins to control CD8α$^+$ cDC and pDC homeostasis in the periphery. Several important issues need to be addressed here. First, the *Cbl* dKO mice carry a germline *Cbl-b* mutation and it is known that *Cbl-b*$^{-/-}$ T cells have a lower threshold for T cell activation. It is therefore necessary to examine whether the observed splenic CD8α$^+$ cDCs expansion and pDCs reduction in *Cbl* dKO mice is due to the DC intrinsic effect rather than an event secondary to *Cbl-b*$^{-/-}$ T cell activation[229]. Secondly, it is known that CD8α$^+$ cDCs contain two subsets, canonical CD8α$^+$ cDCs and non-canonical CD8α$^+$ cDCs, the latter is phenotypically and functionally distinct from the former and is likely derived from failed pDC development[66]. Finally, since CD8α$^+$ cDCs and pDCs require the same environmental factors such as FLT3L for development and survival, it will be interesting to determine whether the CD8α$^+$ cDC expansion and pDC reduction is an inter-connected phenomenon.

IV. 3.1. Overexpansion of SP CD8α$^+$ cDC in Cbl dKO mice is caused by cell intrinsic effects

To address the first issue, I decided to analyze CD8α$^+$ cDC and pDC development in BM chimeric mice that contained both WT and *Cbl* dKO DCs, as well as *Cbl-b*$^{-/-}$ hematopoietic cells. As shown in the scheme, I mixed BM cells from SJL (CD45.1$^+$) and WT or *Cbl* dKO (CD45.2$^+$) mice in 1:1 ratio, and transferred them into lethally irradiated WT SJL mice by i.v. injection (Fig. 4.4A). One month later, donor derived cells were analyzed by flow cytometry. I found that, in the WT/SJL chimeric mice, the CD8α$^+$ cDC derived from B6J origin and SJL origin expand comparably. However, in the *Cbl* dKO/SJL chimeric mice, the CD8α$^+$ cDC derived from B6J origin expanded much more than the CD8α$^+$ cDC derived from SJL origin (Fig. 4.4B and 4.4C). Since in the BM chimeras, the CD8α$^+$ cDCs derived from *Cbl* dKO or WT B6J BM and SJL BM develop in the same environment, these results thus indicate that the CD8α$^+$ cDC overexpansion in *Cbl* dKO mice is due to the cell intrinsic, rather than the environment effect.

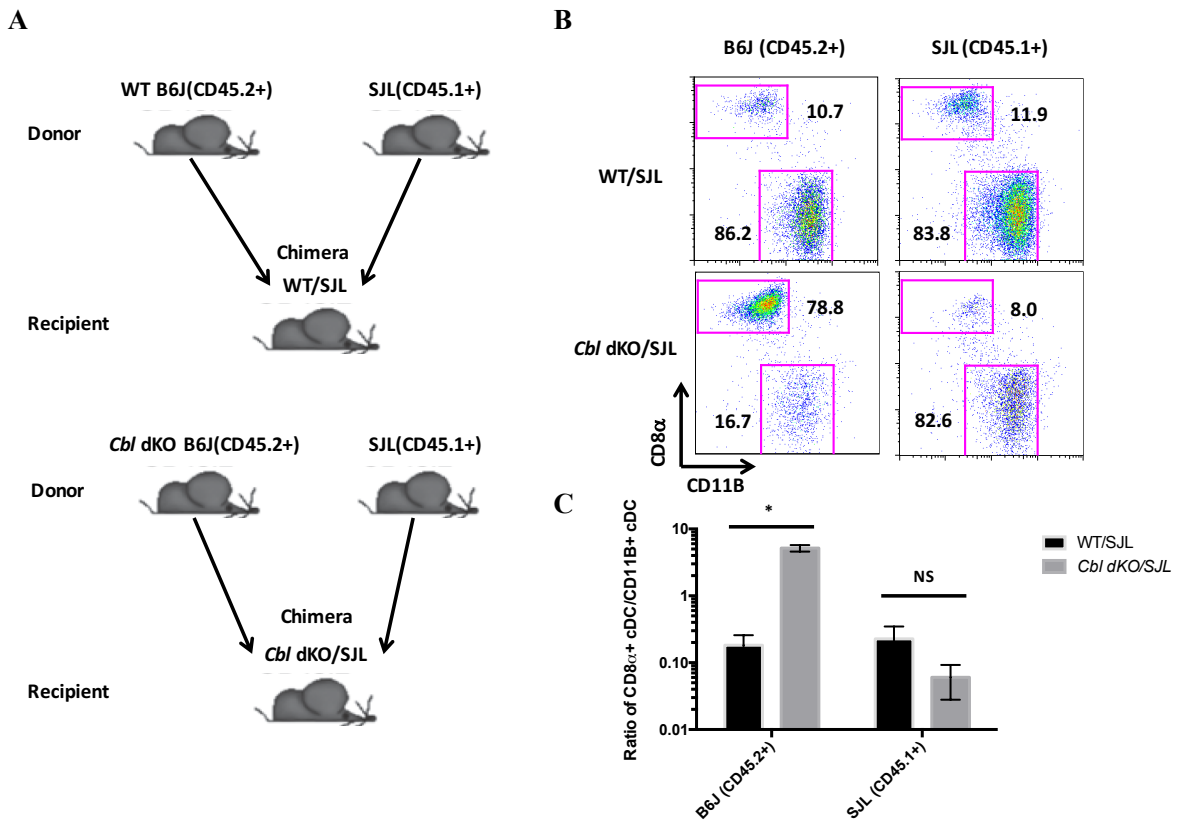

Fig. 4.4. SP CD8α$^+$ cDC overexpansion is caused by cell intrinsic effect.

(A) Generation of WT/SJL and *Cbl* dKO/SJL BM chimeric mice. 1×10^6 BM cells from 10-week-old WT or *Cbl* dKO B6J mice and 1×10^6 BM cells from 10-week-old SJL mice were mixed and transferred to lethally irradiated 3-month-old SJL mice by i.v. injection to make the WT/SJL and *Cbl* dKO/SJL BM chimeric mice. 1 month after BM reconstitution, the chimeric mice were used for FACS analysis.
(B) FACS analysis of CD8α$^+$ vs CD11B$^+$ cDCs in BM chimeras. The percentages of splenic CD8α$^+$ and CD11B$^+$ cDCs in B6J origin derived DCs (CD45.2) or SJL origin derived DCs (CD45.1) from WT/SJL and *Cbl* dKO/SJL chimeric mice are indicated in the plots.
(C) The ratio of CD8α$^+$ cDC versus CD11B$^+$ cDC in B6J origin derived DCs or SJL origin derived DCs from the WT/SJL and *Cbl* dKO/SJL chimeric mice. Multiple t tests with fewer assumptions and Holm-Sidak correction method were applied in the analysis. (n=4) P value <0.05 was considered significant.

IV. 3.2. Splenic pDC reduction in Cbl dKO mice is caused by environmental factors

In the *Cbl* dKO mice, the total number of pDCs in spleen is reduced as compared to that in WT mice. Interestingly, such splenic pDC reduction was also found for both *Cbl* dKO and WT SJL donor derived pDCs in *Cbl* dKO/SJL mice (Fig. 4.5A and 4.5B). There was no significant difference between the ratio of CD45.2$^+$ pDC versus CD45.1$^+$ pDC in WT/SJL mice and *Cbl*

dKO/SJL mice. This finding thus suggests that in addition to the intrinsic factors such as impaired migration, the environmental factors also contribute to the splenic pDCs reduction in the *Cbl* dKO mice. One of the possibilities could be the existence of a competition between the pDCs and expanded CD8α$^+$ cDCs for the same growth factors such as FLT3L. I will discuss this possibility in more detail in the discussion section.

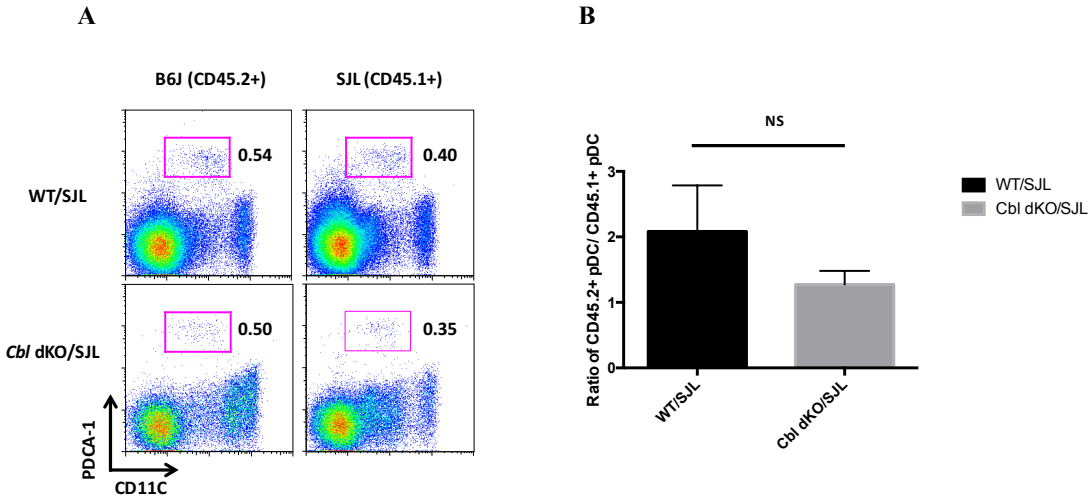

Fig. 4.5. Impaired homeostasis of SP pDC is caused by environmental factors.
(A) The percentage of pDCs (Lin$^-$(CD3$^-$CD19$^-$TER119$^-$NK1.1$^-$)PDCA-1$^+$CD11C$^+$) in B6J origin (CD45.2$^+$) derived cells and SJL origin (CD45.1$^+$) derived cells in the WT/SJL and *Cbl* dKO/SJL BM chimeric mice. The generation of WT/SJL and *Cbl* dKO/SJL BM chimeric mice is followed the same method as described previously.
(B) The statistical analysis of the ratio between the percentage of pDC in B6J origin derived cells vs the percentage of pDC in SJL origin derived cells in the WT/SJL and *Cbl* dKO/SJL BM chimeric mice. Multiple t tests with fewer assumptions and Holm-Sidak correction method were applied in the analysis. (n=3) P value <0.05 was considered significant.

IV. 3.3. Increased SP CD8α$^+$ cDCs are mainly contributed by canonical rather than non-canonical CD8α$^+$ cDCs

A subset of pDC-like non-canonical CD8α$^+$ cDCs has been recently discovered[303]. Their development requires E2-2, the hallmark transcription factor in pDCs development. In addition, these non-canonical CD8α$^+$ cDCs are very distinct from the canonic CD8α$^+$ cDCs by their low CD8α expression, poorer IL-12 production upon CpG stimulation, and low capability of antigen cross-presentation to CD8$^+$ T cells. To examine whether the increased splenic CD8α$^+$ cDCs in *Cbl* dKO mice were contributed by these cells, I analyzed the CD8α expression, IL-12 production and antigen cross-presentation by these cells to OT-I TCR transgenic (Tg) CD8$^+$ T cells. The results

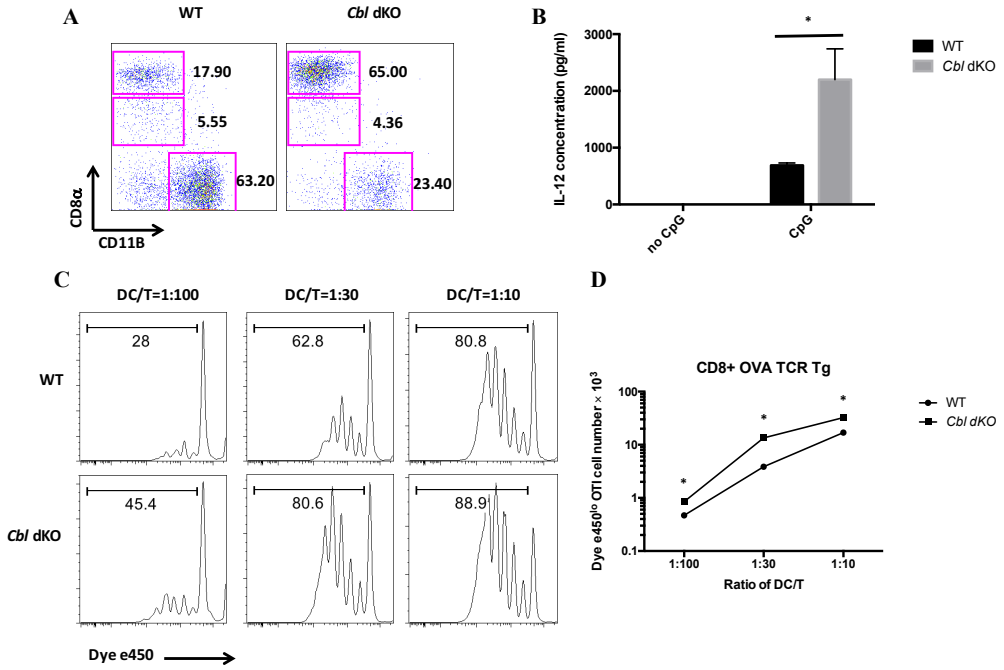

Fig. 4.6. Overexpanded CD8α$^+$ cDCs in *Cbl* dKO mice are canonical CD8α$^+$ cDCs rather than alternative CD8α$^+$ cDCs.

(A) FACS analysis of CD8α expression on splenic WT and *Cbl* dKO CD8α$^+$ cDCs. Percentages of CD8α$^+$, CD8α^{lo}, and CD11B$^+$ cDCs are indicated in the plots.

(B) IL-12 production by splenic WT and *Cbl* dKO CD8α$^+$ cDCs. Splenic WT and *Cbl* dKO CD8α$^+$ cDCs were purified by magnetic-bead based cell separation and FACS sorting as described in the Material and Method section. Triplicates of 1×10^5 CD8α$^+$ cDCs were then stimulated overnight with 5μM CpG. The concentration of IL-12 in the culture medium was quantified by ELISA. Multiple t tests with fewer assumptions and Holm-Sidak correction method were applied in the statistics. (n=3) P value <0.05 was considered significant.

(C) Antigen cross-presentation by CD8α$^+$ cDCs. 5×10^4 purified dye e450 labeled OT-I T cells were co-cultured with different ratios of splenic WT and *Cbl* dKO CD8α$^+$ cDCs in the presence of OVA antigen (40μg/ml) for 72 hours. Percentages of e450^{lo} OT-I T cells were analyzed by FACS.

(D) The statistics of dye e450^{lo} OT-I T cell number in OVA antigen cross-presentation assay. The experiment was done in triplicates in each DC/T ratio. Multiple t tests with fewer assumptions and Holm-Sidak correction method were applied in the statistics. (n=3) P value <0.05 was considered significant. This experiment has been repeated twice.

revealed that the mutant CD8α$^+$ cDCs expressed a comparable high level of CD8α to that of WT CD8α$^+$ cDCs (Fig. 4.6A). In addition, purified *Cbl* dKO CD8α$^+$ DCs produced even higher level of IL-12 upon CpG stimulation compared to the WT canonical CD8α$^+$ DCs (Fig. 4.6B). To examine antigen cross-presentation capability of these mutant CD8α$^+$ cDCs, I purified these cells by FACS sorting, and co-cultured these DCs with dye e450 labeled CD8$^+$ T (OT-I Tg) cells in the

presence of OVA antigens. Since canonic CD8α$^+$ cDCs can cross-present OVA antigen to CD8$^+$ OT-I T cells, they can stimulate OT-I T cells to proliferate, which can be identified based on the dilution of dye e450 in OT-I T cells by FACS analysis (Fig. 4.6C). As shown in Fig. 4.6C and 4.6D, *Cbl* dKO CD8α$^+$ DCs and OT-I T cell co-culture gave rise to more e450 low OT-I T cells compared to the same number of WT DCs, thus indicating that the mutant DCs exhibit even stronger antigen cross-presentation capacity compared to their WT counterparts. Together, these results indicate that the overexpanded splenic *Cbl* dKO CD8α$^+$ DCs are canonical CD8α$^+$ cDCs rather than the alternative lineage of CD8α$^+$ DCs.

IV. 3.4. Overexpansion of CD8α$^+$ cDCs in Cbl dKO mice is caused by preferential proliferation rather than altered lineage commitment from pre-cDCs

The classical development route of SP cDCs starts from the pre-cDCs in the BM. These BM pre-cDCs migrate to peripheral lymphoid organs such as SP where they continue their differentiation into mature CD8α$^+$ cDCs and CD11B$^+$ cDCs[86]. Based on this, it is conceivable that increased CD8α$^+$ cDCs in periphery can be caused by either the preferential lineage commitment from pre-cDCs to CD8α$^+$ cDCs or hyper-proliferation and better survival of mature CD8α$^+$ cDCs than that of CD11B$^+$ cDCs. To examine these two possibilities, I made use of an *in vitro* FLT3L BMDC culture system to determine the differentiation and proliferation of BM derived cDCs. By using this system, I was able to recapitulate the development of cDC and pDC *in vitro*. In brief, total BM cells from WT and *Cbl* dKO mice were seeded into the culture in the presence of different concentrations of FLT3L. After 7-9 days of *in vitro* culture, the BM cells can develop into mature CD11C$^+$B220$^+$ pDCs, and CD11C$^+$B220$^-$ cDCs. The latter can be further resolved into CD11B$^+$ cDCs and CD24$^+$ cDCs that are the equivalents of CD8α$^+$ cDCs generated *in vivo* (Fig. 4.7A). The results revealed that the BM cells from both WT and *Cbl* dKO mice developed into the aforementioned DC lineages in the presence of FLT3L. However, at a low FLT3L concentration, the *Cbl* dKO BM cells could generate a much higher ratio of CD24$^+$ cDC versus CD11B$^+$ cDC compared to WT BM cells and this difference disappeared when a high concentration of FLT3L was provided (Fig. 4.7B and 4.7C). In terms of absolute cell number, there

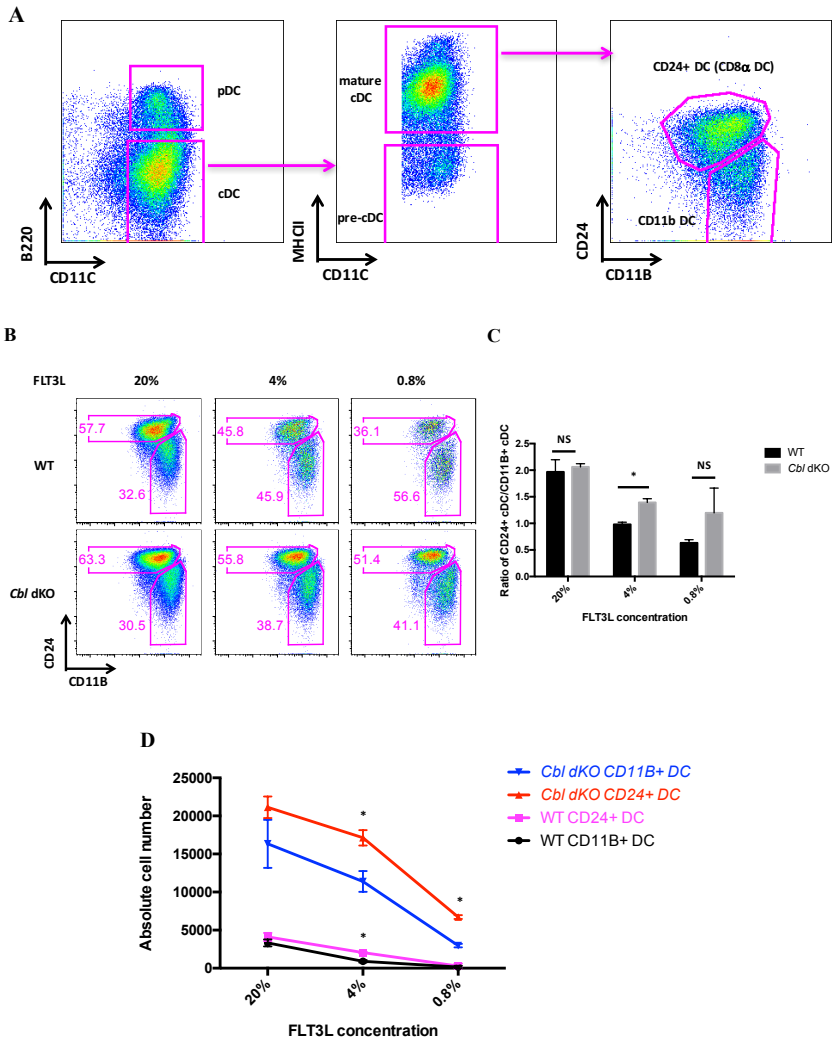

Fig. 4.7. pDC and CD8α$^+$ and CD11B$^+$ cDC lineage development revealed in FLT3L BM culture.

(A) FACS analysis of DC development by *in vitro* FLT3L BMDC culture. Shown are FACS staining of pDCs, pre-cDCc, CD24$^+$ and CD11B$^+$ cDCs generated in FLT3L culture. Gating of different DC subsets is indicated in the plots.

(B) FACS analysis of DC subsets derived from FLT3L culture. Triplicates of 1×10^6 BM cells from WT and *Cbl* dKO mice were cultured in the presence of different concentrations of FLT3L for 7 days *in vitro*. The percentages of CD24$^+$ and CD11B$^+$ cDCs are indicated in the plots.

(C) The statistical analysis of the ratios of CD24$^+$ versus CD11B$^+$ cDCs generated in the presence of different doses of FLT3L. Multiple t tests with fewer assumptions and Holm-Sidak correction method were applied in the analysis. (n=3) P value <0.05 was considered significant. This experiment has been repeated three times.

(D) The absolute cell number of CD24$^+$ and CD11B$^+$ cDCs generated in the presence of different doses of FLT3L. Triplicates of 1×10^6 BM cells from WT and *Cbl* dKO mice were cultured in the presence of different concentrations of FLT3L for 7 days *in vitro*. Multiple t tests with fewer assumptions and Holm-Sidak correction method were applied in the analysis. (n=3) P value <0.05 was considered significant. This experiment has been repeated twice.

were more *Cbl* dKO $CD24^+$ and $CD11B^+$ cDCs generated in the same doses of FLT3L compared to WT $CD24^+$ and $CD11B^+$ cDCs. Moreover, in the presence of low concentration of FLT3L, there were more $CD24^+$ *Cbl* dKO cDCs generated than $CD11B^+$ *Cbl* dKO cDCs. However, this difference was not significant in the presence of high concentration of FLT3L (Fig. 4.7D) These results suggest two things. First, both *Cbl* dKO $CD24^+$ and $CD11B^+$ cDCs have enhanced FLT3 signaling to support their expansion compared to WT $CD24^+$ and $CD11B^+$ cDCs. Second, *Cbl* dKO $CD24^+$ cDCs have relatively higher FLT3 signaling than *Cbl* dKO $CD11B^+$ cDCs. And this difference is dependent on FLT3L concentration, because there is a competition for FLT3L of $CD24^+$ and $CD11B^+$ cDCs in the same culture. In the presence of low concentration of FLT3L, this difference is more obvious, while in the presence of high concentration of FLT3L, this difference is relatively mild.

To further determine whether the preferential expansion of $CD8\alpha^+$ cDCs is due to enhanced proliferation or a preferential lineage commitment to $CD8\alpha^+$ cDCs from the pre-cDCs, I conducted a BrdU incorporation assay by using the same *in vitro* FLT3L culture. After 6 days of FLT3L culture, BrdU was added into the culture for overnight. Since pre-cDCs are only a small portion of cells in the culture, the proliferating ($BrdU^+$) cells detected under this culture condition should be mostly proliferating mature DCs rather than newly committed DCs from the pre-cDCs. The results revealed that *Cbl* dKO pre-cDCs had a slightly increased percentage of $BrdU^+$ cells compared to the WT pre-cDCs. However, the *Cbl* dKO $CD24^+$ cDCs had a more dramatic increase of $BrdU^+$ cells compared to the WT $CD24^+$ cDCs. Although the *Cbl* dKO $CD11B^+$ cDCs also had a significantly increase of $BrdU^+$ cells compared to the WT $CD11B^+$ cDCs, the difference was not as dramatic as the $CD24^+$ cDCs (Fig. 4.8A and 4.8B). To directly examine the cells that are in active cell cycle, a DAPI staining was conducted to determine the percentage of cells that have DNA synthesis. The result of DAPI staining revealed that the *Cbl* dKO $CD24^+$ cDCs had a higher percentage of cells in the S+G2/M phases compared to the WT $CD24^+$ cDCs; in contrast, the percentages of cells in the S+G2/M phase in *Cbl* dKO and WT $CD11B^+$ cDCs were comparable (Fig. 4.8C and 4.8D).

To further exclude the possibility that *Cbl* dKO mutation affects the lineage commitment of $CD8\alpha^+$ vs $CD11B^+$ cDCs, the expression level of several important transcription factors for DC

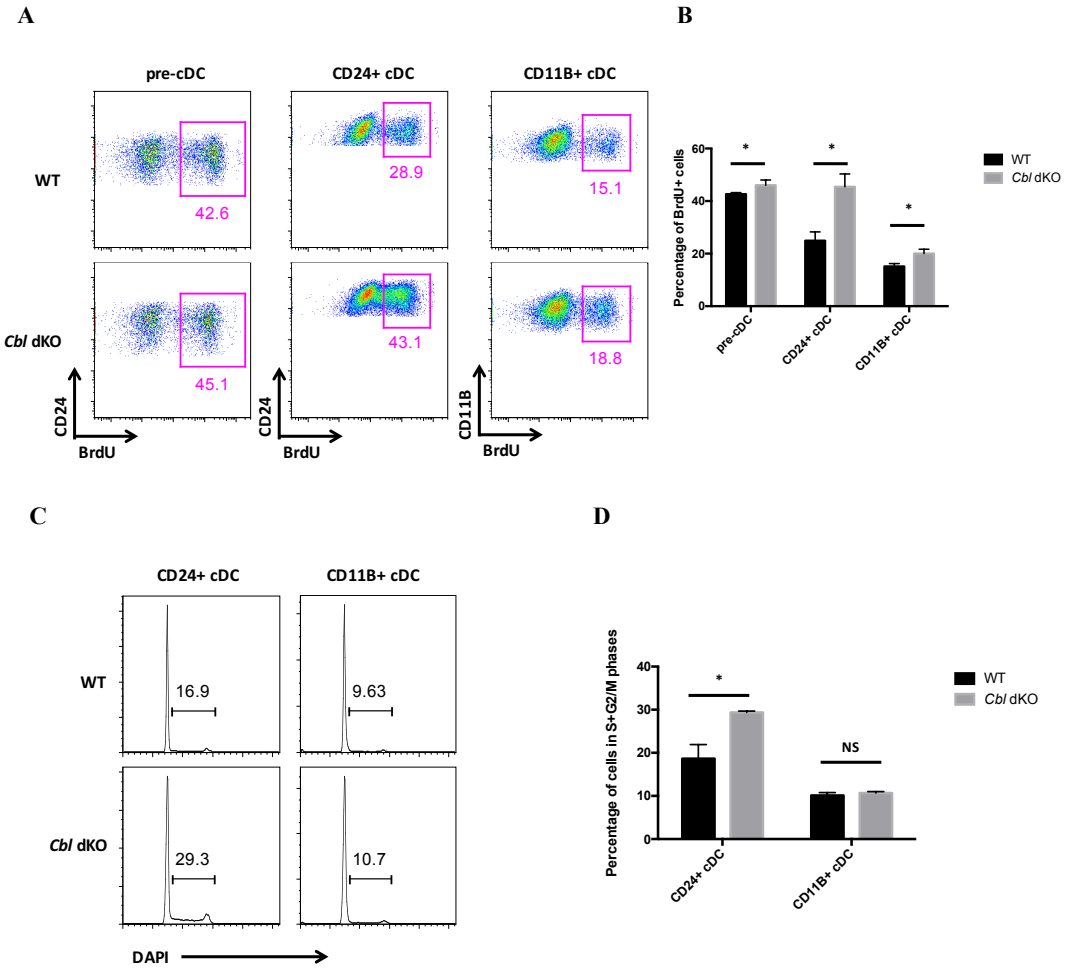

Fig. 4.8. BrdU labeling and cell cycle analyses of *in vitro* FLT3L cultured DC subsets.

(A) BrdU incorporation assay. 2×10^6 BM cells were cultured in 10% FLT3L for 6 days. Cell were labeled with 10μM BrdU for overnight and then subjected to surface and intracellular staining. Shown are BrdU staining of pre-cDCs, $CD24^+$ and $CD11B^+$ cDCs. The percentages of $BrdU^+$ cells in different DC subsets are indicated in the plots.

(B) The statistical analysis of the percentages of $BrdU^+$ cells in different DC subsets generated by *in vitro* FLT3L culture. The experiment was done in triplicates. Multiple t tests with fewer assumptions and Holm-Sidak correction method were applied in the analysis. (n=3) P value <0.05 was considered significant. This experiment has been repeated twice.

(C) Cell cycle analysis by DAPI staining. 2×10^6 BM cells were cultured in 10% FLT3L for 7 days. The DNA contents in the WT or mutant $CD24^+$ and $CD11B^+$ cDCs were stained with 3μM DAPI and then analyzed by FACS. The percentages of cells in S+G2/M phases in different DC subsets are indicated in the plots.

(D) The statistical analysis of the percentages of cells in S+G2/M phases in different DC subsets generated by *in vitro* FLT3L culture. The experiment was done in triplicates. Multiple t tests with fewer assumptions and Holm-Sidak correction method were applied in the analysis. (n=3) P value <0.05 was considered significant. This experiment has been repeated twice.

lineage commitment in pre-cDCs was measured by western blot. The results revealed that the WT and *Cbl* dKO pre-cDC expressed comparable levels of IRF8, which is responsible for the CD8α$^+$ lineage development[30]. The expressions of IRF8 and Id2, a transcription factor that inhibits E2-2 function, were comparable in the mutant and WT CD24$^+$ cDCs. Moreover, the expression of IRF4 was also comparable in the mutant and WT CD11B$^+$ cDCs (Fig. 4.9).

Taken together, these results clearly indicate that the preferential expansion of SP CD8α$^+$ cDCs in *Cbl* dKO mice is mainly due to the hyper-proliferation of CD8α$^+$ cDCs, rather than a biased lineage commitment towards CD8α$^+$ cDCs than to CD11B lineages. In addition, it also suggests that the enhanced FLT3 signaling is perhaps responsible for the altered CD8α$^+$ lineage expansion.

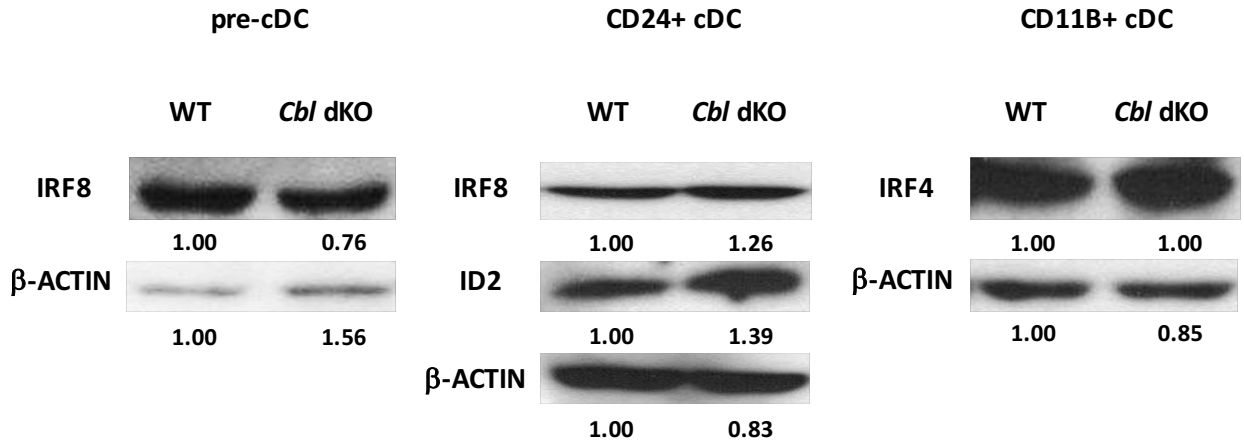

Fig. 4.9. Biochemical analysis of transcription factors required for DC lineage commitment. Western blot analyses of IRF4, IRF8 and ID2 expression in pre-cDCs, CD24$^+$ and CD11B$^+$ cDCs. The WT and mutant DC subsets were purified from *in vitro* FLT3L cultured BMDC through sorting. 5×10^5 pre-cDCs, 1×10^6 CD24$^+$ and CD11B$^+$ cDCs were used for Western blot analysis to detect the expression levels of IRF8, ID2, and IRF4. The Western blot results were then quantified by ImageJ software. The values of *Cbl* dKO samples were normalized by WT samples which were set as 1.00. This experiment has been repeated twice.

IV. 4. CBL proteins control CD8α$^+$ cDC proliferation through FLT3-PKB/AKT-MTOR signaling

The *in vitro* FLT3L culture results suggest that preferential development of CD8α$^+$ cDCs in *Cbl* dKO mice is likely caused by an enhanced FLT3 signaling. To determine whether this is the case,

a series *in vitro* and *in vivo* experiments are conducted to elucidate whether and how CBL proteins regulate FLT3 signaling in DCs.

IV. 4.1. The Cbl dKO mutation enhances PKB/AKT and ERK activation in CD24$^+$ cDCs

It has been reported that FLT3 may activate several downstream signaling pathways such as RAS-MAP kinase and PKB/AKT pathways[215, 272]. Enhanced generation of CD8α$^+$ cDCs in FLT3L cultured BM cells thus prompted me to examine whether these two pathways were enhanced in the mutant DCs. To determine whether this is the case, WT and *Cbl* dKO CD24$^+$ cDCs were purified and the activation of AKT signaling pathway was examined by detecting the phosphorylation of serine 473 (S473) of AKT. The results revealed that there was a higher level of pAKT (S473) in *Cbl* dKO CD24$^+$ cDC than that in WT CD24$^+$ cells even in the absence of FLT3L stimulation, indicating that AKT is constitutively activated in the absence of CBL proteins. As a matter of fact, the AKT activation in the mutant CD24$^+$ cDCs already reached the plateau as the FLT3L stimulation markedly enhanced pAKT (S473) level in WT cells, but not in *Cbl* dKO cells. Interestingly, the augmented AKT activation in CD11B$^+$ cDCs was not as significant as in CD24$^+$ cDCs (Fig. 4.10A and 4.10B). This result is possibly due to the fact that surface FLT3 expression level in CD11B$^+$ cDCs was much lower than that in CD8α$^+$ cDCs (Fig. 4.10D), which is also consistent with the findings that in the FLT3L cultured BMDC, the generation of *Cbl* dKO CD11B$^+$ cDCs was less than *Cbl* dKO CD24$^+$ cDCs. In addition to the constitutive activation of PKB/AKT signaling pathway, EKT1/2 was also shown a constitutive activation in *Cbl* dKO CD24$^+$ cDCs in the absence of FLT3 stimulation. Interestingly, this basal level of activated ERK1/2 in mutant CD24$^+$ cDCs was even higher than that in FLT3L stimulated WT CD24$^+$ cDCs (Fig. 4.10C).

Taken together, these results indicate that CBL proteins are negative regulators for both the PKB/AKT and ERK signaling pathways downstream of FLT3 in DCs. Since these two pathways are simultaneously hyperactive in the *Cbl* dKO CD24$^+$ cDCs, I propose that CBL proteins either simultaneously regulate these two pathways or control a signaling molecule that acts upstream of these two pathways.

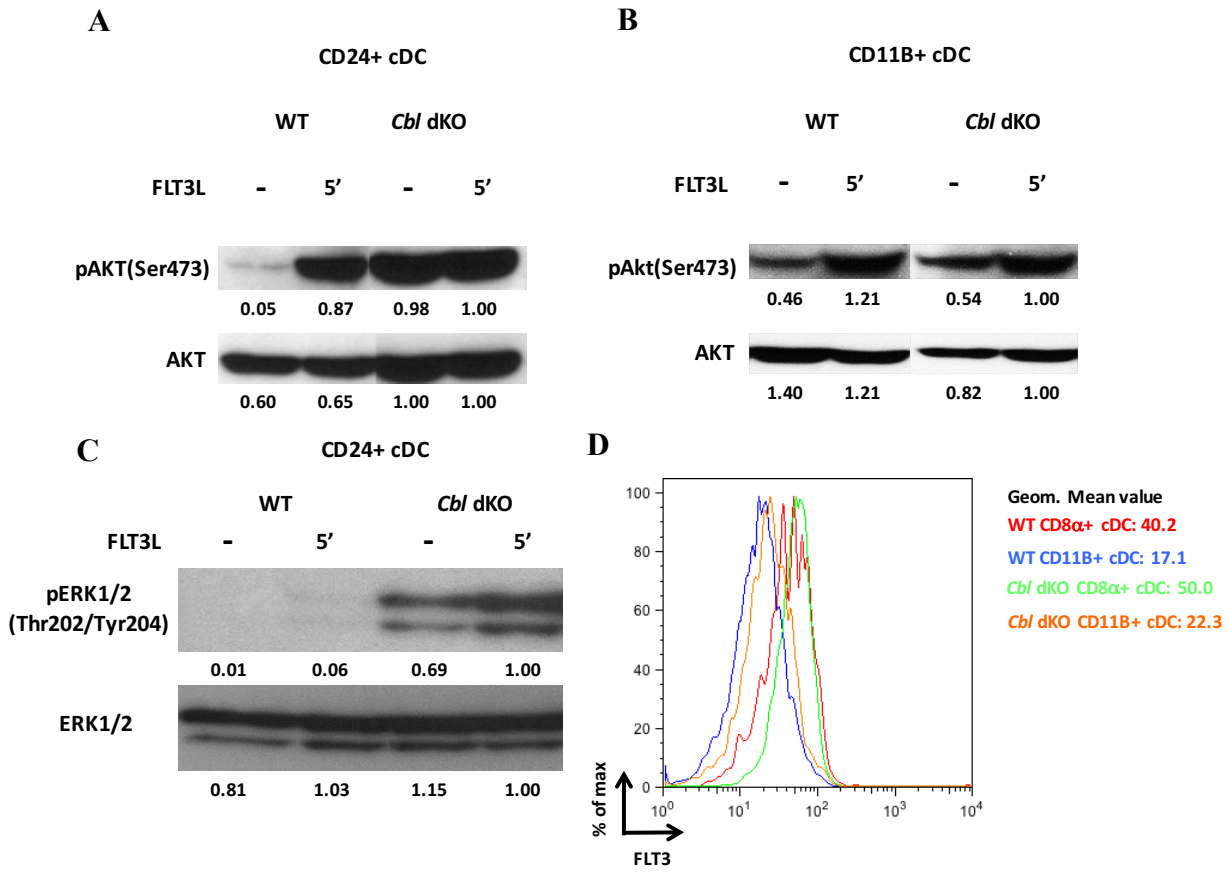

Fig. 4.10. Hyper-activation of PKB/AKT and ERK signaling in *Cbl* dKO CD24$^+$ cDCs.
(A) & **(B)** Western blot analysis of pAKT (Ser473) in WT and *Cbl* dKO CD24$^+$ cDC. CD24$^+$ and CD11B$^+$ cDCs were isolated from FLT3L cultured BMDC by sorting based on the gating strategy shown in Fig. 4.7A. 1×10^6 cells were either stimulated by 100ng/ml FLT3L or without stimulation for 5 mins at 37°C. The levels of pAKT and AKT were detected by western blot. The Western blot results were then quantified by ImageJ software. The value of each sample was normalized by the sample at most right, which was set as 1.00. This experiment has been repeated twice.
(C) Western blot analysis of ERK (Thr202/Tyr204) activation in WT and *Cbl* dKO CD24$^+$ cDCs. CD24$^+$ cDCs were isolated and stimulated as above. The levels of pERK1/2 (Thr202/Tyr204) in the cell lysates were determined by Western blot analysis using an anti-pERK1/2 (Thr202/Tyr204) antibody. The Western blot results were then quantified by ImageJ software. The value of each sample was normalized by the sample at most right, which was set as 1.00. This experiment has been repeated twice.
(D) Flow cytometry analysis of surface FLT3 expression on splenic CD8α$^+$ and CD11B$^+$ cDCs from WT and *Cbl* dKO mice. Splenocytes were stained with MHCII, CD11C, CD8α, CD11B, and FLT3, and the surface FLT3 expressions in different DC subsets were compared. Shown are the histogram presentations and the corresponding geom. mean values of FLT3 expression on the different DC subsets.

IV. 4.2. Attenuation of preferential expansion of *Cbl* dKO CD8α$^+$ cDCs by rapamycin

While the data showed that the *Cbl* dKO mutation resulted in constitutive activation of the PKB/AKT and ERK1/2 signaling pathways, it is not clear whether these activations are relevant to the altered CD8α$^+$ cDC development and if so, which of them is responsible. Since I do not have PKB and ERK KO mice, I decided to investigate this question by using rapamycin, an inhibitor of MTOR, to block the downstream signaling of PKB/AKT pathway. In FLT3L cultured BMDC, addition of rapamycin significantly reduced the expansion of *Cbl* dKO CD24$^+$ cDCs in a dose dependent manner (Fig. 4.11A and 4.11B). The same treatment exhibited only a mild effect on the WT CD24$^+$ cDCs. To examine whether rapamycin treatment could also correct CD8α$^+$ cDC overexpansion in *Cbl* dKO mice *in vivo*, the *Cbl* dKO mice were treated with rapamycin through intraperitoneal (IP) injection for seven consecutive days. The results showed that short-term rapamycin treatment could significantly attenuate the overexpansion of splenic CD8α$^+$ cDCs in *Cbl* dKO mice, although it was only a partial attenuation (Fig. 4.11C and 4.11D). However, the same rapamycin treatment had a relatively mild effect on WT CD8α$^+$ cDCs. It might be due to the reason that *Cbl* dKO CD8α$^+$ cDCs had a higher activation level of pAKT than WT CD8α$^+$ cDCs. These findings thus indicate that the enhanced PKB/AKT-MTOR signaling in *Cbl* dKO CD8α$^+$ cDCs is responsible for the altered homeostasis of CD8α$^+$ cDCs in *Cbl* dKO mice. In addition, the observation that the rapamycin treatment could only partially restore the CD8α$^+$ cDC homeostasis both *in vitro* and *in vivo* suggests that the ERK signaling pathway might also play a role in this regulation.

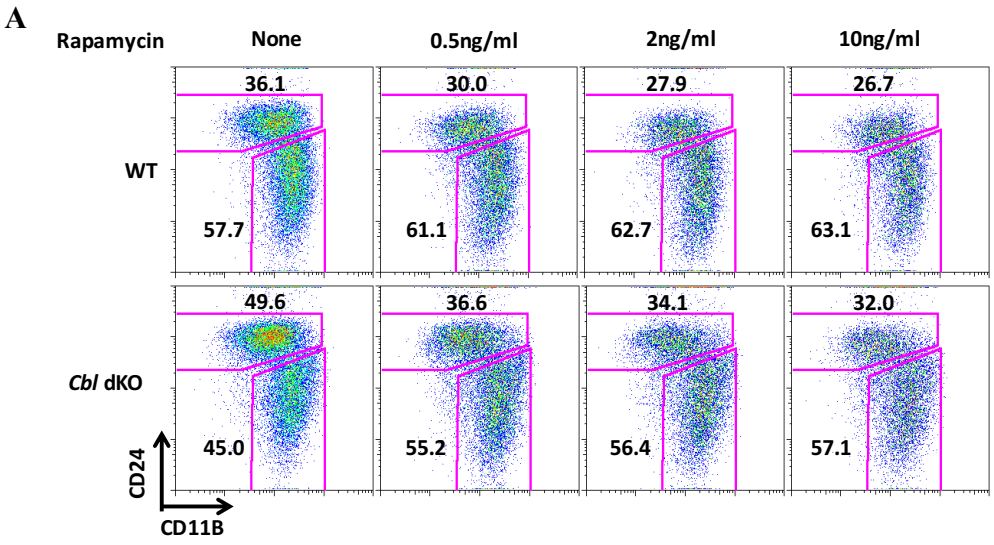

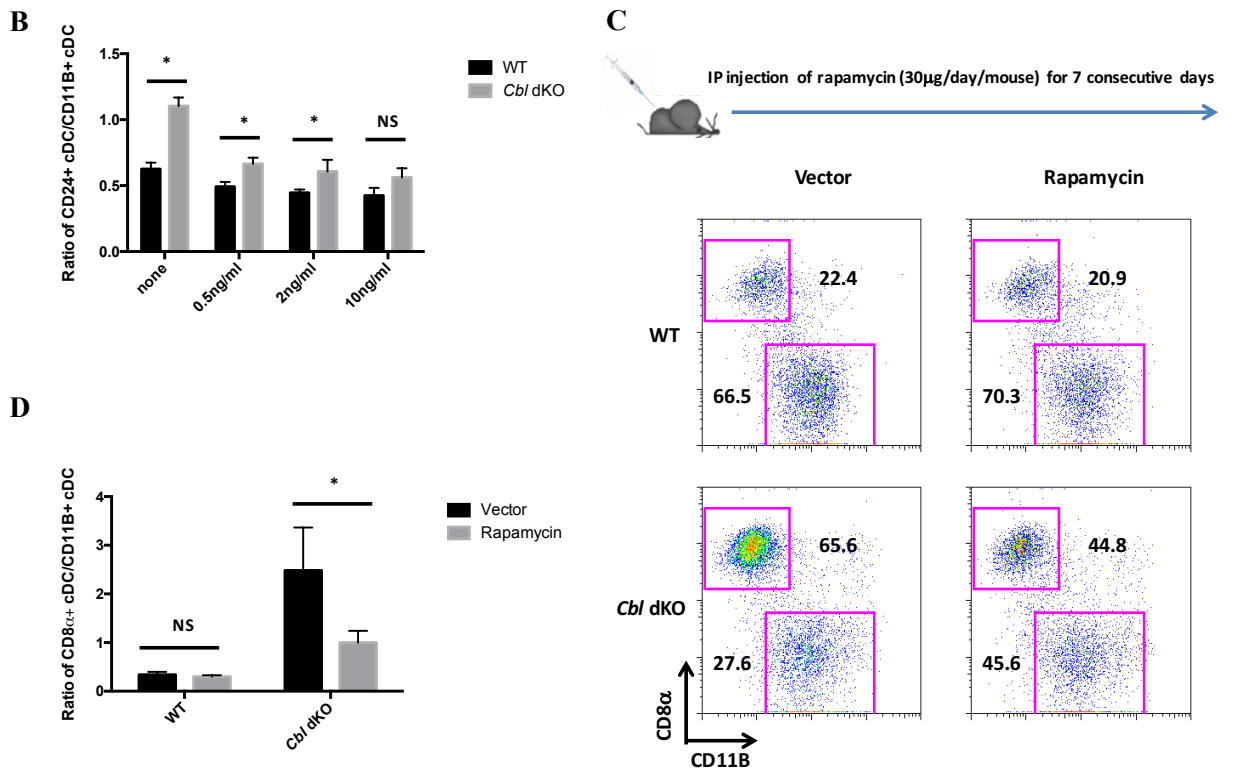

Fig. 4.11. Blockade of MTOR signaling by rapamycin partially corrects *Cbl* dKO CD24$^+$ and SP CD8α$^+$ cDC homeostasis both *in vitro* and *in vivo*.
(A) FACS analysis of *in vitro* FLT3L cultured BMDCs in the presence or absence of rapamycin. 1×10^6 BM cells from WT and *Cbl* dKO mice were cultured in 10% FLT3L for 3 days. Different doses of rapamycin were then added into the culture for an additional culture of 4 days. Cells were then harvested and stained with B220, CD11C, CD24, MHCII, and CD11B for a FACS analysis. Shown are CD24 and CD11B staining of the gated B220$^-$MHCII$^+$CD11C$^+$ cDCs.
(B) The statistical analysis of the ratios of CD24$^+$ versus CD11B$^+$ cDCs in the FLT3L cultured BMDC with different doses of rapamycin. Triplicates were used in this experiment. Multiple t tests with fewer assumptions and Holm-Sidak correction method were applied in the analysis. (n=3) P value <0.05 was considered significant. This experiment has been repeated three times.
(C) FACS analysis of the SP CD8α$^+$ and CD11B$^+$ cDCs from WT and *Cbl* dKO mice with or without rapamycin treatment. Three WT and *Cbl* dKO mice were treated with rapamycin by i.p. injection for 7 consecutive days (30μg/day). Shown are dot plot analyses of CD8α vs CD11B staining of the gated MHCII$^+$CD11C$^+$ splenic cDCs.
(D) The statistical analysis of the ratios of splenic CD8α$^+$ cDC vs CD11B$^+$ cDC from WT and *Cbl* dKO mice with or without rapamycin treatment. Three mice were used in each group. Multiple t tests with fewer assumptions and Holm-Sidak correction method were applied in the statistics. (n=3) P value <0.05 was considered significant.

IV. 4.3. CBL-B and C-CBL directly regulate the activation of FLT3

As described above, it has been revealed that PKB/AKT and ERK1/2 are simultaneously activated in *Cbl* dKO CD24$^+$ cDCs. The mutant CD24$^+$ cDCs also have enhanced FLT3 signaling.

Since FLT3 may act at the upstream of both PKB/AKT and ERK1/2 signaling pathways, I decided to examine whether CBL proteins directly regulate FLT3 signaling in DCs. Since CBL family proteins may interact with their target proteins through their TKB or proline-rich motifs and phosphotyrosines at their C-terminal portions, identifying their association with FLT3 may provide a strong evidence that CBL proteins may directly regulate FLT3 activation.

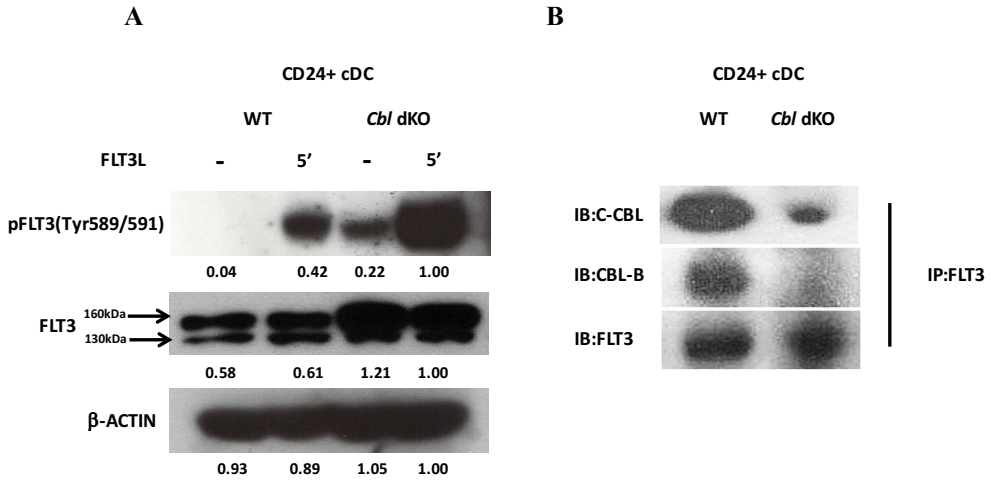

Fig. 4.12. CBL proteins directly regulate FLT3 activity in CD24$^+$ cDCs.
(A) Western blot analysis of pFLT3 (Tyr589/591) in CD24$^+$ cDCs. 1×10^6 WT and *Cbl* dKO CD24$^+$ cDCs were purified from FLT3L cultured BMDC by FACS sorting as described in Material and Method section. 1×10^6 cells were stimulated with 100ng/ml FLT3L or without for 5 min at 37°C. The pFLT3 and FLT3 levels in the cell lysates were measured by Western blot through the antibodies against pFLT3 (Tyr589/591) and FLT3. β-ACTIN was used as an internal control. The Western blot result was further quantified by ImageJ software. The value of each sample was normalized by the sample at most right, which was set as 1.00. This experiment has been repeated at least twice.
(B) The association of CBL-B and C-CBL with FLT3 in WT and *Cbl* dKO CD24$^+$ cDCs. 1×10^6 WT and *Cbl* dKO CD24$^+$ cDCs were purified from FLT3L cultured BMDC by FACS sorting as described previously. The FLT3 complexes in total cell lysates were immunoprecipitated by anti-FLT3 antibody, and the associated proteins in the FLT3 complexes were further detected by immunoblot with anti-C-CBL or anti-CBL-B sequentially. FLT3 was used as an internal control. This experiment has been repeated at least twice.

To test whether FLT3 was hyperactive in the absence of CBL proteins, I examined FLT3 tyrosine phosphorylation at Tyr589/591, the active form of FLT3, by Western blot hybridization. Similar with the PKB/AKT result, a higher level of active form of FLT3 (pFlt3 (Tyr589/591)) was also constitutively present in *Cbl* dKO but not WT CD24$^+$ cDCs (Fig. 4.12A), indicating that FLT3 was indeed constitutively active in the absence of CBL proteins. To further determine whether CBL proteins directly regulate FLT3 activation, I examined the association between CBL proteins

and FLT3 by immunoprecipitation and Western blot hybridization. The results showed that the immunoprecipitated complexes of FLT3 contained both CBL-B and C-CBL, thus supporting the hypothesis that CBL-B and C-CBL regulate FLT3 activation through direct association with FLT3 (Fig. 4.12B).

Previous publication indicates that there are two forms of FLT3: one is the immature form of FLT3 whose molecular weight is 130kDa; the other is the glycosylated mature form of FLT3 whose molecular weight is 160kDa. It is noteworthy that only the glycosylated mature form of FLT3 is expressed extracellularly and can recognize FLT3L, while the immature form of FLT3 is expressed intracellularly and cannot recognize FLT3L[262, 263]. Interestingly, in the result it revealed that the mature form of FLT3 in *Cbl* dKO $CD24^+$ cDCs was markedly increased (Fig 4.10A), suggesting that CBL proteins could be involved in FLT3 degradation.

IV. 4.4. CBL-B and C-CBL promote the downmodulation and degradation of FLT3

It has been shown previously that the CBL family proteins may negatively regulate RTK activity by promoting the internalization and lysosome sorting of the activated RTK[304]. Since the results in my study indicated that the mature form of FLT3 was markedly increased in *Cbl* dKO $CD24^+$ cDCs, it was reasonable to hypothesize that CBL-B and C-CBL regulate the internalization and degradation of FLT3. To test this hypothesis, FLT3 was co-expressed with and without CBL-B or C-CBL in 293T cells. The transfected cells were further stimulated with FLT3L or without. FLT3 downmodulation induced by FLT3L stimulation was then analyzed by flow cytometry. The results revealed that cells co-transfected with FLT3 and CBL-B or C-CBL expressed a constitutively lower level of surface FLT3 compared to the cells transfected with FLT3 alone (Fig. 4.13A and 4.13B). Stimulation of FLT3 and C-CBL or FLT3 and CBL-B co-transfected cells with FLT3L exhibited a much stronger downmodulation of surface FLT3 expression than those transfected with FLT3 alone (Fig. 4.13A and 4.13B).

To further understand the intracellular fate of the internalized FLT3, the FLT3 protein levels were examined by Western blot analysis. The results revealed that in the absence of C-CBL or CBL-B co-transfection, although FLT3L stimulation could induce FLT3 downmodulation (Fig. 4.13B), the internalized FLT3 (160kDa mature form) was not degraded as compared to non-

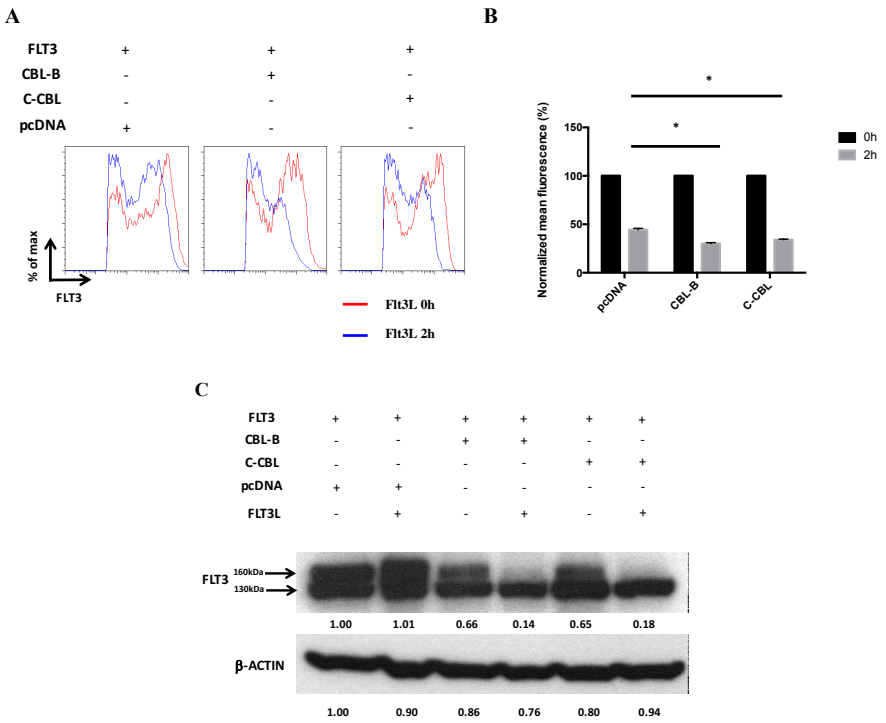

Fig. 4.13. CBL proteins are required for FLT3 degradation.

(A) FACS analysis of surface FLT3 expression in FLT3 or FLT3 and CBL proteins co-transfected cells. 1×10^6 293T cells were seeded in 6-well plate and transfected with either FLT3 (2μg) alone or FLT3 (2μg) and C-CBL (2μg) or CBL-B (2μg) by calcium transfection. 48 hours later, the cells were either non-stimulated or stimulated with 100ng/ml FLT3L for 2 hours at 37°C. The protein synthesis was blocked by 100μg/ml cycloheximide during the stimulation. The surface FLT3 expression was examined by flow cytometry. Red line: Cells before FLT3L stimulation. Blue line: Cells after FLT3L stimulation.

(B) The statistical analysis of FLT3 expression on 293T cells transfected with FLT3 alone or co-transfected with FLT3 and C-CBL or CBL-B. Fluorescence intensities of surface FLT3 on the non-stimulated cells were set as 100%. The fluorescence intensities of surface FLT3 on the FLT3L-stimulated cells were normalized to their non-stimulated baselines. Triplicates were done in this experiment. Ordinary two-way ANOVA and Dunnett's multiple comparisons test was applied to compare the normalized mean fluorescence of CBL-B or C-CBL co-transfected 293T cells with that of FLT3 alone transfected 293T cells, respectively. (n=3) P value <0.05 was considered significant. This experiment has been repeated at least twice.

(C) Western blot analysis of FLT3 expression in FLT3 alone or FLT3 and CBL co-transfected cells. 1×10^6 293T cells were seeded in 6-well plate and transfected with either FLT3 (2μg) alone or FLT3 (2μg) and C-CBL (2μg) or CBL-B (2μg) by calcium transfection. 48 hours later, the cells were either non-stimulated or stimulated with 100ng/ml FLT3L for 2 hours at 37°C. The protein synthesis was blocked by 100μg/ml cycloheximide during the stimulation. The total FLT3 expression level in these cell lysates were detected with anti-FLT3 antibody. β-ACTIN was used as an internal control. The Western blot result was further quantified by ImageJ software. The value of mature form FLT3 in each sample was normalized by the sample at most left, which was set as 1.00. This experiment has been repeated at least twice.

stimulated cells (Fig. 4.13C). The mature form of FLT3 was markedly reduced in C-CBL or CBL-B co-transfected cells with and without FLT3L stimulation (Fig. 4.13C), thus indicating that the degradation of internalized FLT3 requires C-CBL or CBL-B.

IV. 4.5. CBL proteins promote the degradation of FLT3 through both proteasome and lysosome degradation pathways

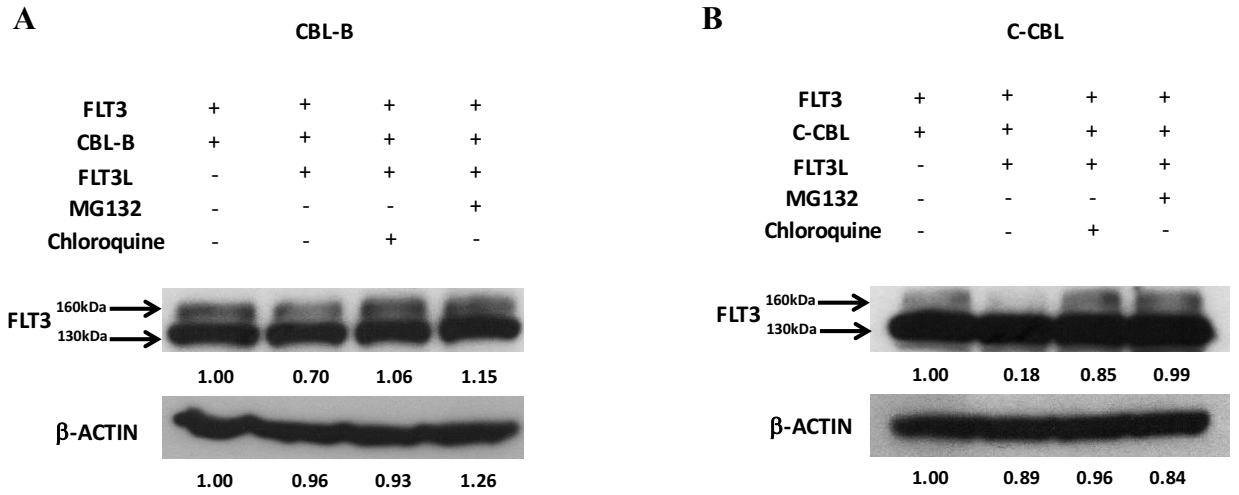

Fig. 4.14. CBL-B and C-CBL promote FLT3 degradation through both proteasome and lysosome dependent manners.
(A & B) Blockade of CBL-B and C-CBL mediated FLT3 degradation by Chloroquine and MG132. 1×10^6 293T cells were seeded in 6-well plate and co-transfected with FLT3 (2μg) and CBL-B (2μg) or C-CBL (2μg) by calcium transfection. 48 hours later, the cells were either non-stimulated or stimulated with 100ng/ml FLT3L for 2 hours at 37°C. The protein synthesis was blocked by 100μg/ml cycloheximide during the stimulation. 10μM MG132 or 50μM chloroquine were also used during the 2 hours' stimulation to block the proteasome and lysosome pathways respectively. 160kDa mature form and 130kDa immature form of FLT3 are indicated by the arrows. β-ACTIN was used as an internal control. The Western blot result was further quantified by ImageJ software. The value of mature form FLT3 in each sample was normalized by the sample at most left, which was set as 1.00. This experiment has been repeated twice.

Protein degradation may occur via either proteasome or lysosome pathways. Since CBL-B or C-CBL was required for FLT3 degradation, the next question is which degradation pathway is involved in CBL family proteins mediated FLT3 degradation. The lysosome pathway, which is mainly used by surface receptors, can be blocked by chloroquine. In contrast, the proteasome pathway, which is mainly used by intracellular proteins, can be blocked by MG132. To examine whether CBL proteins use these pathways to degrade FLT3, the FLT3 expression was examined

in FLT3 and CBL proteins co-transfected cells after chloroquine or MG132 blockade. It was interesting to see that both chloroquine and MG132 blocked FLT3 degradation in the presence of either CBL-B or C-CBL (Fig. 4.14A and 4.14B). This finding thus indicates that CBL proteins can use both proteasome and lysosome pathways for FLT3 degradation.

IV. 4.6. CBL-B and C-CBL mediate the ubiquitination of FLT3

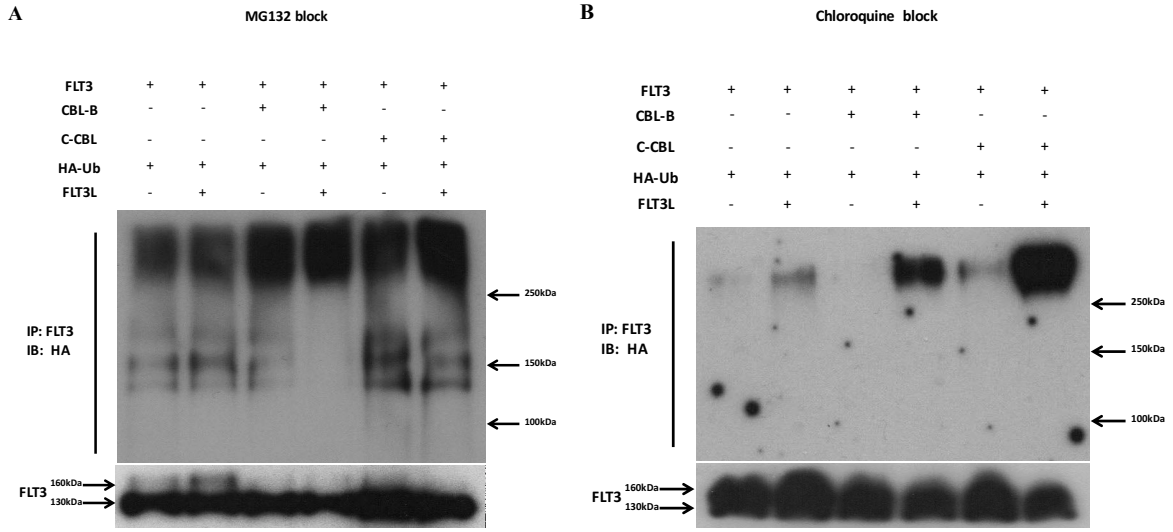

Fig. 4.15. CBL-B and C-CBL promote FLT3 ubiquitination.
(A) Western blot analysis of FLT3 ubiquitination in 293T cells. 1×10^6 293T cells were seeded in 6-well plate. FLT3 (2μg) and HA-Ub (2μg) were co-transfected with CBL-B (2μg) or C-CBL (2μg) by calcium transfection. 48 hours later, the cells were treated with 100μg/ml cycloheximide and 10μM MG132 for 30 mins at 37°C. Then the cells were stimulated with 100ng/ml FLT3L or without for 15 mins at 37°C. The FLT3 in the treated cells was then immunoprecipitated by anti-FLT3 antibody and the ubiquitination of FLT3 was detected by using an anti-HA antibody. FLT3 was used as an internal control. This experiment has been repeated twice.
(B) Western blot analysis of FLT3 ubiquitination in 293T cells. 1×10^6 293T cells were seeded in 6-well plate. FLT3 (2μg) and HA-Ub (2μg) were co-transfected with CBL-B (2μg) or C-CBL (2μg) by calcium transfection. 48 hours later, the cells were treated with 100μg/ml cycloheximide and 50μM chloroquine for 30 mins at 37°C. Then the cells were stimulated with 100ng/ml FLT3L or without for 15 mins at 37°C. The FLT3 in the treated cells was then immunoprecipitated by anti-FLT3 antibody and the ubiquitination of FLT3 was detected by using an anti-HA antibody. FLT3 was used as an internal control. This experiment has been repeated at least twice.

Since both CBL-B and C-CBL are E3 ubiquitin ligases, I decided to examine whether they promote FLT3 ubiquitination. To do so, 293T cells were transfected with either FLT3 alone or FLT3 with CBL-B or C-CBL. A HA-tag ubiquitin expression plasmid was also co-transfected into the cells to increase the sensitivity of detecting the ubiquitination. The transfected cells were then

stimulated with FLT3L or without. MG132 or chloroquine was also used to block the proteasome or lysosome degradation pathway respectively. The cells that co-transfected with CBL-B or C-CBL have markedly enhanced level of FLT3 ubiquitination especially for the chloroquine treated cells (Fig. 4.15A and 4.15B) It thus indicates that both CBL-B and C-CBL may promote FLT3 ubiquitination upon FLT3L stimulation.

IV. 5. E3 ubiquitin ligase function of CBL-B is required for the maintenance of CD8α$^+$ cDC and pDC homeostasis

The CBL family of proteins can function either as E3 ubiquitin ligases or signaling adaptors that transduce signals through assembling of multi-molecular signalosomes. To determine whether CBL-B regulate CD8α$^+$ cDC and pDC homeostasis through its E3 ubiquitin ligase function, I decided to analyze DC homeostasis in a mutant mouse model in which DCs expressed only a ubiquitin ligase function deficient *Cbl-b*, and *C-cbl* was kept absent. To generate the mutant mice, *Cbl* dKO mice were crossed with *C-cbl*$^{f/f}$; *Cbl-b*$^{C373A/C373A}$ mutant mice, and the heterozygous mice (*Cd11c* Cre; *C-cbl*$^{f/f}$; *Cbl-b*$^{C373A/-}$) were used in the experiment. The C373A mutation substitutes the N-terminal consensus cysteine residue in the RING finger domain of CBL-B for an alanine, which still retains the adaptor function but not the ubiquitination function of CBL-B[305]. The results revealed that in the *Cd11c* Cre; *C-cbl*$^{f/f}$; *Cbl-b*$^{C373A/-}$ mutant mice, both splenic CD8α$^+$ cDCs and pDCs recapitulated the phenotypes of their counterparts in the *Cbl* dKO mice (Fig. 4.16A and 4.16B). Thus, these results indicate that E3 ubiquitin ligase function, but not the adaptor function of *Cbl-b* is required for the maintenance of homeostasis of both CD8α$^+$ cDCs and pDCs.

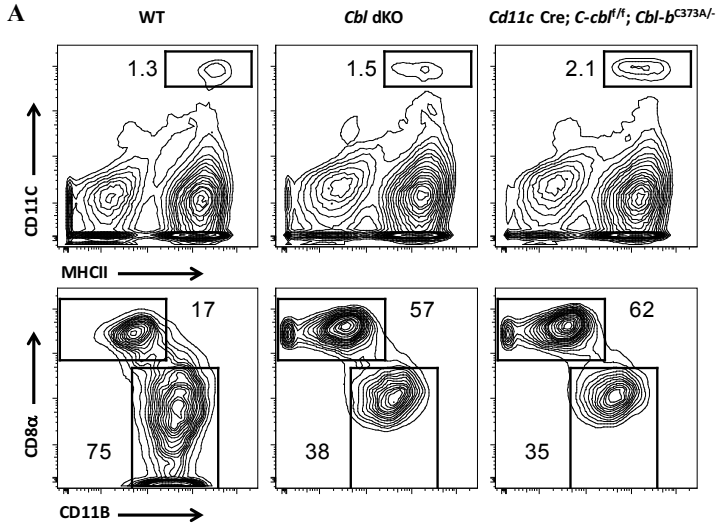

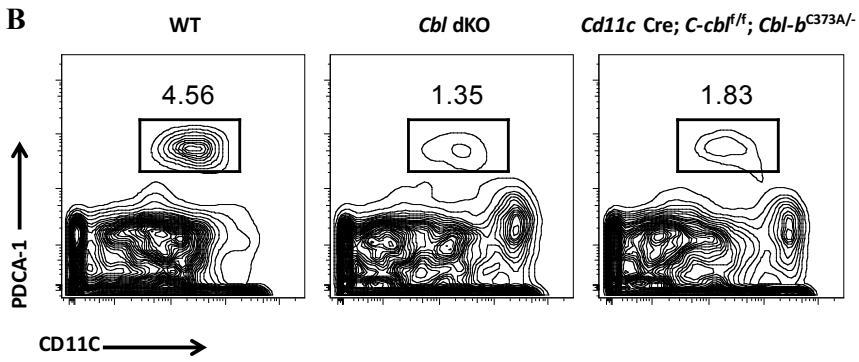

Fig. 4.16. E3 ubiquitin ligase function of CBL-B is required for the maintenance of DC homeostasis.
(A) FACS analysis of DC subsets in the SP of *Cd11c* Cre; *C-cbl*$^{f/f}$; *Cbl-b*$^{C373A/-}$ mutant mice. *Cd11c* Cre; *C-cbl*$^{f/f}$; *Cbl-b*$^{C373A/-}$ mutant mice were generated by crossing *Cbl* dKO mice with *C-cbl*$^{f/f}$; *Cbl-b*$^{C373A/C373A}$ mutant mice. Total splenic cells from 10-week-old WT, *Cbl* dKO, and *Cd11c* Cre; *C-cbl*$^{f/f}$; *Cbl-b*$^{C373A/-}$ mutant mice were stained with anti-CD11C, MHCII, CD11B and CD8α antibodies. Cells were then analyzed on a FACS LSRII. Shown are contour maps of CD11C vs MHCII staining (top panel) and CD8α vs CD11B staining of gated DC population (bottom panel).
(B) FACS analysis of DC subsets in the SP of *Cd11c* Cre; *C-cbl*$^{f/f}$; *Cbl-b*$^{C373A/-}$ mutant mice. *Cd11c* Cre; *C-cbl*$^{f/f}$; *Cbl-b*$^{C373A/-}$ mutant mice were generated by crossing *Cbl* dKO mice with *C-cbl*$^{f/f}$; *Cbl-b*$^{C373A/C373A}$ mutant mice. Total splenic cells from 10-week-old WT, *Cbl* dKO, and *Cd11c* Cre; *C-cbl*$^{f/f}$; *Cbl-b*$^{C373A/-}$ mutant mice were stained with anti-CD11C, PDCA-1, and lineage markers (CD3, CD19, NK1.1 and TER119). Cells were then analyzed on a FACS LSRII. Shown are contour maps of CD11C vs PDCA-1 staining of gated Lin$^-$ cells.

IV. 6. *Cbl* dKO mice develop spontaneous auto-inflammatory disease

IV. 6.1. Cbl dKO mice exhibit a shorter life span and lower body weight

Since DC homeostasis has been significantly altered in *Cbl* dKO mice, I decided to examine whether the immune status is also affected in the mutant mice. The results revealed that the *Cbl* dKO mice had a significantly shorter life span than the WT mice. The death started at less than 5 months of age, and by around 10 months of age, all *Cbl* dKO mice became moribund (Fig. 4.17A). Inspection of the *Cbl* dKO sick mice revealed that they had significantly reduction in body weight, splenomegaly, and lymphadenopathy (Fig. 4.17B, 4.17C, and 4.17D). The sick mice also had yellow skin, suggesting that they could have a severe liver damage.

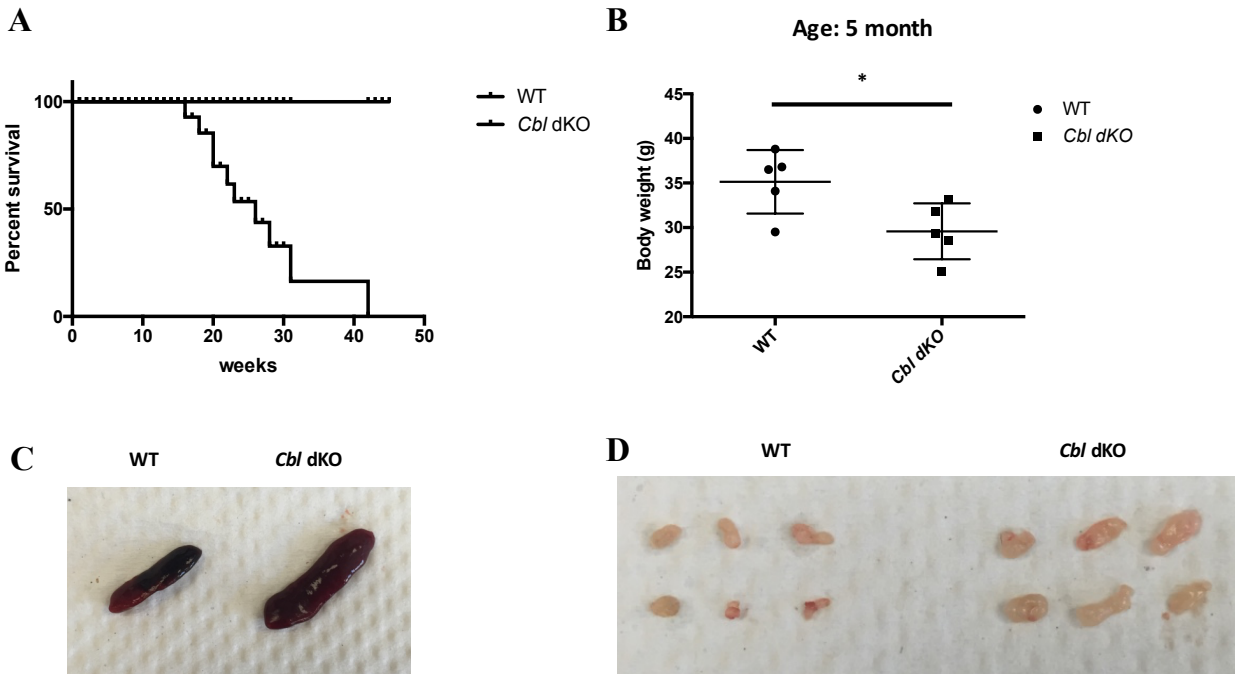

Fig. 4.17. *Cbl* dKO mice have a shorter life span and signs of ongoing inflammation.
(A) *Cbl* dKO mice had a shortened lifespan. Shown are the Kaplan-Meier's survival curves of *Cbl* dKO and WT controls. Gehan-Breslow-Wilcoxon test was applied to compare the survival curve. (n=10) P value <0.05 was considered significant.
(B) Average body weight of 5-month-old WT and *Cbl* dKO mice. Unpaired t test with equal SD was applied to compare the difference. (n=5) P value <0.05 was considered significant.
(C) Images of spleens of 5-month-old WT and *Cbl* dKO mice. *Cbl* dKO mice developed splenomegaly at 5-month of age.
(D) Images of skin draining lymph nodes of 5-month-old WT and *Cbl* dKO mice. *Cbl* dKO mice developed lymphadenopathy at 5-month of age.

IV. 6.2. Cbl dKO mice develop severe inflammatory diseases

To understand the cause of the sickness of the *Cbl* dKO mice, the blood of the sick mice was analyzed. The results revealed that sick *Cbl* dKO mice generally had significantly elevated blood sedimentation rate compared to the healthy WT mice (Fig. 4.18A). However, further analysis could not detect serum autoantibodies against anti-nuclear antigens (ANA) in these sick mutant mice, suggesting that the disease is unlikely mediated by autoantibody (Fig. 4.18B). The further ELISA assay result revealed that *Cbl* dKO mice had significantly higher levels of pro-inflammatory cytokines such as TNF-α and IL-6 in the serum compared to the age-matched WT mice (Fig. 4.18C). This result thus indicates that *Cbl* dKO mice develop severe inflammation rather than autoantibody mediated autoimmune diseases.

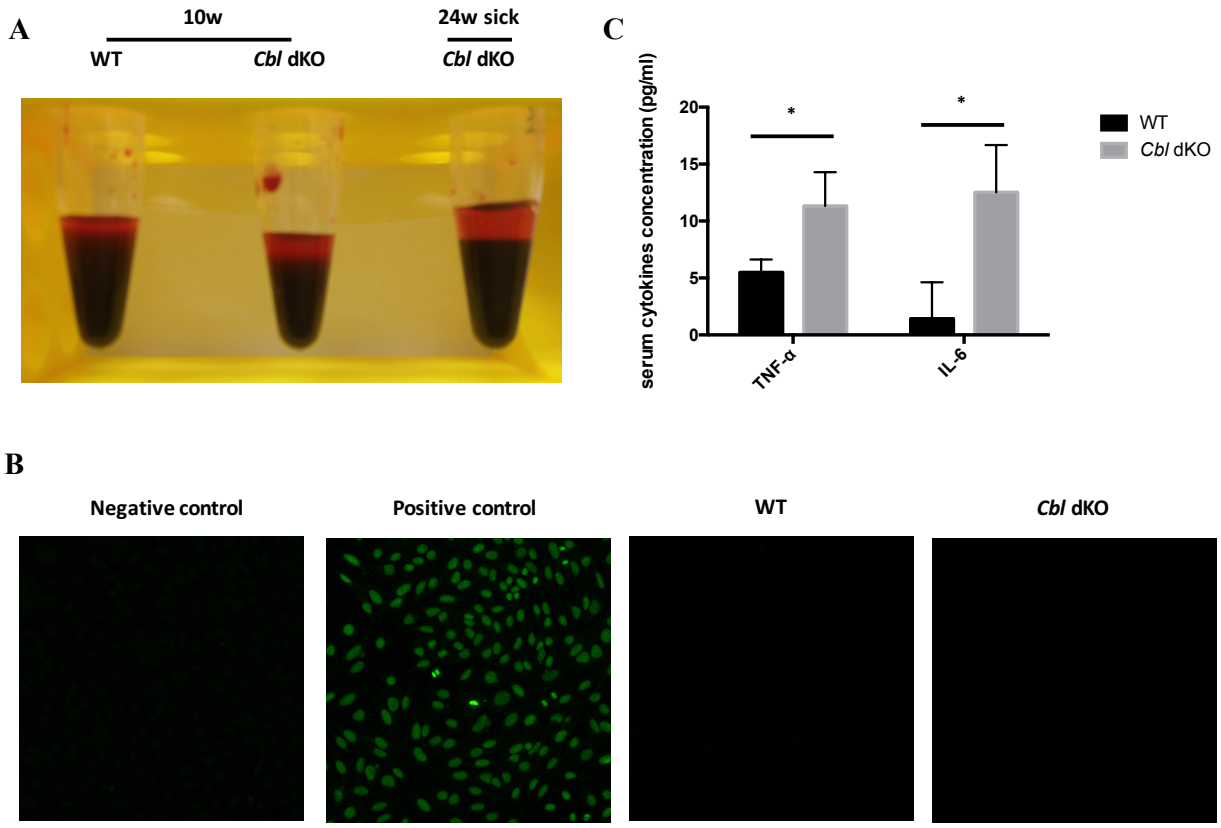

Fig. 4.18. *Cbl* dKO mice have severe inflammatory disease.
(A) *Cbl* dKO mice had increased blood sedimentation rate. The whole blood was collected from 10-week-old WT and *Cbl* dKO mice and 24-week-old sick *Cbl* dKO mice after sacrifice. Sedimentation was allowed to occur without centrifugation for 1 hour at room temperature.
(B) Serum anti-nuclear antigen autoantibody (ANA) detection. 100μl sera were collected from 6-month-old WT and sick *Cbl* dKO mice. ANA in the sera was measured by using a Kallestad HEp-2 kit (#32583, Bio-rad). Negative and positive controls were provided by the manufacturer.
(C) Serum levels of TNF-α and IL-6 in *Cbl* dKO mice. 100μl sera were collected from 3-month-old WT and *Cbl* dKO mice. The TNF-α and IL-6 concentrations were measured by ELISA. Multiple t tests with fewer assumptions and Holm-Sidak correction method were applied in the analysis. (n=5) P value <0.05 was considered significant.

IV. 6.3. Sick Cbl dKO mice have severe leukocyte infiltration in the liver and lung

To further understand the impact of inflammation in the sick mice, pathological analysis was performed on the major organs from the sick *Cbl* dKO mice. The results revealed that the sick mutant mice had exclusively massive leukocyte infiltration in the liver and lung. In some *Cbl* dKO mice, leukocyte infiltration could also be found in the kidney, and salivary gland. Moreover, the

spleen architecture of *Cbl* dKO mice was severely disrupted (Fig. 4.19). In contrast, the heart, intestinal, and pancreas exhibited little change as compared to the WT controls. Based on this result, I conclude that the *Cbl* dKO mice mainly manifest severe liver inflammation. In the later study, I will only focus on the liver and peripheral lymphoid organs for my study.

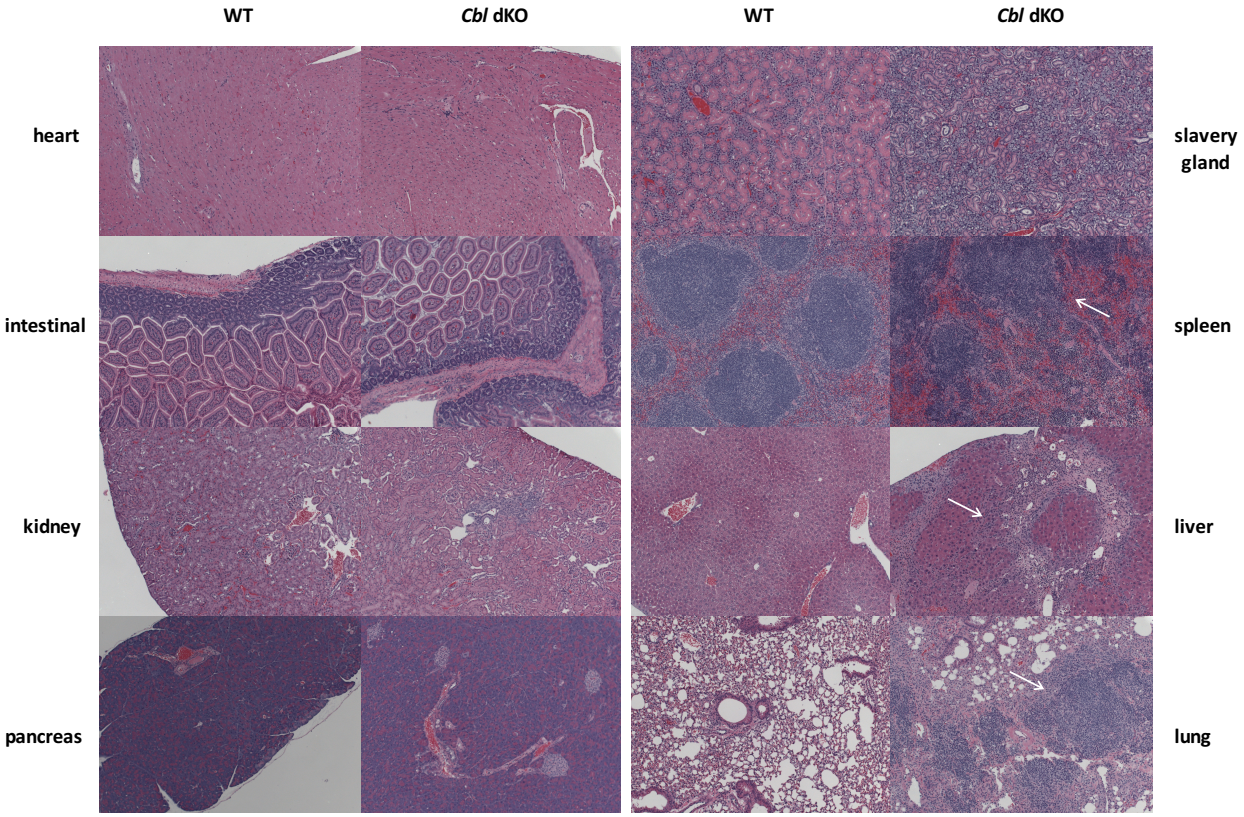

Fig. 4.19. Pathological analysis of major organs of the *Cbl* dKO mice.
Shown are the images of H/E staining of the tissue sections of multiple organs (liver, lung, spleen, slavery gland, pancreas, kidney, intestinal, and heart) from sick *Cbl* dKO mice and age-matched WT mice. The white arrows indicate the areas of leukocyte infiltration.

IV. 6.4. Cbl dKO mice have more activated T cells and Tregs

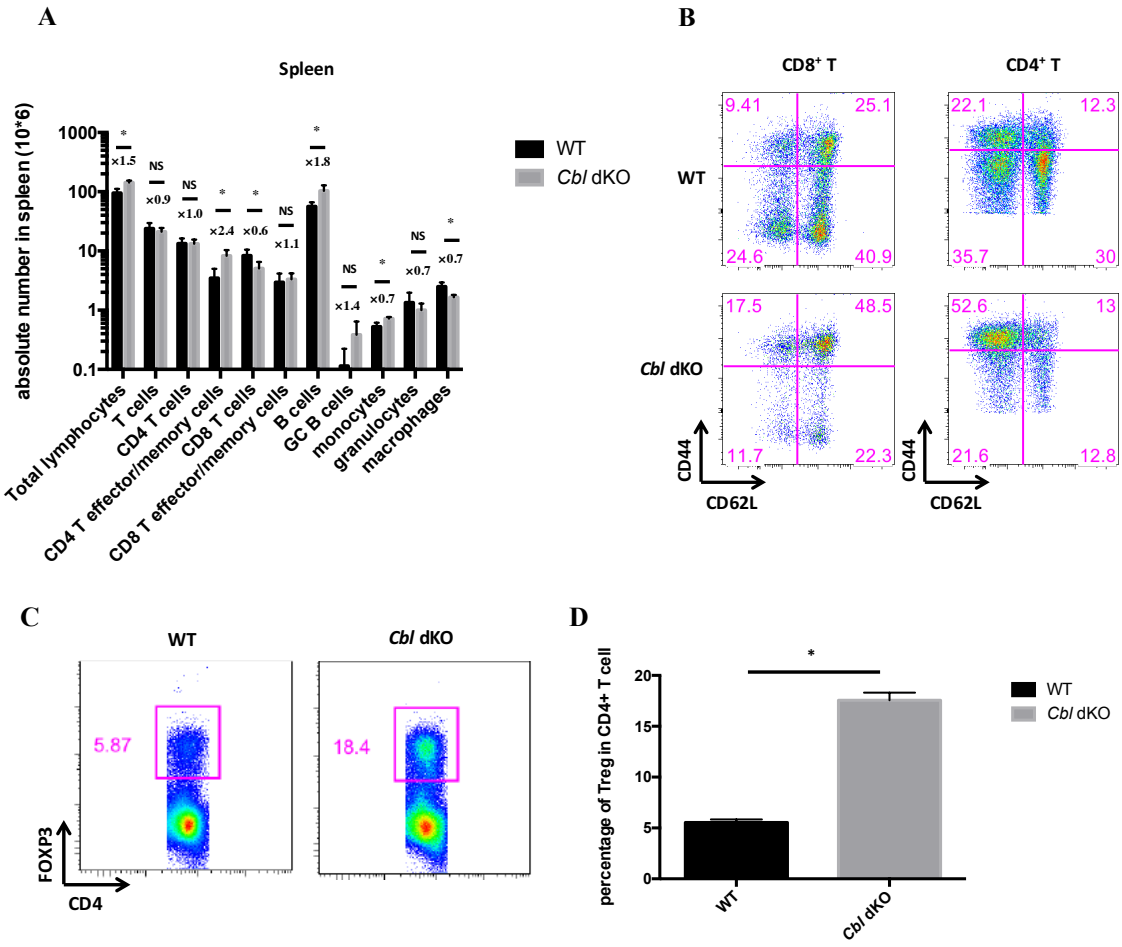

Fig. 4.20. *Cbl* dKO mice have increased numbers of splenic effector/memory T cells and Tregs.

(A) The SP cellularity analysis of *Cbl* dKO mice. Total splenic cells from 5-month-old WT and *Cbl* dKO mice were stained for various cell surface markers and analyzed by flow cytometry. The ratio of absolute numbers of different cell populations between *Cbl* dKO vs WT are also displayed in the figure. Multiple t tests with fewer assumptions and Holm-Sidak correction method were applied in the analysis. (n=5) P value <0.05 was considered significant.

(B) Flow cytometric analysis of T cell activation. Splenic cells from 5-month-old WT and *Cbl* dKO mice were stained with TCRβ, CD4, CD8, CD44 and CD62L. Shown are CD44 vs CD62L staining of gated $TCR\beta^+CD8^+$ T cells and $TCR\beta^+CD4^+$ T cells. Representative data of 5 mice.

(C) FACS analysis of splenic $FOXP3^+$ Treg cells. Shown are FOXP3 vs CD4 staining of gated $TCR\beta^+CD4^+$ splenic T cells from 5-month-old WT and *Cbl* dKO mice. The percentages of $FOXP3^+$ Tregs in the total $TCR\beta^+CD4^+$ splenic T cells were indicated in the plots.

(D) The statistical analysis of the percentages of $FOXP3^+$ splenic Treg cells in 5-month-old WT and *Cbl* dKO mice. Multiple t tests with fewer assumptions and Holm-Sidak correction method were applied in the analysis. (n=3) P value <0.05 was considered significant.

Inflammation in *Cbl* dKO mice can be caused by activated lymphocytes or some other factors. To further understand the status of leukocyte activation in *Cbl* dKO mice, the splenic cellularity analysis was carried out by flow cytometry. The results revealed that the absolute numbers of B cells and $CD4^+$ T effector/memory cells were significantly increased in the spleen of *Cbl* dKO mice compared to age-matched WT mice. In contrast, the numbers of $CD8^+$ T cells, monocytes, and macrophages were significantly reduced (Fig. 4.20A). Furthermore, within both $CD8^+$ and $CD4^+$ T cell populations, there was a dramatic reduction in the percentages of $CD62L^+CD44^-$ naïve T cells and an increase in the percentages of $CD44^+$ effector/memory T cells (Fig. 4.20B). Interestingly, there was also an increase in the percentage of splenic Tregs of *Cbl* dKO mice, a phenotype that is similar with FLT3L triggered WT mice (Fig. 4.20C and 4.20D)[306]. Thus, the constitutive activation of lymphocytes can be one of the reasons contributing to the chronic inflammatory disease in *Cbl* dKO mice.

IV. 6.5. Cbl dKO mice possess increased numbers of activated T cells and $CD103^+$ cDCs in the liver

Because there was severe liver inflammation and leucocyte infiltration in the liver of the sick *Cbl* dKO mice, the cellularity analysis of the leukocytes in the liver was also carried out. The results revealed that there was a significant increase of both $CD4^+$ and $CD8^+$ T cells in the liver of *Cbl* dKO mice compared to the WT mice (Fig. 4.21A). Among these $CD8^+$ and $CD4^+$ infiltrating T cells, the majorities of them were effector/memory T cells as they expressed $CD44^{hi}CD62L^{lo}$ surface markers (Fig. 4.21B). Interestingly, there were also massive infiltrations of myeloid lineage cells including DCs, granulocytes, monocytes, and macrophages in the liver of sick mice (Fig. 4.21A). Most strikingly, among the DC population, there were a 40-fold increase of total DC number and a 79-fold increase of $CD103^+$ cDC number; however, there was only a 2-fold increase of $CD11B^+$ cDC number (Fig. 4.21A). Since DCs are the only cell populations that have *Cbl* double deletion, this finding suggests that $CD103^+$ cDCs, a closely related lineage of splenic $CD8\alpha^+$ cDCs, might be the initial cells that recruit other infiltrating cells to the site.

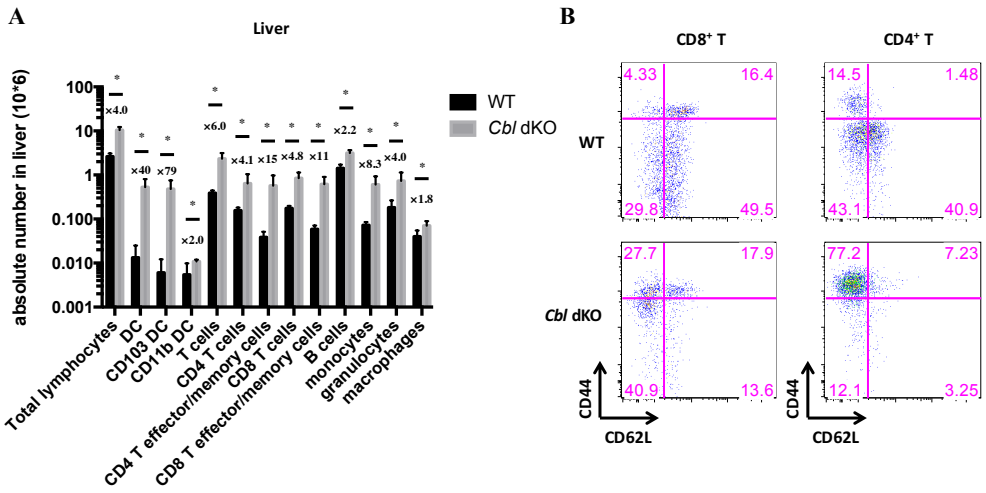

Fig. 4.21. *Cbl* dKO mice have markedly increased numbers of CD103$^+$ cDCs and other infiltrating hematopoietic cells in the liver.
(A) Cellularity analysis of liver infiltrating hematopoietic cells. The mononuclear cells in the liver of 5-month-old WT and *Cbl* dKO mice were isolated through gradient purification method as described in the Material and Method section. The purified liver mononuclear cells were stained for various cell surface markers and analyzed by flow cytometry. The ratio of absolute numbers of different cell populations between *Cbl* dKO vs WT are also displayed in the figure. Multiple t tests with fewer assumptions and Holm-Sidak correction method were applied in the statistics. (n=5) P value <0.05 was considered significant.
(B) Flow cytometric analysis of T cell activation. Liver mononuclear cells from 5-month-old WT and *Cbl* dKO mice were stained with TCRβ, CD4, CD8, CD44 and CD62L. Shown are CD44 vs CD62L staining of gated TCRβ$^+$CD8$^+$ T cells and TCRβ$^+$CD4$^+$ T cells. Representative data of 5 mice.

IV. 6.6. The splenic effector/memory T cells in Cbl dKO mice are Th1 type of T cells

Effector/memory T cells can be classified into Th1, Th2 and Th17[307]. Cytokine production profile of these activated *Cbl* dKO T cells was investigated to understand what type of T help cells they are. Fresh isolated splenocytes were stimulated with PMA/ionomycin, and stained for intracellular IFN-γ, IL-2, and IL-4. To exclude the influence of *Cbl-b* KO mutation, both *Cbl-b* KO and WT T cells were used as controls. The results revealed that the percentages of IFN-γ producing CD4$^+$ and CD8$^+$ T cells were dramatically increased in *Cbl* dKO mice compared to that in *Cbl-b* KO and WT mice (Fig. 4.22A and 4.22C). In contrast, the percentages of IL-2 producing CD4$^+$ and CD8$^+$ T cells was not changed as compared to the controls (Fig. 4.22B and 4.22D). Moreover, the IL-4 producing cells could not be detected in the mutant and WT T cells (data not shown). This result indicates that the activated T cells in *Cbl* dKO mice are primed to Th1 type of effector cells.

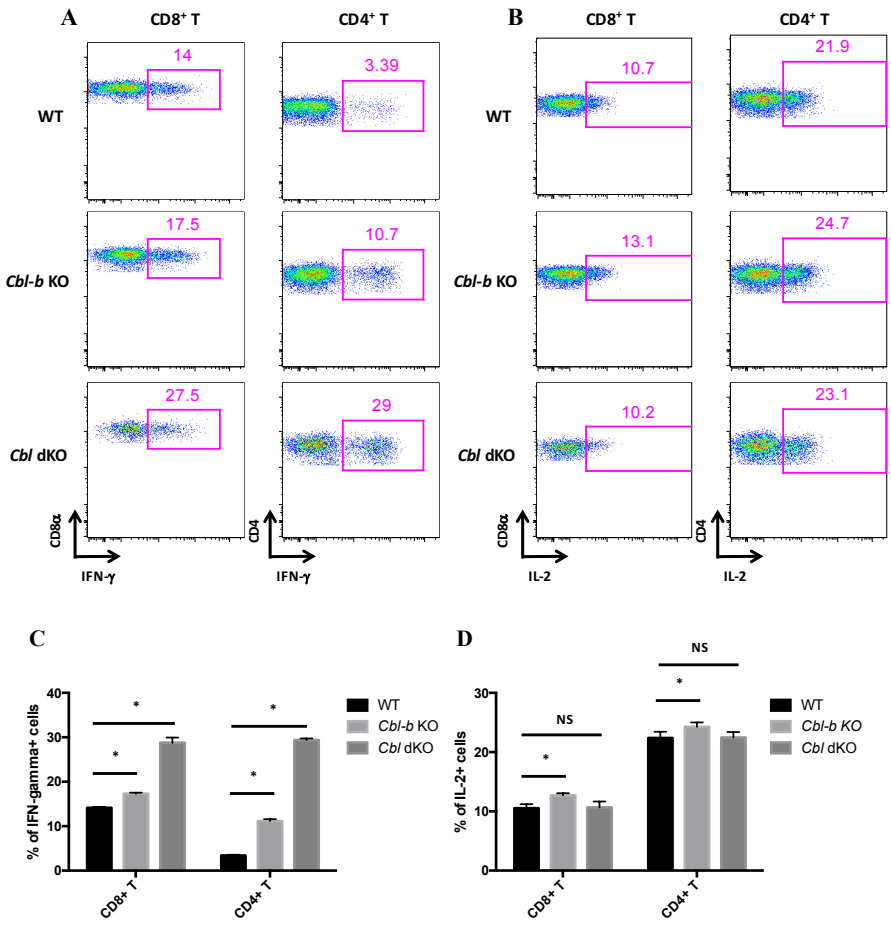

Fig. 4.22. T cells in *Cbl* dKO mice are primed to Th1 type effector T cells.

(A) FACS analysis of IFN-γ producing T cells. 5×10^6 splenocytes were seeded in 12-well plate and stimulated with 20ng/ml PMA, 1μg/ml ionomycin in the presence of 2.5μg/ml brefeldin A for 6 hours at 37°C. The percentages of IFN-γ producing cells were visualized by surface staining of CD3e, CD4, CD8α and intracellular staining of IFN-γ. Shown are dot plots of IFN-γ vs CD4 gated on $CD3^+CD4^+$ T cells, and IFN-γ vs CD8 gated on $CD3^+CD8^+$ T cells.

(B) FACS analysis of IL-2 producing T cells. 5×10^6 splenocytes were seeded in 12-well plate and stimulated with 20ng/ml PMA, 1μg/ml ionomycin in the presence of 2.5μg/ml brefeldin A for 6 hours at 37°C. The percentages of IL-2 producing cells were visualized by surface staining of CD3e, CD4, CD8α and intracellular staining of IL-2. Shown are dot plots of IL-2 vs CD4 gated on $CD3^+CD4^+$ T cells, and IL-2 vs CD8 gated on $CD3^+CD8^+$ T cells.

(C) Statistical analysis of the percentages of IFN-γ producing $CD8^+$ and $CD4^+$ T cells in the SP of WT, *Cbl-b* KO, and *Cbl* dKO mice. Triplicates were done in this experiment. Multiple t tests with fewer assumptions and Holm-Sidak correction method were applied in the analysis. (n=3) P value <0.05 was considered significant. This experiment has been repeated twice.

(D) Statistical analysis of the percentages of IL-2 producing $CD8^+$ and $CD4^+$ T cells in the SP of WT, *Cbl-b* KO, and *Cbl* dKO mice. Triplicates were done in this experiment. Multiple t tests with fewer assumptions and Holm-Sidak correction method were applied in the analysis. (n=3) P value <0.05 was considered significant. This experiment has been repeated twice.

IV.7. Mechanisms leading to the inflammation in *Cbl* dKO mice

IV. 7.1. The Cbl dKO mutation does not alter the expression of co-stimulatory molecules on DCs.

DCs activate T cells through their MHCs, co-stimulatory ligands and cytokines. Flow cytometry was applied to study whether the *Cbl* dKO mutation altered the expression of these co-stimulatory molecules. The results revealed that the expressions of the co-stimulatory molecules such as CD40, CD80, and CD86 were not changed in the *Cbl* dKO $CD8\alpha^+$ cDCs and $CD11B^+$ cDCs as compared to their counterparts in WT, *Cbl-b* KO, and *C-cbl* KO mice (Fig 4.23). The expression of inhibitory ligand PD-L1 was also not changed in both *Cbl* dKO $CD8\alpha^+$ and $CD11B^+$ cDCs (Fig 4.23). It is noteworthy that the expression of PD-L1 was constitutively higher in $CD11B^+$ cDCs than in $CD8\alpha^+$ cDCs (Fig 4.23), suggesting that the $CD11B^+$ cDCs may have more prominent role in immune suppression. Since the ratio of $CD8\alpha^+$ cDCs versus $CD11B^+$ cDCs in *Cbl* dKO mice is much higher than that in WT controls, it could be imagined that the inhibitory effects imposed by $CD11B^+$ cDCs through PD-L1 could be accordingly reduced in *Cbl* dKO mice.

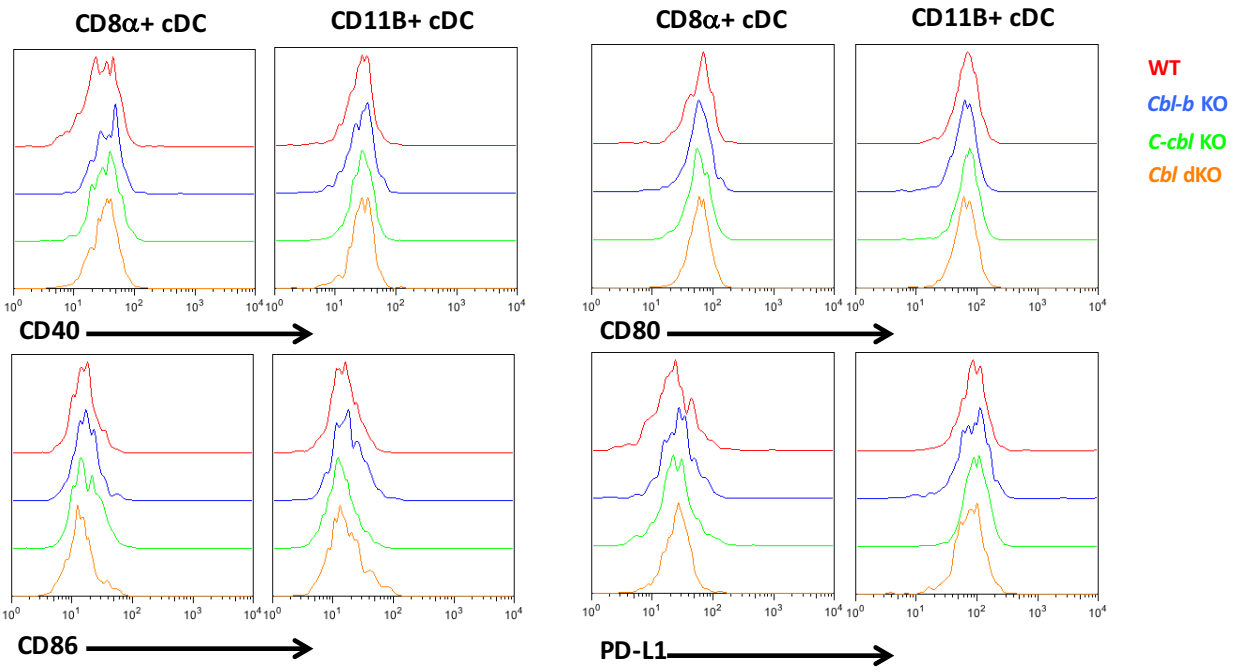

Fig. 4.23. FACS analysis of the expression of co-stimulatory molecules on *Cbl* dKO DCs. Splenic $CD8\alpha^+$ and $CD11B^+$ DCs from 3-month-old WT, *Cbl-b* KO, *C-cbl* KO, and *Cbl* dKO mice were stained with anti-MHCII, CD11C, CD11B, CD8α together with anti-CD40, CD80, CD86, or PD-L1 and then analyzed by flow cytometry. Shown are histograms of CD40, CD80, CD86, and PD-L1 expression gated on $MHCII^+CD11C^+CD8\alpha^+$ cDCs and $MHCII^+CD11C^+CD11B^+$ cDCs. This experiment has been repeated at least twice.

IV. 7.2. Cbl dKO CD8α$^+$ DCs have an enhanced capability to present antigens.

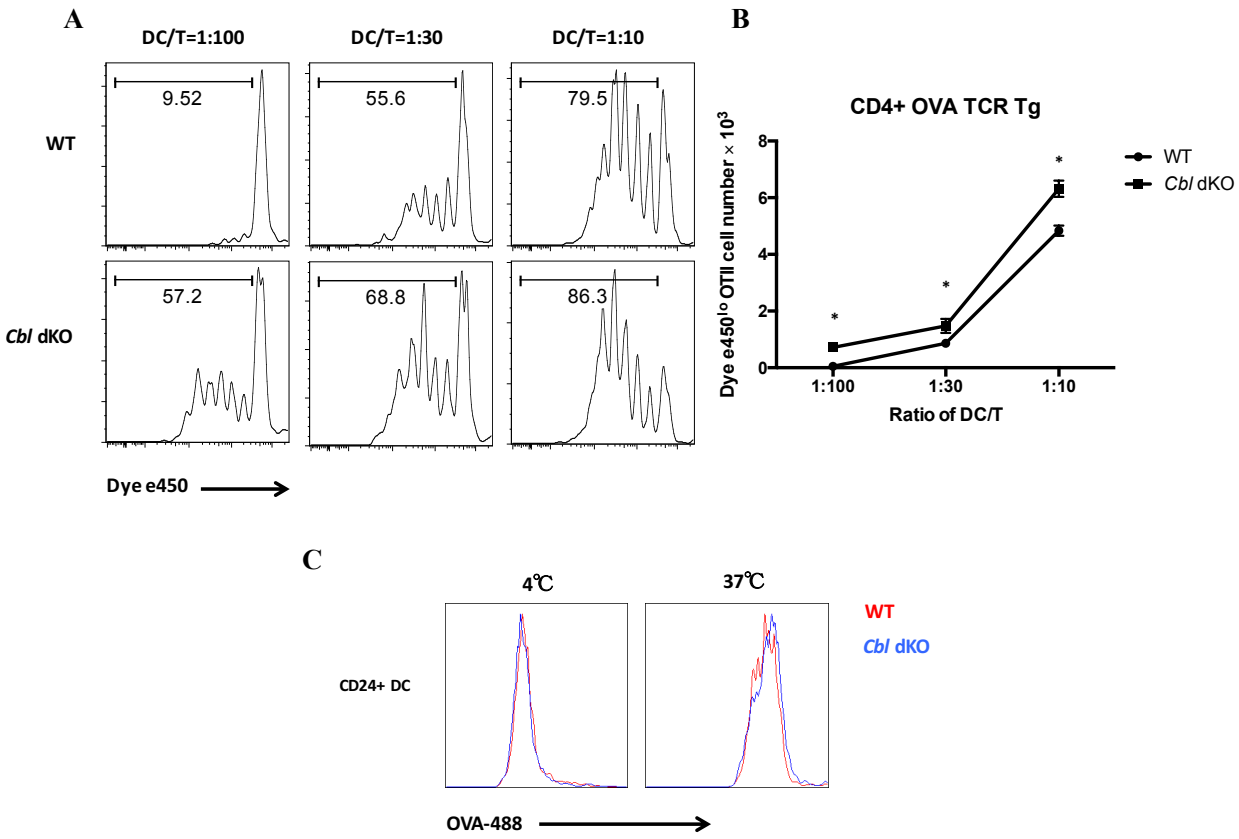

Fig. 4.24. The *Cbl* dKO mutation enhances antigen-presentation capacity of CD8α$^+$ cDCs.
(A) Antigen presentation by CD8α$^+$ cDCs to CD4$^+$ OT-II T cells. 5×10^4 purified dye e450 labeled OT-II T cells were co-cultured with different ratios of splenic WT and *Cbl* dKO CD8α$^+$ cDCs in the presence of OVA antigen (40 μg/ml) for 96 hours. Percentages of e450^{lo} OT-II T cells were analyzed by FACS and shown in the histogram.
(B) The statistical analysis of dye e450^{lo} OT-II T cell number in OVA antigen presentation assay. The experiment was done in triplicates in each DC/T ratio. Multiple t tests with fewer assumptions and Holm-Sidak correction method were applied in the statistics. (n=3) P value <0.05 was considered significant. This experiment has been repeated twice.
(C) Analysis of antigen capture capacity of CD8α$^+$ cDCs. 5×10^5 WT and *Cbl* dKO CD24$^+$ cDCs were cultured at 4°C or 37°C for 30 min in the presence of Alexa488$^+$ OVA antigen (15μg/ml). Shown are histograms of Alexa488 level in WT and *Cbl* dKO CD24$^+$ cDCs.

In addition to the co-stimulation, DCs also influence T cell activation by antigen presentation. Since previous results showed that CD8α+ cDCs had an enhanced capability to cross-present OVA antigens to CD8$^+$ OT-I T cells (Fig. 4.6C and 4.6D), I decided to examine whether antigen

processing and presentation to $CD4^+$ T cells by DCs is also enhanced in the absence of CBL proteins. To do so, purified splenic $CD8\alpha^+$ cDCs from WT and *Cbl* dKO mice were co-cultured with dye e450 labeled $CD4^+$ OT-II T cells in different DC/T ratios. OVA antigen was added to the culture so it could be processed and presented to $CD4^+$ OT-II T cells in the form of MHCII-peptide complexes. The results revealed that *Cbl* dKO $CD8\alpha^+$ cDCs showed significantly enhanced antigen-processing and presenting capacity compared to WT $CD8\alpha^+$ cDCs, with more profound difference found in the culture with a lower DC/T ratio (Fig. 4.24A and 4.24B). The antigen presentation by DCs is a multi-step process including antigen capture, antigen processing, and peptide loading on MHC. To understand which of these steps is affected by CBL-B and C-CBL, the antigen capture step was also investigated. Alexa488 conjugated OVA was incubated with sorted $CD24^+$ cDCs for 30 min at 4°C and 37°C respectively. At 4°C, endocytosis is severely impaired, therefore, there was no antigen capture in both WT and *Cbl* dKO $CD24^+$ cDCs. However, incubation at 37°C led to efficient loading of $Alexa488^+$ OVA antigen into both WT and *Cbl* dKO $CD24^+$ cDCs, suggesting that the antigen capture is not altered by *Cbl* dKO mutation (Fig. 4.24C). Investigation to determine whether antigen degradation and transport inside DCs are altered by *Cbl* dKO mutation is still ongoing.

IV. 7.3. Altered cytokine and chemokine expression profiles in Cbl dKO $CD8\alpha^+$ cDCs and $CD11B^+$ cDCs

In addition to the MHC molecules and co-stimulatory molecules, it was known that cytokine could also dictate the activated T cells into different Th subsets. For example, IL-12 and IFN-γ could drive activated T cells into Th1 cells[308]. IL-4 and IL-10 could inhibit Th1 cell differentiation, but promote Th2 cell differentiation[308]. The RNA seq experiment was conducted to determine the cytokine expression profile of *Cbl* dKO $CD8\alpha^+$ cDCs and $CD11B^+$ cDCs. The results revealed that among the most abundantly expressed cytokines in DCs, IL-6, IL-15, IL-18, and IL-21 expression were dramatically enhanced (Fig. 4.25A). IL-6 was known as a major pro-inflammatory cytokine with also anti-inflammatory properties[309]. IL-15 was known to support NK and T cell proliferation[310, 311]. IL-18 may induce IFN-γ production by NK and T cells[312, 313], which could at least explain the increased percentage of IFN-γ^+ T cells in the SP of *Cbl* dKO mice. IL-21 was known to be required for sustained $CD8^+$ T cell effector activity in viral infection, which could explain the increased proportion of T effector/memory cells in *Cbl* dKO mice[314].

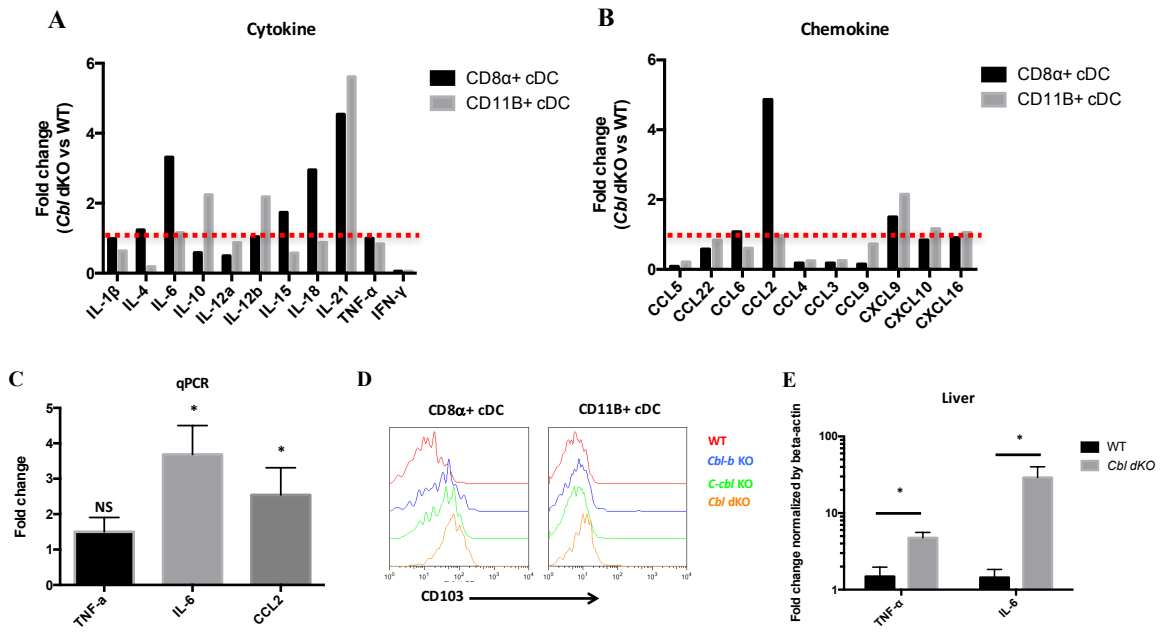

Fig. 4.25. The cytokine and chemokine expression profiles of *Cbl* dKO CD8α$^+$ and CD11B$^+$ cDCs.

(A & B) RNA seq analysis of cytokine and chemokine production by *Cbl* dKO DCs. 5×10^5 CD8α$^+$ and CD11B$^+$ cDCs were purified from pooled splenocytes of several 2-month-old WT or *Cbl* dKO mice following the procedures as described in the Material and Method section. 1μg RNA from CD8α$^+$ and CD11B$^+$ cDCs were provided to the RNA-seq analysis respectively. The RNA-seq data were mapped to GRCm38 mouse reference genome and the calculations of differential gene expression were performed with DESeq or Cufflinks.

(C) qPCR analysis of TNF-α, IL-6, and CCL2 expression in SP CD8α$^+$ cDCs. Splenic CD8a$^+$ cDCs were purified from 3-month-old WT and *Cbl* dKO mice following the procedures as described in the Material and Method section. Data are presented as fold change of the expression of cytokines and chemokines in the mutant cells over WT cells. Triplicates were done in this experiment. Multiple t tests with fewer assumptions and Holm-Sidak correction method were applied in the statistics. (n=3) P value <0.05 was considered significant.

(D) FACS analysis of CD103 expression on cDCs. Splenic CD8α$^+$ and CD11B$^+$ cDCs of WT, *Cbl-b* KO, *C-cbl* KO, and *Cbl* dKO mice were stained with anti-MHCII, CD11C, CD11B, CD8α and CD103. Cell surface CD103 expression of the gated CD8α$^+$ and CD11B$^+$ cDCs was displayed in the histograms. This experiment has been repeated at least twice.

(E) The expression of TNF-α and IL-6 in the liver of 5-month-old WT and *Cbl* dKO mice. mRNA from 30mg liver tissue of each mouse (n=3) was purified and used to generate the cDNA following the procedures as described in the Material and Method section. qPCR was carried out by using the SYBR master mix. Triplicates were used for each sample. Multiple t tests with fewer assumptions and Holm-Sidak correction method were applied in the analysis. (n=3) P value <0.05 was considered significant.

Since *Cbl* dKO mice exhibited massive infiltration of leukocytes in the liver and other organs, the chemokine expression in *Cbl* dKO CD8α$^+$ and CD11B$^+$ cDCs was also studied by using the

same RNA seq data. The results revealed that the CCL family of chemokines CCL5, CCL4, and CCL3 were dramatically downregulated in both *Cbl* dKO CD8α$^+$ and CD11B$^+$ cDCs, except for the inflammatory chemokine CCL2, which was markedly upregulated in *Cbl* dKO CD8α$^+$ cDCs (Fig. 4.25B). The altered expression of TNF-α, IL-6, and CCL2 in *Cbl* dKO CD8α$^+$ cDCs was later confirmed by qPCR (Fig. 4.25C).

Interestingly, the expression of the integrin CD103, the ligand of E-cadherin, was dramatically enhanced in *Cbl* dKO CD8α$^+$ cDCs compared to WT CD8α$^+$ cDCs (Fig. 4.25D), which was consistent with the RNA seq data (data not shown). Since E-cadherin is highly expressed in hepatocytes and biliary epithelial cells[315], this finding thus suggests that the overexpression of CD103 by CD8α$^+$ cDCs may be a reason leading to the migration and accumulation of CD103$^+$ cDC in the liver. In addition, the TNF-α and IL-6 expression levels are also enhanced in the liver of *Cbl* tKO mice than that in *Rag1* KO mice (Fig. 4.25E).

IV. 8. Inflammatory disease can develop in *Cbl* dKO mice in the absence of T and B cells

The previous results indicated that *Cbl* dKO mice had massive activation of T cells. However, it is not clear whether the development of inflammatory disease in *Cbl* dKO mice depends on T and B cells. To examine this possibility, I crossed *Cbl* dKO mice with *Rag1*$^{-/-}$ mice to generate *Cd11c* Cre; *C-cbl*$^{f/f}$; *Cbl-b*$^{-/-}$; *Rag1*$^{-/-}$ mice (*Cbl* triple knockout (*Cbl* tKO) mice). By using these mutant mice, it allowed me to study the disease development in the absence of T and B cells.

IV. 8.1. Cbl tKO mice develop more severe inflammatory disease than Cbl dKO mice

Inspection of *Cbl* tKO mice revealed that they had even shorter lifespan than *Cbl* dKO mice (Fig. 4.26A). In addition, *Cbl* tKO mice also had significant loss of body weight when they were 6-month-old and sick (Fig. 4.26B). The mutant mice seemed to be growth retarded as their size was smaller than the age and sex-matched *Rag1* KO mice (Fig. 4.26C). Similar with *Cbl* dKO mice, *Cbl* tKO mice also had splenomegaly, but not lymphadenopathy (Fig. 4.26D), probably due to the lack of T and B cells. Further autopsy analysis showed that *Cbl* tKO mice exclusively developed hepatomegaly (Fig. 4.26E and 4.26F), suggesting that they also had severe liver inflammation and liver fibrosis. Consistent with this assumption, *Cbl* tKO mice had jaundice phenotype characterized by yellow skin, yellow serum, and yellow gallbladder, a phenotype

suggesting the existence of obstruction of the bile duct (Fig. 4.26G and 4.26H). Collectively, these data indicate that *Cbl* tKO mice develop an inflammatory disease similar with that found in *Cbl* dKO mice. The relative more severe disease progression in *Cbl* tKO mice than in *Cbl* dKO mice is likely due to the fact that the former did not have the expanded Treg cells found in the latter.

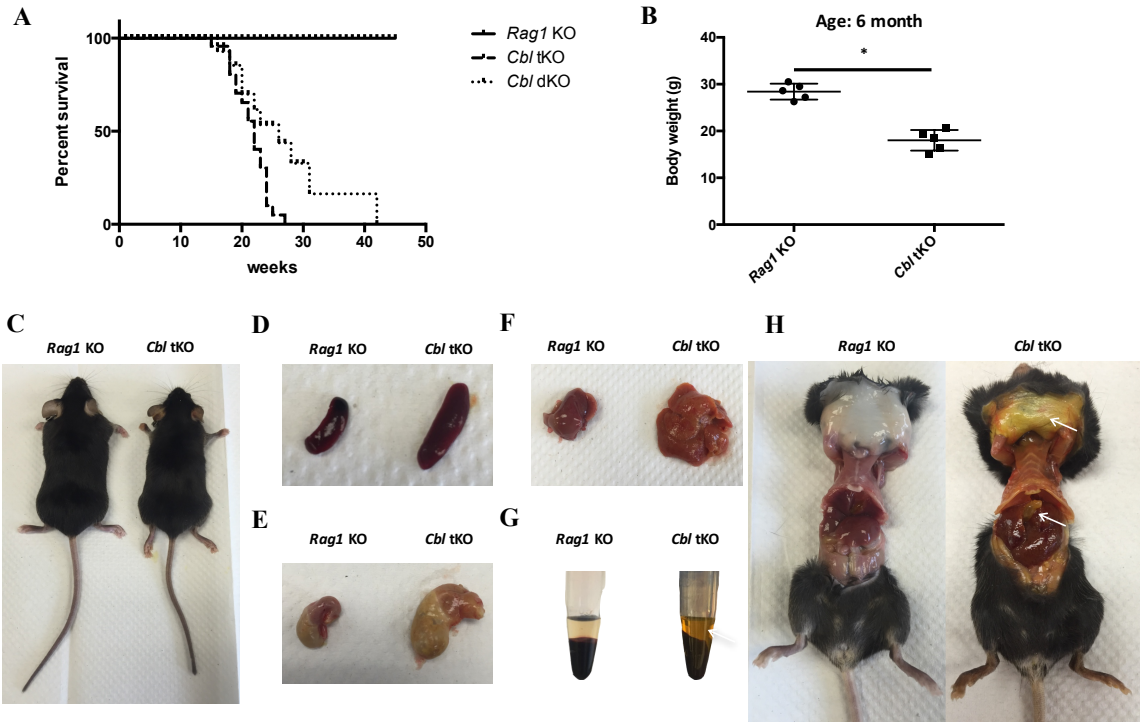

Fig. 4.26. The *Cbl* tKO mice develop a similar but more severe inflammatory disease than *Cbl* dKO mice.

(A) Kaplan-Meier survival curves of *Cbl* tKO mice. Shown are the lifespan of *Rag1* KO, *Cbl* dKO, and *Cbl* tKO mice. Gehan-Breslow-Wilcoxon test was applied to compare the survival curve. (n=10) P value <0.05 was considered significant. *Cbl* tKO mice had significantly shorter lifespan than *Cbl* dKO mice. (p=0.0407)

(B) Average body weight of 6-month-old *Rag1* KO and *Cbl* tKO mice. Unpaired t test with equal SD was applied to compare the difference. (n=5) P value <0.05 was considered significant.

(C) Comparison of the body size of 6-month-old sick *Cbl* tKO and the age and sex-matched *Rag1* KO mice.

(D) Images of spleens from 6-month-old sick *Cbl* tKO mice and age and sex-matched healthy *Rag1* KO mice.

(E) Enlarged stomach from 6-month-old sick *Cbl* tKO mice compared with age and sex-matched healthy *Rag1* KO mice.

(F) Hepatomegaly of 6-month-old sick *Cbl* tKO mice compared with age and sex-matched healthy *Rag1* KO mice.

(G) and **(H)** Jaundice phenotype of 6-month-old sick *Cbl* tKO mice compared with age and sex-matched healthy *Rag1* KO mice. The jaundice phenotype was characterized by yellow skin, yellow serum, and yellow gallbladder.

IV. 8.2. Cbl tKO mice have increased levels of serum inflammatory cytokines and chemokines

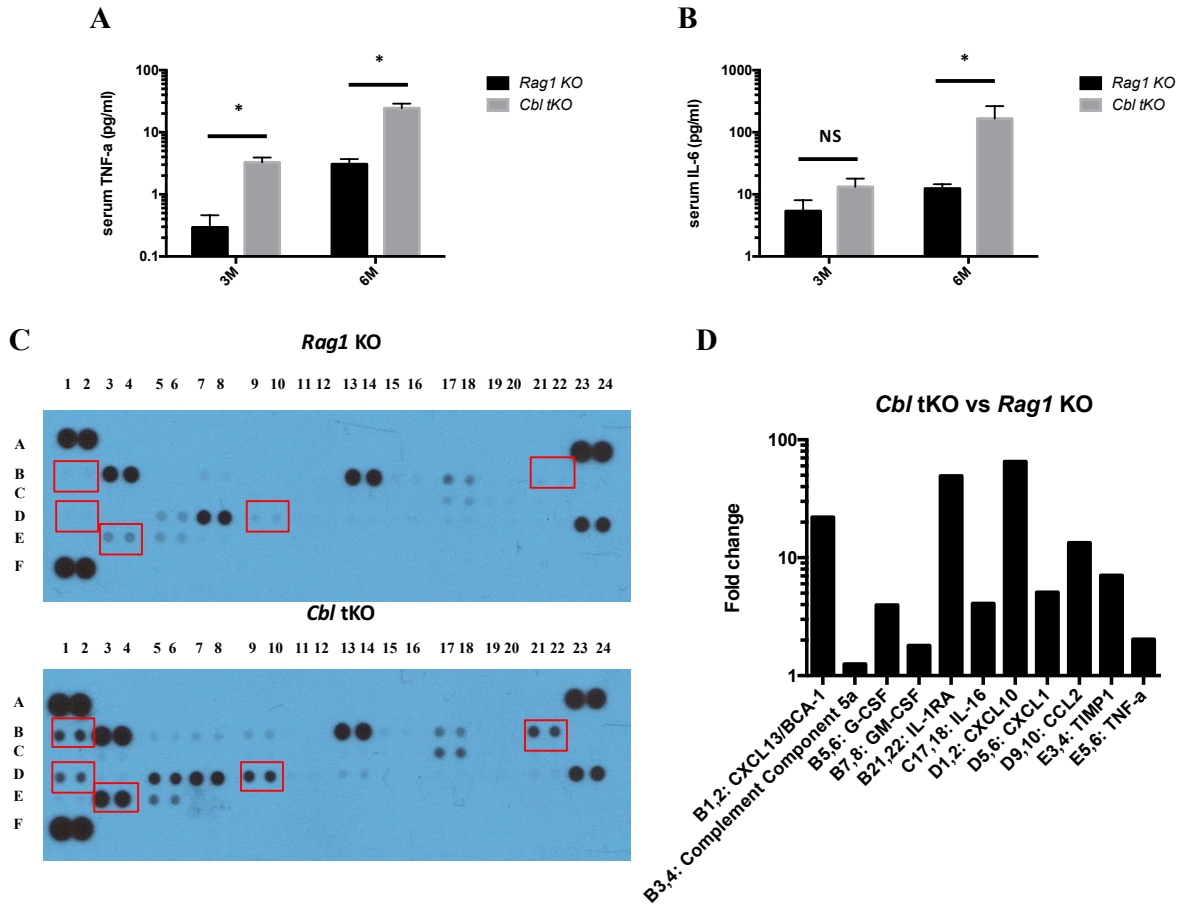

Fig. 4.27. *Cbl* tKO mice have increased levels of serum inflammatory cytokines and chemokines.
(A & B) ELISA analysis of serum TNF-α and IL-6 concentrations in 3 and 6-month-old *Rag1* KO and *Cbl* tKO mice. Multiple t tests with fewer assumptions and Holm-Sidak correction method were applied in the analysis. (n=4) P value <0.05 was considered significant.
(C) Chip array assay of serum cytokines and chemokines' expression profiles in the sera from 3 sick *Cbl* tKO mice or 3 age-matched *Rag1* KO mice. The sera were pooled together respectively and analyzed by cytokine array panel A kit following the procedures described in Material and Method section. The most significantly overexpressed cytokines and chemokines were marked in red.
(D) The quantification of several highly upregulated cytokines and chemokines were done by the software ImageStudioLite.

Since *Cbl* tKO mice showed similar chronic auto-inflammation phenotype as *Cbl* dKO mice, I decided to measure whether these mice also had abnormal expression of inflammatory cytokines and chemokines. The results revealed that serum TNF-α and IL-6 levels were also dramatically increased in *Cbl* tKO mice as compared to that in *Rag1* KO mice (Fig. 4.27A and 4.27B).

Furthermore, a broad screen of other inflammatory cytokines and chemokines was conducted by using a chip assay. The results showed that CXCL13, CXCL10, and CCL2 were most dramatically enhanced chemokines in the serum of *Cbl* tKO mice compared to *Rag1* KO mice. In addition, IL-1Rα and TIMP1 were also significantly enhanced in the serum of *Cbl* tKO mice (Fig. 4.27C). This result is consistent with the ongoing inflammation in the *Cbl* tKO mice.

IV. 8.3. *Cbl* tKO mice have severe leukocyte infiltration and fibrosis in the liver

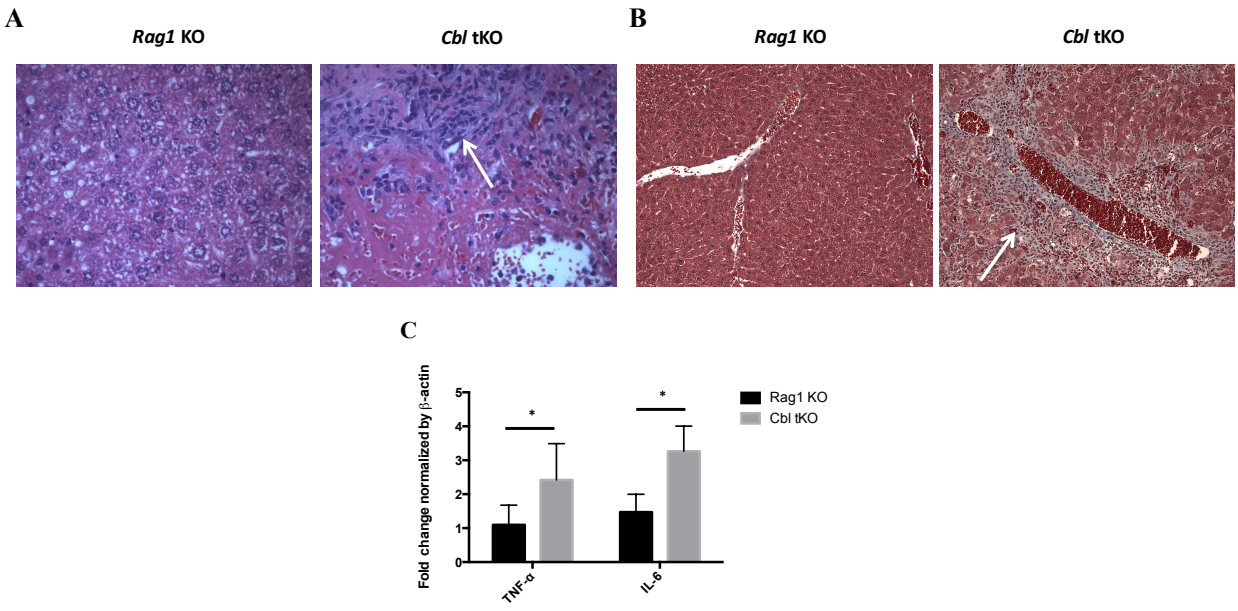

Fig. 4.28. *Cbl* tKO mice develop severe liver inflammation.
(A) Pathological analysis of liver tissue of *Rag1* KO and *Cbl* tKO mice. Shown are H/E staining of the liver sections of 6-month-old sick *Cbl* tKO mice and age and sex-matched healthy *Rag1* KO mice. White arrow indicated the area with leukocyte infiltration. Representative data of at least 5 mice.
(B) Analysis of liver fibrosis in *Rag1* KO and *Cbl* tKO mice. Shown are Masson's trichrome staining of the liver sections of 6-month-old sick *Cbl* tKO mice and age and sex-matched healthy *Rag1* KO mice. White arrow indicated the blue collagen-rich region.
(C) Inflammatory cytokine expression in *Cbl* tKO liver. mRNA from 30mg liver tissue of each mouse (n=5) was purified and used to generate the cDNA following the procedures as described in the Material and Method section. qPCR was carried out by using the SYBR master mix. Triplicates were used for each sample. Multiple t tests with fewer assumptions and Holm-Sidak correction method were applied in the statistics. (n=5) P value <0.05 was considered significant.

The observed hepatomegaly and jaundice phenotype in *Cbl* tKO mice suggested that these mice had developed liver inflammatory disease. To investigate whether this is the case as the *Cbl* dKO mice, pathological analysis was carried out on these *Cbl* tKO mice. The results revealed that

similar with *Cbl* dKO mice, *Cbl* tKO mice also had severe leukocyte infiltration in the liver (Fig. 4.28A). Masson's trichrome staining also showed that the liver tissue of *Cbl* tKO mice developed severe fibrosis, with most profound fibrosis observed in the area around the portal region of the liver (Fig. 4.28B), suggesting that there was ongoing liver tissue damaging and repairing process. qPCR analysis revealed that both TNF-α and IL-6 levels were significantly enhanced in the liver tissue of *Cbl* tKO mice, suggesting that the pathological change in the liver is probably caused by ongoing inflammation (Fig. 4.28C).

IV. 8.4. The cellularity analysis of the liver in Cbl tKO mice

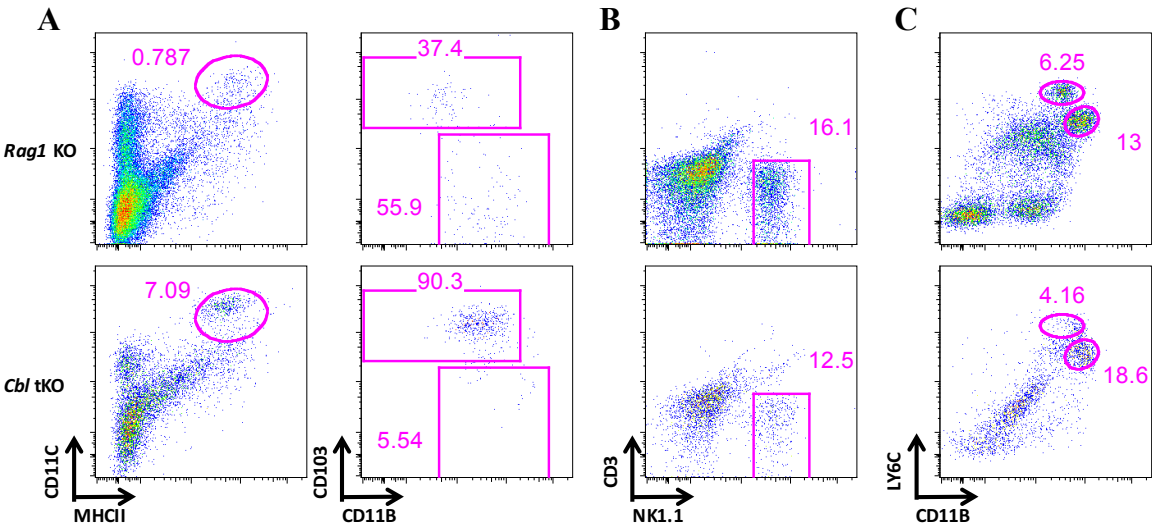

Fig. 4.29. *Cbl* tKO mice have markedly expanded CD103$^+$ DCs in the liver.
(A) FACS analysis of DCs in the liver of *Rag1* KO and *Cbl* tKO mice. Liver mononuclear cells from *Rag1* KO and *Cbl* tKO mice were purified following the procedures as described in the Material and Method section. The purified liver mononuclear cells were then stained with anti-CD11C, MHCII, CD11B and CD103. Shown are the dot plots of MHCII vs CD11C staining, and CD103 vs CD11B staining of the gated CD11C$^+$MHCII$^+$ cells. Representative data of 5 mice.
(B) FACS analysis of infiltrated NK cells in the liver of *Rag1* KO and *Cbl* tKO mice. Liver mononuclear cells from *Rag1* KO and *Cbl* tKO mice were purified following the procedures as described in the Material and Method section. The purified liver mononuclear cells were then stained with anti-NK1.1 and CD3. Shown are dot plots of NK cells (NK1.1$^+$CD3$^-$). Representative data of 5 mice.
(C) FACS analysis of granulocytes and monocytes in the liver of *Rag1* KO and *Cbl* tKO mice. Liver mononuclear cells from *Rag1* KO and *Cbl* tKO mice were purified following the procedures as described in the Material and Method section. The purified liver mononuclear cells were then stained with anti-CD11B and LY6C. Shown are the dot plots of CD11B vs LY6C staining. Percentages of granulocytes (LY6C^{int}CD11B^{hi}) and monocytes (LY6C^{hi}CD11B^{int}) are indicated in the plots. Representative data of 5 mice.

Given that *Cbl* tKO mice developed severe liver inflammatory disease, I decided to analyze the cellularity of the infiltrating inflammatory cells in the liver. Similar with that observed in the liver of *Cbl* dKO mice, there was a dramatic expansion of DC population in the liver of *Cbl* tKO mice as compared to *Rag1* KO controls. Within the DC population, $CD103^+$ cDC was the most dramatically expanded cells (Fig. 4.29A). Other cell population, such as granulocytes was also significantly increased. In contrast, NK cells (Fig. 4.29B) and monocyte (Fig. 4.29C) were even slightly reduced. Although the study to obtain the final statistics is still ongoing, the current data at least suggest that the expanded $CD103^+$ DCs is likely the initial reason leading to the observed liver inflammation.

IV. 9. Potential mechanisms that cause the inflammation in *Cbl* tKO mice

IV. 9.1 Expression of co-stimulatory molecules is not changed in Cbl tKO DCs

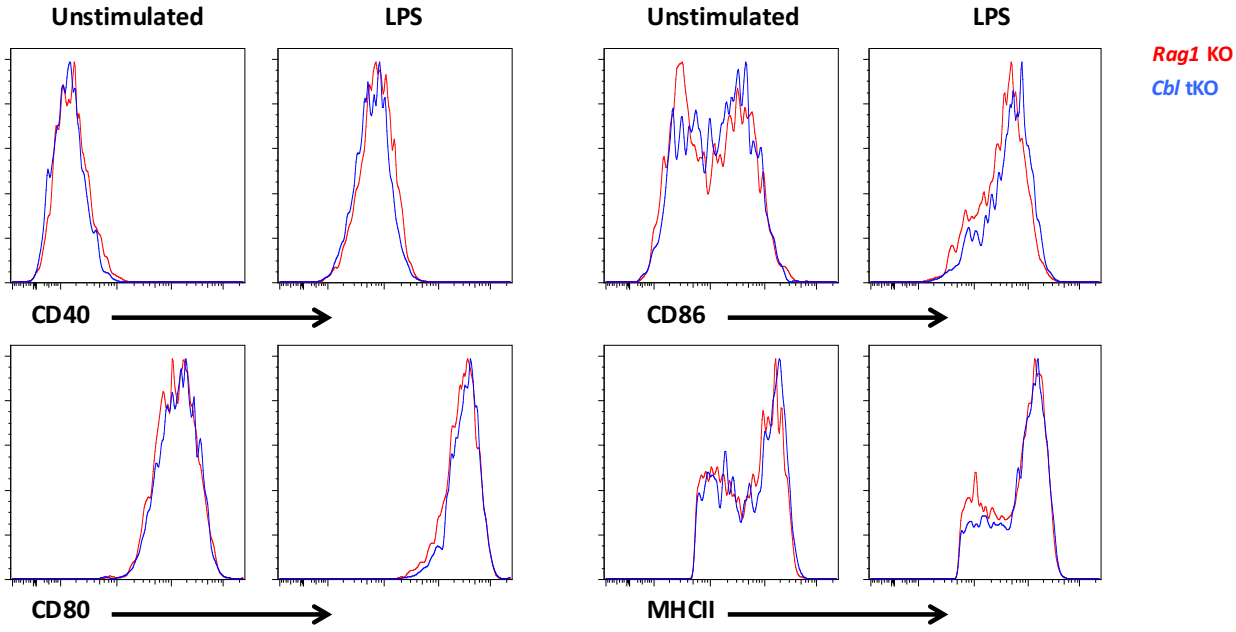

Fig. 4.30. The *Cbl* tKO mutation does not affect the expression of co-stimulatory molecules in DCs.
1×10^7 BM cells from *Rag1* KO or *Cbl* tKO mice were cultured in 10% GM-CSF supernatant for 9 days in 10cm dish to generate the GM-CSF derived DCs. 1×10^6 GM-CSF derived *Rag1* KO and *Cbl* tKO DCs were stimulated with 100ng/ml LPS or without at 37°C for overnight. Cells were then stained with anti-CD40, CD86, CD80, CD11C and MHCII. Shown are histograms of CD40, CD80, CD86, and MHCII expression of gated $MHCII^+CD11C^+$ DCs. Representative data of two experiments.

In *Cbl* dKO mice, there is not any alteration in the expression of co-stimulatory molecules and MHCII in the mutant DCs compared with the WT DCs. To examine whether this is the case in *Cbl* tKO DCs, I examined the expressions of co-stimulatory molecules such as CD40, CD80, CD86, and MHCII on *Rag1* KO and *Cbl* tKO DCs by flow cytometry. The results revealed that the expressions of these molecules were comparable between *Rag1* KO and *Cbl* tKO DCs. LPS stimulation upregulated the expressions of these co-stimulatory molecules in *Cbl* tKO DCs to a similar extent as that in the *Rag1* KO DCs (Fig. 4.30). This result suggested that CBL-B and C-CBL regulate DC function not through regulation of the expression of these co-stimulatory molecules and LPS/TLR4 signaling pathway. Although it was proposed previously by some other group that CBL-B could regulate MyD88 ubiquitination[223], it seemed not true based on my results.

IV. 9.2. The inflammatory cytokine expression of liver and SP Cbl tKO cDCs

To determine whether *Cbl* tKO DCs exhibited a similar dysregulated cytokine expression as *Cbl* dKO DCs, I examined the inflammatory cytokine expression profile of the liver infiltrating cells in the *Cbl* tKO mice. The results revealed that liver $CD45^+$ leukocytes from *Cbl* tKO mice produced significantly more IL-6 than those from *Rag1* KO mice; however, TNF-α production was not altered (Fig. 4.31A). In the liver cDCs populations, there was a significant decrease of TNF-α expression, and a significant increase of IL-6 expression (Fig. 4.31B). Although total number of liver granulocytes was increased in *Cbl* tKO mice, they produced lower levels of TNF-α and IL-6 compared to the *Rag1* KO liver granulocytes (Fig. 4.31C).

To determine whether cytokine production by SP *Cbl* tKO $CD8\alpha^+$ cDCs was altered, I examined TNF-α and IL-6 production of SP *Cbl* tKO $CD8\alpha^+$ cDCs with or without CpG stimulation. The results revealed that TNF-α production by *Cbl* tKO $CD8\alpha^+$ cDCs was comparable to the *Rag1* KO $CD8\alpha^+$ cDCs after CpG stimulation. However, the IL-6 production in the *Cbl* tKO $CD8\alpha^+$ cDCs was moderately but significantly increased compared to the *Rag1* KO $CD8\alpha^+$ cDCs after CpG stimulation (Fig. 4.31D and 4.31E). These data thus suggest that the liver inflammation observed in *Cbl* tKO mice might be caused by an accumulating effect of the infiltrated leukocytes and $CD103^+$ DCs rather than the hyper-activation of individual DCs.

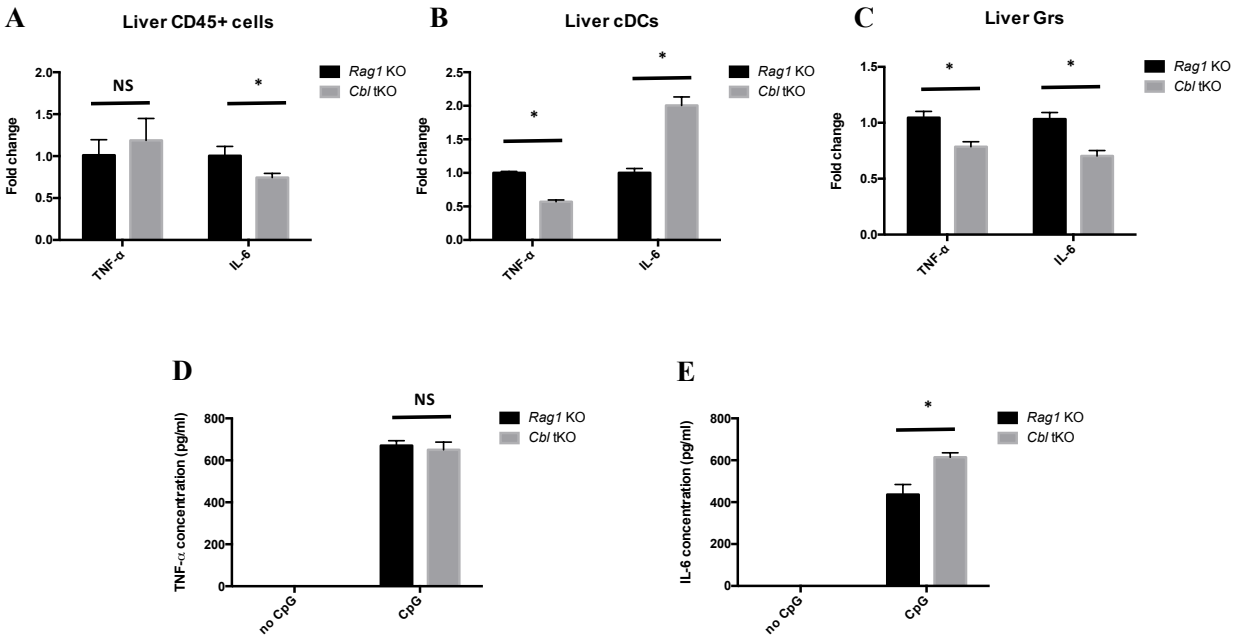

Fig. 4.31. Inflammatory cytokine production by liver infiltrating cell subsets and splenic CD8α$^+$ cDCs in *Cbl* tKO mice.

(A & B & C) qPCR analysis of TNF-α and IL-6 expression in different liver infiltrating cell subsets including CD45$^+$ leukocytes, MHCII$^+$CD11C$^+$ cDCs, and LY6G$^+$CD11B$^+$ granulocytes. Liver mononuclear cells from three 6-month-old *Rag1* KO or *Cbl* tKO mice were pooled together and stained with different antibodies for cell sorting to purify the CD45$^+$ leukocytes, MHCII$^+$CD11C$^+$ cDCs, and LY6G$^+$CD11B$^+$ granulocytes. The TNF-α and IL-6 expression in these cell subsets were quantified by qPCR following the procedures as described in the Material and Method section. This experiment was done in triplicates. Multiple t tests with fewer assumptions and Holm-Sidak correction method were applied in the analysis. (n=3) P value <0.05 was considered significant.

(D & E) ELISA analysis of TNF-α and IL-6 production by SP CD8α$^+$ cDCs from 3-month-old *Rag1* KO and *Cbl* tKO mice with and without CpG stimulation. Splenocytes from three 3-month-old *Rag1* KO or *Cbl* tKO mice were pre-enriched and stained with anti-MHCII, CD11C, CD11B and CD8α for cell sorting to purify the CD8α$^+$ cDCs. 5×10^4 sorted CD8α$^+$ cDCs were then stimulated by 5μM CpG for overnight at 37°C. The TNF-α and IL-6 concentration in the supernatant were measured by ELISA. This experiment was done in triplicates. Multiple t tests with fewer assumptions and Holm-Sidak correction method were applied in the analysis. (n=3) P value <0.05 was considered significant.

IV. 9.3. Rapamycin treatment prevents auto-inflammation development in Cbl tKO mice

Cbl dKO and *Cbl* tKO mice developed a similar liver inflammatory disease. Since in both mice there was an expansion of CD8α$^+$ cDCs and the development of these cell populations is controlled by PKB/AKT-MTOR signaling, I decided to examine whether treatment of *Cbl* tKO mice with rapamycin, which could restore the homeostasis of CD8α$^+$ cDCs, could prevent or even cure the

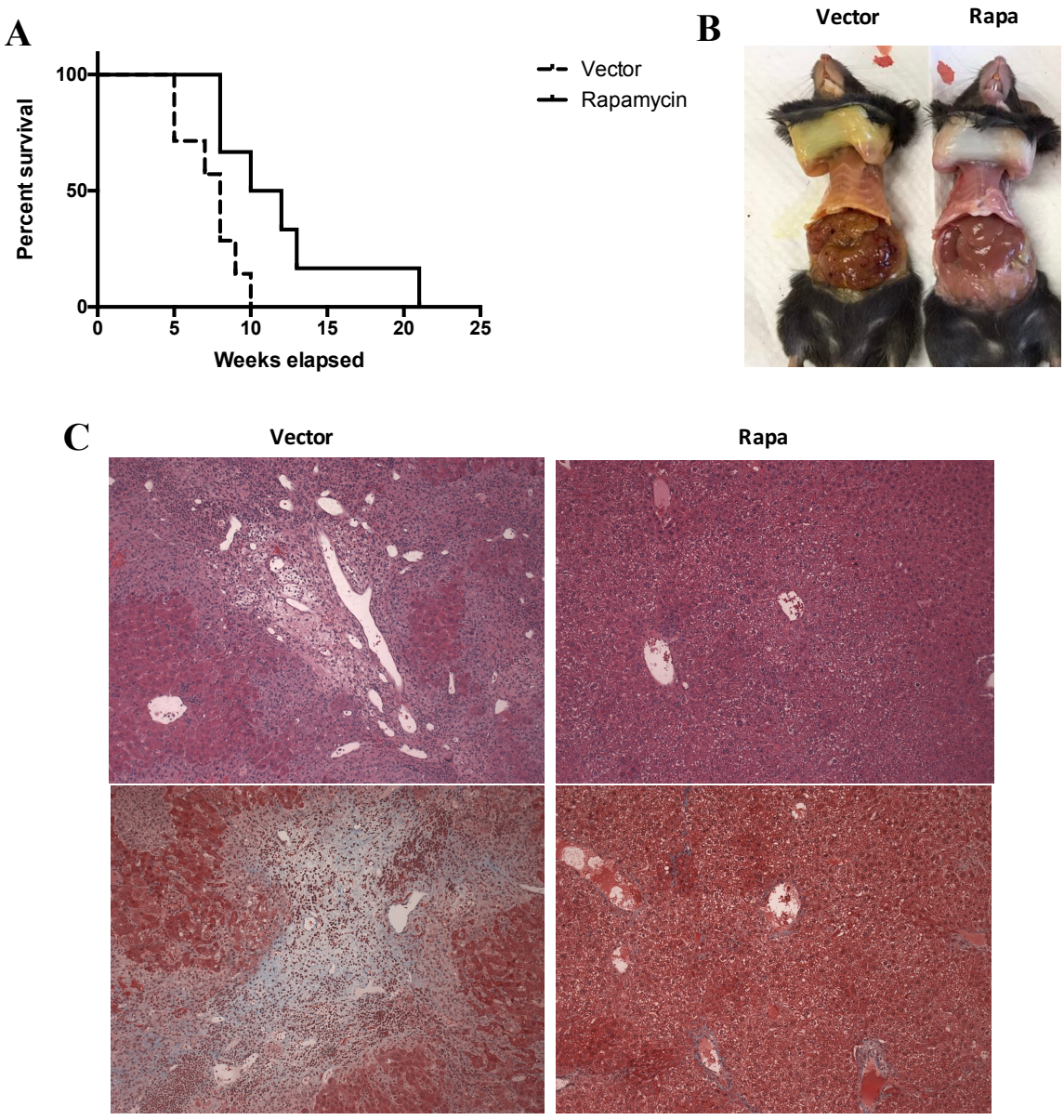

Fig. 4.32. Long-term rapamycin treatment could prevent *Cbl* tKO mice from developing chronic liver inflammation.

(A) Shown are Kaplan-Meier survival curves of *Cbl* tKO mice with either rapamycin or vector treatment. 90-day-old *Cbl* tKO mice were treated with rapamycin (300μg/week, 3 times/week) or vector through i.p. injection until the mice were dead. Gehan-Breslow-Wilcoxon test was applied to compare the survival curve. (n=7) P value <0.05 was considered significant. *Cbl* tKO mice with rapamycin treatment had significantly longer lifespan than vector treated *Cbl* tKO mice. (p=0.033) **(B & C)** *Cbl* tKO mice with long-term rapamycin treatment showed alleviated jaundice and hepatomegaly phenotype compared to the vector treated *Cbl* tKO mice. 90-day-old *Cbl* tKO mice were treated with rapamycin (300μg/week, 3 times/week) or vector through i.p. injection for 45 days. The mice were sacrificed and the liver leukocyte infiltration and fibrosis were analyzed by HE and Masson's trichrome staining respectively. These are the representative results of five rapamycin vs vector treated mice.

disease. To do so, 90-day-old *Cbl* tKO mice were either treated with rapamycin or vector for long-term follow up to study their survival curves and disease progression. The results revealed that rapamycin treatment could dramatically prevent the jaundice and hepatomegaly phenotype and extend the lifespan of *Cbl* tKO mice for up to more than 20 weeks, which was significantly longer than the vector treated *Cbl* tKO mice (Fig. 4.32A and 4.32B). The H/E and Masson's trichrome staining results further revealed that long-term rapamycin treatment could dramatically prevent the liver leukocyte infiltration and fibrosis of *Cbl* tKO mice, which was consistent with the alleviated jaundice and hepatomegaly phenotype (Fig. 4.32C).

To further understand whether rapamycin treatment could also inhibit the inflammatory cytokine expression in *Cbl* tKO mice, the levels of TNF-α and IL-6 in the serum and liver of rapamycin treated *Cbl* tKO mice were measured. The results revealed that although there were reductions of TNF-α and IL-6 levels in both serum and liver of rapamycin treated *Cbl* tKO mice compared to those of vector treated *Cbl* tKO mice, they were not significant (Fig. 4.33A and 4.33B). It has been shown previously that rapamycin treatment could alleviate liver leukocyte infiltration in *Cbl* tKO mice. To further understand which cell subsets maybe involved in this process, the cellularity analysis for both splenocytes and liver mononuclear cells was conducted. The results revealed that there was a general and dramatic cell number reduction in both SP and liver of rapamycin treated *Cbl* tKO mice compared to vector treated *Cbl* tKO mice (Fig. 4.33C and 4.33D). Furthermore, the DC number and $CD103^+$ cDC number had a 36-fold and 38-fold reduction in the liver of rapamycin treated *Cbl* tKO mice compared to vector treated *Cbl* tKO mice. These results suggest that blockade of mTOR signaling could be an effective way to prevent the development of auto-inflammation in *Cbl* tKO mice, probably through restoring the homeostasis of DCs. However, since rapamycin could only partially restore the homeostasis of DCs, its treatment could not completely rescue the chronic inflammation in *Cbl* tKO mice. Further investigations are required to understand whether there will be a better protective effect if both MTOR inhibitor and ERK inhibitor are used together.

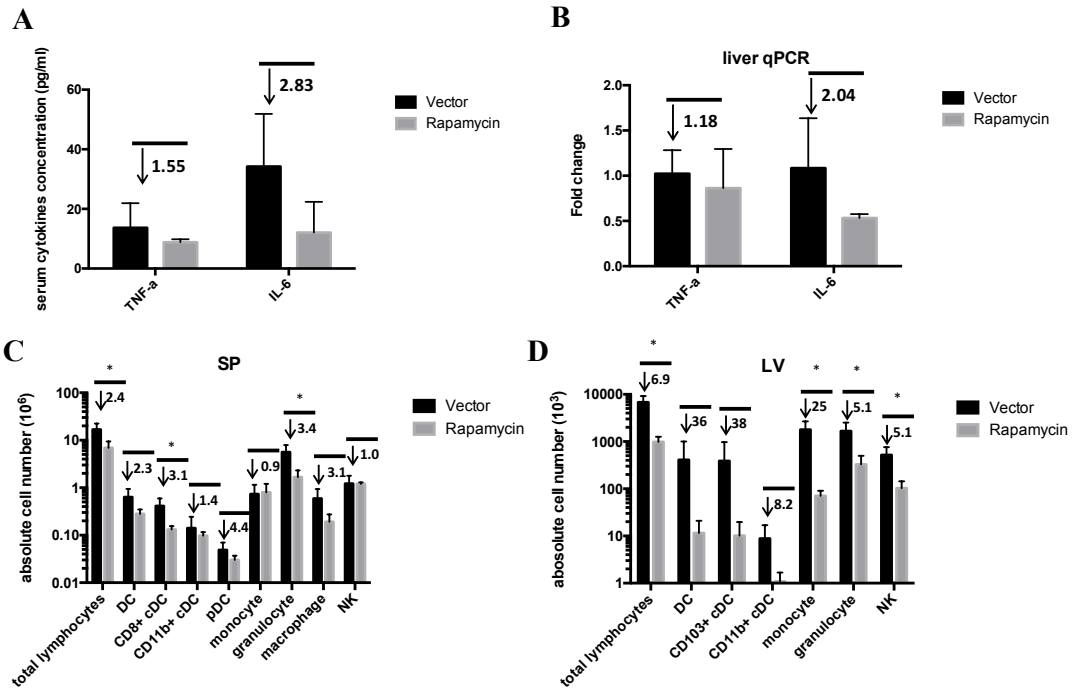

Fig. 4.33. Long-term rapamycin treatment could prevent *Cbl* tKO mice from developing chronic liver inflammation through restoring DC homeostasis in the liver.

(A) Serum levels of TNF-α and IL-6 in *Cbl* tKO mice treated with rapamycin or vector. 100μl sera were collected from rapamycin or vector treated *Cbl* tKO mice. The TNF-α and IL-6 concentrations were measured by an ELISA. Multiple t tests with fewer assumptions and Holm-Sidak correction method were applied in the analysis. (n=5) P value <0.05 was considered significant.

(B) Inflammatory cytokine expression in the liver of rapamycin or vector treated *Cbl* tKO mice. mRNA of the liver tissue from rapamycin or vector treated *Cbl* tKO mice (30mg/mouse, n=5) was purified and used to generate the cDNA following the procedures as described in the Material and Method section. qPCR was carried out by using the SYBR master mix. Triplicates were used for each sample. Multiple t tests with fewer assumptions and Holm-Sidak correction method were applied in the analysis. (n=5) P value <0.05 was considered significant.

(C) The SP cellularity analysis of rapamycin or vector treated *Cbl* dKO mice. Total splenic cells from rapamycin or vector treated *Cbl* dKO mice were stained for various cell surface markers and analyzed by flow cytometry. The ratios of the absolute numbers of different cell populations between rapamycin treated vs vector treated are also displayed in the figure. Multiple t tests with fewer assumptions and Holm-Sidak correction method were applied in the analysis. (n=5) P value <0.05 was considered significant.

(D) Cellularity analysis of liver infiltrating hematopoietic cells. The mononuclear cells in the liver of rapamycin or vector treated *Cbl* dKO mice were isolated through gradient purification method as described in the Material and Method section. The purified liver mononuclear cells were stained for various cell surface markers and analyzed by flow cytometry. The ratios of the absolute numbers of different cell populations between rapamycin treated vs vector treated are also displayed in the figure. Multiple t tests with fewer assumptions and Holm-Sidak correction method were applied in the analysis. (n=5) P value <0.05 was considered significant.

V. DISCUSSION

V.1. The major role of DC on organismal health

As an adaptor, DC is so important to bridge the innate immunity and adaptive immunity in mammals. As I mentioned before, different DC subsets are specialized to commit different functions. $CD8\alpha^+$ cDCs are specialized to present intracellular and extracellular antigens to $CD8^+$ T cells through the MHCI molecules. In addition, they are also specialized to secret IL-12 upon TLR stimulation, which can help to promote the Th1 immune response. Moreover, $CD8\alpha^+$ cDCs also have an effect to boost Treg generation through DC-T cell contact[280]. As the other major DC subset, $CD11B^+$ cDCs are specialized to present antigens to $CD4^+$ T cells through the MHCII molecules. In addition, $CD11B^+$ cDCs have constitutively highly expressed PD-L1 compared with $CD8\alpha^+$ cDCs, which suggest they may have immune suppression function to keep the organism under steady-state. Interestingly, a very recent study showed that T cell-mediated anti-tumor immunity could be boosted by depleting $CD11B^+$ cells[316]. In the inflammatory conditions, there is another highly expanded non-classical DC subset, the $CD11B^+$ moDCs, which is normally absent in steady-state. These $CD11B^+$ moDCs have even stronger antigen presentation capacity than $CD8\alpha^+$ and $CD11B^+$ cDCs, which suggest they contribute a lot to the immunity to against infection[106]. Interestingly, based on my result, the *in vitro* GM-CSF generated $CD11B^+$ moDCs do not express PD-L1 (data not shown). Since different DC subsets have so different functions in terms of immune suppression and immune boost, it requires a very delicate regulation of these DC subsets to keep the organism immune quiescent under steady-state, but boost the immune response under inflammation.

One of the mechanisms which fine-tune such delicate regulation is through manipulating the ratio among these different DC subsets by cytokines. For example, FLT3L can fine-tune the ratio of $CD8\alpha^+$ vs $CD11B^+$ cDCs[306], which is probably due to the fact that $CD8\alpha^+$ cDCs have different level of surface FLT3 expression as $CD11B^+$ cDCs. Another cytokine M-CSF might also be involved in this regulation, because $CD11B^+$ cDCs have relatively higher surface M-CSFR expression than $CD8\alpha^+$ cDCs. Even though, it has to be noted that the major *in vivo* effect of M-CSF is to boost monocyte proliferation, because these cells have much higher surface M-CSFR expression compared to $CD8\alpha^+$ and $CD11B^+$ cDCs. It is also noteworthy that during the *in vitro* moDC generation, the moDCs have dramatic downregulation of M-CSFR compared to the original monocytes[106]. Therefore, in the inflammatory conditions, the control of moDC population may

through the control of monocyte population. Based on these knowledges, it will be very interesting to investigate how the host responds to different stimuli in terms of FLT3L and M-CSF production to fine-tune the ratios among different DC subsets.

V. 2. C-CBL and CBL-B control lineage development of CD8α$^+$ cDC and pDC

It has been previous reported that the development of CD11B$^+$ and CD8α$^+$ cDC and pDC is controlled by distinct mechanisms, each is dictated by a unique transcription factor. While pDC development requires helix-loop helix transcription factor E2-2, development of CD11B$^+$ and CD8α$^+$ cDC depends on transcription factors such as IRF4 and IRF8 respectively[30, 51, 74]. At present, it is not clear whether expression of E2-2, IRF4, and IRF8 is regulated by extracellular signals through unknown receptors or is merely a default process during DC development. Association between different genetic backgrounds and their inherited ratios of different DC lineages indicates that genetic factors are one of the pre-deposited factor that influence the homeostasis of different DC subsets. My experiments presented here demonstrate that, in addition to the transcription factors, cell external signals also play a critical role in the control of DC homeostasis, in particular, the ratio among different DC subsets. Using gene knockout mice, it is found that in the absence of both E3 ubiquitin ligases C-CBL and CBL-B (*Cbl* dKO), homeostasis of DC lineages is dramatically altered, as the number of CD8α$^+$ cDC is significantly increased whereas that of pDC is markedly reduced. In contrast, the total number of CD11B$^+$ cDC is barely influenced, indicating that CBL signaling only selectively affect CD8α$^+$ cDC and pDC lineage development in mice. Based on these findings, I conclude that similar with the aforementioned transcription factors, the CBL family of proteins also plays a critical role in the maintenance of DC lineage homeostasis. Since any significant alteration in DC population could not been found in individual *C-cbl* or *Cbl-b* gene deficient mice, I conclude that this is a redundant function shared by C-CBL and CBL-B.

V. 3. CBL proteins control DC homeostasis mainly by regulating CD8α$^+$ cDC proliferation

Homeostasis of DC subsets can be influenced by either cell lineage commitment, preferential proliferation and/or survival of the committed mature DCs. The results in my study suggest that CBL proteins control CD8α$^+$ but to less extent CD11B$^+$ cDC proliferation rather than the commitment of these DC subsets, because the expression of *Irf8* gene, which is responsible for

CD8α$^+$ lineage commitment, remains similar in both WT and *Cbl* dkO DC precursors (Fig. 4.9). In contrast, the *in vitro* BrdU incorporation assay showed that in FLT3L BM culture, the proliferation of *Cbl* dKO CD24$^+$ cDCs, an equivalent DC population to *in vivo* CD8α$^+$ cDCs, is significantly enhanced as compared to WT counterparts, suggesting that CBL proteins influence CD8α$^+$ cDC homeostasis by regulating their proliferation (Fig. 4.8A and Fig. 4.8B).

V. 4. Why *Cbl* dKO mutation preferentially influences FLT3 signaling in CD8α$^+$ cDC

The results in my study support a conclusion that CBL proteins regulate CD8α$^+$ cDC proliferation through FLT3 signaling. This conclusion is based on the evidences that 1) In the *in vitro* FLT3L BM culture, addition of FLT3L enhances CD24$^+$ cDC proliferation and such effect is more profound in a low FLT3L concentration, suggesting that the *Cbl* dKO mutation leads to the augmentation of FLT3 signaling; 2) The biochemical studies directly show that *Cbl* dKO cDCs exhibit hyper-activation of FLT3 even in the absence of FLT3L stimulation, indicating that CBL proteins are negative regulators of FLT3 kinase activity.

A question that remains unanswered is that FLT3 is expressed by all lineages of DCs, why the *Cbl* dKO mutation only leads to an increase in CD8α$^+$ but not CD11B$^+$ lineage cDCs and even a reduction in pDCs? The results show that the alteration of DC subsets in *Cbl* dKO mice exhibits different tissue specific patterns. For example: in the BM, there is no change in the total number of pDCs and the reduced number of pDCs is only found in the SP. In the SP and liver, a marked increase of CD8α$^+$ cDCs and CD103$^+$ cDCs were found respectively; whereas CD11B$^+$ cDCs in these tissues are normal. I conceive that several mechanisms might contribute to this phenomenon. Firstly, it was found that different DC subsets had different levels of surface FLT3 expression. For example, splenic CD8α$^+$ cDCs have a higher level of surface FLT3 than CD11B$^+$ cDCs (Fig. 4.10D). Although the FLT3 expression level of pDC has not been investigated in my experiment, based on the previous data on mRNA expression of FLT3 in different DC subsets, it is clearly showed that the splenic pDCs have similar mRNA level of FLT3 as the spleen CD11B$^+$ cDCs, which are both lower than that expressed by splenic CD8α$^+$ cDCs (NCBI immunological genome project). This observation thus suggests that the FLT3 signaling in CD8α$^+$ cDCs would be stronger than that in CD11B$^+$ cDCs and pDCs. The stronger FLT3 signaling could favor their proliferation

and survival over the *Cbl* dKO CD11B$^+$ cDCs and *Cbl* dKO pDCs. This notion is supported by the observation that low concentration of FLT3L has a more profound effect on CD24$^+$ cDC and a high does FLT3L also enhances the ratio of CD24$^+$ cDC vs CD11B$^+$ cDC in WT FLT3L cultured BMDC, a phenomenon similar with that found in *Cbl* dKO FLT3L cultured BMDC.

Secondly, for the impaired homeostasis of splenic pDCs in *Cbl* dKO mice, it could be a consequence of growth niche competition by the expanded CD8α^+ cDCs in the spleen. It is known that the survive and expansion of both pDC and cDC requires FLT3L. Since *Cbl* dKO CD8α^+ cDCs express more FLT3, they may have an advantage over pDC to compete for the FLT3L. As a result, the expanded *Cbl* dKO CD8α^+ cDCs would consume more FLT3L, consequently reducing the FLT3L in the environment, leading to the impaired pDC survival and neutralizing the enhanced FLT3 signaling in *Cbl* dKO CD11B$^+$ cDCs. This assumption is supported by the *Cbl* dKO/SJL chimeric mouse, in which the splenic pDCs derived from SJL BM cells are also severely reduced, suggesting that they lack the survival factor such as FLT3L to support their proliferation (Fig. 4.5).

Finally, for the overexpansion of CD103$^+$ cDC in the liver of *Cbl* dKO mice and *Cbl* tKO mice, I think there are two possible factors that might be involved. Firstly, CD103$^+$ cDCs were considered as the counterpart of CD8α^+ cDCs in the periphery, and they were known to share many similar features such as FLT3L dependence. In this regard, one explanation could be that the enhanced FLT3 signaling pathway in *Cbl* dKO CD103$^+$ cDCs similarly favors the expansion of CD103$^+$ cDCs over the CD11B$^+$ cDCs in the liver. Secondly, it is possible that the increased surface CD103 expression in *Cbl* dKO CD8α^+ cDCs promotes their migration from the spleen to the liver, since CD103 is a ligand of tissue-resident hematopoietic cells and its receptor E-cadherin is highly expressed in both hepatocytes and biliary epithelial cells. It should be noteworthy that the liver CD103$^+$ cDCs did not express CD8α based on previous studies, however in my experiment, the liver CD103$^+$ cDCs from both WT mice and *Cbl* dKO mice do express CD8α (Fig. 5.1A and 5.1B). This discrepancy is likely caused by different methods used to isolate the liver cells. The *in vivo* anti-CD103 blocking experiment can provide the evidence whether this is a valid assumption. Moreover, it will be interesting to further study whether CBL-B and C-CBL regulate CD103 expression directly. Given that our RNA seq data indicate that the mRNA level of CD103 is already enhanced in the *Cbl* dKO CD8α^+ cDCs, I propose that the regulation of CD103

expression by C-CBL and CBL-B already occurs at the transcriptional level instead of the post-translational level.

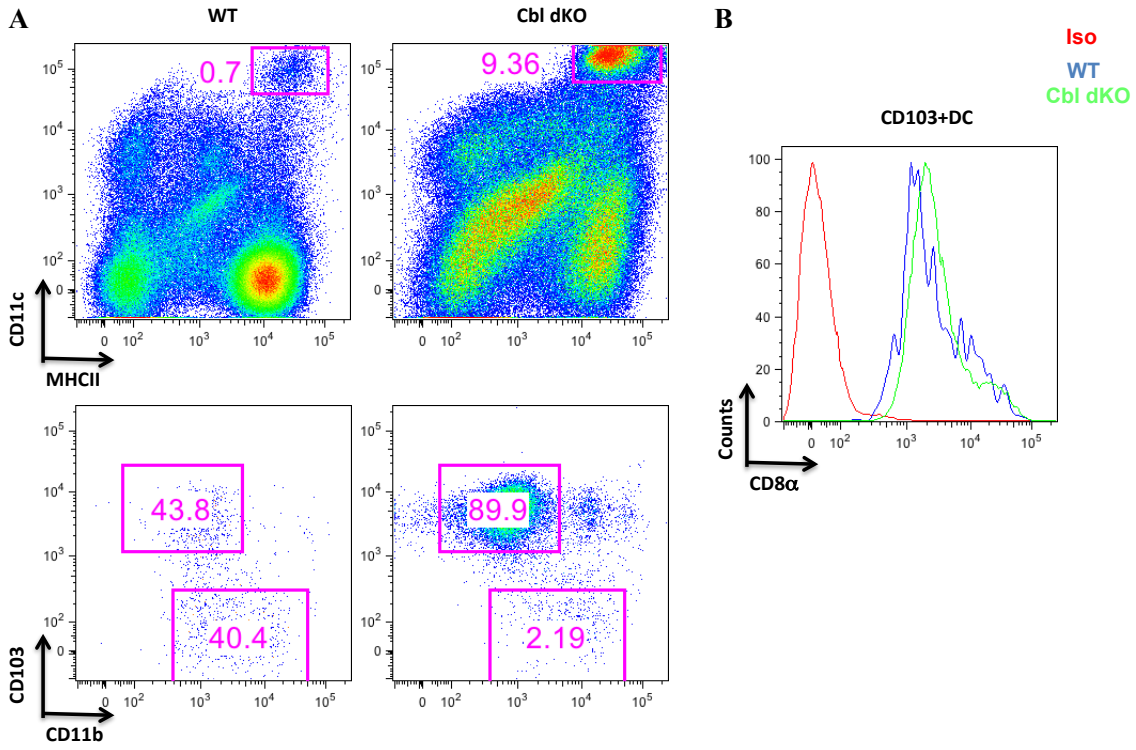

Fig. 5.1. CD8α expression on liver CD103$^+$ cDC of WT and *Cbl* dKO mice.
(A) FACS analysis of liver infiltrating CD103$^+$ DCs. Liver mononuclear cells from WT and *Cbl* dKO mice were purified and stained with anti-MHCII, CD11C, CD8α, CD11B, and CD103. Shown are CD11B vs CD103 expression (bottom panel) on the gated CD11C$^+$MHCII$^+$ liver infiltrating DCs. This experiment has been repeated for at least 3 times.
(B) FACS analysis of CD8α expression on gated CD11B$^-$CD103$^+$ liver cDC from WT and *Cbl* dKO mice. Representative data of at least 5 mice.

However, there is still another issue needs to addressed here. Since the BrdU incorporation assay and DAPI staining were carried out *in vitro*, questions still exist what will the *in vivo* situation look like in *Cbl* dKO mice. The *in vivo* BrdU incorporation experiment and Ki67 staining results revealed that both splenic *Cbl* dKO CD8α$^+$ and CD11B$^+$ cDCs have enhanced proliferation rate compared to the WT CD8α$^+$ and CD11B$^+$ cDCs (data not shown). This result suggests three things. Firstly, compared to WT CD11B$^+$ cDCs, the *Cbl* dKO CD11B$^+$ cDCs may have slightly expansion to a certain extend which requires more samples to distinguish this difference. But even that, it is true that the difference in CD8α$^+$ cDCs is more dramatic than in CD11B$^+$ cDCs. Secondly, some other factors other than FLT3 are involved in CD8α$^+$ and CD11B$^+$ cDCs proliferation *in vivo*. For

example, WT CD11B$^+$ cDCs have relatively higher M-CSFR surface expression than WT CD8α^+ cDCs, and CBL proteins can regulate the ubiquitination and degradation of M-CSFR[317]. Therefore, it may cause the difference between the *in vitro* and *in vivo* results. But even that, it should still be kept in mind that the absolute expression of FLT3 is higher than the M-CSFR in CD11B$^+$ cDC, which suggests that the effect by FLT3 should be more dominant than that by M-CSFR. Thirdly, since in mutant CD8α^+ cDCs, the FLT3 signaling is stronger than in mutant CD11B$^+$ cDCs, which may suggest that the mutant CD8α^+ cDCs have better survival compared to the mutant CD11B$^+$ cDCs. However, it still needs further experiments to prove this hypothesis that the mutant CD8α^+ cDCs survive better than the mutant CD11B$^+$ cDCs *in vivo*.

V. 5. The mechanism by which CBL proteins regulate FLT3 signaling

FLT3 is a receptor tyrosine kinase that delivers signal through its multiple intracellular signaling modules. It has been shown that the major intracellular signaling pathways that act downstream FLT3 include, but are not limited to, the PKB/AKT-MTOR, RAS-MEK-ERK kinases cascade, and Ca^{2+} mobilization. My data indicate that CBL proteins regulate at least the PKB/AKT-MTOR and RAS-MEK-ERK signaling pathways during DC development through regulating FLT3. The results in my study have shown that both PKB/AKT and ERK1/2 kinases are constitutively activated in *Cbl* dKO CD24$^+$ cDC (Fig. 4.10A, 4.10B, and 4.10C). Stimulation of FLT3 markedly enhances the activity of PKB/AKT and ERK1/2 in WT cells, however, to much less extent the activation of these kinases in *Cbl* dKO DCs, suggesting that in the mutant DCs their activities almost reach the plateau even in the absence of FLT3 stimulation. The enhanced activity of PKB/AKT is relevant to the altered DC homeostasis, because blockade of MTOR signaling, which acts downstream of PKB/AKT, by rapamycin normalizes the total number of CD8α^+ cDC in both the FLT3L bone marrow culture or in mice.

Given that both PKB/AKT and ERK signals are enhanced in the mutant DCs, I propose that CBL proteins regulate these signals at the top of these signaling cascades, namely at the level of FLT3 receptor. It has been reported that C-CBL and CBL-B regulate receptor signaling either by promoting their ubiquitination and degradation or by acting as an adaptor to bridge the receptor signaling to downstream signalosomes. My data favor the notion that CBL proteins regulate FLT3 signaling by promoting FLT3 ubiquitination and degradation. Indeed, the results in my study show

that expression of mature form of FLT3, but not the immature form of FLT3, is dramatically increased in the mutant DCs as compared to WT cells (Fig. 4.12A). In addition, the *in vitro* biochemical analysis reveals that CBL proteins can promote FLT3 ubiquitination (Fig. 4.15). Moreover, since both PKB/AKT and ERK1/2 activities are enhanced rather than weakened in the mutant DCs than in WT DCs, it is unlikely that CBL proteins function as bridge to link the FLT3 and its downstream PKB/AKT and ERK signaling. Altogether, I propose a working model that explains how CBL proteins regulate cDC homeostasis as depicted in Fig. 5.2. In this model, I propose that FLT3 is a key regulator that senses environmental signal (FLT3L) to determine the genesis of $CD8\alpha^+$ cDC vs $CD11B^+$ cDC ratio during DC development. CBL proteins play a critical role in this regulation by dictating the level of FLT3 expression through promoting its ubiquitination and degradation. In a certain microenvironment, there is a homeostasis among $CD8\alpha^+$ cDCs, $CD11B^+$ cDCs and pDCs. However, when CBL proteins were deficient in these three DC subsets, $CD8\alpha^+$ cDCs have advantages in proliferation over $CD11B^+$ cDCs and pDCs, which is probably due to two reasons. First, $CD8\alpha^+$ cDCs have higher surface FLT3 expression than $CD11B^+$ cDCs and pDCs, which makes them have stronger signals to keep themselves survive and proliferate better. Second, the expanded $CD8\alpha^+$ cDCs can manipulate the local FLT3L concentration to suppress $CD11B^+$ cDCs and pDCs proliferation, which consequently changes the homeostasis of all these DC subsets. It is noteworthy that this phenotype is very similar with the phenotype found in high dose FLT3L treated WT mice. In the high dose FLT3L treated mice, these three DC subsets all have dramatic overexpansion in the spleen, and $CD8\alpha^+$ cDCs have a more prominent overexpansion than the other two DC subsets[306]. Also in FLT3L treated mice, there is a Treg expansion in the spleen, which is similar with the results in my study[318].

FLT3 is a membrane protein. It is generally believed that membrane protein degradation after ubiquitination usually occurs via the endocytosis and lysosome pathway. It is interesting to find that blockade of lysosome pathway with chloroquine or proteasome pathways with MG132 reduces FLT3 degradation (Fig. 4.14). At present, it is not so clear how these degradation pathways are involved in CBL proteins mediated FLT3 degradation, however, it will be interesting to dissect these mechanisms in the future.

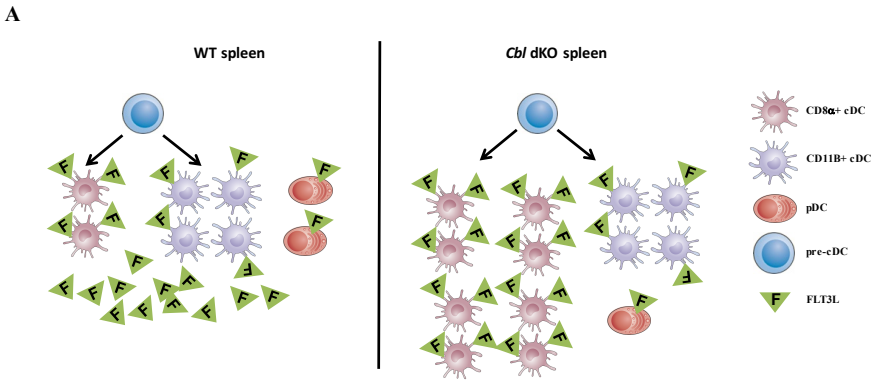

Fig. 5.2. The regulatory mechanisms of CBL proteins on the homeostasis of DCs.
(A) The regulation of CBL proteins on the homeostasis of DCs in the spleen. In the spleen of WT mice, the attenuation of FLT3 signaling due to the existence of CBL proteins is essential for keeping the homeostasis of DC subsets. And there are still some free FLT3L in the environmental niche (left panel). However, in the spleen of *Cbl* dKO mice, $CD8\alpha^+$ cDCs have more prominent overexpansion due to their higher surface FLT3 expression and the consequent stronger FLT3 signaling than $CD11B^+$ cDCs and pDCs. The overexpanded $CD8\alpha^+$ cDCs also consume the free FLT3L in the environmental niche, which leads to a stress of survive for $CD11B^+$ cDCs and pDCs (right panel). Some components of this figure are taken from Ref.319.

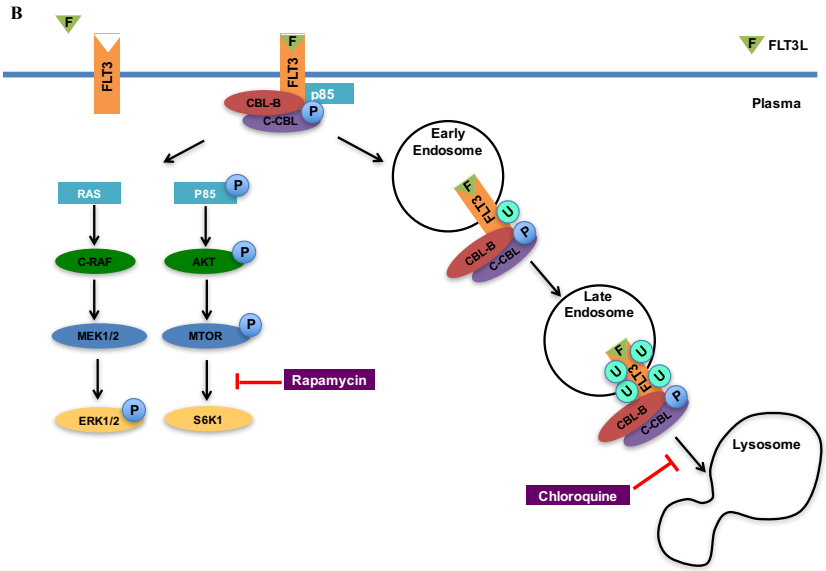

(B) The redundant negative regulatory roles of CBL-B and C-CBL in FLT3 signaling pathway. When FLT3 receive the extracellular signal from FLT3L, it will form homodimer and activate each other by the phosphorylation of Try589/591. On one hand, the phosphorylated FLT3 will transfer the signal through its associated adaptors such as P85, GRB2, and etc to activate downstream PKB/AKT-MTOR and RAS-MEK-ERK signaling pathways. On the other hand, the phosphorylated FLT3 will be recognized by the TKB domain of CBL-B and C-CBL, which leads to the multi-mono-ubiquitination and lysosome sorting mediated degradation of FLT3 to attenuate FLT3 signaling.

V. 6. CBL proteins are required for the maintenance of immune quiescence at the steady-state

Based on the previous results in the lab, it has been shown that CBL proteins play a redundant role in the control of immune quiescence of both T and B cells. The simultaneous ablation of CBL proteins in either T or B lineage cells leads to the development of spontaneous autoimmune and SLE like diseases respectively[236]. Here, the results in my study reveals that mice with simultaneous inactivation of C-CBL and CBL-B in DCs have impaired DC homeostasis, which leads to severe liver inflammation and sporadic inflammation in other organs including lung, kidney, and salivary gland. Mice start to become moribund younger than 5-month-old, most likely due to the development of severe liver fibrosis and functional failure. These findings thus demonstrate that in addition to T and B cells, DCs also require CBL proteins to maintain their functional quiescence and homeostasis under steady state.

The question here is by which mechanisms CBL proteins control the immune quiescence of DCs under steady-state. The results in my study show that in the absence of *in vitro* stimulation, freshly isolated splenic CD8α^+ DCs from *Cbl* dKO mice produce more amounts of inflammatory cytokines and chemokines such as IL-6 and CCL2 (Fig. 4.25). The production of these inflammatory cytokines and chemokines can promote the chronic inflammation in the *Cbl* dKO mice, though it is unknown whether block of IL-6 or CCL2 can alleviate the inflammatory disease. The production of IL-6 is also slightly enhanced in *Cbl* dKO splenic CD8α^+ cDCs compared to the WT counterparts after CpG stimulation (Fig. 4.31), suggesting that CBL proteins may negatively regulate TLRs, at least TLR9 involved in CpG recognition. It is noteworthy that *Cbl* dKO mice contain a markedly expanded cDC population in the liver than WT mice, and these cells also exhibit enhanced production of IL-6. Although the enhancement of these inflammatory cytokines and chemokines' production is slight in the mutant DCs, the accumulative effect of the dramatically expanded DC population in the liver might provide a very detrimental influence to the liver.

At present, it is still not so clear what mechanisms do DCs use to keep their functional quiescence when they sense the self-cues. It is a still unanswered question whether CBL proteins are required to suppress conventional pattern recognition receptors from being hyperactive under

steady state. Alternatively, if it is the case that in the absence of CBL proteins, these pattern recognition receptors can become spontaneously active so that minimal stimulation from environmental pathogen or pathogen products can trigger DC hyper-activation, and lead to the development of inflammatory disease. However, the results of the antibiotic treatment experiment reveal that CBL proteins are not involved in this process (data not shown). Given that CBL proteins can negatively regulate the sensing of environmental pathogens or pathogen products, antibiotics treated *Cbl* dKO mice are supposed to have less severe liver inflammation. However, opposite to the hypotheses, the antibiotics treated *Cbl* dKO mice have even more severe inflammatory disease (data not shown).

V. 7. How do CBL-B and C-CBL regulate antigen presentation capacity of DCs

In the *in vitro* results, it is clearly shown that *Cbl* dKO CD8α^+ cDCs have enhanced antigen-presenting capacities to both CD8$^+$ OT-I and CD4$^+$ OT-II T cells (Fig. 4.6C, 4.6D, 4.24A, 4.24B). The result that *Cbl* dKO mice possess more activated T cells also indicate that *Cbl* dKO DCs indeed prime and activate more T cells *in vivo* (Fig. 4.20, 4.21, 4.22). There is still one unsolved question that how CBL proteins regulate the antigen presentation capacity of DCs. Antigen presentation is a multi-step process, which includes antigen capture, antigen processing, antigen transport, and presentation in the form of MHC-peptide complexes. The results in my study indicate that the antigen capture by CD24$^+$ cDCs is not affected by *Cbl* dKO mutation (Fig 4.26C). Since the mutant DCs have unchanged surface expression of co-stimulatory molecules, MHC-I and MHC-II, it is more reasonable to speculate that CBL proteins might regulate DC antigen presentation through other mechanisms. Previous studies showing that MARCH family, another RING finger containing E3 ubiquitin ligase family, was involved in the regulation of MHC-II and CD86 ubiquitination and degradation. Therefore, it is reasonable to speculate that CBL family proteins could also be involved in this regulation through their RING finger domains. However, based on the results in my study, this speculation seems not likely, because the *Rag1* KO and *Cbl* tKO GM-CSF cultured BMDCs show equivalent surface expression of MHC-II and CD86 with or without LPS stimulation (Fig. 4.30). Since *Cbl* dKO DCs have constitutively activated AKT and ERK signaling pathways, the higher antigen-presenting capacity of *Cbl* dKO CD8α^+ cDCs could be probably due to the fact that the mutant cells have higher viability which facilitates the antigen presentation of DCs. Another explanation is related to the upregulated surface CD103 expression

in *Cbl* dKO CD8α$^+$ cDCs (Fig 4.25D). It has been reported in other studies that CD103 expression on DCs is positively correlated with their antigen presenting capacities[45]. Although the detailed mechanism how CD103 expression regulates antigen presentation has not been clarified yet, it will be certainly interesting to investigate this mechanism in the future.

V. 8. Why there is more Th1 type of effector cells in the *Cbl* dKO mice

The results in my study showed that there were more CD4$^+$ T effector/memory cells in the SP and liver of *Cbl* dKO mice (Fig. 4.20 and 4.21). Among these splenic CD4$^+$ T effector/memory cells, there was also an increased percentage of IFN-γ producing Th1 type of cells compared to the WT counterparts (Fig. 4.22). Therefore, the question is that what mechanism do *Cbl* dKO DCs use to polarize CD4$^+$ T cells to Th1 cells. Based on the results, this phenomenon could be contributed from two parts: the intrinsic part and the extrinsic part. First, *Cbl-b* single KO has the effect on promoting the Th1 polarization of CD4$^+$ T cells (Fig. 4.22). Since *Cbl-b* are germline KO in the *Cbl* dKO mice, the T cells in the *Cbl* dKO mice also have *Cbl-b* deletion (Fig. 4.1). Therefore, *Cbl-b* deletion in T cells themselves will contribute an intrinsic effect to promote Th1 polarization in the *Cbl* dKO mice. Second, the percentage of CD4$^+$ IFN-γ producing cells in *Cbl* dKO mice is higher than that in *Cbl*-b KO mice, suggesting that there must be an extrinsic effect involved (Fig. 4.22). One possibility of this extrinsic effect could be that the *Cbl* dKO CD8α$^+$ cDCs produce more IL-12 upon CpG stimulation compared to WT CD8α$^+$ cDCs (Fig. 4.6B). However, the RNA-seq data do not show a dramatic increase of IL-12 expression in *Cbl* dKO CD8α$^+$ cDCs compared to the WT CD8α$^+$ cDCs. Therefore, this possibility seems less likely. Another possibility of this extrinsic effect could be contributed by the enhanced ratio of CD8α$^+$ cDCs vs CD11B$^+$ cDCs in *Cbl* dKO mice. It is noteworthy that the inhibitory co-stimulatory molecule PD-L1 is specifically highly expressed on CD11B$^+$ cDCs surface compared to CD8α$^+$ cDCs. The enhanced ratio of CD8α$^+$ cDCs vs CD11B$^+$ cDCs in *Cbl* dKO mice provide a microenvironment where the activated T cells have less chances to contact with inhibitory ligand PD-L1, thus leading to an enhanced Th1 polarization.

V. 9. The revelations from the entire study

There are still several other issues need to be addressed here. Firstly, why long-term rapamycin treatment could only partially prevent the liver inflammation? Based on the results of the long-term rapamycin treatment experiment, it clearly shows that restoring DC homeostasis can significantly but not completely extend the lifespan of *Cbl* tKO mice and protect them from chronic liver inflammation (Fig. 4.32 and 4.33). It is probably due to the fact that both AKT and ERK signaling pathways are activated in *Cbl* tKO CD8α^+ cDCs, and rapamycin treatment could only block the AKT pathway, thus leading to a partial restoration of DC homeostasis. In the future, it will be worthy to investigate whether a combination of AKT and ERK inhibitors or FLT3 inhibitor could completely restore DC homeostasis and protect *Cbl* tKO mice from liver inflammation even better. Meanwhile, it should also be noted that rapamycin has a general anti-aging effect in both flies and mice[320, 321]. Although the mechanism behind is not very clear yet, this effect should be put into consideration.

Secondly, is FLT3L treatment a good method to boost immunity? The answer depends on the context. Based on the results in my study, I think, short-term FLT3L treatment might boost the immunity through an enhanced ratio of CD8α^+ cDCs vs CD11B$^+$ cDCs. Actually, there are already some studies showing that short-term FLT3L treatment could effectively boost immunity to protein vaccine or against tumor[306, 322]. However, based on the results in my study, long-term FLT3L treatment should be used with caution, because it may cause chronic liver inflammation.

Thirdly, is it a good idea to use FTL3L as an anti-autoimmune drug? In many studies including my study, it clearly shows that there is a positive correlation between CD8α^+ cDCs expansion and Tregs expansion. This correlation is even proved true in human subjects[280]. Because Tregs are considered to have anti-autoimmune effect, some researchers suggests FLT3L may represent a promising agent for promoting immune tolerance in a variety of clinical settings[280]. However, based on my results, this notion should be used with caution. Because the majorities of anti-autoimmune treatments are chronic processes, long-term FLT3L treatment may cause chronic liver inflammation. Moreover, based on my results, the enhanced FLT3 signaling in DCs could also promote Th1 immune response, which may deteriorate some types of autoimmune diseases.

Altogether, the effect of long-term FLT3L treatment should be investigated before its clinical application. Unfortunately, such experiments have not been reported yet.

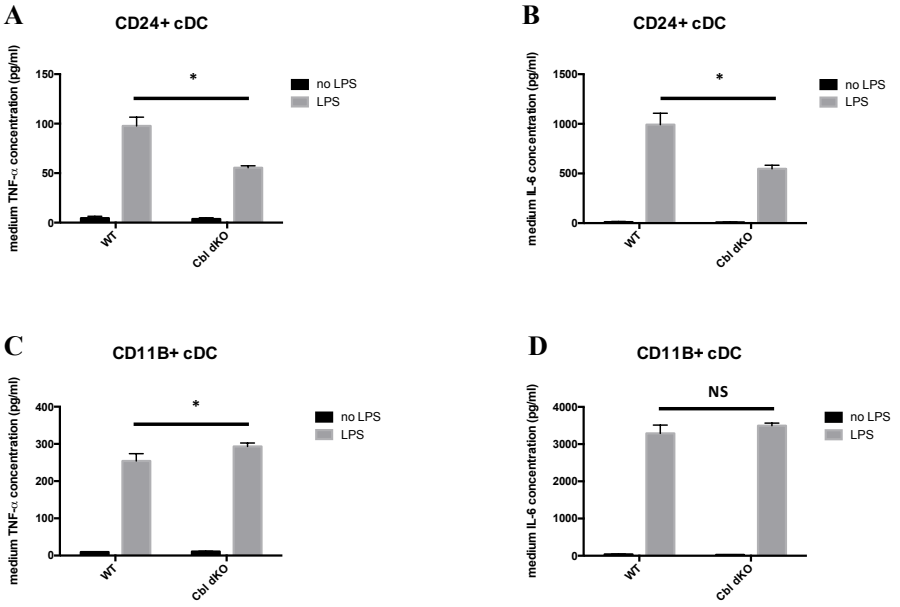

Fig. 5.3. *Cbl* dKO CD24$^+$ cDC produce less inflammatory cytokines upon LPS stimulation.
(A & B) TNF-α and IL-6 production by WT and *Cbl* dKO CD24$^+$ cDCs. Pooled BM cells from WT or *Cbl* dKO mice (n=3) were cultured in 10% FLT3L conditional medium. CD24$^+$ cDCs were sorted following the same procedures as described in the Material and Method section. Triplicates of 1×10^5 CD24$^+$ cDCs were then stimulated overnight with 100ng/ml LPS. The concentration of TNF-α and IL-6 in the culture medium was quantified by ELISA. Multiple t tests with fewer assumptions and Holm-Sidak correction method were applied in the statistics. (n=3) P value <0.05 was considered significant.
(C & D) TNF-α and IL-6 production by WT and *Cbl* dKO CD11B$^+$ cDCs. Pooled BM cells from WT or *Cbl* dKO mice (n=3) were cultured in 10% FLT3L conditional medium. CD11B$^+$ cDCs were sorted following the same procedures as described in the Material and Method section. Triplicates of 1×10^5 CD11B$^+$ cDCs were then stimulated overnight with 100ng/ml LPS. The concentration of TNF-α and IL-6 in the culture medium was quantified by ELISA. Multiple t tests with fewer assumptions and Holm-Sidak correction method were applied in the statistics. (n=3) P value <0.05 was considered significant.

Last but not least, do CBL proteins regulate the ubiquitination and degradation of MYD88? As it is mentioned in the introduction section, there is one study showing that CBL-B could regulate the ubiquitination and degradation of MYD88 with the help of SYK[223]. However, there are still several questions remain unsolved. First, in another study by using the same *in vitro* 293T system, the results showed that CBL-B could regulate the ubiquitination and degradation of TLR4, but not MYD88[323]. It might be argued that the impaired MYD88 degradation in the second study is possibly due to the absence of SYK. However, from a more biological point of view to think about

these results, it seems not very reasonable for CBL-B to regulate both the ubiquitination and degradation of two molecules which act the upstream and downstream of the same signaling pathway. Second, since C-CBL has similar structure as CBL-B, is there any similar effect of C-CBL on the ubiquitination and degradation of MYD88 or TLR4? Unfortunately, there is no such report yet. Last but not least, if it is the case that CBL proteins could regulate the ubiquitination and degradation of MYD88, *Cbl* dKO cDCs are supposed to produce more inflammatory cytokines such as TNF-α and IL-6 upon LPS stimulation. However, it is not the case based on my results (Fig. 5.3). In the result, it clearly shows that, upon LPS stimulation, there is dramatic reduction of TNF-α and IL-6 production of *Cbl* dKO $CD24^+$ cDCs compared to WT $CD24^+$ cDCs.

VI. CONCLUSION REMARKS AND FUTURE DIRECTION

The results of my study have demonstrated that CBL proteins play an important role in DC development and homeostasis by their redundant functions of regulating FLT3 ubiquitination and degradation. Since $CD8\alpha^+$, and $CD11B^+$ cDCs and pDCs have different surface FLT3 expression, the ablation of CBL proteins also causes an extrinsic effect on the development of these three DC subsets through creating a local FLT3L competition environment. This FLT3L competition environment leads to the net outcome of $CD8\alpha^+$ cDCs overexpansion, pDCs reduction, unchanged $CD11B^+$ cDCs in spleen, and $CD103^+$ cDCs overexpansion in liver. This impaired homeostasis of DC subsets could further cause a chronic liver inflammation in the mice without the help of T cells and B cells. Moreover, the chronic liver inflammation could be partially blocked by long-term rapamycin treatment.

However, there are still several critical questions worth to be investigated in the future. Firstly, it is known that FLT3 receptor activation involves multiple signaling pathways, such as the PKB/AKT-MTOR, RAS-MEK-ERK, and Ca^{2+} mobilization. My study also indicates that in the absence of CBL proteins, both PKB/AKT-MTOR and RAS-MEK-ERK pathways are activated in DCs, which leads to the question whether double block of AKT and ERK signaling pathways could rescue the liver inflammation of the *Cbl* tKO mice. Secondly, it has been noticed the inflammatory cytokines and chemokines such as TNF-α, IL-6 and CCL2 are highly expressed in the serum of Cbl tKO mice. However, what are the cell sources that mostly contribute to the overproduction of these cytokines or chemokines are still not very clear. The accumulating effect of overexpanded $CD103^+$ cDCs in liver could be one explanation. However, it is still worth to explore any other possible mechanisms. Thirdly, all the results in my study point out to the regulation of CBL proteins on RTKs, but not TLRs. However, it will still be interesting to investigate whether depletion of *Myd88* gene in mutant DCs could help to alleviate the liver inflammation in *Cbl* dKO mice. By doing so, it can help us to confirm whether CBL proteins are involved in the regulation of TLR/MYD88 signaling pathway. Fortunately, the *Cd11c* Cre; *C-cbl*$^{f/f}$; *Myd88*$^{f/f}$; *Cbl-b*$^{-/-}$ have been created in the lab. Fourthly, since in my result it clearly shows that there is a specifically highly expression of PD-L1 on $CD11B^+$ cDCs, it will be worth to investigate the biological significance of PD-L1 on $CD11B^+$ cDCs, and biological consequences of manipulating the ratio among different DC subsets. Fifthly, it will also be interesting to investigate whether and how some other factors such as inflammation or metabolic products could be involved in regulating the

ratio among different DC subsets. Last but not least, given that *Cbl* dKO mice develop predominantly severe liver inflammatory diseases, it will be a great interest to examine whether the same molecules or other molecules regulated by CBL proteins are involved in human liver inflammation diseases.

VII. ACKNOWLEDGMENTS

First, I would like to thank my supervisor, Dr. Hua Gu, for his meticulous guidance on me during the past 5 years in his lab. I still remember the tough moment when I just changed to this new lab after the first year of my PhD study. At that time, I had very few knowledge on immunology and molecule biology compared with the knowledge that I have now. Dr. Hua Gu is a very smart and knowledgeable person, and he is always willing to share his knowledge with us. I also appreciate the lessons learned from him and this lab. Next, I would like to thank my committee members, Dr. Artur Kania, Dr. Woong-Kyung Suh, and Dr. Éric Cohen for their critical help to my research and thesis. I would also like to thank my thesis committee members, Dr. André Veillette, Dr. Connie Krawczyk, Dr. Sylvie Lesage, and Dr. Jean-Philippe Gratton for their suggestions to improve the quality of my thesis. Especially, I would like to thank Dr. Dominique Davidson for her tremendous help and contribution to the French abstract of my thesis, and also her other helps to my experiments.

Secondly, I would also like to acknowledge other amazing mentors who provide me tremendous helps to my PhD study. Dr. Cheolho Cheong, thank you for your generosity and teaching me how to generate FLT3L derived DCs and the basic knowledge about different DC subsets. Dr. Yong-Rui Zou, thank you for the contribution to the cytokine and chemokine screen experiment. Dr. Woong-Kyung Suh, thank you for your generosity of providing me the *Rag1* KO mice. Dr. André Veillette, thank you for your generosity of sharing the OT-I, OT-II mice and J588 GM-CSF-secreting myeloma cell line. Dr. Wallace Langdon, thank you for your generosity of providing me the *Cbl-b*^{C373A} mice. Dr. Boris Reizis, thank you for your generosity of providing me the FLT3L-secreting B16 melanoma cell line. Thanks to Adeline for your contribution to the long-term rapamycin treatment experiment.

Thirdly, I would like to acknowledge the amazing IRCM core facility members. Without your professional work, my research will never go such easy and enjoyable, and will become much tougher. Thanks to the animal facility members: Marie-Claude Lavallée, Ève-Lyne Thivierge, Dimitar Dimitrov, Manon Laprise, Suzie Riverin, Stéphanie Lemay, Caroline Dubé, Sara Demontigny, Julie D Amours, and Ovidiu Jumanca. Thanks to the histology core facility members: Simone Terouz and Dominique Lauzier. Thanks to the FACS core facility members: Éric Massicotte, Julie Lord, Julien Leconte, and Philippe St-Onge. Thanks to the molecular biology

core facility members: Odile Neyret, Agnes Dumont, and Myriam Rondeau. Thanks to the microscope core facility member: Dominic Filion. Thanks to the bioinformatics core facility members: Virginie Calderon and Alexis Blanchet-Cohen.

Fourthly, I would like to acknowledge the people or institution who give tremendous help to my life during my PhD study. Thanks to CSC and CIHR to provide me the financial support of my PhD study. I cannot imagine how can I, as a student from a Chinese working class family, afford my 6 years' PhD study in Canada without your support. Thanks to the previous and present lab mates for your company. Five years is a long journey, and it has been always a pleasure to work with you and share different points of view on science and social issues. Thanks to the kindness help from IRCM secretaries Virginie Leduc and Daniela Baggio, and secretary France Fauteux from the department. Thanks to the IRCM cafeteria for serving the delicious and affordable meals.

Fifthly, I would like to show my great gratitude to the sacrifice of the experimental mice. Thanks to their contribution to the scientific researches.

Last but not least, I want to acknowledge my parents for their unwavering support and understanding of my decision to come to Canada for my PhD study. I want to acknowledge them for their understanding for me to spend so few time with them during the past 6 years.

VIII. REFERENCE LIST

1. Steinman, R.M., Identification of a novel cell type in the peripheral lymphoid organs of mice. I. Morphology, quantitation, tissue distribution. J. Exp. Med, 1973. 137(5): p. 1142-1162.
2. Steinman, R.M., Identification of a novel cell type in the peripheral lymphoid organs of mice. II. Function properties in vitro. J. Exp. Med, 1974. 139(2): p. 380-397.
3. Steinman, R.M., Identification of a novel cell type in the peripheral lymphoid organs of mice. III. Function properties in vivo. J. Exp. Med, 1974. 139(6): p. 1431-1445.
4. Steinman, R.M., Lymphoid dendritic cells are potent stimulators of the primary mixed leukocyte reaction in mice. Proc Natl Acad Sci U S A. 1978. 75(10): p. 5132-5136.
5. Nussenzweig, M.C., Dendritic cells are accessory cells for the development of anti-trinitrophenyl cytotoxic T lymphocytes. J. Exp. Med. 1980. 152(4): p. 1070-1084.
6. Liu K, In vivo analysis of dendritic cell development and homeostasis. Science. 2009. 324(5925): p. 392-397.
7. Ginhoux F, The origin and development of nonlymphoid tissue CD103+ DCs. J. Exp. Med. 2009. 206(13): p. 3115-3130.
8. Merad M, The dendritic cell lineage: ontogeny and function of dendritic cells and their subsets in steady state and the inflamed setting. Annu Rev Immunol. 2013. 31: p. 563-604.
9. Lieping Chen, Molecular mechanisms of T cell co-stimulation and co-inhibition. Nav Rev Immunol. 2013. 13(4): p. 227-242.
10. Bergtold A, Cell surface recycling of internalized antigen permits dendritic cell priming of B cells. Immunity. 2005. 23(5): p. 503-514.
11. Trombetta ES, Activation of lysosomal function during dendritic cell maturation. Science. 2003. 299(5611): p. 1400-1403.
12. Maria Rescigno, Dendritic cell survival and maturation are regulated by different signaling pathways. J. Exp. Med. 1998. 188(11): p. 2175-2180.
13. Ken Shortman, Steady-state and inflammatory dendritic-cell development. Nat Rev Immunol. 2007. 7(1): p. 19-30.
14. Crowley M, The cell surface of mouse dendritic cells: FACS analyses of dendritic cells from different tissues including thymus. Cell Immunol. 1989. 118(1): p. 108-125.
15. Vremec D, The surface phenotype of dendritic cells purified from mouse thymus and spleen: investigation of the CD8 expression by a subpopulation of dendritic cells. J. Exp. Med. 1992. 176(1): p. 47-58.

16. del Rio ML, CD103- and CD103+ bronchial lymph node dendritic cells are specialized in presenting and cross-presenting innocuous antigen to CD4+ and CD8+ T cells. J Immunol. 2007. 178(11): p. 6861-6866.
17. Waskow C, The receptor tyrosine kinase Flt3 is required for dendritic cell development in peripheral lymphoid tissues.
18. Heath WR, Cross-presentation in viral immunity and self-tolerance. Nat Rev Immunol. 2001. 1(2): p. 126-134.
19. Blum JS, Pathways of antigen processing. Annu Rev Immunol. 2013. 31: p. 443-473.
20. Joffre OP, Cross-presentation by dendritic cells. Nat Rev Immunol. 2012. 12(8): p. 557-569.
21. den Haan JM, Constitutive versus activation-dependent cross-presentation of immune complexes by CD8(+) and CD8(-) dendritic cells in vivo. J. Exp. Med. 2002. 196(6): p. 817-827.
22. GeurtsvanKessel CH, Clearance of influenza virus from the lung depends on migratory langerin+CD11b- but not plasmacytoid dendritic cells. J. Exp. Med. 2008. 205(7): p. 1621-1634.
23. Desch AN, CD103+ pulmonary dendritic cells preferentially acquire and present apoptotic cell-associated antigen. J. Exp. Med. 2011. 208(9): p. 1789-1797.
24. Segura E, Different cross-presentation pathways in steady-state and inflammatory dendritic cells. Proc Natl Acad Sci U S A. 2009. 106(48): p. 20377-20381.
25. Meredith MM, Expression of the zinc finger transcription factor zDC (Zbtb46, Btbd4) defines the classical dendritic cell lineage. J. Exp. Med. 2012. 209(6): p. 1153-1165.
26. Satpathy AT, Zbtb46 expression distinguishes classical dendritic cells and their committed progenitors from other immune lineages. J. Exp. Med. 2012. 209(6): p. 1135-1152.
27. Meredith MM, Zinc finger transcription factor zDC is a negative regulator required to prevent activation of classical dendritic cells in the steady state. J. Exp. Med. 2012. 209(9): p. 1583-1593.
28. Schiavoni G, ICSBP is essential for the development of mouse type I interferon-producing cells and for the generation and activation of CD8alpha(+) dendritic cells. J. Exp. Med. 2002. 196(11): p. 1415-1425.
29. Edelson BT, Peripheral CD103+ dendritic cells form a unified subset developmentally related to CD8alpha+ conventional dendritic cells. J. Exp. Med. 2010. 207(4): p. 823-836.
30. Tailor P, The BXH2 mutation in IRF8 differentially impairs dendritic cell subset development in the mouse. Blood. 2008. 111(4): p. 1942-1945.
31. Hacker C, Transcriptional profiling identifies Id2 function in dendritic cell development. Nat

Immunol. 2003. 4(4): p. 380-386.
32. Kusunoki T, TH2 dominance and defective development of a CD8+ dendritic cell subset in Id2-deficient mice. J Allergy Clin Immunol. 2003. 111(1): p. 136-142.
33. Spits H, Id2 and Id3 inhibit development of CD34(+) stem cells into predendritic cell (pre-DC)2 but not into pre-DC1. Evidence for a lymphoid origin of pre-DC2. J. Exp. Med. 2000. 192(12): p. 1775-1784.
34. Hildner K, Batf3 deficiency reveals a critical role for CD8alpha+ dendritic cells in cytotoxic T cell immunity. Science. 2008. 322(5904): p. 1097-1100.
35. Jason Waithman, Resident CD8+ and migratory CD103+ dendritic cells control CD8 T cell immunity during acute influenza infection. Plos One. 2013. 8(6): p. e66136.
36. Wu L, Cell-autonomous defects in dendritic cell populations of Ikaros mutant mice point to a developmental relationship with the lymphoid lineage. Immunity. 1997. 7(4): p. 483-492.
37. Carotta S, The transcription factor PU.1 controls dendritic cell development and Flt3 cytokine receptor expression in a does-dependent manner. Immunity. 2010. 32(5): p. 628-641.
38. Crozat K, The XC chemokine receptor 1 is a conserved selective marker of mammalian cells homologous to mouse CD8alpha+ dendritic cells. J. Exp. Med. 2010. 207(6): p. 1283-1292.
39. Miller JC, Deciphering the transcriptional network of the dendritic cell lineage. Nat Immunol. 2012. 13(9): p. 888-899.
40. Greter M, GM-CSF controls nonlymphoid tissue dendritic cell homeostasis but is dispensable for the differentiation of inflammatory dendritic cells. Immunity. 2012. 36(6): p. 1031-1046.
41. Martinez-López M, Batf3-dependent CD103+ dendritic cells are major producers of IL-12 that drive local Th1 immunity against Leishmania major infection in mice. Eur J Immunol. 2015. 45(1): p. 119-129.
42. Vremec D, The influence of granulocyte/macrophage colony-stimulating factor on dendritic cell levels in mouse lymohoid organs. Eur J Immunol. 1997. 27(1): p. 40-44.
43. King IL, GM-CSF-dependent, CD103+ dermal dendritic cells play a critical role in Th effector cell differentiation after subcutaneous immunization. J. Exp. Med. 2010. 207(5): p. 953-961.
44. Kingston D, The concerted action of GM-CSF and Flt3-ligand on in vivo dendritic cell homeostasis. Blood. 2009. 114(4): p. 835-843.
45. Sathe P, The acquisition of antigen cross-presentation function by newly formed dendritic cells. J Immunol. 2011. 86(9): p. 5184-5192.

46. Dudziak D, Differential angtigen processing by dendritic cell subsets in vivo. Science. 2007. 315(5808): p. 107-111.
47. Lewis KL, Notch2 receptor signaling controls functional differentiation of dendritic cells in the spleen and intestine. Immunity. 2011. 35(5): p. 780-791.
48. Kabashima K, Intrinsic lymphotoxin-beta receptor requirement for homeostasis of lymphoid tissue dendritic cells. Immunity. 2005. 22(4): p. 439-450.
49. Wang YG, Stimulating lymphotoxin beta receptor on the dendritic cells is critical for their homeostasis and expansion. J Immunol. 2005. 175(10): p. 6997-7002.
50. Wu L, RelB is essential for the development of myeloid-related CD8alpha- dendritic cells but not of lymphoid-related CD8alpha+ dendritic cells. Immunity. 1998. 9(6): p. 839-847.
51. Suzuki S, Critical roles of interferon regulatory factor 4 in CD11bhighCD8alpha- dendritic cell development. Proc Natl Acad Sci U S A. 2004. 101(24): p. 8981-8986.
52. Esashi E, The signal transducer STAT5 inhibits plasmacytoid dendritic cell development by suppressing transcription factor IRF8. Immunity. 2008. 28(4): p. 509-520.
53. Caton ML, Notch-RBP-J signaling controls the homeostasis of CD8- dendritic cells in the spleen. J. Exp. Med. 2007. 204(7): p. 1653-1664.
54. Kim TS, Respiratory dendritic cell subsets differ in their capacity to support the induction of virus-specific cytotoxic CD8+ T cell responses. PLoS One. 2009. 4(1): p. e4204.
55. Ballesteros-Tato A, Temporal changes in dendritic cell subsets, cross-priming and costimulation via CD70 control CD8(+) T cell responses to influenza. Nat Immunol. 2010. 11(3): p. 216-224.
56. Kastenmüller K, Protective T cell immunity in mice following protein-TLR7/8 agonist-conjugate immunization requires aggregation, type I IFN, and multiple DC subsets. J Clin Invest. 2011. 121(5): p. 1782-1796.
57. Helft J, Cross-presenting CD103+ dendritic cells are protected from influenza virus infection. J Clin Invest. 2012. 122(11): p. 4037-4047.
58. Siegal FP, The nature of the principal type 1 interferon-producing cells in human blood. Science. 1999. 284(5421): p. 1835-1837.
59. Asselin-Paturel C, Mouse type I IFN-producing cells are immature APCs with plasmacytoid morphology. Nat Immunol. 2001. 2(12): p. 1144-1150.

60. Reizis B, Plasmacytoid dendritic cells: recent progress and open questions. Annu Rev Immunol. 2011. 29: p. 163-183.
61. Corcoran L, The lymphoid past of mouse plasmacytoid cells and thymic dendritic cells. J Immunol. 2003. 170(10): p. 4926-4932.
62. Onai N, Identification of clonogenic common Flt3+M-CSFR+ plasmacytoid and conventional dendritic cell progenitors in mouse bone marrow. Nat Immunol. 2007. 8(11): p. 1207-1216.
63. Naik SH, Development of plasmacytoid and conventional dendritic cell subtypes from single precursor cells derived in vitro and in vivo. Nat Immunol. 2007. 8(11): p. 1217-1226.
64. Onai N, A clonogenic progenitor with prominent plasmacytoid dendritic cell developmental potential. Immunity. 2013. 38(5): p. 943-957.
65. Schlitzer A, Identification of CCR9- murine plasmacytoid DC precursors with plasticity to differentiate into conventional DCs. Blood. 2011. 117(24): p. 6562-6570.
66. Swiecki M, The multifaceted biology of plasmacytoid dendritic cells. Nat Rev Immunol. 2015. 15(8): p. 471-485.
67. Onai N, Activation of the Flt3 signal transduction cascade rescues and enhances type I interferon-producing and dendritic cell development. J. Exp. Med. 2006. 203(1): p. 227-238.
68. Sathaliyawala T, Mammalian target of rapamycin control dendritic cell development downstream of Flt3 ligand signaling. Immunity. 2010. 33(4): p. 597-606.
69. Scheffler JM, LAMTOR2 regulates dendritic cell homeostasis through FLT3-dependent mTOR signaling. Nat Commun. 2014. 5: p. 5138.
70. Fancke B, M-CSF: a novel plasmacytoid and conventional dendritic cell poietin. Blood. 2008. 111(1): p. 150-159.
71. MacDonald KP, The colony-stimulating factor 1 receptor is expressed on dendritic cells during differentiation and regulates their expansion. J Immunol. 2005. 175(3): p. 1399-1405.
72. Li HS, The signal transducers STAT5 and STAT3 control expression of Id2 and E2-2 during dendritic cell development. Blood. 2012. 120(22): p. 4363-4373.
73. Xu Y, Differential development of murine dendritic cells by GM-CSF versus Flt3 ligand has implications for inflammation and trafficking. J Immunol. 2007. 179(11): p. 7577-7584.
74. Cisse B, Transcription factor E2-2 is an essential and specific regulator of plasmacytoid dendritic cell development. Cell. 2008. 135(1): p. 37-48.

75. Nagasawa M, Development of human plasmacytoid dendritic cells depends on the combined action of the basic helix-loop-helix factor E2-2 and the Ets factor Spi-B. Eur J Immunol. 2008. 38(9): p. 2389-2400.
76. Sasaki I, Spi-B is critical for plasmacytoid dendritic cell function and development. Blood. 2012. 120(24): p. 4733-4743.
77. Ghosh HS, ETO family protein Mtg16 regulates the balance of dendritic cell subsets by repressing Id2. J. Exp. Med. 2014. 211(8): p. 1623-1635.
78. Sawai CM, Transcription factor Runx2 controls the development and migration of plasmacytoid dendritic cells. J. Exp. Med. 2013. 210(11): p. 2151-2159.
79. Fuchsberger M, Activation of plasmacytoid dendritic cells. Immunol Cell Biol. 2005. 83(5): p. 571-577.
80. Kenya Honda, IFR-7 is the master regulator of type-I interferon-dependent immune responses. Nature. 2005. 434(7034): p. 772-777.
81. Young LJ, Differential MHC class II synthesis and ubiquitination confers distinct antigen-presenting properties on conventional and plasmacytoid dendritic cells. Nat Immunol. 2008. 9(11): p. 1244-1252.
82. Mouriès J, Plasmacytoid dendritic cells efficiently cross-prime naïve T cells in vivo after TLR activation. Blood. 2008. 112(9): p. 3713-3722.
83. Di Pucchio T, Direct proteasome-independent cross-presentation of viral antigen by plasmacytoid dendritic cells on major histocompatibility complex class I. Nat Immunol. 2008. 9(5): p. 551-557.
84. Merad M, Origin, homeostasis and function of Langerhans cells and other langerin-expressing dendritic cells. Nat Rev Immunol. 2008. 8(12): p. 935-947.
85. Banchereau J. Dendritic cells and the control of immunity. Nature. 1998. 392(6673): p. 245-252.
86. Romani N, Langerhans cells and more: langerin-expressing dendritic cell subsets in the skin. Immunol Rev. 2010. 234(1): p. 120-141.
87. Tang A, Adhesion of epidermal Langerhans cells to keratinocytes mediated by E-cadherin. Nature. 1993. 361(6407): p. 82-85.

88. Keisuke Nagao, Murine epidermal Langerhans cells and langerin-expressing dermal dendritic cells are unrelated and exhibit distinct functions. Proc Natl Acad Sci U S A. 2009. 106(9): p. 3312-3317.
89. Jiang W, The receptor DEC-205 expressed by dendritic cells and thymic epithelial cells is involved in antigen processing. Nature. 1995. 375(6527): p. 151-155.
90. Idoyaga J, Specialized role of migratory dendritic cells in peripheral tolerance induction. J Clin Invest. 2013. 123(2): p. 844-854.
91. Clydesdale GJ, Ultraviolet light induced injury: immunological and inflammatory effects. Immunol Cell Biol. 2001. 79(6): p. 547-568.
92. Merad M, Langerhas cell renew in the skin throughout life under steady-state conditions. Nat Immunol. 2002. 3(12): p. 1135-1141.
93. Chang-Rodriguez S, Fetal and neonatal murine skin harbors Langerhans cell precursors. J Leukoc Biol. 2005. 77(3): p. 352-360.
94. Chorro L, Langerhans cell (LC) proliferation mediates neonatal development, homeostasis, and inflammation-associated expansion of the epidermal LC network. J. Exp. Med. 2009. 206(13): p. 3089-3100.
95. Hoeffel G, Adult Langerhans cells derive predominantly from embryonic fetal liver monocytes with a minor contribution of yolk sac-derived macrophages. J. Exp. Med. 2012. 209(6): p. 1167-1181.
96. Ginhoux F, Langerhans cells arise from monocytes in vivo. Nat Immunol. 2006. 7(3): p. 265-273.
97. Witmer-Pack MD, Identificaion of macrophages and dendritic cells in the osteopetrotic (op/op) mouse. J Cell Sci. 1993. (Pt4): p. 1021-1029.
98. Lin H, Discovery of a cytokine and its receptor by functional screening of the extracellular proteome. Science. 2008. 320(5877): p. 807-811.
99. Kaplan DH, Autocrine/paracrine TGFbeta1 is required for the development of epidermal Langerhans cells. J. Exp. Med. 2007. 204(11): p. 2545-2552.
100. Chopin M, Langerhans cells are generated by two distinct PU.1-dependent transcriptional networks. J. Exp. Med. 2013. 210(13): p. 2967-2980.
101. Renn CN, TLR activation of Langerhans cell-like dendritic cells triggers an antiviral immune response. J Immunol. 2006. 177(1): p. 298-305.

102. Henri S, CD207+CD103+ dermal dendritic cells cross-present keratinocyte-derived antigens irrespective of the presence of Langerhans cells. J. Exp. Med. 2010. 207(1): p. 189-206.
103. Bedoui S, Cross-presentation of viral and self antigens by skin-derived CD103+ dendritic cells. Nat Immunol. 2009. 10(5): p. 488-495.
104. Bobr A, Acute ablation of Langerhans cells enhances skin immune responses. J Immunol. 2010. 185(8): p. 4724-4728.
105. Sallusto F, Efficient presentation of soluble antigen by cultured human dendritic cells is maintained by granulocyte/macrophage colony-stimulating factor plus interleukin 4 and downregulated by tumor necrosis factor alpha. J. Exp. Med. 1994. 179(4): p. 1109-1118.
106. Cheong C, Microbial stimulation fully differentiates monocytes to DC-SIGN/CD109(+) dendritic cells for immune T cell areas. Cell. 2010. 143(3): p. 416-429.
107. Serbina NV. TNF/iNOS-producing dendritic cells mediate innate immune defense against bacterial infection. Immunity. 2003. 19(1): p. 59-70.
108. Greter M, GM-CSF controls nonlymphoid tissue dendritic cell homeostasis but is dispensable for the differentiation of inflammatory dendritic cells. Immunity. 2012. 36(6): p. 1031-1046.
109. Hammer GE, Molecular control of steady-state dendritic cell maturation and immune homeostasis. Annu Rev Immunol. 2013. 31: p. 743-791.
110. Lemaitre B, The dorsoventral regulatory gene cassette spätzle/Toll/cactus controls the potent antifungal response in Drosophila adults. Cell. 1996. 86(6): p. 973-983.
111. Poltorak A, Defective LPS signaling in C3H/HeJ and C57BL/10ScCr mice: mutations in Tlr4 gene. Science. 1998. 282(5396): p. 2085-2088.
112. Dalod M, Dendritic cell maturation: functional specialization through signaling specificity and transcriptional programming. EMBO J. 2014. 33(10): p. 1104-1116.
113. Deane JA. Control of toll-like receptor 7 expression is essential to restrict autoimmunity and dendritic cell proliferation. Immunity. 2007. 27(5): p. 801-810.
114. Mouchess ML, Transmembrane mutations in Toll-like receptor 9 bypass the requirement for ectodomain proteolysis and induce fatal inflammation. Immunity. 2011. 35(5): p. 721-732.
115. Iwami KI, Cutting edge: naturally occurring soluble form of mouse Toll-like receptor 4 inhibits lipopolysaccharide signaling. J Immunol. 2000. 165(12): p. 6682-6686.
116. LeBouder E, Soluble forms of Toll-like receptor (TLR)2 capable of modulating TLR2 signaling are present in human plasma and breast milk. J Immunol. 2003. 171(12): p. 6680-6689.

117. Chuang TH, Triad3A, an E3 uniquitin-protein ligase regulating Toll-like receptors. Nat Immunol. 2004. 5(5): p. 495-502.
118. McCartney-Francis N, Aberrant Toll receptor expression and endotoxin hypersensitivity in mice lacking a functional TGF-beta 1 signaling pathway. J Immunol. 2004. 172(6): p. 3814-3821.
119. Wan YY, 'Yin-Yang' functions of transforming growth factor-beta and T regulatory cells in immune regulation. Immunol Rev. 2007. 220: p. 199-213.
120. Abreu MT, Decreased expression of Toll-like receptor-4 and MD-2 correlates with intestinal epithelial cell protection against dysregulated proinflammatory gene expression in response to bacterial lipopolysaccharide. J Immunol. 2001. 167(3): p. 1609-1616.
121. Sadanaga A, Protection against autoimmune nephritis in MyD88-deficient MRL/lpr mice. Arthritis Rheum. 2007. 56(5): p. 1618-1628.
122. Silver KL, MyD88-dependent autoimmune disease in Lyn-deficient mice. Eur J Immunol. 2007. 37(10): p. 2734-2743.
123. Kaisho T, Endotoxin-induced maturation of MyD88-deficient dendritic cells. J immunol. 2001. 166(9): p. 5688-5694.
124. Liew FY, Negative regulation of toll-like receptor-mediated immune responses. Nat Rev Immunol. 2005. 5(6): p. 446-458.
125. Janssens S, Regulation of interleukin-1- and lipopolysaccharide-induced NF-kappaB activation by alternative splicing of MyD88. Curr Biol. 2002. 12(6): p. 467-471.
126. Burns K, Inhibition of interleikin 1 receptor/Toll-like receptor signaling through the alternatively spliced, short form of MyD88 is due to its failure to recruit IRAK4. J. Exp. Med. 2003. 197(2): p. 263-268.
127. Dumitru CD, TNF-alpha induction by LPS is regulated posttranscriptionally via a Tpl2/ERK-dependent pathway. Cell. 2000. 103(7): p. 1071-1083.
128. Huang Q, Differential regulation of interleukin 1 receptor and Toll-like receptor signaling by MEKK3. Nat Immunol. 2004. 5(1): p. 98-103.
129. Kinjyo I, SOCS1/JAB is a negative regulator of LPS-induced macrophage activation. Immunity. 2002. 17(5): p. 583-591.
130. Nakagawa R, SOCS-1 participates in negative regulation of LPS responses. Immunity. 2002. 17(5): p. 677-687.

131. Fukao T, PI3K-mediated negative feedback regulation of IL-12 production in DCs. Nat Immunol. 2002. 3(9): p. 875-881.
132. Baker AK, Rapamycin enhances LPS induction of tissue factor and tumor necrosis factor-alpha expression in macrophages by reducing IL-10 expression. Mol Immunol. 2009. 46(11-12): p. 2249-2255.
133. Zhang G, Negative regulation of toll-like receptor-mediated signaling by Tollip. J Biol Chem. 2002. 277(9): p. 7059-7065.
134. Boone DL, The ubiquitin-modifying enzyme A20 is required for termination of Toll-like receptor responses. Nat Immunol. 2004. 5(10): p. 1052-1060.
135. Hammer GE, Expression of A20 by dendritic cells preserves immune homeostasis and prevents colitis and spondyloarthritis. Nat Immunol. 2011. 12(12): p. 1184-1193.
136. Geijtenbeek TB, Signalling through C-type lectin receptors: shaping immune responses. Nat Rev Immunol. 2009. 9(7): p. 465-479.
137. Hawiger D, Dendritic cells induce peripheral T cell unresponsiveness under steady state conditions in vivo. J. Exp. Med. 2001. 194(6): p. 769-779.
138. Osorio F, Myeloid C-type lectin receptors in pathogen recognition and host defense. Immunity. 2011. 34(5): p. 651-664.
139. Kerrigan AM, Syk-coupled C-type lectin receptors that mediate cellular activation via single tyrosine based activation motifs. Immunol Rev. 2010. 234(1): p. 335-352.
140. Robinson MJ, Myeloid C-type lectins in innate immunity. Nat Immunol. 2006. 7(12): p. 1258-1265.
141. Mócsai A, The SYK tyrosine kinase: a crucial player in diverse biological functions. Nat Rev Immunol. 2010. 10(6): p. 387-402.
142. Hughes CE, CLEC-2 activates Syk through dimerization. Blood. 2010. 115(14): p. 2947-2955.
143. Sancho D, Identification of a dendritic cell receptor that couples sensing of necrosis to immunity. Nature. 458(7240): p. 899-903.
144. Tanne A, A murine DC-SIGN homologue contributes to early host defense against Mycobacterium tuberculosis. J. Exp. Med. 2009. 206(10): p. 2205-2220.
145. Barrett NA, Dectin-2 recognition of house dust mite triggers cysteinyl leukotriene generation by dendritic cells. J Immunol. 2009. 182(2): p. 1119-1128.

146. Yamasaki S, Mincle is an ITAM-coupled activating receptor that senses damaged cells. Nat Immunol. 2008. 9(10): p. 1179-1188.
147. Meyer-Wentrup F, Targeting DCIR on human plasmacytoid dendritic cells results in antigen presentation and inhibits IFN-alpha production. Blood. 2008. 111(8): p. 4245-4253.
148. Meyer-Wentrup F, DCIR is endocytosed into human dendritic cells and inhibits TLR8-mediated cytokine production. J Leukoc Biol. 2009. 85(3): p. 518-525.
149. Fujikado N, Dcir deficiency causes development of autoimmune disease in mice due to excess expansion of dendritic cells. Nat Med. 2008. 14(2): p. 176-180.
150. Gringhuis SI, Dectin-1 directs T helper cell differentiation by controlling noncanonical NF-kappaB activation through Raf-1 and Syk. Nat Immunol. 2009. 10(2): p. 203-213.
151. Krishnaswamy JK, Beyond pattern recognition: NOD-like receptors in dendritic cells. Trends Immunol. 2013. 34(5): p. 224-233.
152. van de Veerdonk FL, Inflammasome activation and IL-1b and IL-18 processing during infection. Trends Immunol. 2011. 32(3): p. 110-116.
153. Kanneganti TD, Central roles of NLRs and inflammasomes in viral infection. Nat Rev Immunol. 2010. 10(10): p. 688-698.
154. Lim HX, Principal role of IL-12p40 in the decreased Th1 and Th17 responses driven by dendritic cells of mice lacking IL-12 and IL-18. Cytokine. 2013. 63(2): p. 179-186.
155. Strober W, NOD2, an intracellular innate immune sensor involved in host defense and Crohn's disease. Mucosal Immunol. 2011. 4(5): p. 484-495.
156. Maeda S, Nod2 mutation in Crohn's disease potentiates NF-kappaB activity and Il-1beta processing. Science. 2005. 307(5710): p. 734-738.
157. Watanabe T, Nucleotide binding oligomerization domain 2 deficiency leads to dysregulated TLR2 signaling and induction of antigen-specific colitis. Immunity. 2006. 25(3): p. 473-485.
158. Kato H, Cell type-specific involvement of RIG-I in antiviral response. Immunity. 2005. 23(1): p. 19-28.
159. Kato H, RIG-I-like receptors and autoimmune disease. Curr Opin Immunol. 2015. 37: p. 40-45.
160. Funabiki M, Autoimmune disorders associated with gain of function of the intracellular sensor MDA5. Immunity. 2014. 40(2): p. 199-212.

161. Chen GY, Sterile inflammation: sensing and reacting to damage. Nat Rev Immunol. 2010. 10(12): p. 826-837.
162. Vabulas RM, Endocytosed HSP60s use toll-like receptor 2 (TLR2) and TLR4 to activate the toll/interleukin-1 receptor signaling pathway in innate immune cells. J Biol Chem. 2001. 276(33): p. 31332-31339.
163. Gao B, Endotoxin contamination in recombinant human heat shock protein 70 (Hsp70) preparation is responsible for the induction of tumor necrosis factor alpha release by murine macrophages. J Biol Chem. 2003. 278(1): p. 174-179.
164. Chen CJ, Identification of a key pathway required for the sterile inflammatory response triggered by dying cells. Nat Med. 2007. 13(7): p. 851-856.
165. Imaeda AB, Acetaminophen-induced hepatotoxicity in mice is dependent on Tlr9 and the Nalp3 inflammasome. J Clin Invest. 2009. 119(2): p. 305-314.
166. Zhang JG, The dendritic cell receptor Clec9A binds damaged cells via exposed actin filaments. Immunity. 2012. 36(4): p. 646-657.
167. Neumann K, Clec12a is an inhibitory receptor for uric acid crystals that regulates inflammation in response to cell death. Immunity. 2014. 40(3): p. 389-399.
168. Chu H, Innate immune recognition of the microbiota promotes host-microbial symbiosis. Nat Immunol. 2013. 14(7): p. 668-675.
169. Vaishnava S, The antibacterial lectin RegIIIgamma promotes the spatial segregation of microbiota and host in the intertine. 2011. 334(6053): p. 255-258.
170. Cash HL, Symbiotic bacteria direct expression of an intertinal bactericidal lectin. Science. 2006. 313(5790): p. 1126-1130.
171. Brandl K, MyD88-mediated signals induce the bactericidal lectin RegIII gamma and protect mice against intestinal Listeria monocytogenes infection. J. Exp. Med. 2007. 204(8): p. 1891-1900.
172. Petnicki-Ocwieja T, Nod2 is required for the regulation of commensal microbiota in the intestine. Proc Natl Acad Sci U S A. 2009. 106(37): p. 15813-15818.
173. Rakoff-Nahoum S, Recognition of commensal microflora by toll-like receptors is required for intestinal homeostasis. Cell. 2004. 118(2): p. 229-241.
174. Round JL, The Toll-like receptor 2 pathway establishes colonization by a commensal of the human microbiota. Science. 2011. 332(6032): p. 974-977.

175. Chassaing B, Intestinal epithelial cell toll-like receptor 5 regulates the intestinal microbiota to prevent low-grade inflammation and metabolic syndrome in mice. Gastroenterology. 2014. 147(6): p. 1363-1377.
176. Lupher ML Jr, The Cbl protooncoprotein: a negative regulator of immune receptor signal transduction. Immunol Today. 1999. 20(8): p. 375-382.
177. Rao N, The Cbl family of ubiquitin ligases: critical negative regulators of tyrosine kinase signaling in the immune system. J Leukoc Biol. 2002. 71(5): p. 753-763.
178. Griffiths EK, Cbl-3-deficient mice exhibit normal epithelial development. Mol Cell Biol. 2003. 23(21): p. 7708-7018.
179. Blake TJ, The truncation that generated the v-cbl oncogene reveals an ability for nuclear transport, DNA binding and acute transformation. EMBO J. 1993. 12(5): p. 2017-2026.
180. Langdon WY, The c-cbl proto-oncogene is preferentially expressed in thymus and testis tissues and encodes a nuclear protein. J Virol. 1989. 63(12): p. 5420-5424.
181. Ota Y, The product of the proto-oncogene c-cbl: a negative regulator of the Syk tyrosine kinase. Science. 1997. 276(5311): p. 418-420.
182. Murphy MA, Tissue hyperplasia and enhanced T-cell signaling via ZAP-70 in c-Cbl-deficient mice. Mol Cell Biol. 1998. 18(8): p. 4872-4882.
183. Levkowitz G, c-Cbl/Sli-1 regulates endocytic sorting and ubiquitination of the epidermal growth factor receptor. Genes Dev. 1998. 12(23): p. 3663-3674.
184. Keane MM, cbl-3: a new mammalian cbl family protein. Oncogene. 1999. 18(22): p. 3365-3375.
185. Ohashi PS, T-cell signaling and autoimmunity: molecular mechanisms of disease. Nat Rev Immunol. 2002. 2(6): p. 427-438.
186. Meng W, Structure of the amino-terminal domain of Cbl complexed to its binding site on ZAP-70 kinase. Nature. 1999. 398(6722): p. 84-90.
187. Zheng N, Structure of a c-Cbl-UbcH7 complex: RING domain function in ubiquitin-protein ligases. Cell. 2000. 102(4): p. 533-539.
188. Sanjay A, Cbl associates with Pyk2 and Src to regulate Src kinase activity, alpha(v)beta(3) integrin-mediated signaling, cell adhesion, and osteoclast motility. J Cell Biol. 2001. 152(1): p. 181-195.

189. Meisner H, Interactions of Drosophila Cbl with epidermal growth factor receptors and role of Cbl in R7 photoreceptor cell development. Mol Cell Biol. 1997. 17(4): p. 2217-2225.
190. Miura-Shimura Y, Cbl-mediated ubiquitinylation and negative regulation of Vav. J Biol Chem. 2003. 278(40): p. 38495-38504.
191. Hunter S, Phosphorylation of cbl after stimulation of Nb2 cells with prolactin and its association with phosphatidylinositol 3-kinase. Mol Endocrinol. 1997. 11(9): p. 1213-1222.
192. Sawasdikosol S, Tyrosine-phosphorylated Cbl binds to Crk after T cell activation. J Immunol. 1996. 157(1): p. 110-116.
193. Komander D, The emerging complexity of protein ubiquitination. Biochem Soc Trans. 2009. 37(Pt 5): p. 937-953.
194. Giles J, Chemistry Nobel for trio who revealed molecular death-tag. Nature. 2004. 431(7010): p. 729.
195. Pickart CM, Mechanisms underlying ubiquitination. Annu Rev Biochem. 2001. 70: p. 503-533.
196. Dye BT, Structural mechanisms underlying posttranslational modification by ubiquitin-like proteins. Annu Rev Biophys Biomol Struct. 2007. 36: p. 131-150.
197. Deshaies RJ, RING domain E3 uniquitin ligases. Annu Rev Biochem. 2009. 78: p. 399-434.
198. Markson G, Analysis of the human E2 ubiquitin conjugating enzyme protein interaction network. Genome Res. 2009. 19(10): p. 1905-1911.
199. Haglund K, Multiple monoubiquitination of RTKs is sufficient for their endocytosis and degradation. Nat Cell Biol. 2003. 5(5): p. 461-466.
200. Garcia-Higuera I, Interaction of the Fanconi anemia proteins and BRCA1 in a common pathway. Mol Cell. 2001. 7(2): p. 249-262.
201. Lei CQ, FoxO1 negatively regulates cellular antiviral response by promoting degradation of IRF3.
202. Duncan LM, Lysine-63-linked ubiquitination is required for endolysosomal degradation of class I molecules. EMBO J. 2006. 25(8): p. 1635-1645.
203. Chen ZJ, Nonproteolytic functions of ubiquitin in cell signaling. Mol Cell. 2009. 33(3): p. 275-286.
204. Zheng N, Structure of a c-Cbl-UbcH7 complex: RING domain function in ubiquitin-protein ligases. Cell. 2000. 102(4): p. 533-539.

205. Dou H, Structureal basis for autoinhibition and phosphorylation-dependent activation of c-Cbl. Nat Struct Mol Biol. 2012. 19(2): p. 184-192.
206. Kobashigawa Y, Autoinhibition and phosphorylation-induced activation mechanisms of human cancer and autoimmune disease-related E3 protein Cbl-b. Proc Natl Acad Sci U S A. 2011. 108(51): p. 20579-20584.
207. Miyake S, Cbl-mediated negative regulation of platelet-derived growth factor receptor-dependent cell proliferation. A critical role for Cbl tyrosine kinase-binding domain. J Biol Chem. 1999. 274(23): p. 16619-16628.
208. Ohrt T, c-Cbl binds to tyrosine-phosphorylated neurotrophin receptor p75 and induces its ubiquitination. Cell Signal. 2004. 16(11): p. 1291-1298.
209. Haugsten EM, Ubiquitination of fibroblast growth factor receptor 1 is required for its intracellular sorting but not for its endocytosis. Mol Biol Cell. 2008. 19(8): p. 3390-3403.
210. Abella JV, Met/Hepatocyte growth factor receptor ubiquitination suppresses transformation and is required for Hrs phosphorylation. Mol Cell Biol. 2005. 25(21): p. 9632-9645.
211. Saur SJ, Ubiquitination and degradation of the thrombopoietin receptor c-Mpl. Blood. 2010. 115(6): p. 1254-1263.
212. Lee PS, The Cbl protooncoprotein stimulates CSF-1 receptor multiubiquitination and endocytosis, and attenuates macrophage proliferation. EMBO J. 1999. 18(13): p. 3616-3628.
213. Zeng S, Regulation of stem cell factor receptor signaling by Cbl family proteins (Cbl-b/c-Cbl). Blood. 2005. 105(1): p. 226-232.
214. Masson K, Direct binding of Cbl to Tyr568 and Tyr936 of the stem cell factor receptor/c-Kit is required for ligand-induced ubiquitination, internalization and degradation. Biochem J. 2006. 399(1): p. 59-67.
215. Rathinam C, Myeloid leukemia development in c-Cbl RING finger mutant mice is dependent on FLT3 signaling. Cancer Cell. 2010. 18(4): p. 341-352.
216. Rao N, The non-receptor tyrosine kinase Syk is a target of Cbl-mediated ubiquitylation upon B-cell receptor stimulation. EMBO J. 2001. 20(24): p. 7085-7095.
217. Xiao Y, Targeting CBLB as a potential therapeutic approach for disseminated candidiasis. Nat Med. 2016. 22(8): p. 906-914.
218. Zhu LL, E3 ubiquitin ligase Cbl-b negatively regulates C-type lectin receptor-mediated antifungal innate immunity. J Exp Med. 213(8): p. 1555-1570.

219. Wang HY, Cbl promotes ubiquitination of the T cell receptor zeta through an adaptor function of Zap-70. J Biol Chem. 2001. 276(28): p. 26004-26011.
220. Bulut GB, Cbl uniquitination of p85 is essential for Epo-induced EpoR endocytosis. Blood. 2013. 122(24): p. 3964-3972.
221. Xiong H, Ubiquitin-dependent degradation of interferon regulatory factor-8 mediated by Cbl down-regulates interleukin-12 expression. J Biol Chem. 2005. 280(25): p. 23531-23539.
222. Shen M, Interferon regulatory factor-1 binds c-Cbl, enhances mitogen activated protein kinase signaling and promotes retinoic acid-induced differentiation of HL-60 human myelo-monoblastic leukemia cells. Leuk Lymphoma. 2011. 52(12): p. 2372-2379.
223. Han C, Integrin CD11b negatively regulates TLR-triggered inflammatory responses by activating Syk and promoting degradation of MyD88 and TRIF via Cbl-b. Nat Immunol. 2010. 11(8): p. 734-742.
224. Bachmaier K, E3 ubiquitin ligase Cblb regulates the acute inflammatory response underlying lung injury. Nat Med. 13(8): p. 920-926.
225. Ashton-Rickardt PG, Evidence for a differential avidity model of T cell selection in the thymus. Cell. 1994. 76(4): p. 651-663.
226. Hogguist KA, T cell receptor antagonist peptides induce positive selection. Cell. 1994. 76(1): p. 17-27.
227. Sebzda E, Positive and negative thymocyte selection induced by different concentrations of a single peptide. Science. 1994. 263(5153): p. 1615-1618.
228. Naramura M, Altered thymic positive selection and intracellular signals in Cbl-deficient mice. Proc Natl Acad Sci U S A. 1998. 95(26): p. 15547-15552.
229. Huang F, Establishment of the major compatibility complex-dependent development of CD4+ and CD8+ T cells by the Cbl family proteins. Immunity. 2006. 25(4): p. 571-581.
230. Naramura M, c-Cbl and Cbl-b regulate T cell responsiveness by promoting ligand-induced TCR down-modulation. Nat Immunol. 2002. 3(12): p. 1192-1199.
231. Janeway CA Jr, Signals and signs for lymphocyte responses. Cell. 1994. 76(2): p. 275-285.
232. Leung J, The CD28-B7 Family in Anti-Tumor Immunity: Emerging Concepts in Cancer Immunotherapy. Immune Netw. 2014. 14(6): p. 265-276.
233. McCoy KD, The role of CTLA-4 in the regulation of T cell immune response. Immunol Cell Biol. 1999. 77(1): p. 1-10.

234. Chiang YJ, Cbl-b regulates the CD28 dependence of T-cell activation. Nature. 2000. 403(6766): p. 216-220.
235. Bachmaier K, Negative regulation of lymphocyte activation and autoimmunity by the molecular adaptor Cbl-b. Nature. 2000. 403(6766): p. 211-216.
236. Huang F, Negative regulation of lymphocyte development and function by the Cbl family of proteins. Immunol Rev. 2008. 224: p. 229-238.
237. Chiang JY, Ablation of Cbl-b provides protection against transplanted and spontaneous tumors. J Clin Invest. 2007. 117(4): p. 1029-1036.
238. Loeser S, Spontaneous tumor rejection by cbl-b-deficient CD8+ T cells. J Exp Med. 2007. 204(4): p. 879-891.
239. Sohn HW, Cbl-b negatively regulates B cell antigen receptor signaling in mature B cells through unbiquitination of the tyrosine kinase Syk. J Exp Med. 2003. 197(11): p. 1511-1524.
240. Kitaura Y, Control of the B cell-intrisic tolerance programs by ubiquitin ligases Cbl and Cbl-b. Immunity. 2007. 26(5): p. 567-578.
241. Vivier E, Functions of natural killer cells. Nat Immunol. 2008. 9(5): p. 503-510.
242. Paolino M, The E3 ligase Cbl-b and TAM receptors regulate cancer metastasis via natural killer cells. Nature. 2014. 507(7493): p. 508-512.
243. Ginhoux F, Monocytes and macrophages: development pathways and tissue homeostasis. Nat Rev Immunol. 2014. 14(6): p. 392-404.
244. Fogg DK, A clonogenic bone marrow progenitor specific for macrophages and dendritic cells. Science. 2006. 311(5757): p. 83-87.
245. Auffray C, CX3CR1+CD115+CD135+ common macrophage/DC precursors and the role of CX3CR1 in their response to inflammation. J Exp Med. 2009. 206(3): p. 595-606.
246. Hirasaka K, Deficiency of Cbl-b gene enhances infiltration and activation of macrophages in adipose tissue and causes peripheral insulin resistance in mice. Diabetes. 2007. 56(10): p. 2511-2522.
247. Chiou SH, The E3 ligase c-Cbl regulates dendritic cell activation. EMBO Rep. 2011. 12(9): p. 971-979.
248. Wallner S, The role of the e3 ligase cbl-B in murine dendritic cells. PLos One. 2013. 8(6): p. e65178.

249. Wirnsberger G, Inhibition of CBLB protects from lethal Candida albicans sepsis. Nat Med. 2016. 22(8): p. 915-923.
250. Sargin B, Flt3-dependent transformation by inactivating c-Cbl mutations in AML. Blood. 2007. 110(3): p. 1004-1012.
251. Caligiuri MA, Novel c-CBL and CBL-b uniquitin ligase mutations in human acute myeloid leukemia. Blood. 2007. 110(3): p. 1022-1024.
252. Vainchenker W, New mutations and pathogenesis of myeloproliferative neoplasms. Blood. 2011. 118(7): p. 1723-1735.
253. Naramura M, Mutant Cbl proteins as oncogenic drivers in myeloproliferative disorders. Oncotarget. 2011. 2(3): p. 245-250.
254. Grunwald MR, FLT3 inhibitors for acute myeloid leukemia: a review of their efficacy and mechanisms of resistance. Int J Hematol. 2013. 97(6): p. 683-694.
255. Matthews W, A receptor tyrosine kinase specific to hematopoietic stem and progenitor cell-enriched populations. Cell. 1991. 65(7): p. 1143-1152.
256. Mackarehtschian K, Targeted disruption of the flk2/flt3 gene leads to deficiencies in primitive hematopoietic progenitors. Immunity. 1995. 3(1): p. 147-161.
257. Maraskovsky E, Dramatic increase in the numbers of functionally mature dendritic cells in Flt3 ligand-treated mice: multiple dendritic cell subpopulations identified. J Exp Med. 1996. 184(5): p. 1953-1962.
258. McKenna HJ, Mice lacking flt3 ligand have deficient hematopoiesis affecting hematopoietic progenitor cells, dendritic cells, and natural killer cells. Blood. 2000. 95(11): p. 3489-3497.
259. Svensson MN, Murine germinal center B cells require functional Fms-like tyrosine kinase 3 signaling for IgG1 class-switch recombination. Proc Natl Acad Sci U S A. 2015. 112(48): p. E6644-6653.
260. Annesley CE, The Biology and Targeting of FLT3 in Pediatric Leukemia. Front Oncol. 2014. 4.
261. Hamilton JA, Colony-stimulating factors in inflammation and autoimmunity. Nat Rev Immunol. 2008. 8(7): p. 533-544.
262. Maroc N, Biochemical characterization and analysis of the transforming potential of the FLT3/FLK2 receptor tyrosine kinase. Oncogene. 1993. 8(4): p. 909-918.

263. Lyman SD, Characterization of the protein encoded by the flt3 (flk2) receptor-like tyrosine kinase gene. Oncogene. 1993. 8(4): p. 815-822.
264. Graddis TJ, Structure-function analysis of FLT3 ligand-FLT3 receptor interactions using a rapid functional screen. J Biol Chem. 1998. 273(28): p. 17626-17633.
265. Savvides SN, Flt3 ligand structure and unexpected commonalities of helical bundles and cysteine knots. Nat Struct Biol. 2000. 7(6): p. 486-491.
266. Yamamoto Y, Activating mutation of D835 within the activation loop of FLT3 in human hematologic malignancies. Blood. 2001. 97(8): p. 2434-2439.
267. Mitina O, Src family tyrosine kinases phosphorylate Flt3 on juxtamembrane tyrosines and interfere with receptor maturation in a kinase-dependent manner. Ann Hematol. 2007. 86(11): p. 777-785.
268. Beslu N, Phosphatidylinositol-3' kinase is not required for mitogenesis or internalization of the Flt3/Flk2 receptor tyrosine kinase. J Biol Chem. 1996. 271(33): p. 20075-20081.
269. Zhang S, Flt3 ligand induces tyrosine phosphorylation of gab1 and gab2 and their association with shp-2, grb2, and PI3 kinase. Biochem Biophys Res Commun. 2000. 277(1): p. 195-199.
270. Zhang S, Flt3 signaling involves tyrosyl-phosphorylation of SHP-2 and SHIP and their association with Grb2 and Shc in Baf3/Flt3 cells. J Leukoc Biol. 1999. 65(3): p. 372-380.
271. Takahashi S, Downstream molecular pathways of FLT3 in the pathogenesis of acute myeloid leukemia: biology and therapeutic implications. J Hematol Oncol. 2011. p. 4-13.
272. Gilliland DG, The roles of FLT3 in hematopoiesis and leukemia. Blood. 2002. 100(5): p. 1532-1542.
273. Spiekermann K, Overexpression and constitutive activation of FLT3 induces STAT5 activation in primary acute myeloid leukemia blast cells. Clin Cancer Res. 2003. 9(6): p. 2140-2150.
274. Manfra DJ, Conditional expression of murine Flt3 ligand leads to expansion of multiple dendritic cells subsets in peripheral blood and tissues of transgenic mice. J Immunol. 2003. 170(6): p. 2843-2852.
275. Guimond M, In vivo role of Flt3 ligand and dendritic cells in NK cell homeostasis. J Immunol. 2010. 184(6): p. 2769-2775.
276. Zou T, Dendritic cells induce regulatory T cell proliferation through antigen-dependent and –independent interactions. J Immunol. 2010. 185(5): p. 2790-2799.

277. Yamazaki S, CD8+ CD205+ splenic dendritic cells are specialized to induce Foxp3+ regulatory T cells. J Immunol. 2008. 181(10): p. 6923-6933.
278. Sathaliyawala T, Mammalian target of rapamycin controls dendritic cell development downstream of Flt3 ligand signaling. Immunity. 2010. 33(4): p. 597-606.
279. Pulendran B, Prevention of peripheral tolerance by a dendritic cell growth factor: flt3 ligand as an adjuvant. J Exp Med. 1998. 188(11): p. 2075-2082.
280. Klein O, Flt3 ligand expands CD4+ FoxP3+ regulatory T cells in human subjects. Eur J Immunol. 2013. 43(2): p. 533-539.
281. Jabbouor M, Discrete domains of MARCH1 mediate its localization, functional interactions, and posttranscriptional control of expression. J Immunol. 2009. 183(10): p. 6500-6512.
282. Bartee E, Downregulation of major histocompatibility complex class I by human unbiquitin ligases related to viral immune evasion proteins. J Virol. 2004. 78(3): p. 1109-1120.
283. De Gassart A, MHC class II stabilization at the surface of human dendritic cells is the result of maturation-dependent MARCHI down-regulation. Proc Natl Acad Sci U S A. 2008. 105(9): p. 3491-3496.
284. Corcoran K, Ubiquitin-mediated regulation of CD86 protein expression by the ubiquitin ligase membrane-associated RING-CH-1 (MARCH1). J Biol Chem. 2011. 286(43): p. 37168-37180.
285. Baravalle G, Ubiquitination of CD86 is a key mechanism in regulating antigen presentation by dendritic cell. J Immunol. 2011. 187(6): p. 2966-2973.
286. Ohmura-Hoshino M, Inhibition of MHC class II expression and immune responses by c-MIR. J Immunol. 2006. 177(1): p. 341-354.
287. Vereecke L, The ubiquitin-editing enzyme A20 (TNFAIP3) is a central regulator of immunopathology. Trends Immunol. 2009. 30(8): p. 383-391.
288. Krikos A, Transcriptional activation of the tumor necrosis factor alpha-inducible zinc finger protein, A20, is mediated by kappa B elepments. J Biol Chem. 1992. 267(25): p. 17971-17976.
289. Tewari M, Lymphoid expression and regulation of A20, an inhibitor of programmed cell death. J Immunol. 1995. 154(4): p. 1699-1706.
290. Lee EG, Failure to regulate TNF-induced NF-kappaB and cell death responses in A20-deficient mice. Science. 2000. 289(5488): p. 2350-2354.

291. Wertz IE, De-ubiquitination and ubiquitin ligase domains of A20 downregulate NF-kappaB signaling. Nature. 2004. 430(7000): p. 694-699.
292. Boone DL, The ubiquitin-modifying enzyme A20 is required for termination of Toll-like receptor responses. Nat Immunol. 2004. 5(10): p. 1052-1060.
293. Shembade N, Inhibition of NF-kappaB signaling by A20 through disruption of ubiquitin enzyme complexes. Science. 2010. 327(5969): p. 1135-1139.
294. Kool M, The ubiquitin-editing protein A20 prevents dendritic cell activation, recognition of apoptotic cells, and systemic autoimmunity. Immunity. 2011. 35(1): p. 82-96.
295. Kobayashi T, TRAF6 is a critical factor for dendritic cell maturation and development. Immunity. 2003. 19(3): p. 353-363.
296. Han D, Dendritic cell expression of the signaling molecule TRAF6 is critical for gut microbiota-dependent immune tolerance. Immunity. 2013. 38(6): p. 1211-1222.
297. Duran-Struuck R, Principles of bone marrow transplantation (BMT): providing optimal veterinary and husbandry care to irradiated mice in BMT studies. J Am Assoc Lab Anim Sci. 2009. 48(1): p. 11-22.
298. Ojielo CI, Defective phagocytosis and clearance of Pseudomonas aeruginosa in the lung following bone marrow transplantation. J Immunol. 2003. 171(8): p. 4416-4424.
299. Kim D, TopHat2: accurate alignment of transcriptomes in the presence of insertions, deletions and gene fusions. Genome Biol. 2013. 14(4): R36.
300. Liao Y, featureCounts: an efficient general purpose program for assigning sequence reads to genomic features. Bioinformatics. 2014. 30(7): p. 923-930.
301. Sabir M, Impact of traumatic brain injury on sleep structure, eletrocorticographic activity and transcriptome in mice. Brain Behav Immun. 2015. 47: p. 118-130.
302. Trapnell C, Transcript assembly and quantification by RNA-Seq reveals unannotated transcripts and isoform switching during cell differentiation. Nat Biotechnol. 2010. 28(5): p. 511-515.
303. Bar-On L, CX3CR1+ CD8alpha+ dendritic cells are a steady-state population related to plasmacytoid dendritic cells. Proc Natl Acad Sci U S A. 2010. 107(33): p. 14745-14750.
304. Thien CB, Cbl: many adaptations to regulate protein tyrosine kinases. Nat Rev Mol Cell Biol. 2001. 2(4): p. 294-307.

305. Ettenberg SA, Cbl-b-dependent coordinated degradation of the epidermal growth factor receptor signaling complex. J Biol Chem. 2001. 276(29): p. 27677-27684.
306. Anandasabapathy N, Classical Flt3L-dependent dendritic cells control immunity to protein vaccine. J Exp Med. 2014. 211(9): p. 1875-1891.
307. Zhu J, CD4 T cells: fates, functions, and faults. Blood. 2008. 112(5): p. 1557-1569.
308. Szabo SJ, Molecular mechanisms regulating Th1 immune responses. Annu Rev Immunol. 2003. 21: p. 713-758.
309. Scheller J, The pro- and anti-inflammatory properties of the cytokine interleukin-6. Biochi Biophys Acta. 2011. 1813(5): p. 878-888.
310. Cho D, Expansion and activation of natural killer cells for cancer immunotherapy. Korean J Lab Med. 2009. 29(2): p. 89-96.
311. Berard M, IL-15 promotes the survival of naïve and memory phenotype CD8+ T cells. J Immunol. 2003. 170(10): p. 5018-5026.
312. Micallef MJ, Interferon-gamma-inducing factor enhances T helper 1 cytokine production by stimulated human T cells: synergism with interleukin-12 for interferon-gamma production. Eur J Immunol. 1996. 26(7): p. 1647-1651.
313. Chaix J, Cutting edge: Priming of NK cells by IL-18. J Immunol. 2008. 181(3): p. 1627-1631.
314. Johnson LD, Immunology. A chronic need for IL-21. Science. 2009. 324(5934): p. 1525-1526.
315. Gonzalez-Sanchez E, E-cadherin, guardian of liver physiology. Clin Res Hepatol Gastroenterol. 2015. 39(1): p. 3-6.
316. Zhang Y, Myeloid cells are required for PD-1/PD-L1 checkpoint activation and the establishment of an immunosuppressive environment in pancreatic cancer. Gut. 2017. 66(1): p. 124-136.
317. Wang Y, CSF-1 stimulated multiubiquitination of the CSF-1 receptor and of Cbl follows their tyrosine phosphorylation and association with other signaling proteins. J Cell Biochem. 1999. 72(1): p. 119-134.
318. Swee LK, Expansion of peripheral naturally occurring T regulatory cells by Fms-like tyrosine kinase 3 ligand treatment. Blood. 2009. 113(25): p. 6277-6287.
319. Belz GT, Transcriptional programming of the dendritic cell network. Nat Rev Immunol. 2012. 12(2): p. 101-113.

320. Bjedov I, Mechanisms of life span extension by rapamycin in the fruit fly Drosophila melanogaster. Cell Metab. 2010. 11(1): p. 35-46.
321. Harrison DE, Rapamycin fed late in life extends lifespan in genetically heterogeneous mice. Nature. 2009. 460(7253): p. 392-395.
322. Disis ML, Flt3 ligand as a vaccine adjuvant in association with HER-2/neu peptide-based vaccines in patients with HER-2/neu-overexpressing cancers. Blood. 2002. 99(8): p. 2845-2850.
323. Abe T, Cbl-b is a critical regulator of macrophage activation associated with obesity-induced insulin resistance in mice. Diabetes. 2013. 62(6): p. 1957-1969.